The Chromatic Aberration of the Eye and its Importance in the Modern World

FINCH, ABIGAIL,POPPY

The Chromatic Aberration of the Eye and its Importance in the Modern World

Abigail P. Finch

A thesis presented for the degree of
Doctor of Philosophy

Centre for Advanced Instrumentation
Department of Physics
Durham University
United Kingdom
September 2019

The Chromatic Aberration of the Eye and its Importance in the Modern World

Abigail P. Finch

Abstract

The human eye has various aberrations that distort the image formed on the retina. Monochromatic aberrations are the distortions present at a single wavelength and chromatic aberrations are wavelength dependent. Longitudinal chromatic aberration (LCA) describes the difference in defocus at different wavelengths. The LCA of the human eye is approximately 2 dioptres (D) across the visible spectrum. Normally we are unaware of these distortions, however, they do play an important role in our vision. The aim of this thesis was to investigate the importance of these aberrations in the context of the modern world.

The illuminant spectra that we are exposed to today are quite different from 100 years ago. Because LCA results in a difference in defocus with wavelength this means that the amount of defocus blur in the retinal image will change depending on the spectrum of light. In this thesis findings are reported indicating that there are certain illuminant spectra for which the chromatic fringes due to LCA were more visible. We also investigated how people accommodated to spectra made up of two distinct narrowband LEDs. The findings suggest that people do not accommodate optimally to these spectra.

There is also increasing interest in blurring stimuli realistically. This is partly with the emergence of virtual reality, so that 3D scenes appear as realistic as possible, but also has more clinical applications in trialling the effects of different corrective lenses on vision before the lenses are made (or inserted in the case of intraocular lenses). We investigated the importance of including monochromatic aberrations when rendering out of focus stimuli. It seems that monochromatic aberrations do make the stimuli appear more realistic, however, they did not have a significant impact on visual acuity.

Supervisors: Gordon D. Love and John M. Girkin

Acknowledgements

Firstly I would like to thank my supervisor Gordon Love. His support and encouragement throughout the PhD has been wonderful and his guidance has been invaluable. I would also like to thank Andrew Kirby for always being there to answer any questions and for all his help with setting up the experiments, and Laura Young for all her advice and the time she has spent explaining things to me over the years. I would like to thank our collaborators, Martin Banks and Steven Cholewiak from UC Berkeley and Jenny Read and Maydel Fernandez Alonso from Newcastle University for all of their support and advice. I would also like to acknowledge the Engineering and Physical Sciences Research Council (EPSRC) for funding this PhD.

I would like to thank everyone who encouraged me to start the PhD. In particular I would like to thank Hannah Smithson for kindling my interest in vision science, encouraging me to apply for the PhD, and for all her support before and since. I would also like to thank Sam for his support and encouragement in starting the PhD.

I would like to thank all of my office mates and the other CfAI members both for giving up their time to help me with my work and for helping me take my mind off work when needed with the many pub trips. I would especially like to thank Dougie for all of his support and reassurance. I would also like to thank everyone who gave up their time to participate in my experiments.

Throughout the PhD I have been very lucky to have the support of the Grey MCR community for which I am extremely grateful. I am so grateful to my old housemates for making Durham feel like a home. I would especially like

to thank Hannah and Ana for always being there for me no matter what, and to Ryan and Hannah for giving me somewhere to stay while I was writing up. Thank you also to my parents and my sister. They have been so supportive throughout and always make time for me when I need them even when I'm at my most difficult.

Contents

Declaration

The work in this thesis is based on research carried out at the Centre for Advanced Instrumentation, Department of Physics, University of Durham, England. No part of this thesis has been submitted elsewhere for any other degree or qualification. Everything presented below is the sole work of the author unless referenced to the contrary in the text with the following exceptions:

- In Chapter 5 the experimental data was collected in collaboration with Maydel Fernandez Alonso at Newcastle University. The author worked together with Maydel to set up the apparatus and collect the data. However, the statistical analysis and simulations were all the work of the author.
- Andrew K Kirby built the wavefront sensor described in chapters 5 and 6 and was responsible for collecting the wavefront data used in both of these chapters. The author then processed the data from the wavefront sensors to extract the relevant information.
- For Chapter 6 Andrew K Kirby helped to build the relay lens system used to view the projector screen and altered the projector itself by adding a filter.

List of Figures

List of Tables

Chapter 1

Introduction

The optics of the human eye are far from perfect, and as a result the light entering the eye is distorted in a variety of ways. These distortions can be classified as either chromatic aberrations (those that vary with the wavelength of light), or monochromatic aberrations (the aberrations present at a single wavelength). All eyes have both chromatic and monochromatic aberrations that vary across individuals. However, one particularly dramatic aberration is longitudinal chromatic aberration (LCA), which is generally constant across all individuals. LCA describes the difference in defocus at different wavelengths. Across the range of visible wavelengths there is a difference in defocus of about 2 dioptres (D) due to LCA. Given that people can be given glasses for anything above 0.5 D of refractive error, this 2 D due to LCA seems quite dramatic.

Since monochromatic and chromatic aberrations both blur the retinal image, we might expect them to be detrimental to our vision. In fact, it has been suggested that as well as correcting for refractive error and astigmatism, it may be beneficial to correct for other monochromatic aberrations and even chromatic aberrations using contact lenses, intraocular lenses (López-Gil and Montés-Micó, 2007), or laser eye surgery (Seiler et al., 2000). A number of studies have suggested that correcting monochromatic and/or chromatic aberrations can result in significant improvements in visual acuity (Campbell and Gubisch, 1967; Liang and Williams, 1997; Liang et al., 1997; Seiler et al., 2000; Yoon and Williams, 2000, 2002; Benny et al., 2007; Schwarz et al., 2014).

However, it also seems that the visual system is able to adapt to the aberra-

tions of the eye. In fact as long as they are not too dramatic, the magnitude of aberrations does not seem to correlate with visual acuity (Villegas et al., 2008; Artal, 2014). There is also evidence that both chromatic and monochromatic aberrations may actually be useful in some cases. For example, they both increase the depth of focus of the eye (Campbell and Gubisch, 1967) and they could also provide a cue for determining the direction of an accommodative response.

In this thesis the aberrations of the eye are investigated in relation to modern illuminant spectra and the possibility of realistically rendering blur in stimuli. These are introduced briefly below.

1.1 Modern illuminant spectra

In the past humans would have mostly been exposed to broadband spectra with relatively smooth intensity distributions as a function of wavelength, whether these be from natural daylight or lamps. The top two panels of Figure 1.1 show two examples of common broadband illuminants, one for a standard daylight illumination (D65) and the other for a typical tungsten bulb (Illuminant A).

However, in the modern world we are increasingly exposed to artificial illuminants and displays with more unnatural spectra. The bottom panel of Figure 1.1 shows two examples of modern spectra with intensity distributions that are much less smooth as a function of wavelength. What is particularly noticeable is that these more modern spectra have a series of distinct peaks in intensity at different wavelengths.

LCA results in different defocus values for different wavelengths and therefore spectra with different wavelength distributions may result in different blurring in the retinal images and different optimal accommodation responses. In this thesis we investigate the effects of different spectra on the appearance of chromatic fringes at object boundaries due to LCA and on people's accommodation responses.

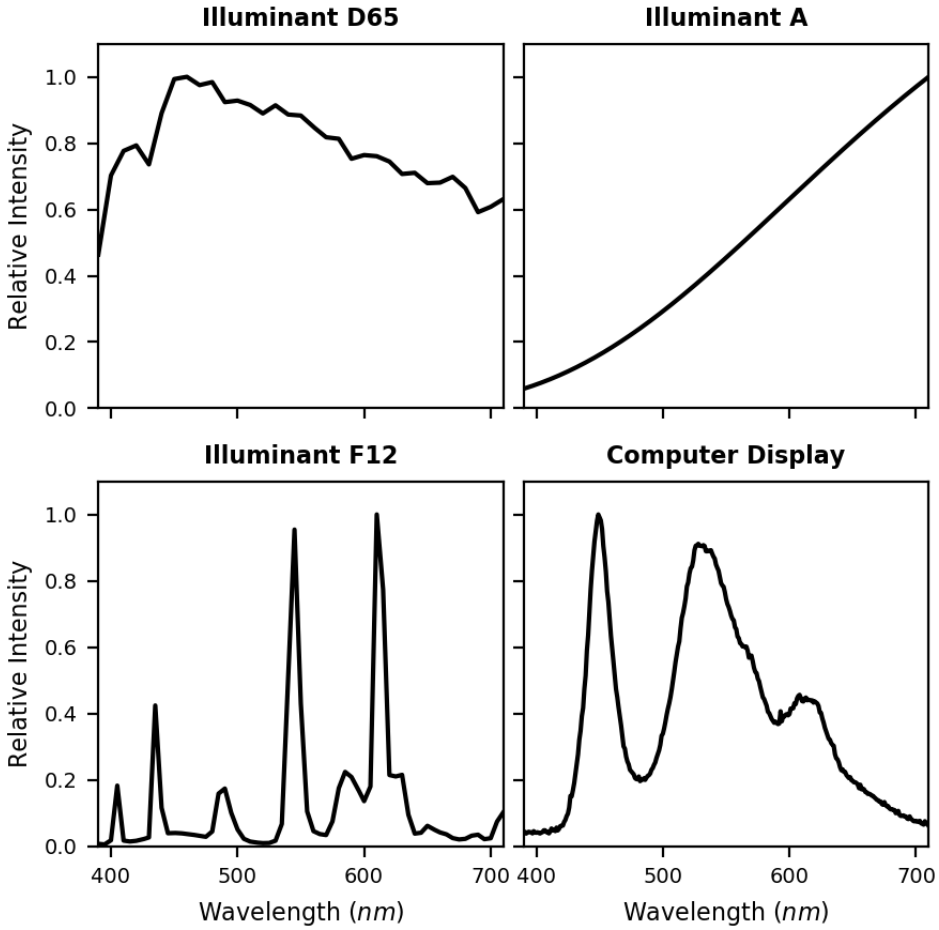

Figure 1.1: The spectra of four example illuminants. The top left panel shows D65, which is a CIE standard spectrum for natural daylight. The top right panel shows Illuminant A, which is a CIE standard spectrum from a tungsten filament bulb. The bottom left panel shows Illuminant F12 (CIE), which is an example of a CIE florescent lamp spectrum. The bottom right panel shows the spectrum of the white light coming from a MacBook screen. The spectra have all been normalised to have a maximum intensity of one.

1.2 Rendering blur realistically

It is useful to be able to realistically render blur both for displaying 3D scenes realistically such as in virtual reality, and in order to simulate the effects of certain optical corrections for patients without the expense of making the lenses. It seems logical to assume that in order to realistically render blur we

would need to account for the ways in which the aberrations of the eye would normally interact with stimuli in the real world. The final part of this thesis investigates whether it is important to include monochromatic aberrations when rendering blur.

1.3 Synopsis

This thesis investigates the impact of the aberrations of the eye on our vision by referencing the work of previous studies and advancing this work through both simulations and experiments. The following six chapters are summarised below.

- Chapter 2 is an overview of the workings of the human eye. This chapter has two main sections. The first describes the optics of the eye and the second describes detection of the light within the eye by the photoreceptors and the subsequent processing into neural signals that are relayed to the brain.
- Chapter 3 describes the accommodation response of the eye in greater detail. Firstly, the accommodation response curve and some potential reasons for the typical 'lead' and 'lag' in accommodation are discussed. Secondly, some of the potential cues to accommodation are examined the evidence for the use of each of these cues is discussed.
- Chapter 4 addresses the question of why it is that we do not generally notice the effects of LCA, and, in particular, why we do not see the chromatic fringes at image boundaries due to LCA. In this chapter the effect of the spectrum of light on the visibility of chromatic fringes is also investigated both through simulations and through an experiment in which participants were asked to give subjective reports of whether they could see chromatic fringes.
- Chapter 5 investigates whether different illuminant spectra alter our accommodative accuracy. An experiment is described in which observers' accommodative responses were measured for a selection of spectra made up of various combinations of two narrowband LEDs. Simulations are also described in this chapter predicting where observers would accommodate to the spectra using various potentials cues and rules for ac-

commodation. These simulation results are compared to the measured accommodation responses to evaluate which rule the observers might be using to accommodate and whether they are accommodating optimally.

- Chapter 6 explores the question of whether it is possible to render blur so that it is equivalent to real optical blur. A series of experiments are described in this chapter, in which various types of rendered blur are compared to real optical blur. These comparisons are made both in terms of the effect on visual acuity and in terms of the appearance.

- Chapter 7 Summarises the findings from the other chapters and presents ideas for future research.

Chapter 2

The Human Eye and Chromatic Aberration

This chapter gives an overview of the human eye and how it works. It covers the optics of the eye and the way that the light is focussed, as well as the way that the light is detected within the eye and processed into neural signals that feed into the brain.

The human eye is an imaging system. Figure 2.1 shows a diagram of a cross section of the human eye. As the light from an object in the environment enters the eye it passes through the tear film, the cornea, the aqueous humour, the lens, and the vitreous humour before reaching the retina. The cornea and the lens refract the light bringing it into a focus on the retina.

The retina is a multilayered structure lining the inner surface of the eye. This is where the photoreceptors which detect the light are located and where the first stages of visual processing occur. A roughly 5° visual angle central region of the retina is covered by a yellowish pigment known as macular pigment. Within this macular region lies the fovea. The fovea is a pit in the retina where the spatial resolution is greatest. When we fixate on an object in the outside world, the image of the object comes to a focus at the fovea.

At the back of the eye, towards the nasal side, the optic nerve leaves the eye. This is where axons carry the visual information towards the brain. The point at which the optic nerve leaves the eye is known as the optic disc. At the optic disc there is a gap in the retina which corresponds to a blind spot in our visual field.

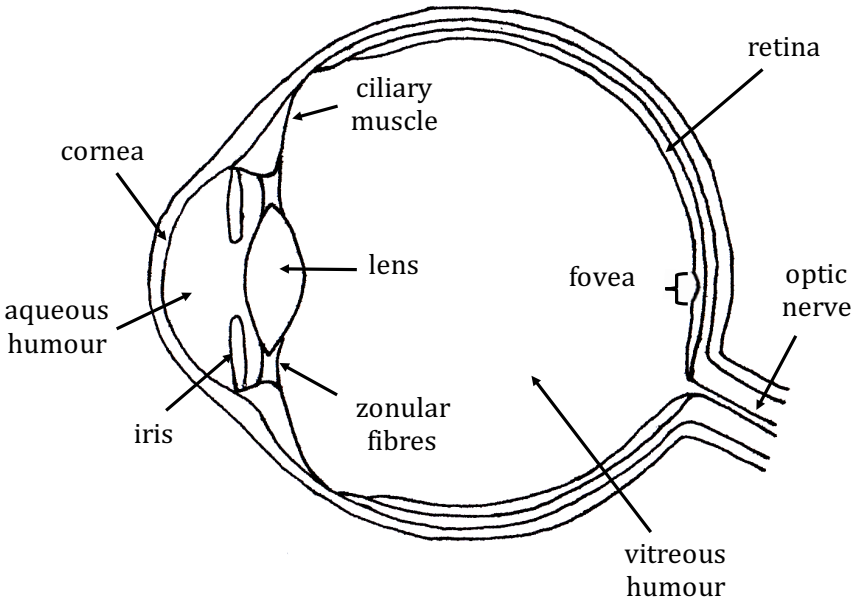

Figure 2.1: A representation of the cross section of a human eye (not to scale).

The following sections describe first the optics and then the neural pathways within the eye in greater detail.

2.1 Optics of the eye

Overall the eye has a refractive power of approximately 60 dioptres (D) when it is in focus for far objects. This is needed in order to focus images onto the retina. There are two main optical components of the eye that contribute to this refractive power: the cornea, and the crystalline lens. The cornea is the domed transparent layer right at the front of the eye. The crystalline lens is a convex structure that sits within the eye just behind the iris and is suspended in place by fibres called zonules (see Figure 2.1). The cornea has a fixed shape and accounts for the majority of the refraction (approximately 40 D) whereas the lens only accounts for about 20 D of the refraction when.

The lens is adjustable and responsible for fine tuning the focus of the eye through a process called accommodation. The shape of the lens is controlled by the ciliary muscle, which attaches to the zonules. When the ciliary muscle is

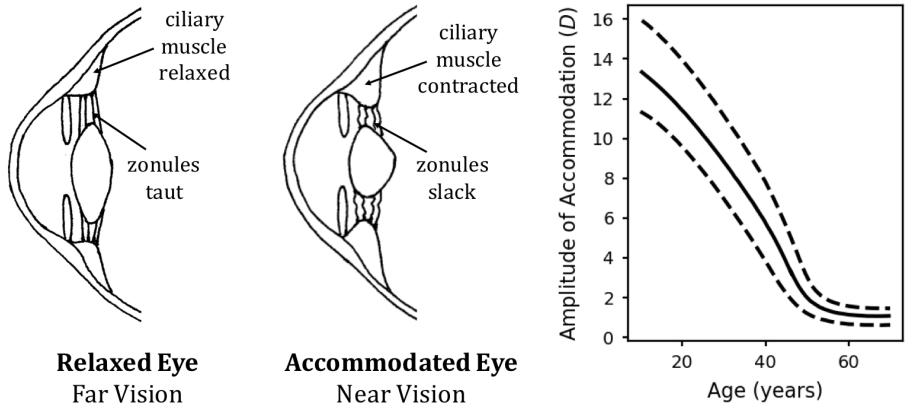

Figure 2.2: The accommodation of the human eye. The left panel shows a representation of the cross section of the front of a human eye in an accommodated and relaxed state (not to scale). In the graph on the right the solid line shows the amplitude of accommodation as a function of age for the average case. The two dashed lines show the upper and lower limits of the amplitude of accommodation as a function of age for normal cases. The data in the graph was taken from Duane (1912).

relaxed, the zonules are taut. This stretches out the lens reducing its effective power. In this state the accommodation is relaxed and the eye is focussed for distant objects. When the ciliary muscle is contracted, the zonules become slack and the lens forms a rounder shape. In the state the eye is focussed for near objects. The left panel of Figure 2.2 shows diagrams of a cross section of a relaxed eye (far vision) and an accommodated eye (near vision).

Myopia (short sightedness) and hyperopia (long sightedness) are accommodative errors that can occur within the eye. Myopia is caused by the eye being too long for the focal length of the lens. This means that even when the ciliary muscles are in their most relaxed state the eye is not in focus for 0 D. Therefore, myopia results in an inability to bring far away objects into focus. Hyperopia, on the other hand, is caused by the eye being too short for the focal length of the lens. This means that when the ciliary muscles are in their most relaxed state the eye is in focus for <0 D (i.e. beyond infinity). This means that a hyperopic eye cannot bring close up objects into focus.

The lens also changes with age becoming less flexible (Glasser and Campbell, 1998) and less transparent (Pokorny et al., 1987; Weale, 1988). The loss of

flexibility results in a loss of accommodative range with age. Young people have approximately 10-16 D of accommodation. However, by the age of around 50 the amplitude of accommodation is usually less than 2 D (Duane, 1912). This loss of accommodation with age is know as presbyopia. The right panel of Figure 2.2 shows the amplitude of accommodation as a function of age as measured by Duane (1912).

The loss of transparency of the lens with age results in less light getting through the lens to the retina. This particularly affects light in the blue part of the spectrum meaning that the light reaching the retina becomes more yellow. However, people adapt to this change so they do not notice colours changing with age.

It is interesting to note that although the cornea has a single refractive index, the refractive index of the lens actually varies throughout the structure so that it is different in the centre than at the edge. This is known as a gradient index (GRIN).

Another important part of the optics of the eye is the pupil. This is the circular aperture that the light passes through between the cornea and the lens. The pupil is formed by the circular iris muscle, which contracts and relaxes to control the size of the pupil. The pupil size varies depending on the amount of light entering the eye to limit the amount of light that reaches the retina.

2.1.1 Image quality

The image formed by any optical system will not be a perfect representation of the scene being imaged. This is because information will be lost as the light travels through the optics of the system. The eye is no exception to this rule.

One good way of assessing the quality of the images produced by an optical system such as the eye, is to examine the quality of the image that would be formed of an infinitely small point of light. The image of a single point of light is known as the point spread function (PSF). All images can be thought of as a collection of single points of light. Therefore, the quality of any image formed by an optical system is limited by the quality of the PSF of that optical system. The PSF of an optical system can be calculated using the equation,

$$\mathrm{PSF}(r_i, \theta_i) = |\mathcal{F}(P(r_p, \theta_p) e^{i \frac{2\pi}{\lambda} Z(r_p, \theta_p)})|^2, \tag{2.1}$$

where $\mathrm{PSF}(r_i, \theta_i)$ is the PSF defined over the image plane (the retina) with the radial coordinates r_i and θ_i, $\mathcal{F}$ is a Fourier transform, $P(r_p, \theta_p)$ is the pupil function, which describes the shape of the pupil, $Z(r_p, \theta_p)$ is the phase function, which describes the phase distortions of the light across the pupil, r_p, θ_p are the radial coordinates in the pupil plane, and λ is the wavelength of the light.

In order to approximate what the image formed on the retina (retinal image) for a specific eye will look like, we can convolve the perfect 2D representation of the scene being imaged with the PSF of the eye. This convolution can be done in Fourier space using the equation

$$\mathrm{Image} = \mathcal{F}^{-1}[\mathcal{F}(\mathrm{Scene}) \times \mathcal{F}(\mathrm{PSF})], \tag{2.2}$$

where Image is the retinal image, Scene is a 2D representation of the scene being imaged, and $\mathcal{F}^{-1}$ is an inverse Fourier transform. It is worth bearing in mind that this approximation of the retinal image relies on the assumption that the PSF remains constant across the field of view and as we will see in the later sections on aberrations, this is not actually the case. Therefore the approximation of the retinal image produced by this equation is more accurate for small angles.

Another way of representing the quality of images produced by a particular optical system is in Fourier (or frequency) space. This is based on the Fourier theorem named after J. B. Fourier, which states that any image can be represented as the sum of a series of sinusoidal gratings (Fourier, 1808). Therefore, instead of the image being represented as a series of intensity values over a two dimensional space, it is transformed so that it is represented as a series of amplitudes and phases each corresponding to a sinusoidal grating of a different spatial frequency. These two representations are mathematically equivalent and we can refer to the first as being the representation of the image in image space and the second as the representation of the image in Fourier space. To convert between these two representations a Fourier transform is needed. A standard Fourier transform takes us from image space into Fourier space and an inverse Fourier transform takes us back from Fourier space to image space.

If we take the Fourier transform of the PSF, we get the optical transfer function (OTF). Therefore,

$$\mathrm{OTF} = \mathcal{F}(\mathrm{PSF}). \tag{2.3}$$

The OTF of an optical system contains information as to how the contrast and phase of each spatial frequency component of the image will be altered from the object plane to the image plane. By taking the absolute value of the OTF we get the modulation transfer function (MTF). So

$$\text{MTF} = |\mathcal{F}(\text{PSF})|. \tag{2.4}$$

The MTF contains just the contrast information for each spatial frequency and not the phase information. Therefore, the MTF is simply a description of the loss in contrast for each spatial frequency component of the image.

If the PSF is not radially symmetric then the MTF also won't be radially symmetric. In these cases it is standard to calculate the radially averaged MTF as

$$\text{rMTF}(f_i) = \frac{1}{2\pi}\int_0^{2\pi} \text{MTF}_{\text{2D}}(f_i, \theta_i)d\theta, \tag{2.5}$$

where f_i is the spatial frequency in the image plane and θ_i is the angle.

As well as the optics of the eye, neural factors also influence the quality of the visual information that our brains can use. These factors include the distribution of the photoreceptors in the retina, the receptive fields of the post-receptoral pathways, and the way that the visual information is then processed by the brain.

The combined effect of the optics of the eye and the neuronal influences can be described in frequency space by the Contrast Sensitivity Function (CSF). The CSF describes the sensitivity of the visual system as a function of spatial frequency. In this way the CSF is very similar to the MTF just with the neuronal influences also accounted for.

The CSF can be measured psychophysically by presenting sinusoidal gratings to an observer at a range of spatial frequencies. At each spatial frequency the contrast at which the stimulus is at threshold can be determined experimentally to get the contrast threshold function. The CSF is simply the inverse of the contrast threshold function.

The CSF can also be calculated for an eye with a known wavefront error using the equation

$$\text{CSF}(f_i) = \text{MTF}(f_i) \times \text{nCSF}(f_i). \tag{2.6}$$

From the wavefront error the MTF can be calculated. The MTF is essentially the optical component of the CSF. Then all that is needed is the neural

component of the CSF or the neural Contrast Sensitivity Function (nCSF). The nCSF can be calculated by rearranging Equation 2.6 to get,

$$\text{nCSF}(f_i) = \frac{\text{CSF}(f_i)}{\text{MTF}(f_i)}. \tag{2.7}$$

Mannos and Sakrison (1974) modelled the CSF for the eye with the equation,

$$\text{CSF}(f_i) = 2.6(0.0192 + 0.114f_i)e^{-(0.114f_i)^{1.1}}. \tag{2.8}$$

This model was based on measurements taken with a pupil size of roughly 3mm. By assuming this eye to be diffraction limited, which is reasonable given the small pupil size, we can estimate the MTF for this standard eye by calculating the diffraction limited MTF for an eye with a 3mm pupil. An estimation for the nCSF can then be calculated using Equation 2.7 as was shown in Young (2011) and Parnell (2015). Once the nCSF has been calculated in this way it can then be used to compute the CSF for any eye with a known MTF using Equation 2.6.

The optical causes of degradation in the images formed by the eye can be broken down into three main categories. These are the effects of diffraction, the monochromatic aberrations of the eye, and the chromatic aberrations of the eye. In the following subsections, each of these optical effects will be described in turn.

2.1.2 Diffraction

The first source of optical error in the retinal image is diffraction. This is a phenomenon that applies to any optical system, even one without any optical imperfections or aberrations. Diffraction occurs when a wavefront of light is obstructed. In the case of the eye this obstruction is the circular pupil. After the light has travelled through the pupil, diffraction causes it to spread out. The light from different points within the pupil will then interfere both constructively and destructively resulting in diffraction rings in the image formed on the retina. Because diffraction is unavoidable, the best possible image that can be formed by an optical system is the diffraction limited image.

The effects of diffraction can be modelled in two ways. The Fresnel approximation describes diffraction effects in the near-field (i.e. when the image plane

is close to the aperture) while the Fraunhofer approximation describes diffraction in the far-field (i.e. when the image plane is far from the aperture). In the case of the eye, the cornea and the lens combined result in an optical power of approximately 60 dioptres. This optical power has essentially the same effect as having a very large distance between the retina and the pupil. Therefore, the Fraunhofer approximation is valid for the eye. Equation 2.1 for calculating the PSF includes the Fraunhofer approximation of diffraction.

Using Equation 2.1 with a constant phase function (no aberrations), the PSF of a diffraction limited eye can be generated. This diffraction limited PSF is known as an Airy disc and consists of a central peak in intensity with a series of successively fainter concentric rings surrounding it. The intensity profile of a cross-section through the centre of an Airy disc is shown in Figure 2.3.

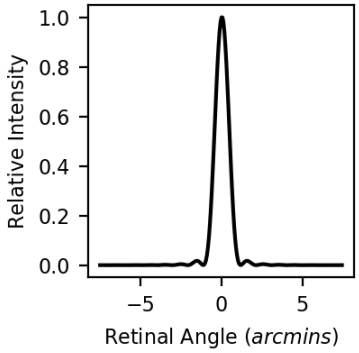

Figure 2.3: The profile of an Airy disc for a diffraction limited eye with a 2mm pupil and 550nm light.

The amount of diffraction that occurs within an eye is dependent on both the size of the aperture and the wavelength of the light. The smaller the aperture and the longer the wavelength, the greater the effect of diffraction, and therefore the more spread out the PSF, will be. Figure 2.4 shows the Airy discs for different pupil sizes and wavelengths. It is clear from these images that the PSF becomes more blurred as the pupil size decreases and as the wavelength increases.

2.1.3 Monochromatic aberrations

The second source of degradation in the retinal image are the monochromatic aberrations of the eye. These are caused by the structure and arrangement of the optical components of the eye and cause distortions to the retinal image that are not wavelength dependent. This means that they are present even in monochromatic light.

There are a variety of monochromatic aberrations each of which have different effects on the retinal image. In this section I will firstly describe the different ways in which monochromatic aberrations can degrade the image formed of

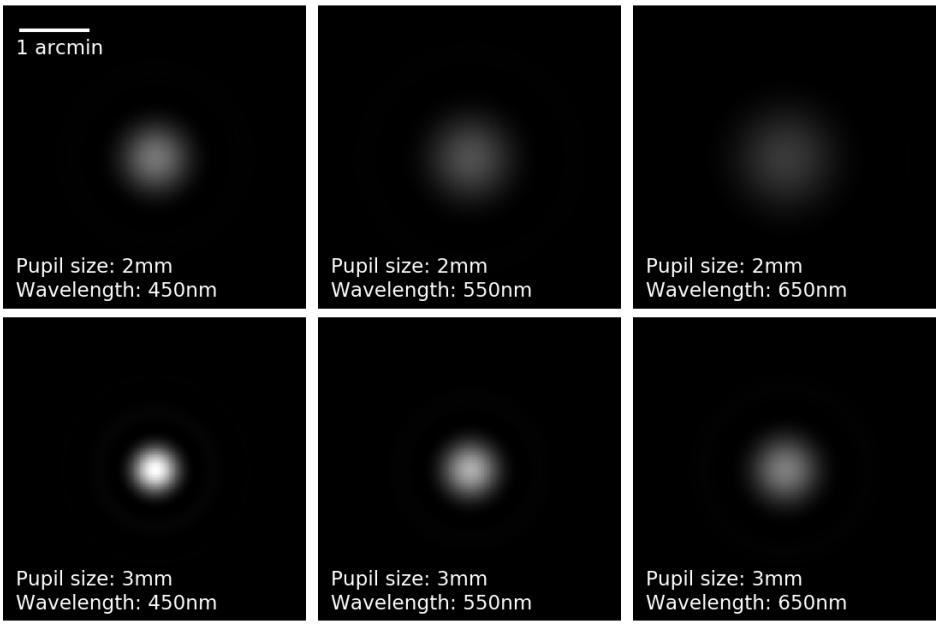

Figure 2.4: Images of Airy discs formed by an eye with pupil diameters of 2mm and 3mm and with wavelengths of 450nm, 550nm and 650nm. The scale bar in the top left image applies to all of the images. In order for the scale to be accurate the images would need to be viewed from approximately 31 meters.

a single point of light. I will then briefly describe some of the ways that monochromatic aberrations can affect the image formed across the visual field.

Monochromatic aberrations for a single point

These aberrations alter the relative phase of the wavefront of light across the pupil. This means that rays of light passing through different points on the pupil will not all come into a focus at the same point on the retina.

Monochromatic aberrations can distort the light in many different ways. Therefore, in order to characterise the monochromatic aberrations in a particular eye it is useful to break them down into categories or modes. The standard method for describing the monochromatic aberrations of human eyes is to approximate them using Zernike modes (Zernike, 1934; Thibos et al., 2000). Zernike modes describe the wavefront distortion in the pupil plane for a series of different aberrations. They can be calculated using the Zernike polynomi-

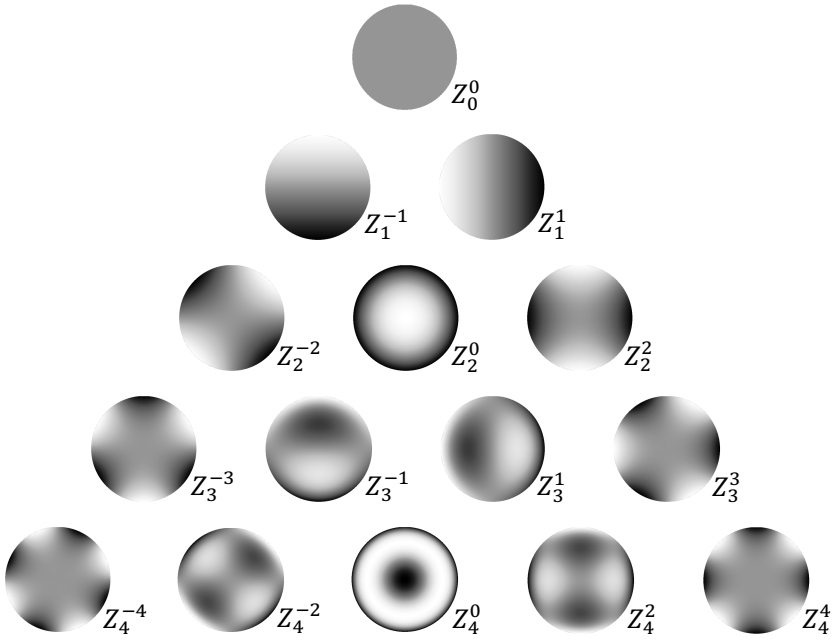

Figure 2.5: Representations of the phase functions described by the Zernike polynomials up to $n = 4$. The greyscale colourmap shows the wavefront error across the pupil. Darker areas have negative phase and lighter areas have positive phase. The n and m parameter values are given for each Zernike mode in the form Z_n^m.

als. One useful feature of the Zernike modes is that they are all orthogonal to each other. This means that the magnitude of each Zernike aberration within a wavefront can be determined independently of the other Zernike aberrations within that wavefront.

The Zernike modes are grouped by two parameters, n, which corresponds to the radial frequency of the aberration, and m, which corresponds to the angular (azimuthal) frequency, where $n \geq 0$ and $-n \leq m \leq n$. The order of a Zernike mode is also given by its n value. The standard notation is to write n as subscript and m as superscript, so each Zernike mode can be referred to as Z_n^m. Figure 2.5 shows the phase functions for the first 4 orders of Zernike polynomials.

The Zernike modes can be calculated using the equation

$$Z_n^m(r_p, \theta_p) = N_n^m \; R_n^m(r_p) \; A_n^m(\theta_p) \tag{2.9}$$

where $Z_n^m(r_p, \theta_p)$ is the Zernike mode defined over a unit circle with the polar coordinates $0 \leq r \leq 1$ and $0 \leq \theta \leq 2\pi$. N_n^m is the normalisation term, which makes the root mean squared (RMS) error equal to one, and is given by

$$N_n^m = \sqrt{\frac{2(n+1)}{1+\delta}}, \tag{2.10}$$

where

$$\delta = \begin{cases} 1 & \text{if } m = 0, \\ 0 & \text{otherwise.} \end{cases} \tag{2.11}$$

$R_n^m(r_p)$ is the radial component and is defined as

$$R_n^m(r_p) = \sum_{k=0}^{\frac{n-|m|}{2}} \frac{-1^k \, (n-k)! \, r_p^{n-2k}}{k! \, (\frac{n+|m|}{2} - k)! \, (\frac{n-|m|}{2} - k)!}. \tag{2.12}$$

$A_n^m(\theta_p)$ is the angular component where

$$A_n^m(\theta_p) = \begin{cases} \sin(m\theta_p) & \text{if } m < 0, \\ 1 & \text{if } m = 0, \\ \cos(m\theta_p) & \text{if } m > 0. \end{cases} \tag{2.13}$$

Some of the Zernike modes are more familiar, such as defocus (Z_2^0), which causes all of the rays from the pupil to come to a focus either behind or in front of the focal plane. Astigmatism is also relatively well known (Z_2^{-2} and Z_2^2), and results in the rays of light along one axis in the pupil coming into focus in a different plane to those along the orthogonal axis. However, the Zernike modes include a whole host of other aberrations that distort the light in different ways.

Using this standardised system the aberrations of a particular eye can be described by giving a single coefficient for each of these Zernike modes up to a certain order. Because the Zernike polynomials are normalised by the normalisation function $N(n, m)$, the coefficient for each aberration is also the RMS error of that aberration.

The monochromatic aberrations in the human eye are mainly caused by the shapes of the lens and the cornea as well as the structure of the gradient index within the lens (Marcos et al., 2001; Smith et al., 2008). The tear film, which is a thin layer of fluid on the surface of the cornea, can also have an impact. Individual variation in these factors cause monochromatic aberrations vary dramatically between eyes (Marcos et al., 2001).

The monochromatic aberrations within an individual eye can also vary. This can be caused by changes in the way that the light is passing through the optics of the eye or by actual variations in the shape and structure of the lens, cornea, and tear film.

The path that the light is taking through the optics of the eye changes with field angle. Therefore, the monochromatic aberrations change with field angle. We will come back to this when we describe monochromatic aberrations across the visual field.

The path of the light also changes with pupil size. As pupil size increases the effect of monochromatic aberrations increases too (Thibos et al., 2002; Wilson et al., 2002). This is because the light reaching the retina has travelled through a greater area of the lens and cornea and is therefore more aberrated by these structures. With a small pupil of around 1.22mm the eye is approximately diffraction limited (Thibos et al., 2002). However, as the pupil size increases, as it does in dimmer lighting, the image formed on the retina becomes more affected by the aberrations of the eye.

There are various processes that lead to changes in the shape and structure of the lens, cornea and tear film. In order for the eye to accommodate the lens changes shape and it has been found that the monochromatic aberrations of the eye change as it accommodates (He et al., 2000). In particular, spherical aberration has been found to vary linearly with accommodation in a way that is consistent across individuals, with the Zernike coefficient for spherical aberration becoming increasingly negative the greater the accommodation response is (Plainis et al., 2005). The shape of the cornea and the lens, and the gradient index of the lens also change with age (Smith et al., 2008). This results in the wavefront error increasing with age (McLellan et al., 2001; Artal et al., 2002; Plainis and Pallikaris, 2008). The tear film also changes with every blink. It is worth noting, however, that Miranda et al. (2009) found monochromatic aberrations to be relatively stable over the course of a week

with any variation being too small to be clinically significant.

Monochromatic aberrations across the visual field

As was mentioned previously, the monochromatic aberrations described above vary with field angle. This means that the blur in the image will vary across the visual field. The variations can be in the amount and nature of the blur in the retinal image, and in the magnification of the retinal image.

It has been shown that as field angle increases the monochromatic aberrations of the eye also increase. This means that retinal image quality becomes worse at greater eccentricities (Navarro et al., 1998; Guirao and Artal, 1999; Atchison and Scott, 2002; Smith et al., 2008).

There can also be a difference in magnification across the image, known as distortion. Although this could distort the image in a large number of ways, typically the distortion introduced by optical systems is symmetrical and can be described either as barrel or pincushion distortion, or as some combination of the two. Barrel distortion is when the image has a greater magnification in the centre of the field, with the magnification decreasing with eccentricity. Pincushion distortion is the opposite of barrel distortion and results in the magnification being the lowest at the centre of the image and increasing with eccentricity. Distortion results in straight lines in the scene appearing curved in the image.

2.1.4 Chromatic Aberrations

The refractive indices of the optical components of the eye are dependent on the wavelength of light. This means that the aberrations of the eye are also dependent on wavelength resulting in chromatic aberration. There are two types of chromatic aberration that occur within the eye. These are longitudinal chromatic aberration (LCA) and transverse chromatic aberration (TCA).

Longitudinal Chromatic Aberration

The wavelength dependence of the refractive indices of the optical components of the eye results in different focal lengths for different wavelengths of light. This difference in the focal length, and therefore defocus, with wavelength is known as longitudinal or axial chromatic aberration (LCA).

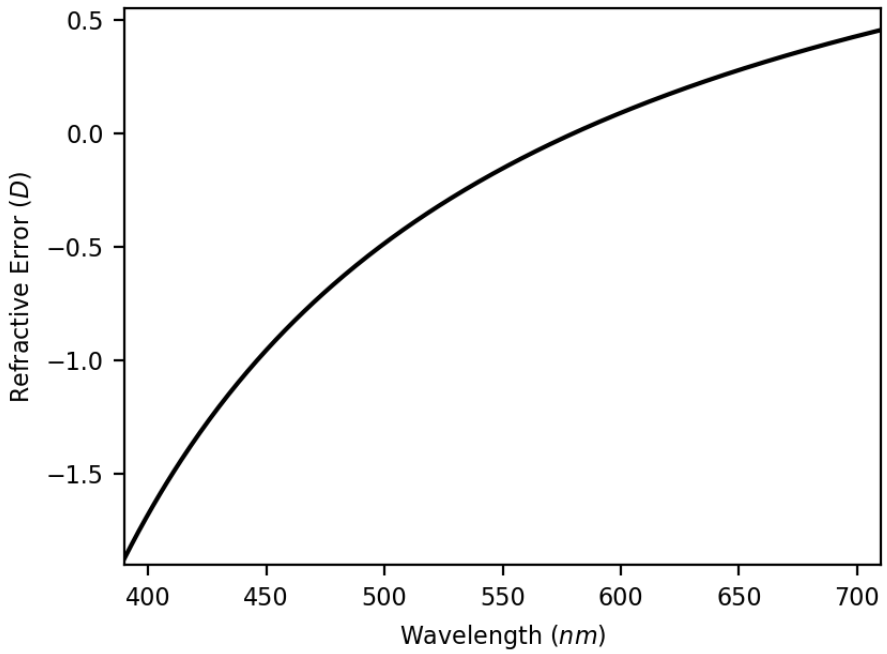

Figure 2.6: The LCA of the human eye as a function of wavelength calculated from Equation 2.14. The reference wavelength is 580nm.

Many studies have been conducted to measure the LCA of the eye using various techniques (e.g. Bedford and Wyszecki, 1957; Charman and Jennings, 1976; Howarth and Bradley, 1986; Marcos et al., 1999; Burns, 2000; McLellan et al., 2002; Grieve et al., 2006). The general agreement is that LCA is essentially the same across individuals, and that across the whole of the visible spectrum the LCA of the human eye is approximately 2 D. Figure 2.6 shows a plot of the LCA of the eye as a function of wavelength calculated from the equation

$$D(\lambda) = 1.7312 - \frac{633.46}{\lambda - 214.10} \tag{2.14}$$

where λ is the wavelength of light in nanometres and $D(\lambda)$ is refractive error in dioptres. This equation was described by Marimont and Wandell (1994) based on the work of Thibos et al. (1992). In this case the refractive error is calculated relative to a reference wavelength of 580nm.

Transverse Chromatic Aberrations

Transverse or lateral chromatic aberration (TCA) describes lateral shifts in the images produced on the retina at different wavelengths. This effect is due to differences in the magnification power and aberrations of the optical components of the eye at different wavelengths.

Unlike with LCA there is a large amount of variation in TCA between eyes (Marcos et al., 2001). There is also evidence for a link between the TCA and the monochromatic aberrations introduced by an eye. Marcos et al. (2001) found that eyes with large amplitudes of monochromatic aberrations also tended to have more TCA as well.

Zhai et al. (2014) showed that TCA has a negligible impact on visual quality relative to LCA. Therefore, the following chapters will focus on LCA rather than TCA. It is also easier to study the effects of LCA because it does not vary much between individuals.

2.2 Physiology of the retina

The retina is the structure that covers the back surface of the eye. It is made up of a series of layers of cells know as plexiform layers. Within these layers, the photoreceptors detect the light reaching the retina, and it is also where the first stages of visual processing occur. This processing takes place in cells which receive inputs from the photoreceptors and combine them in various ways.

The structure of the retina is slightly counter intuitive because the layers of cells responsible for processing the information from the photoreceptors actually lie in front of the layer of photoreceptors. This means that the light reaching the retina must first past through these processing cell layers before it can reach the photoreceptors.

Behind the photoreceptors is the pigment epithelium. This is a layer of cells containing pigment that absorbs the light that was not detected by the photoreceptors. This prevents light that was not initially detected from scattering and potentially being detected by photoreceptors elsewhere and confusing the image.

In this section I will firstly describe the types of photoreceptor in the eye. I will then go on to describe the structure of the other plexiform layers and some of the ways in which the visual information is processed in these layers.

2.2.1 Photoreceptors

The photoreceptors in the eye are composed of an inner segment and an outer segment. The outer segment absorbs photons and generates a neural signal. It is composed of a highly folded membrane with a large surface area. This membrane is where the photons are detected so the large surface area increases the chance of photon detection. The inner segment is where the cell body is located containing the nucleus of the cell. The inner segment also includes an extrusion that carries the signal initiated in the outer segment to a synapse with other cells. Figure 2.7 shows diagrams of the structures of the photoreceptors in the retina.

There are two main types of photoreceptors in the human eye, rods and cones. These are named after the shapes of the outer segments. Cones have a more conical shaped outer segment whereas rods have a long, rod shaped, outer segment (see Figure 2.7).

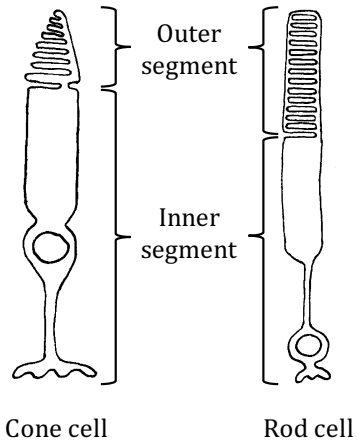

Figure 2.7: A diagram of the cone and rod photoreceptors of the human eye (not to scale).

There are many functional differences between rods and cones. Rods work better under dim lighting conditions and they become saturated under bright light. The cones, on the other hand, work better under brighter conditions and they are not as sensitive to dim light. The cones also have a greater spatial resolution than the rods. This is due to the fact that the cones are very densley packed at the fovea. In fact, in the central fovea (foveola) there are no rod cells at all, only cone cells.

Another difference between the rods and the cones is that they contain different types of pigment. This results in rods and cones being sensitive to light of different wavelengths.

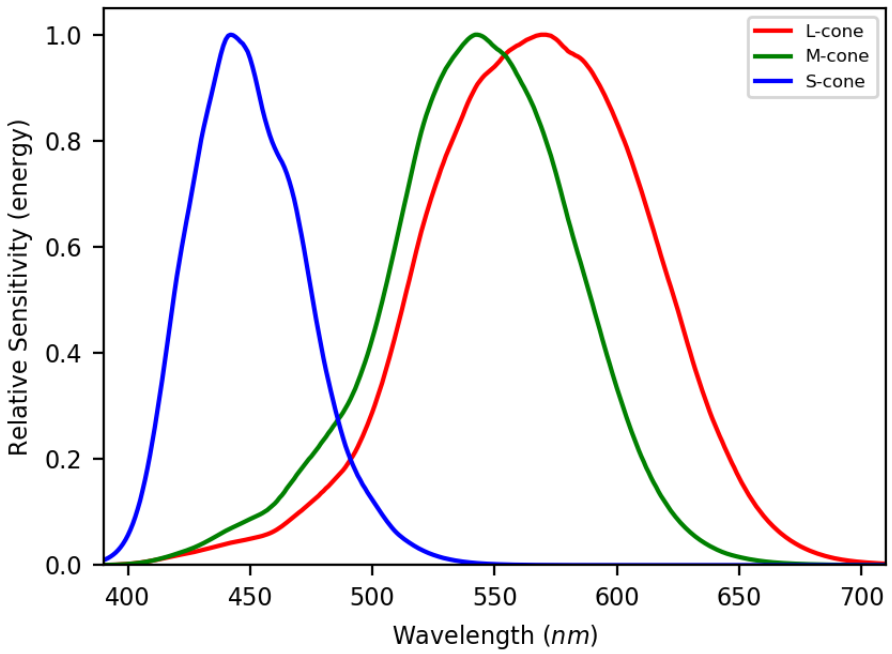

Figure 2.8: The standard spectral sensitivities of the L, M, and S cones for the central 2° visual field, normalised so that the peak sensitivity for each cone type is one. These standards were defined by Stockman et al. (1999) and Stockman and Sharpe (2000) and were taken from www.cvrl.org.

There is only one type of rod cell with one type of photopigment. Therefore, all of the rod cells in the eye have the same spectral sensitivity. The rods have a peak sensitivity at around 498nm and their sensitivity drops of at about 640nm. There are, however, three types of cone cells each with a different spectral sensitivity. These are referred to as short wavelength cones (S cones), middle wavelength cones (M cones), and long wavelength cones (L cones), after the wavelength ranges they are most sensitive to. Figure 2.8 shows the spectral sensitivities of these three cone types.

Both rods and cones are univarient. This means that each type of receptor can only alter the intensity of their signal and therefore they cannot disambiguate intensity of the stimulus from wavelength of the stimulus. However, by comparing the signal between the three different types of cone cell we are able to help solve this ambiguity between wavelength and intensity. The dif-

ferences in the spectral sensitivities of these three cone types is therefore the basis of our ability to perceive colour. As there is only one type of rod cell, we cannot make these comparisons and therefore we cannot distinguish colours when using the rod cells alone.

As rods and cones operate under different light levels, lighting conditions can be broken down into three categories. These are scotopic, mesopic and photopic from darkest to brightest. Under scotopic conditions, there is not enough light for the cones to function and therefore it is the rods alone that are responsible for our vision. Therefore under scotopic conditions we cannot perceive colour. Under mesopic conditions, both the rods and the cones contribute to our vision. Under photopic conditions, the light saturates the rods so only the cones contribute to our vision. We can perceive colour in both mesopic and photopic conditions since the cones are active in both.

The rods and cones also vary in terms of their distribution across the retina. The cones are most concentrated at the fovea with the cone density trailing off dramatically into the peripheral retina. The rods, on the other hand, are not present at all in the central fovea, although there is a much higher density of rods than cones in the periphery. This is the reason that our visual acuity and colour vision are best at the fovea. It also is the reason that we often can detect dimmer objects in our periphery which seem to disappear when we fixate them.

The different cone types also have different distributions across the retina. The S cones are a lot sparser in the photoreceptor mosaic, making up only about 5 to 10% of cones overall. There are also no S cones at all in the central fovea. On average there are somewhere between 1.5 and 2 times more L cones than M cones in the retina (Cicerone et al., 1994; Sharpe et al., 2005). However, there are dramatic individual differences in the relative numbers of L and M cones (Hofer et al., 2005).

There is also a third type of photoreceptor in the eye which contains the pigment melanopsin. However, I will describe this in more detail in the following section.

2.2.2 Post-receptoral processing

Once the light has been detected by the photoreceptors, the photoreceptors excite other cells to respond. This sets off a chain of responses that eventually carries information via the optic nerve to the lateral geniculate nucleus (LGN), and then to the visual cortex in the brain. For the purposes of this thesis we are just concerned with the first few stages of this visual processing which occur in the retina itself.

The processing in the human retina involves four main types of cell. These are the amacrine cells, bipolar cells, horizontal cells, and the ganglion cells (Kolb et al., 1992).

The bipolar cells are essentially the relay cells that carry information from the photoreceptors to the ganglion cells. The amacrine and horizontal cells mostly make lateral connections along the retina. The amacrine cells are located next to the photoreceptors whereas the horizontal cells are located next to the ganglion cells.

The ganglion cells make up the inner most layer in the retina and are the final cells in the retinal processing chain. It is the axons of the ganglion cells that make up the optic nerve to carry the information from the eye to the LGN.

There are many different types of ganglion cell, each of which makes different comparisons and combinations of the signals from the photoreceptors. These ganglion cells form the basis of important visual pathways in the early visual system, with different pathways corresponding to different layers within the LGN. Here I will be describing four key types of ganglion cells and their associated pathways.

Parvocellular Pathway

The most common type of ganglion cell in the primate retina are those that feed into the parvocellular layers of the LGN and form the basis of the parvocellular pathway. For this reason these ganglion cells are sometimes referred to as P-cells.

In the central retina these P-cells have very small receptive fields and are known as midget ganglion cells (Rodieck et al., 1985). The midget ganglion cells have spatially opponent receptive fields with a concentric structure. At

the centre of their receptive field they take an input from a single L or M cone. In the surround they take an opponent input from a mixture of L and M cones.

Because the central input comes from a single cone, whereas the surrounding input is from a seemingly random combination of L and M cones, the average spectral sensitivity is different for the centre and the surround of the receptive field. As a result of this the midget ganglion cells are chromatically opponent in the $L-M$ colour direction. This means that they are sensitive to changes along the red-green colour axis.

These features of the midget ganglion cells lead to properties that are characteristic of the parvocellular pathway. These properties include a high spatial resolution and an important role in colour vision. The midget ganglion cells and the parvocellular pathway form the basis of the red-green or $L-M$ dimension in human colour space.

Magnocellular Pathway

The second most common type of ganglion cells in the primate retina are called parasol ganglion cells. These feed into the magnocellular layers of the LGN. These are vastly outnumbered by midget ganglion cells in the retina but are more common in the periphery.

The parasol ganglion cells also have spatially opponent, concentric receptive fields. However, their receptive fields are much larger than those of the midget ganglion cells (Rodieck et al., 1985), giving them a poorer spatial resolution. In the parasol ganglion cells the input to both the centre and the surround of the receptive field comes from a mixture of L and M cones. This means that unlike the midget ganglion cells, the parasol ganglion cells are not chromatically opponent.

These features of the parasol ganglion cells result in the magnocellular pathway having a lower spatial resolution that the parvocellular pathway. The magnocellular pathway also has no chromatic opponency. It does have a greater sensitivity than the parvocellular pathway though.

The magnocellular pathway has often been associated with the luminance pathway, which is responsible for detecting changes in luminance and luminance boundaries. The luminance pathway has a much faster response than the

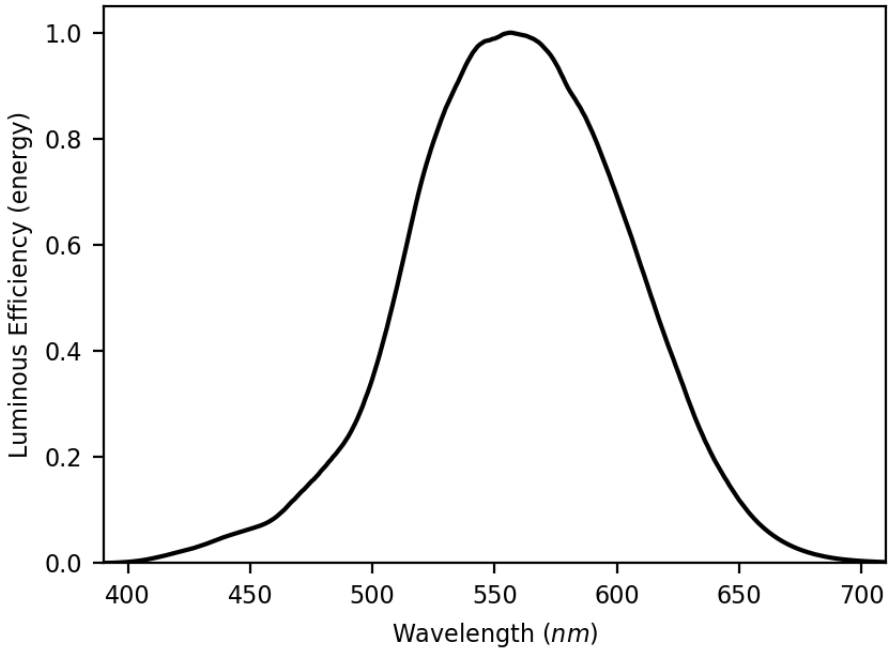

Figure 2.9: The 2° luminous efficiency as a function of wavelength expressed in units of energy. These data were taken from www.cvrl.org.

chromatic pathways. It also has a spectral sensitivity, known as the luminous efficiency function or $V(\lambda)$ (shown in Figure 2.9), which combines the spectral sensitivities of the L and M cones in the following equation

$$V(\lambda) = 0.68990272\ L(\lambda) + 0.34832189\ M(\lambda), \tag{2.15}$$

where $V(\lambda)$ is the energy based luminous efficiency function, and $L(\lambda)$ and $M(\lambda)$ are the energy based L and M cone spectral sensitivity functions normalised to have peak sensitivities of one (Stockman and Sharpe, 2000; Sharpe et al., 2005; CIE, 2006; Stockman et al., 2008).

Koniocellular Pathway

Another type of retinal ganglion cell is the small bistratified ganglion cell (Dacey and Lee, 1994). These project to the koniocellular layers of the LGN and form the start of the koniocellular pathway.

The small bistratified ganglion cell has a very large receptive field with no surround. This means that it is not spatially opponent. It receives excitatory input from the S cones and an inhibitory input from L and M cones making it chromatically opponent in the $S-(L+M)$ or blue-yellow colour direction.

This pathway is important for colour vision as it allows for colour discrimination in the $S-(L+M)$ or blue-yellow dimension. Combined with the parvocellular pathway this forms the basis of human colour vision. However, the koniocellular pathway has very poor spatial resolution.

Intrinsically Photosensitive Retinal Ganglion Cells

As was mentioned previously, there is also a third type of photoreceptor. These are fundamentally different from rods and cones in that they are in fact intrinsically photosensitive retinal ganglion cells (ipRGCs). The ipRGCs are ganglion cells which contain a light sensitive photopigment called melanopsin.

The receptive field structure of the ipRGCs is similar to that of the small bistratified ganglion cells in that they are very large and are not spatially opponent. However, unlike the small bistratified ganglion cells, the ipRGCs receive excitatory input for L and M cones and inhibitory input from the S cones (Dacey et al., 2005). The melanopsin in the ipRGCs also contributes an excitatory input to the cells. This means that they are also chromatically opponent.

The ipRGCs show a very sustained light response (Wong, 2012). This suits them to non-image forming visual functions. ipRGCs are thought to play a key role in several non-image forming functions including the pupillary light response (Gamlin et al., 2007; Spitschan et al., 2014) and the control of circadian rhythms (Berson et al., 2002).

2.2.3 Summary

All optical systems are imperfect and therefore there is always some image degradation. In the eye this degradation is caused by a combination of diffraction, monochromatic aberrations, and chromatic aberrations.

There are various ways to represent the quality of the images formed by the eye. The PSF is a representation of the image formed of an infinitely small

point of light. The PSF can then be used to generate and approximation of the retinal image of any given scene.

The OTF and MTF also represent the quality of the retinal image, but in Fourier space. This means that they show the contrast (and phase for the OTF) for each spatial frequency relative to the theoretical perfect image. The CSF is another Fourier space metric, but it takes into account not only the optical effects of the eye but neuronal effects as well.

Photoreceptors in the retina detect the light entering the eye. There are two main types of photoreceptor: rods and cones. The rods work in darker conditions and are saturated in bright light. There is only one type of rod and therefore the rods have no colour discrimination. The cones work in brighter conditions and are less sensitive to low light levels. There are three types of cone and comparisons between these form the basis of human colour vision.

Ganglion cells received a combination of inputs from various photoreceptors and carry this information from the eye to the LGN. Different types of ganglion cells compare and combine the signals from the photoreceptors differently and form the basis of different visual pathways.

There are three main post-receptoral pathways. The magnocellular pathway is responsible for the luminance dimension. The parvocellular pathway is responsible for the $L{-}M$ colour dimension and has a very high spatial resolution at the fovea. The koniocellular pathway is responsible for the $S{-}(L{+}M)$ colour dimension and has a low spatial resolution.

Chapter 3

The Accommodation Response

This chapter goes into the accommodation response of the human eye in greater detail. The first section describes the general shape of the accommodation response function. The second section describes the potential optical cues that the human visual system could use to accommodate and evaluates the evidence for the use of each of these cues.

3.1 Accommodation response curve

When the steady state accommodation response is plotted as a function of the stimulus distance there is not a simple linear relationship over the range of values that the eye can accommodate to. Instead the slope of the accommodation response is less than one indicating over-accommodation to far stimuli and under-accommodation to near stimuli. The accommodation response function also tails off at the furthest and nearest distances. An example of this curve can be seen in Figure 3.1. This characteristic shape of the accommodation response function has been known for many years (Toates, 1972).

It has been suggested that this apparent 'lead' and 'lag' in the accommodation response function is due to a 'laziness' of the accommodation response. Perhaps we 'spare accommodation' by not fully bringing the stimulus into focus.

Leading on from this idea, it has been suggested that perhaps the longitudinal chromatic aberration (LCA) of the eye results in a greater depth of field, which in turns allows for this sparing of accommodation. Campbell and Gubisch

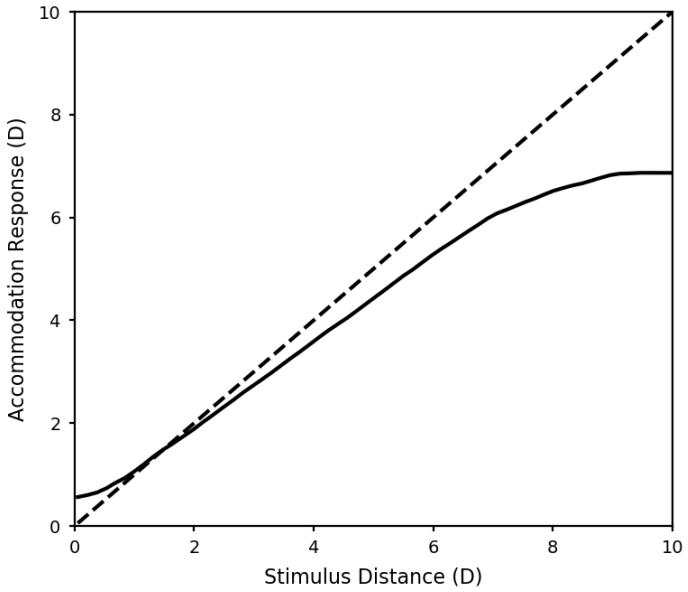

Figure 3.1: The dotted line shows a 'perfect' one to one relationship between the stimulus distance and the accommodation response, and the solid line shows a typical accommodation response function. This graph was adapted from Bobier, Campbell, and Hinch (1992).

(1967) actually showed that there is a greater depth of focus for white light than for monochromatic light. Perhaps the reason for the lead and lag in the accommodation response function is that at closer distances the eye is in focus for blue light while at further distances the eye is in focus for red light. This way the eye is always in focus for some wavelength but the accommodation is spared.

Ivanoff (1949) was the first to make the suggestion that at different distances we may accommodate for different wavelengths. In his experiment subjects accommodated to a white light source with various levels of defocus. For each defocus level Ivanoff determined which wavelength of monochromatic light was also in focus. He found that when the the eye was accommodating to a white light source at infinity, red wavelengths of almost 700nm were in focus. However, when the eye was accommodating to a white light source at 2.5 dioptres (D), wavelengths of approximately 500nm were in focus. Similarly Bobier and Sivak (1978) found that red light is more out of focus when the eye is accommodating to a near stimulus and green light is more out of focus

when the eye is accommodating to a far stimulus.

These studies show that the apparent shape of the accommodation response function along with the LCA of the eye result in the lowest defocus at longer wavelengths for near objects and the lowest defocus at shorter wavelengths for far objects. However, they do not show that it is because of the LCA of the eye that the accommodation response curve has these 'leads' and 'lags'

There is actually increasing evidence that the apparent 'lead' and 'lag' in the accommodation response function is not due to the LCA of the eye. Charman and Tucker (1978) compared the accommodation response function for white and monochromatic light and found that the apparent 'leads' and 'lags' in the accommodation response function were also present under monochromatic light suggesting that LCA was not responsible for them. Similarly Bobier et al. (1992) investigated whether the 'leads' and 'lags' in the accommodation response function were still present when LCA was increased, reduced, or reversed. They found that varying LCA did not significantly affect the stimulus response function, again indicating that LCA is not responsible for the shape of the accommodation response function.

Therefore, it seems that there must be another explanation behind the shape of the accommodation response function. One more recent idea is that rather than resulting from a 'sparing' of accommodation, the shape of the accommodation response function actually represents the optimal response. It has been shown that when the higher order aberrations of the eye, and in particular spherical aberration, are taken into account, the accommodation response that optimises image quality is not actually the same as the one to one linear accommodation response that eliminates defocus (Plainis et al., 2005; Buehren and Collins, 2006; Tarrant et al., 2010; Thibos and Bradley, 2013). In fact, it has been found that positive defocus can improve the image quality in an optical system with positive spherical aberration and negative defocus can improve the image quality in an optical system with negative spherical aberration (Tarrant et al., 2010). Therefore, given that spherical aberration becomes increasingly negative with accommodation (Plainis et al., 2005), it follows that the optimal accommodation response would have a lag for near targets and a lead for distant targets just as the actual measured accommodation response does.

3.2 Cues to accommodation

When it comes to working out the accommodation response needed to bring a defocussed image into focus, there are two pieces of information that the visual system needs. Firstly, it needs the magnitude of the defocus, in order to produce the correct magnitude of response, and secondly, it needs the sign of the defocus, to produce the correct direction of response.

Generally, the greater the magnitude of defocus, the more blurred the image formed on the retina will be, regardless of the sign of the defocus. Therefore, working out the magnitude of the accommodation response needed should not be too difficult a task. The more blurry the image is, the further it is from focus, and therefore, the greater the necessary accommodative response is.

However, defocus is an even order aberration. This means that, all other things being equal, the image formed by an eye with defocus of a dioptres will be identical to the image formed by an eye with defocus of $-a$ dioptres. This is demonstrated in Figure 3.2. This means that defocus blur on its own is an even-error cue, because it gives information about the magnitude but not the sign of defocus. Therefore, the visual system must be using some other cue in order to judge the direction of the accommodation response needed. This cue must give an odd-error signal for accommodation.

Under natural conditions we tend to be confronted with scenes made up of familiar objects where there are many pictorial cues that could be used to determine the direction of an accommodation response. For example, we know what the relative sizes of familiar objects should be and can use this to judge whether an object is closer or further away. Surface textures can also provide useful cues because there will be a gradient in the spatial frequency of these textures as they become further away or closer to us.

Most of the time we will also be viewing scenes binocularly (with both eyes). This means that there are also cues from the vergence of our eyes and from binocular disparity that could help to guide the direction of our accommodation responses. When we are fixated on an object with both eyes the angle of the eyes, or the vergence, gives us a cue to how far away that object is. Binocular disparity refers to the difference in the location of the images of objects in the scene on both retinas. This provides cues to the depth within the scene.

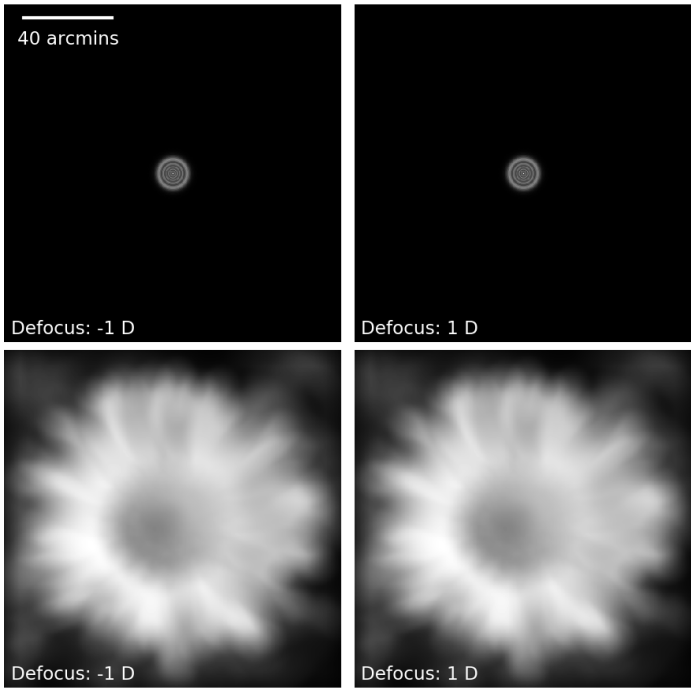

Figure 3.2: The top row shows greyscale images of the simulated PSFs for both -1 D and 1 D of defocus, for 550nm light and a 5mm pupil. The bottom row shows greyscale images of a daisy convolved with these PSFs to give the generated retinal images of a daisy with -1 D and 1 D of defocus. The scale bar in the top left image applies to all of the images. In order for the scale to be accurate the images would need to be viewed from approximately 1 meter.

Another possibility is that the human visual system could be using a trial and error approach by accommodating slightly in one direction. If it is the correct direction, then the defocus blur should reduce slightly, whereas if it is the wrong direction, then the defocus blur should increase slightly. From this additional information it would then be possible for the visual system to determine the actual direction of response needed.

It has, however, been found that the human visual system is capable of making accurate accommodation responses for stimuli presented monocularly (to only one eye) in the absence of any pictorial cues (Smithline, 1974). It has also been found that these responses are initiated in the correct direction suggesting that the visual system is not using a trial and error approach.

There must, therefore, be an odd-error optical cue that the visual system is

using to accommodate. There are actually a number of potential candidates for this cue. These include the monochromatic aberrations of the eye, the chromatic aberrations of the eye, the microfluctuations of the eye, and the Stiles-Crawford effect. All of these potential cues will be discussed below.

The studies investigating the accommodation response can be broken up into two main categories. There are those that monitor accommodation responses for a step change in defocus and those that monitor accommodation responses to a sinusoidally modulating stimulus. The need for a directional cue most obviously applies to the first type of study where the defocus step is in a random direction. However, I will be discussing both types of study in this chapter.

3.2.1 Monochromatic Aberrations

As was described in the previous section, the eye actually has many monochromatic aberrations of various magnitudes that distort the wavefront of light. Although these aberrations are orthogonal in the pupil plane, they actually interact in their effects on the retinal image. It has often been suggested that these monochromatic aberrations could provide a directional cue to accommodation (Fincham, 1951; Campbell and Westheimer, 1959).

One result of these interactions is that although on its own, defocus only provides an even-error cue, when it is combined with other even order aberrations, a difference can be seen in the retinal images formed depending on the sign of the defocus, providing a potential odd-error cue. This means that there are a whole range of monochromatic aberrations that could contribute a directional cue for accommodation. Next I will describe the ways that astigmatism and spherical aberration in particular might provide such a cue. I will then discuss whether there is convincing evidence for monochromatic aberrations being used as a directional cue for accommodation.

Vertical and oblique astigmatism (Z_2^{-2} and Z_2^2) are even order aberrations. These cause light from one axis in the pupil to come into focus at a different depth from the orthogonal axis. When astigmatism is combined with defocus, the sign of the defocus determines which axis has the best focus, this therefore determines the orientation of the blur in the PSF. This results in a clear change in the retinal image with the sign of defocus as can be seen in Figure 3.3.

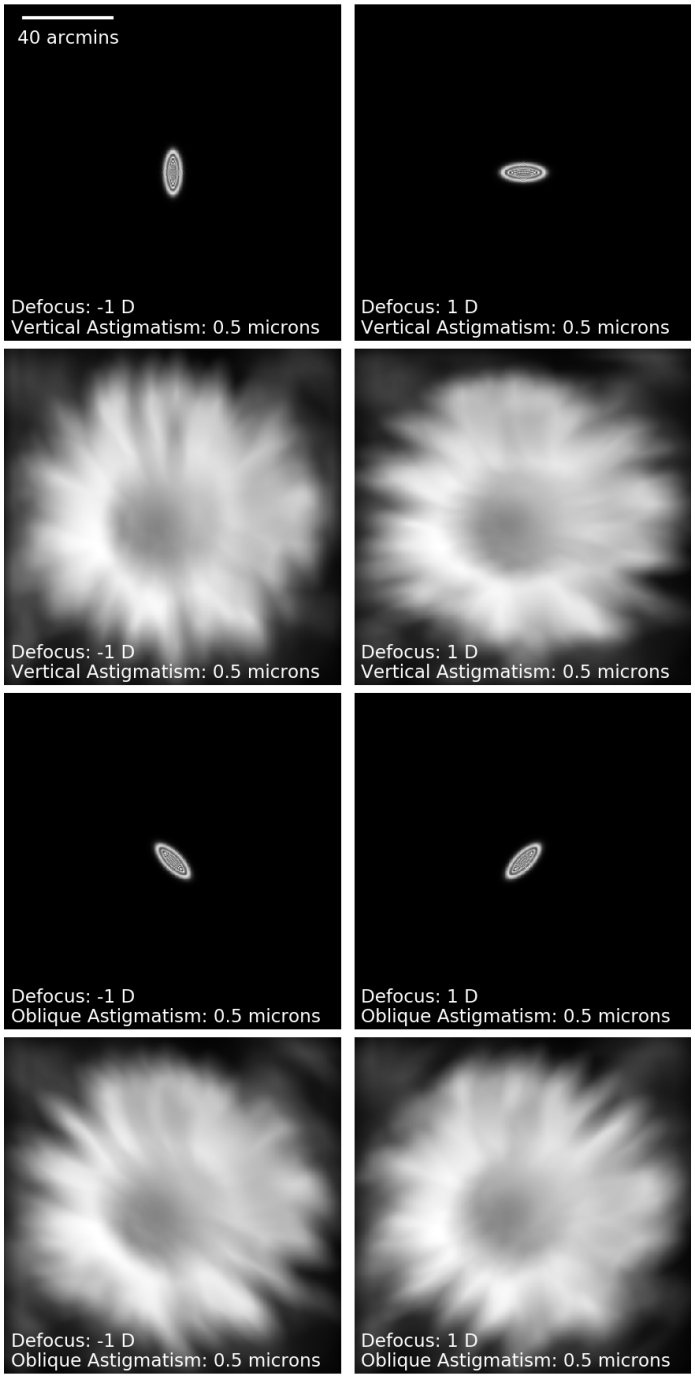

Figure 3.3: Simulated PSFs and retinal images of a daisy for defocus and astigmatism with 550nm light and a 5mm pupil. The top 2 rows are for vertical astigmatism and the bottom 2 rows are for oblique astigmatism. The two columns are for -1 D and 1 D defocus respectively. The scale bar in the top left image applies to all of the images. In order for the scale to be accurate the images need to be viewed from approximately 1 meter.

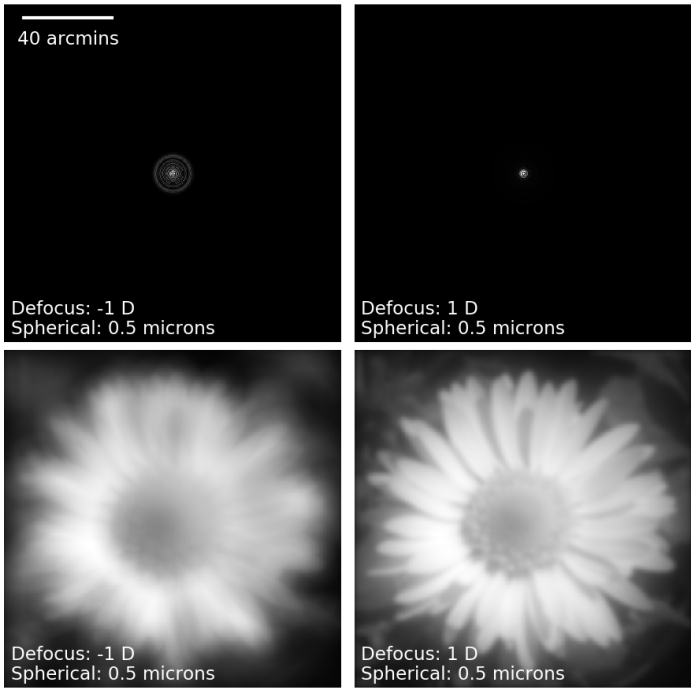

Figure 3.4: The top row shows greyscale images of the simulated PSFs for an eye with spherical aberration and either -1 D or 1 D of defocus, for 550nm light and a 5mm pupil. The bottom row shows greyscale images of a daisy convolved with these PSFs to give the retinal images. The scale bar in the top left image applies to all of the images. In order for the scale to be accurate the images would need to be viewed from approximately 1 meter.

Although astigmatism would provide a clear cue for the direction of accommodation, it is not clear whether real eyes have enough astigmatism to provide a strong cue. Astigmatism is also routinely corrected using spectacles or contact lenses to below 0.25D. This means that those people with large enough magnitudes of astigmatism to provide a cue to accommodation may have this corrected.

Spherical aberration is also an even order aberration which could provide a cue to the sign of defocus. The differences in the PSFs and retinal images with the sign of defocus in an eye with spherical aberration can be seen in Figure 3.4. However, although there is clearly a difference between the retinal images with positive and negative defocus, it is not so clear what this difference is and how it might be distinguished from the magnitude of the defocus.

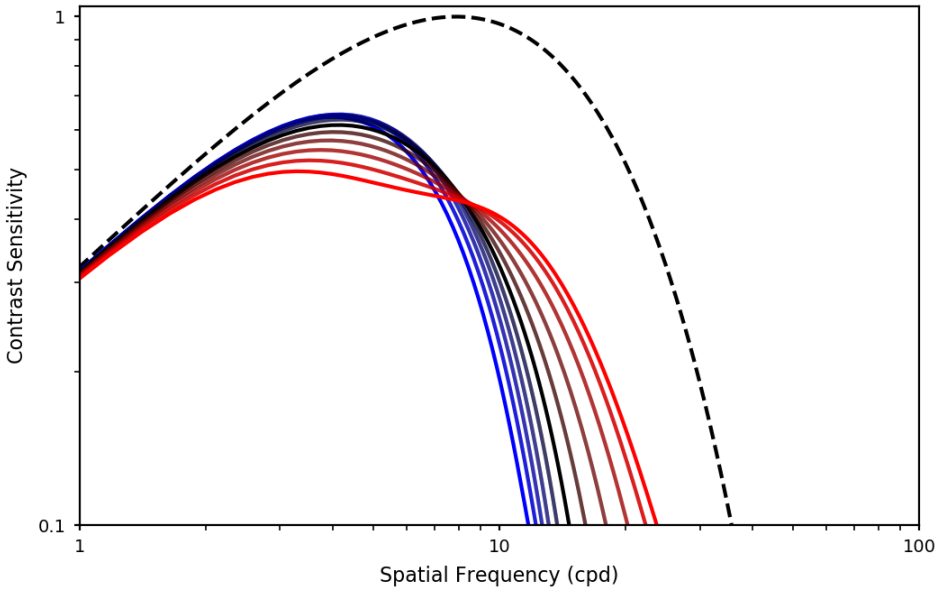

Figure 3.5: The solid lines show the CSFs generated for a an eye with a 3mm pupil and 0.13 microns of spherical aberration. The black solid line is with 0 D defocus, the red lines are for positive defocus values in equal steps up to 0.5 D, and the blue lines are for negative defocus in equal steps down to -0.5 D. The black dotted line shows the diffraction limited CSF for an eye with a 3mm pupil. All of the CSFs were calculated for 550nm light.

The effect of defocus sign for an eye with spherical aberration can be seen more clearly by plotting the Contrast Sensitivity Functions (CSFs). The CSFs for an optical system with 0.13 microns of spherical aberration and various amounts of defocus can be seen in Figure 3.5. These CSFs were calculated using Equations 2.6, 2.7, and 2.8 as described in the previous chapter on pages 11 and 12. It can be seen from this figure that there is a reduced sensitivity to higher spatial frequencies and increased sensitivity to lower spatial frequencies as defocus becomes more negative. This effect was also shown by Parnell (2015). Green and Campbell (1965) showed a similar effect with the measured CSFs for an eye with natural aberrations. It is possible that this difference in the shape of the CSF due to spherical aberration could be used by the visual system to determine the direction for accommodation.

A number of studies have investigated whether the human visual system does use cues from monochromatic aberrations to guide the accommodation re-

sponse A selection of these studies are described below.

Campbell and Westheimer (1959) presented monochromatic stimuli both with and without an annular pupil. The annular pupil was designed to remove the spherical aberration. The target would then move out of focus by 0.5 or 1 dioptres in a random direction and the subjects' task would be to adjust the target until it was in focus again. In the condition without the annular pupil, with enough practice all of the subjects could respond correctly on all trials. However, with the annular pupil, even after a large number of trials the subjects could not respond in the correct direction every time. There was also another condition where a cylindrical lens was added as well at the annular pupil. This introduced astigmatism to the stimulus. Once this astigmatism was added all subjects were able to respond correctly after a few trials. This experiment indicated that both spherical aberration and astigmatism can be used by the visual system to determine the sign of defocus. However, as this study did not measure accommodation it is not clear from these results whether the odd-error signals from spherical aberration and astigmatism could actually drive accommodation.

Wilson et al. (2002) presented a point source target to subjects with various amounts of defocus. The subjects' task was to indicate the sign of the defocus. They performed this task at three different pupil sizes (1mm, 2mm and 5mm). Measures were taken to minimise other potential cues, ensuring that the subjects were using the cues from monochromatic aberrations. They found that as the pupil size (and therefore the magnitude of the monochromatic aberrations) increased, so did the subjects' ability to detect the correct sign of defocus. This provides evidence that the visual system can use the cues from monochromatic aberrations to work out the sign of the defocus. However, this study also did not investigate the accommodation response itself so the findings may not extend to the accommodative system.

There have also been studies that have measured the accommodation response while manipulating the monochromatic aberrations using an adaptive optics (AO) system. An AO system is an optical system that includes a wavefront sensor and a device to manipulate the wavefront of light such as a deformable mirror. The wavefront sensor measures the wavefront of the light that is reflected back out through the optics of the eye and the deformable mirror can manipulate the wavefront of the light entering the eye. This system can

be used to alter or cancel out the aberrations introduced by the eye.

Chin et al. (2009a) used an AO system to manipulate monochromatic aberrations while observers accommodated to 0.5 D step changes in defocus. The step changes were randomised so that the subject could not predict the direction of the defocus shift. The monochromatic aberrations were either unchanged, corrected or inverted following the change in defocus. They found that, although correcting the aberrations had no significant effect on the accommodation response, inverting the aberrations resulted in a reduction in the accommodation response gain for outward steps in defocus and led to more accommodation responses in the wrong direction. This suggests that the visual system does, in part, use cues from monochromatic aberrations as a directional cue for accommodation. However, it seems that in that in the absence of a cue from monochromatic aberrations other cues can be used.

Gambra et al. (2009) also used an AO system to manipulate monochromatic aberrations while subjects responded to step changes in defocus. However, in this case the step changes were always in the same direction so the direction of the required response was always the same. They found that correcting aberrations actually tended to improve the accommodative response. This may be because the subjects did not need to determine the direction of the response but only the magnitude.

Chin et al. (2009b) measured the accommodation response to sinusoidal rather than step changes in defocus while manipulating the monochromatic aberrations using an AO system. However, they found that overall there was no significant effect of correcting monochromatic aberrations on the accommodation response. Again this could be in part due to the more predictable nature of the stimulus.

Similarly, Bernal-Molina et al. (2017) measured dynamic accommodation responses to sinusoidal accommodation stimuli under a range of aberration correction conditions. These ranged from natural aberrations to completely corrected aberrations (except defocus) and included conditions where just spherical aberration was left uncorrected and just astigmatism was left uncorrected. They also found no significant differences in the gain or phase lag of the accommodation responses between the conditions.

Cholewiak et al. (2018) used a different kind of approach to investigate whether

cues from astigmatism or spherical aberration could drive accommodation. Instead of optically manipulating the observers' aberrations, they measured their aberrations and then used these to render realistically blurred stimuli for various step changes in defocus. For the astigmatism experiment there were three subjects, two had uncorrected astigmatism with magnitudes of 1 D or more and the third had less than 1 D of astigmatism. The subjects' accommodation responses were measured for three different conditions. For the first condition there were real step changes in optical defocus with the subjects' astigmatism uncorrected. For the second condition the step changes in defocus were rendered with the astigmatism in the image rendered correctly for that specific subject. The third condition was the same as the second condition with the only difference being that the rendered astigmatism was rotated by 45° from normal. For the two rendered conditions the subjects' actual astigmatism was corrected optically. It was found that the subjects with 1 D or more of astigmatism were usually able to accommodate in the correct direction for the rendered defocus when the rendered astigmatism was in the correct axis, although the response was smaller than for a real defocus change. However, when the rendered astigmatism was rotated by 45° there was no consistent response. They concluded that astigmatic blur can drive accommodation but the responses tend to be small and inconsistent. They also conducted a similar experiment investigating whether spherical aberration can drive accommodation. However, they found that none of the 3 subjects showed consistent accommodation responses to a stimulus with their rendered spherical aberration and step changes in defocus. This suggests that the odd-error cue resulting from spherical aberration was not used by these subjects to accommodate.

The general trend in the literature seems to be that removing the monochromatic aberrations does not impair the accommodation response, suggesting that there are other important cues that the visual system can use. However, when the monochromatic aberrations are reversed, so that the cue from the monochromatic aberrations conflicts with other potential cues, there is an impairment in the accommodation response. This suggest that although monochromatic aberrations are not the only cue used by the visual system to guide the accommodation response, they are one of the cues that is used. There may also be differences in the extent to which the cue from monochromatic aberrations is used between individuals due to differences in the

magnitude of monochromatic aberrations and therefore differences in the effectiveness of the cue.

3.2.2 Longitudinal Chromatic Aberration

The LCA of the human eye could also act as a cue for accommodation. This is because each wavelength of light is defocussed by a different amount when it is imaged by the eye. Therefore, for polychromatic images, instead of the image on the retina representing a single focal plane, it essentially covers a range of focal planes spanning approximately 2D across the range of visible wavelengths.

Figure 3.6 shows an approximation of what the polychromatic PSFs and retinal images would look like with the LCA of the eye and either positive or negative defocus. What can be seen from these images is that when the defocus is positive, the shorter wavelength, blue, light is the sharpest and the longer wavelength, red, light is the most blurred. However, when the sign of the defocus is negative it is the longer wavelength, red, light that is the sharpest and the shorter wavelength, blue, light is the most blurred. This results in a clear difference in the retinal images. Burge and Geisler (2011) actually demonstrated that CA could fully resolve the sign ambiguity of defocus.

Crane (1966) described how the combination of the two factors of the LCA of our eyes and the different spectral sensitivities of different cone channels, essentially results in the different cone channels sampling retinal images on different focal planes. This would mean that the relative blur in these three channels could provide information about the sign and magnitude of the accommodation response needed.

Flitcroft (1990) developed a computational model to explain how the visual system might use the chromatic aberration of the eye to increase the accuracy of accommodation. In this paper, Flitcroft suggested that double opponent neurons might allow for a comparison in image quality between different wavelength ranges. This comparison of image quality could then be used to guide the accommodation response in the correct direction. It could be that the accommodation system aims to balance the level of blur in different cone channels and in doing so brings wavelengths in the middle of the spectrum into focus.

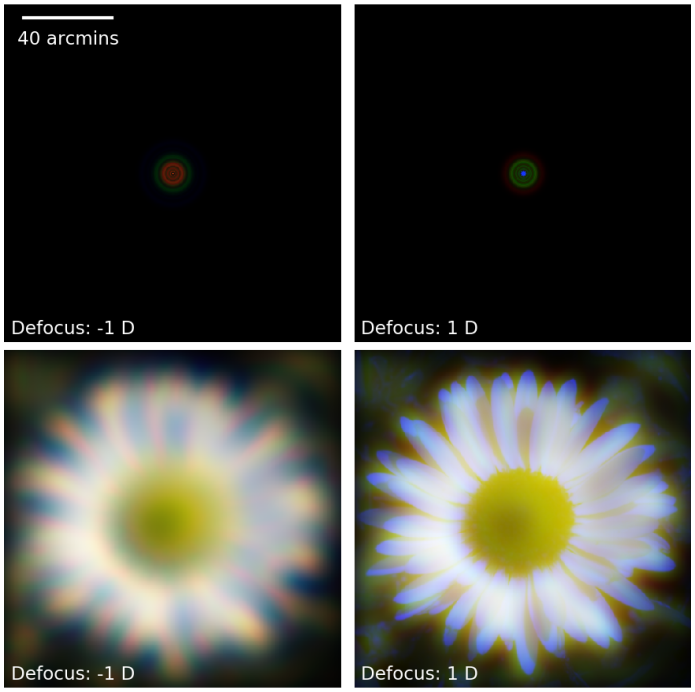

Figure 3.6: The top row shows the simulated RGB PSFs for an eye with normal LCA and either -1 D or 1 D of defocus. The second row shows RGB images of a daisy convolved with the PSFs in the top row to give the retinal images. These were calculated assuming wavelengths of 650nm, 550nm, and 450nm respectively for the R, G and B channels and a 5mm pupil. The scale bar in the top left image applies to all of the images. In order for the scale to be accurate the images would need to be viewed from approximately 1 meter.

Many studies have investigated the effect of manipulating LCA on subjects' accommodative responses. Below the findings from some of these studies are reviewed.

Campbell and Westheimer (1959) devised a task in which subjects were in a fixed state of relaxed accommodation and had to bring a target into focus by adjusting its axial position in an optical system. Although all subjects had got to the stage where they were always adjusting the target correctly for white light, they found that when the light source was switched from being white light to monochromatic light some subjects started making errors again for the first few trials. This suggests that these subjects were using LCA as a cue to the direction of defocus for the white light stimuli. However, they

were able to switch to using a different cue relatively quickly. Although this experiment did not actually record accommodation responses, it does indicate that the visual system can use the cue from chromatic aberrations.

Fincham (1951) actually recorded the accommodation response to step changes in defocus under broadband and narrowband light. They found that some subjects showed impaired accommodation performance under monochromatic light. However, some subjects showed roughly the same responses for white and monochromatic light. Very similar findings were obtained when they used an achromatising lens with broadband light to cancel out the LCA of the eye, instead of the monochromatic light condition. This indicates that at least some of the subjects were using a cue from LCA in the white light condition. However, it is clear that there were also other cues that the visual system was able to use to accommodate, at least for some subjects.

Charman and Tucker (1978) found that although initially white light targets allow more accurate accommodation responses for some people, after training equally accurate responses can be made in monochromatic light. This suggests that although LCA can be used as a cue for accommodation, it is not necessary for accurate accommodation.

Rucker and Kruger (2004) also recorded accommodation responses for both static stimuli and stimuli with a defocus step. The stimulus was made up of a grating of yellow (580nm) light and a grating of blue (420nm) light superimposed. In one condition they eliminated the effect of LCA by altering the optical defocus in the yellow grating to cancel out the LCA of the eye. They found no significant difference in either the static or the dynamic accommodation response between the normal LCA and the removed LCA conditions. This indicated that the cue from LCA was not necessary for accommodation under these conditions.

Many studies have also investigated the effect of manipulating LCA on accommodation responses to stimuli with sinusoidally modulated defocus. Several of these studies have found some degree of impairment of the accommodation response when the LCA cue is removed or reduced (e.g., Kruger and Pola, 1986; Kruger et al., 1993; Stone et al., 1993; Aggarwala et al., 1995a,b; Kruger et al., 1995, 1997).

Kruger et al. (1993) found that when LCA was eliminated, the gain of the

accommodative response decreased and the phase-lag increased. They also found that reversing the LCA substantially disrupted the accommodative response. Similarly, Kruger et al. (1995) found that a normal amount of LCA led to good accommodation. However, when LCA was reversed, the accommodation response was disrupted. Kruger et al. (1997) found that neutralizing and reversing LCA led to a reduced accommodative gain, as did using monochromatic as opposed to white light. However, they found that a few subjects did still perform relatively well in monochromatic light, indicating that there must be other cues that can be used for accommodation.

It has also been found that accommodative gain increases and phase lag decreases with increasing spectral bandwidth and, therefore, increasing LCA (Aggarwala et al., 1995a). Aggarwala et al. (1995b) additionally found that accommodation in white light with LCA corrected was similar to that in monochromatic light. These too provide evidence that LCA is used as a cue to accommodation.

In a different kind of study Cholewiak et al. (2017) investigated the effect of rendering defocus with the LCA of the eye included. They found that in stimuli with rendered defocus and LCA the cue provided by the rendered LCA could actually drive the accommodation response.

Overall, there is substantial evidence suggesting that the visual system does use LCA as a directional cue for accommodation. Although previous studies also suggest that it is not the only odd-error cue that the visual system uses to accommodate. This is interesting as it suggests that although LCA increases the amount of blur in the retinal image, it actually could be advantageous to vision in general as it could allow the visual system to accommodate more effectively. This could also suggest why our eyes have not evolved to eliminate LCA.

3.2.3 Microfluctuations

When the eye is accommodating on an object, rather than maintaining a constant level of accommodation, it fluctuates. It has been found that there are in fact two main temporal frequency components to these microfluctuations. These are a low frequency component, which is at approximately ≤ 0.6 Hz, and a high frequency component, which is somewhere between 1.0 Hz and 2.5 Hz.

It has been suggested that these microfluctuations could provide a directional cue, which could be used to initiate an accommodation response in the correct direction (Alpern, 1958). The idea is that these microfluctuations allow for a trial and error approach accommodation. Fender (1964) actually described these microfluctuations as a "'hunting" motion' used to find the correct direction for the accommodation response.

The way this cue could work is that the microfluctuations result in the eye covering a range of accommodative states between two limits. At one extreme the accommodation will be further from the optimum point meaning that there will be more defocus blur in the retinal image, and therefore a lower contrast. At the other extreme the accommodation will be closer to the optimum point meaning that there will be less defocus blur in the retinal image and a greater contrast. It has been suggested that the visual system could compare the retinal image contrast between the two extremes of the microfluctuations and use this to determine the direction needed for the accommodative response.

The visual system can only use this contrast comparison technique if the difference in contrast at the two extremes of the microfluctuations is above threshold. Metlapally et al. (2014) measured the wavefront error over time for four subjects. They used this to estimate the magnitude of the microfluctuations and to calculate the higher order aberrations. They then simulated modulation transfer functions (MTFs) for a range of defocus values. They found that for each of the spatial frequencies they investigated there was a range of defocus values for which the contrast difference between the two extremes of the microfluctuations was above threshold. This was true regardless of whether or not the higher order aberrations were included in the simulations, although the signals were generally smaller when higher order aberrations were included.

The next question is whether the visual system actually uses the odd-error cue from these microfluctuations. This is difficult to test experimentally as no-one has yet found a way to actually null or manipulate the microfluctuations in real time. However, Metlapally et al. (2016) tried another simpler tactic, which was to introduce simulated defocus noise to the stimuli with similar temporal frequencies as the microfluctuations. The idea was that this noise would mask contrast changes due to the actual microfluctuations and impair the visual system's ability to use this as a cue. They measured the observers'

accommodative responses to step changes in defocus both with and without the noise. They did find that accommodation performance was worse for the noise condition compared to the control condition. This is consistent with microfluctuations acting as a directional cue to accommodation. However, it may be that the noise condition made the task more difficult for other reasons. Therefore this study does not give conclusive evidence that microfluctuations are used as a cue.

It has also been pointed out that the accommodation response is very fast with a reaction time of about 0.4 seconds. This means that only the faster microfluctuations could possibly provide a directional cue in time. However, there is also evidence that these faster microfluctuations may just be a by product of other functions such as the pulse. It is unclear how the visual system could extract useful information from the direction of these microfluctuations if they are not under active control.

An alternative suggestion is that the microfluctuations do play an important role for accommodation but not in determining the direction of the initial accommodation response. Instead microfluctuations could play a role in maintaining the average accommodation at the right level after the initial response has been made rather than in actually driving this initial response. For this the speed is not so important so the lower frequency fluctuations could be used.

3.2.4 Stiles-Crawford effect

The Stiles-Crawford effect was first reported by Stiles and Crawford (1933) who found that the eye is not equally sensitive to light entering at different points on the pupil. They found that the peak sensitivity is towards the nasal side of the pupil rather than right at the centre and the sensitivity tails of towards the edges of the pupil. We now know that this effect is due to the acceptance angle of the individual cones. In other words, each cone is not equally sensitive to light from all angles, and therefore, is not equally sensitive to light from all parts of the pupil.

Fincham (1951) suggested that the Stiles-Crawford effect may provide a directional cue for accommodation. More recently Kruger et al. (2001) described an updated model for the way that the Stiles-Crawford effect could provide this cue. This model is based on the fact that when the light is focussed

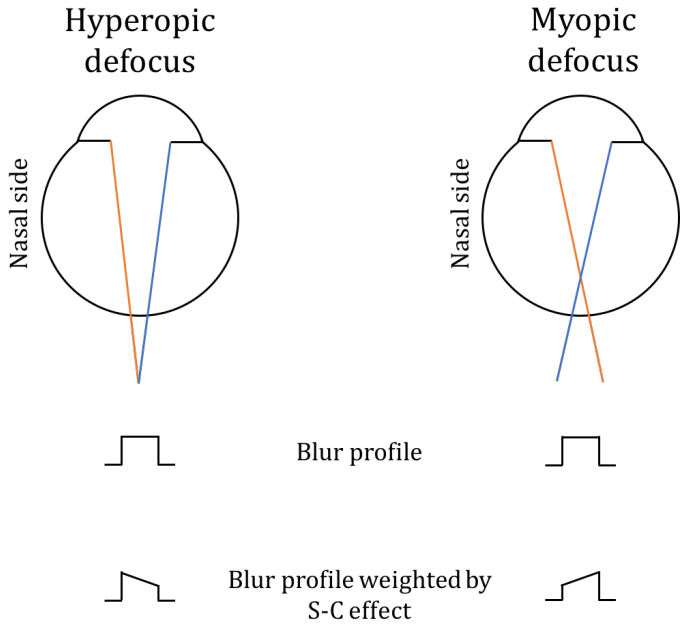

Figure 3.7: A demonstration of the way that the Stiles-Crawford effect could provide a directional cue for accommodation (not to scale). The diagrams at the top show an eye with hyperopic defocus (left) and an eye with myopic defocus (right). The orange line represents the path of the light from the nasal side of the pupil and the blue line represents the path of light from the opposite side of the pupil. Below this is a representation of the profiles of the blur discs formed on the retina. These are identical for the two types of defocus. At the bottom the same profiles are shown but this time as they might appear if they were weighted by a Stiles-Crawford effect biased to the nasal side of the pupil. This is based on a diagram from Kruger et al. (2001).

behind the retina, the light from the nasal side of the pupil will fall on the nasal side of the retina, and when the light is focussed in front of the retina, the light from the nasal side of the pupil with fall on the opposite side of the retina. They suggested that because the Stiles-Crawford effect is generally biased towards the nasal side of the pupil, the photoreceptors will generally be more sensitive to the light from the nasal side of the pupil. Therefore, when the light is focussed behind the retina the photoreceptors will be more sensitive to the nasal side of the blur circle and vice versa when the light is focussed in front of the retina. This will lead to asymmetric blur circles which could then be used to determine the direction of the accommodation response

needed. A diagram illustrating this model is shown in Figure 3.7.

There is evidence that the human visual system is able to use a monochromatic cue for accommodation other than monochromatic aberrations. Kruger et al. (1997) and Chen et al. (2006) both found that some subjects were able to accommodate under narrowband light with very little signal from monochromatic or chromatic aberrations. One suggestion is that these participants could have been using a cue from the Stiles-Crawford effect in order to accommodate.

A few studies have investigated more directly whether the Stiles-Crawford effect is in fact used by the visual system to accommodate. Kruger et al. (2001) used apodising filters to either neutralise, reverse, or double the Stiles-Crawford effect in a single participant while monitoring their accommodation response. They found no significant reduction in accommodative gain for either the neutralised or reversed conditions as compared to the natural Stiles-Crawford effect condition. In fact, for the 5mm pupil there was an increased gain for the neutralised and reversed conditions, although this was not significant.

Stark et al. (2009) measured the Stiles-Crawford functions and monochromatic aberrations for 21 participants. They then used these to simulate retinal images for -1, 0, and 1 D of defocus with a 3mm pupil under 4 conditions. These 4 conditions were: no Stiles-Crawford effect or monochromatic aberrations, Stiles-Crawford effect but no monochromatic aberrations, monochromatic aberrations but no Stiles-Crawford effect, or both Stiles-Crawford effect and monochromatic aberrations. They then recorded the participants accommodation responses as they viewed these stimuli through a pinhole. They found that the Stiles-Crawford effect on its own did not provide a significant cue to accommodation.

Neither of these studies show any evidence that the Stiles-Crawford effect is used by the visual system to accommodate. Therefore, it seems unlikely that this is an important cue for accommodation.

3.2.5 Summary

The visual system is able to accommodate accurately under very impoverished conditions, where all of the pictorial and binocular cues are stripped away. In

order to do this it must be using an odd-error signal from some optical cue.

There is strong evidence that people are able to use an odd-error cue from LCA in order to accommodate. However, it has been found that many subjects are able to accommodate accurately even in monochromatic light when the cue from LCA is no longer available. This means that there must also be a monochromatic cue. There are three main candidates for this cue. These are the monochromatic aberrations of the eye, the microfluctuations of the eye, and the Stiles-Crawford effect.

There is quite a bit of evidence suggesting that at least some people can use the cue from monochromatic aberrations in order to accommodate. However, some studies have shown that even in cases when the monochromatic aberrations are optically corrected or reduced by inserting a small artificial pupil, and the light is near to monochromatic, some subjects are still able to accommodate. It may be that in these cases there is still a strong enough residual signal from either the LCA or the monochromatic aberrations to drive accommodation. However, it may also be that in these cases the microfluctuations or the Stiles-Crawford effect are being used.

There is no strong evidence that the odd-error cues from either the microfluctuations or the Stiles-Crawford effect are used by the visual system to accommodate. More research in this area is needed to establish whether either of these cues is actually used or whether there may be another cue that the visual system is using when the signals from LCA and monochromatic aberrations are impoverished.

Chapter 4

Why can't we see LCA?

As has been described in previous chapters, the human eye has a significant amount of longitudinal chromatic aberration (LCA). LCA results in different defocus values for different wavelengths and, therefore, different amounts of blur at different wavelengths. We would expect this to result in chromatic fringes in the retinal image. However, generally people do not notice these chromatic fringes. This chapter addresses the question of why we don't generally notice the LCA of our eyes and why we don't generally perceive the chromatic fringes that should result from this LCA.

There are three main explanations as to why people do not usually perceive the LCA of their eyes. Firstly, it is possible that when the monochromatic aberrations and other optical features of the eye are taken into account, the chromatic fringes in the retinal image due to LCA are actually insignificant. Secondly, it could be that the inherent way in which our visual systems process the information in the retinal image results in any chromatic fringes being lost. For example, it could that the inherent way in which colour is processed prevents the detection of these chromatic fringes. Finally, it could be that our visual systems have adapted to the specific chromatic aberrations of our eyes. If this were the case then it may mean that a change in chromatic aberration would result in the detection of the chromatic fringes formed on the retina. Throughout this chapter the evidence for each of these explanations will be evaluated. The results of simulations and an experiment will also be presented in order to gain further insight into this question.

Figure 4.1: The top image is the stimulus of a daisy. This stimulus was multiplied by the R, G, and B primary spectra from a MacBook retina display to give the HSI for the image viewed on the MacBook display. The bottom left panel shows the retinal image calculated from the HSI of the daisy for an eye with natural LCA and a 5mm pupil. The bottom right panel shows another retinal image for the daisy but this time with monochromatic aberrations measured from a real eye focussed at 3 D as well as the LCA. The one degree scale bar in the top image applies to all three images. In order for the scale to be accurate the images would need to be viewed from approximately half a meter away.

4.1 Is LCA too insignificant to notice?

I will first address the possibility that the chromatic fringes formed on the retina are actually too subtle to be seen. Although 2 dioptres (D) of LCA across the visible spectrum sounds like a lot, it may be that once the other optical effects in the eye have been taken into account, the fringes on the retina are actually too subtle to detect.

Figure 4.1 shows the simulated retinal image formed of the daisy shown in the top panel both with (bottom right panel) and without (bottom left panel)

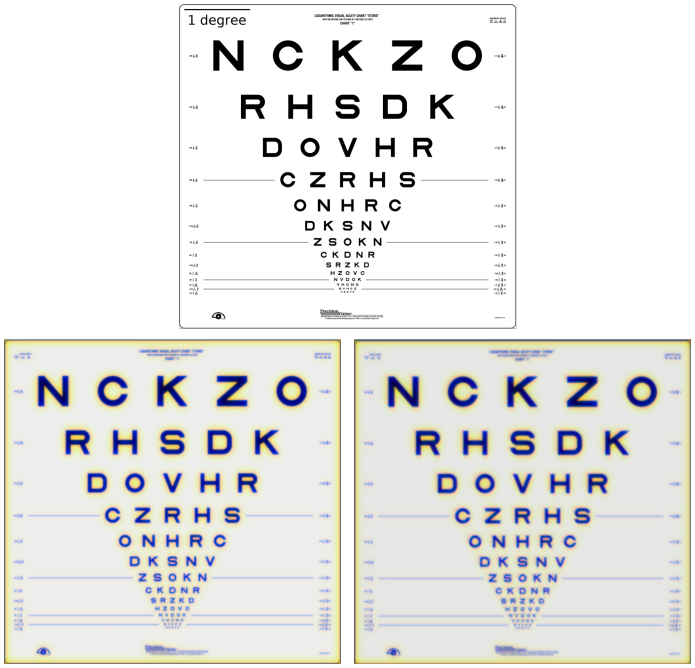

Figure 4.2: The top image is the stimulus of an ETDRS logMAR visual acuity chart. This stimulus was multiplied by the R, G, and B primary spectra from a MacBook retina display to give the HSI for the image viewed on the MacBook display. The bottom left panel shows the retinal image calculated from the HSI of the chart for an eye with natural LCA and a 5mm pupil. The bottom right panel shows another retinal image for the chart but this time with monochromatic aberrations measured from a real eye focussed at 3 D as well as the LCA. The one degree scale bar in the top image applies to all three images. In order for the scale to be accurate the images would need to be viewed from approximately half a meter away.

monochromatic aberrations, using method 2 described in Appendix A. The chromatic fringes do not seem to be particularly obvious in either of the retinal images. Looking closely it is possible to see some fringing around the edges of this petals, however this is very faint and the main difference between the retinal images and the original, is that overall the retinal images are more blurred. From these simulated retinal images it seems unsurprising that we don't generally notice the chromatic fringes as they are very subtle indeed.

Figure 4.2 shows the retinal images generated using method 3 described in Appendix A for an ETDRS logMAR visual acuity chart (shown in the top

panel) with a D65 spectrum. This scene has a lot more contrast than the daisy, and the chromatic fringing in the retinal images shown in the bottom two panels are a lot more obvious. There is, however, little difference between the retinal image generated with monochromatic aberrations (bottom right) and that generated without monochromatic aberrations (bottom left). This makes it seem that monochromatic aberrations do not substantially reduce the chromatic fringing in the retinal image. However, it is important to bear in mind that the monochromatic aberrations included in the simulation above were only measured at a single wavelength and there is evidence that the aberrations of the eye actually change with wavelength (Marcos et al., 1999). It is possible that if the aberrations of the eye were measured across a range of wavelengths they could hide the fringes more.

To investigate the interaction between the monochromatic and chromatic aberrations of the eye, McLellan et al. (2002) measured the aberrations for real eyes at a series of wavelengths. From this data they computed modulation transfer functions (MTFs) for eyes with these aberrations. They found that, although monochromatic aberrations reduce the resolution at the wavelengths near focus, they actually improve the resolution at the spectral extremes. In this way, the monochromatic aberrations result in the resolution for polychromatic light being roughly constant for all wavelengths. It is possible that this could also reduce the appearance of fringes. In agreement with this, Ravikumar et al. (2008) found that the effect of LCA was greatly reduced in the presence of typical monochromatic aberrations. Unfortunately we were not able to measure monochromatic aberrations separately at different wavelengths and therefore we could not simulate the retinal images for those aberrations.

It has also been suggested that the macular pigment within the eye could mitigate the effects of LCA. The macular pigment covers the fovea, which is the region of the retina with the highest spatial resolution. This pigment mostly absorbs blue wavelengths, where the defocus due to LCA is greatest. Reading and Weale (1974) calculated the spectral transmittance necessary to reduce the blur resulting from chromatic aberration to threshold level. They found that the necessary characteristics were similar to those of macular pigment. In the simulated retinal images shown above the effect of macular pigment in the central 2 degrees of the retina was accounted for.

These findings and simulations indicate that the chromatic fringes formed on

the retina may not be as dramatic as we initially suspected, especially when factors such as the monochromatic aberrations and the macular pigment of the eye are taken into account, and especially when the scene being viewed is a complex colourful scene like the daisy above. However, it seems that these effects do not completely eliminate the effects of LCA especially for high contrast stimuli like the logMAR acuity chart. Therefore, it seems that the optical factors of the eye cannot fully explain why we do not generally notice the chromatic fringes due to LCA.

4.2 Does the inherent nature of visual processing eliminate the chromatic fringes?

The second possibility is that the way in which the visual system processes information, results in the chromatic fringes being lost. In this section evidence for this hypothesis will be presented and evaluated.

One way of explaining this is at the level of the cone cells. There are three different types of cone cell, each with a different spectral sensitivity. Most of the blur due to LCA occurs at shorter wavelengths where the S cones have the highest sensitivity. However, the S cones are also the most sparsely distributed in the retina and therefore have the lowest spatial resolution. The L and M cones, on the other hand, are distributed a lot more densely in the retina and have a higher spatial resolution. However, both the L and M cones have a relatively low sensitivity to the shorter wavelengths where the LCA has the greatest impact. This could help to explain why we do not notice the chromatic fringes on the retina.

Another way of addressing this is by looking at the roles of the different postreceptoral pathways. There are three main postreceptoral pathways that project from the retina into distinct layers in the lateral geniculate nucleus (LGN). These are the magnocellular, parvocellular and koniocellular pathways. The koniocellular pathway is responsible for the $S-(L+M)$ colour discrimination. This colour dimension is the one that should be most affected by LCA. Therefore it is in this colour dimension that we can expect the majority of the chromatic fringing due to LCA to occur. However, the koniocellular pathway also has a very low spatial resolution and has no spatial-opponency in its receptive fields, so it seems reasonable to assume that the

visual information in this pathway is not the key information used to detect edges in an image. For this reason it may well be that the chromatic fringes in this channel are not detected. The parvocellular pathway is responsible for the $L - M$ colour discrimination. This pathway does have a good spatial resolution and its receptive fields are spatially as well as chromatically opponent, meaning that it could be useful for detecting edges in the image. However, the spectral sensitivities for the L and M cones are actually very similar and largely overlap. This means that there may not be an obvious difference in defocus due to LCA between L and M channels and, therefore, the chromatic fringes in the parvocellular pathway may be below threshold. The magnocellular pathway is responsible for the $L + M$ or luminance dimension in colour space. This could provide useful information for edge detection as it also has relatively good spatial resolution and spatially opponent receptive fields. However, as this pathway does not compare the signals between cone channels, it cannot detect colour differences. Therefore, the magnocellular pathway could never detect chromatic fringes.

Figure 4.3 gives a rough indication of the information available in each of the three cone channels and in each of the three main postreceptoral channels for a simple luminance edge in D65 illumination. The top panel shows a profile of the luminance edge of the scene. The second panel shows the relative stimulation of the L, M, and S cone channels across the luminance edge. From this we can see that the blur profile in the L and M channels is very similar, with significantly more blur present in the S channel. The similarity between L and M channels should be interpreted with caution though, as it is dependent on the accommodative state of the eye. The simulations were run for an eye focussed at 580nm, however, it is not clear which wavelength the eye actually focusses on in natural daylight. The third panel shows the profile of the L+M channels, an approximation of the information available to the magnocellular pathway. All this pathway can detect is a blurred luminance edge, as it does not make any comparisons between cone types. The fourth panel shows the profile for the $L - M$ channels, an approximation of the information available to the parvocellular pathway. Differences in signal in this pathway represent differences in colour along the $L - M$ (approximately red-green) axis. There is a colour difference around the luminance edge, but this is very subtle. The fifth panel shows the profile for the $S - (L + M)$ channels, approximating the information available to the koniocellular pathway. Differences in signal

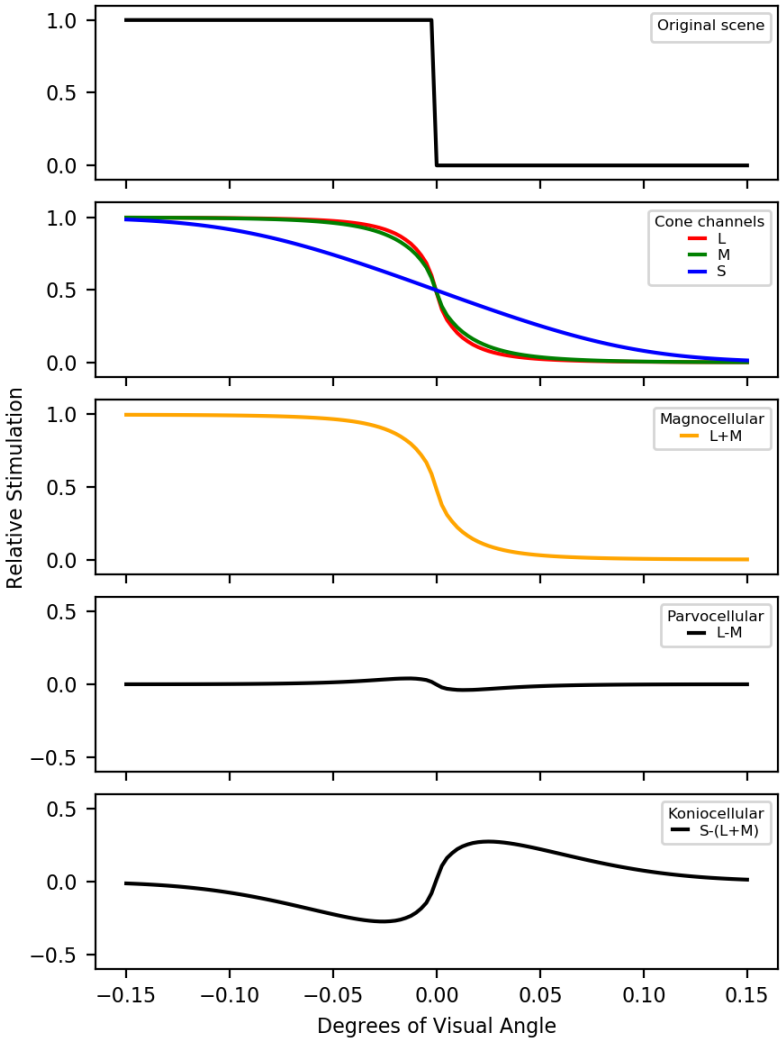

Figure 4.3: The top panel shows the intensity profile of a luminance edge. The retinal image was simulated for this luminance edge with the D65 spectrum, for an eye with natural LCA and a 5mm pupil. The second panel shows the profile of stimulation for the L (red), M (green), and S (blue) cone channels resulting from the generated retinal image. The third panel shows the profile of stimulation in the $L + M$ channels. This roughly represents the information available to the magnocellular or luminance pathway. The fourth panel shows the profile of stimulation in the $L - M$ channels. This represents the information available to the parvocellular pathway. The bottom panel shows the profile of stimulation in the $S - (L + M)$ channels. This represents the information available to the koniocellular pathway.

here indicate differences in colour in the $S - (L + M)$ (approximately blue-yellow) axis. Here the colour difference around the luminance edge is a lot more dramatic. However, as was mentioned above, the koniocellular pathway has a much lower spatial resolution than the other pathways.

It is relatively well established that luminance information dominates the detection of edges. Many studies have found evidence for a phenomenon known as "filling in" for certain stimuli. This is where a luminance boundary appears to constrain coloured regions so people perceive a coloured area filling the space defined by a luminance boundary even when the chromatic boundary is different.

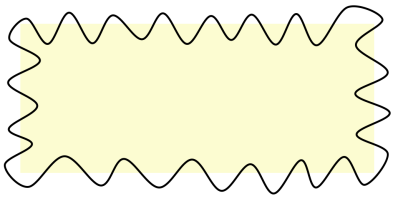

Figure 4.4: An example of the Boynton illusion. When viewed from close up a yellow rectangle can be seen with a separate wavy back line. However, when viewed from far away the yellow colour seems to stop at the wavy black line.

One case of such an effect is the Boynton illusion (Stockman and Brainard, 2009). An example of this illusion is shown in Figure 4.4. There is a clear luminance boundary defined by the black wavy line. However, the boundary between the white and yellow regions is a straight line. The yellow and the white parts of the image have a very similar luminance and are also very similar in their L and M cone stimulation. This means that the difference between the yellow and white areas provides the strongest signal to the S cone channel. People tend to perceive the yellow region filling in the area defined by the black line when viewing this image from a distance. This suggests that there is a tendency for our visual system to use the luminance boundaries in an image to indicate where the S cone channel chromatic boundaries will be. This is relevant in the context of LCA because, as was shown in Figure 4.3, it is in the S opponent colour axis that the fringes due to LCA are most dramatic.

There is also evidence that luminance information dominates our detection of blur. Wandell (1995) split up an image into a "light-dark" (luminance) channel, a "red-green" channel, and a "blue-yellow" channel. They then created three separate images each with one of the channels blurred and the other two sharp. The image where the luminance information was blurred looked noticeably blurry. However, the images where either the "red-green" or the "blue-

yellow" information were blurred by the same amount did not look blurred. Sharman et al. (2013) investigated this effect further by measuring blur detection thresholds. They found that the blur detection threshold in the chromatic (isoluminant) channels increased significantly when sharp luminance information was added compared with when the chromatic information was shown with no luminance information. There was no equivalent masking effect when sharp chromatic information was added to blurred luminance information. This effect was found even when the stimuli were altered so that the threshold for detecting chromatic blur on its own was not significantly different from that for detecting luminance blur on its own. This could help to explain why we do not perceive the chromatic fringes caused by chromatic blur at luminance edges, because the luminance edge information has a masking effect on the chromatic edge information so that we cannot detect the chromatic blur.

The results discussed in this chapter do suggest that there are various features in the way that our visual systems process information that could prevent us detecting chromatic blur and chromatic fringes due to LCA. Not only does the pathway most affected by LCA have the lowest spatial resolution, but even when the chromatic fringing would be visible on its own, previous findings suggest that when this fringing occurs at a luminance boundary, the sharp luminance edge could mask the chromatic blur.

4.3 Does the visual system adapt to the specific LCA of the eye?

As the LCA of our eyes generally remains constant throughout our lives another possibility is that the reason we don't notice the chromatic aberration of our eyes is that our brains have adapted to it. If the visual system has adapted to the specific LCA of our eyes, then if the chromatic aberrations were to change suddenly, we should notice the chromatic fringes until we have re-adapted to the new chromatic aberrations. One way that the chromatic aberrations affecting our eyes might change in an every day scenario is if we use spectacles or contact lenses which introduce their own chromatic aberrations. Many people do report noticing chromatic fringes when they put on or take off their glasses or lenses, but generally report that these fade away relatively quickly. This is presumably due to their eyes adapting to the new chromatic

aberration.

A study carried out by Hay et al. (1963) supports the theory that the visual system can adapt to specific chromatic aberrations. In this study six participants wore prism glasses continuously for a ten day adaptation period. These prisms caused chromatic dispersion which appeared to the participants as coloured fringes. Every day the participants removed the glasses for an hour in order to carry out some tests. In these tests the subjects viewed vertical gratings through a variable prism and were required to adjust the power of the prism in order to eliminate the apparent coloured fringes. These tests were carried out under both narrowband and broadband (tungsten) light. Under broadband light, the subjects were always able to find a prism setting that eliminated the apparent fringes. Before the adaptation period the settings to eliminate fringes were around 0 minutes of arc of chromatic dispersion. However, once the subjects were in the adaptation period their prism settings to eliminate the fringes became closer to those of the prisms that they were adapting to. Interestingly, three subjects actually reported seeing chromatic fringes for monochromatic light after they had been wearing the prism glasses for 10 days. In these cases, adjusting the variable prism had no effect on the perceived fringes so the subjects were not able to eliminate them. This shows that the apparent fringes were not actually present in the retinal image but resulted from visual processing. These findings suggest that people are able to adapt to even quite dramatic changes in chromatic aberration and that this adaptation is specific to the chromatic aberration present.

The evidence presented above suggests that the human visual system is capable of adapting to chromatic fringing on the retina and can adapt to even quite dramatic fringes over a relatively short space of time. If there were any residual chromatic fringes after the optical factors and the inherent way that the visual information is processed are taken into account then it seems likely that the visual system would be able to adapt to these fringes.

4.4 The effect of the illuminant spectrum on chromatic blur

As well as lenses or prisms with different chromatic aberrations influencing the chromatic fringes on the retina, it seems logical that the spectral content of the

light entering the eye could affect the chromatic fringes resulting from LCA. Monochromatic light will eliminate the chromatic fringes and it is conceivable that a spectrum of light with most of its energy at the extremes of the visible spectrum would enhance these fringes. Therefore, it is possible that, there are certain types of spectrum for which people are more likely to see chromatic fringes.

As was mentioned in Chapter 1, historically humans would have been exposed to relatively broadband illuminant spectra. However, in the modern world we are exposed to many different types of spectra, many of which do not have such a smooth broadband intensity distribution as a function of wavelength. Below simulations are shown of the retinal images with a variety of different illuminant spectra.

The CIE standard illuminant, D65, is the standard spectrum for average daylight conditions consisting of a mixture of sunlight and skylight with a colour temperature of approximately 6500K. Figure 4.5 shows the spectrum of D65 light and the retinal image for a square patch of D65 light (as generated using method 3 described in Appendix A with high wavelength resolution). Looking closely at the simulated retinal image there is some chromatic fringing around the edge of the square, with the inside edge of the square having a yellowish colour and a blue halo just outside the edge of the square. However, when the square is held at approximately half a meter away so that the scale bar is the right size, the fringing is not very obvious.

Figure 4.6 shows the spectrum of Illuminant A, which is the CIE standard illuminant for a typical tungsten lamp, and the retinal image of a square with this spectrum. Illuminant A also has a broadband spectrum. Here the chromatic fringing around the square is not visible even when viewed closely. This may be due to the lack of shorter wavelengths in this spectrum.

Figure 4.7 shows the spectrum of one of the CIE standard fluorescent lamp spectra (Illuminant F7) and the corresponding retinal image and Figure 4.8 shows the spectrum of a mixture of three narrowband LEDs (red, green, and blue) and the corresponding retinal image. These spectra have very different shapes from the D65 spectrum shown in Figure 4.5. Instead of having a smooth broadband shape they are made up of a series of short sharp peaks. However, even though the spectra are so different from D65, the retinal images in all three look quite similar. They all have subtle chromatic fringing around

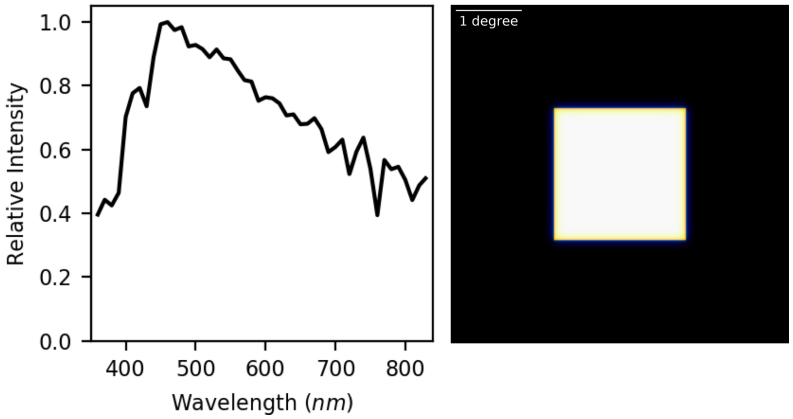

Figure 4.5: The left panel shows the CIE D65 spectrum. The right panel shows the retinal image of a square patch with this spectrum for an eye with natural LCA and a 5mm pupil. The scale bar represents one degree of visual angle. In order for the scale to be accurate the image would need to be viewed from approximately half a meter away.

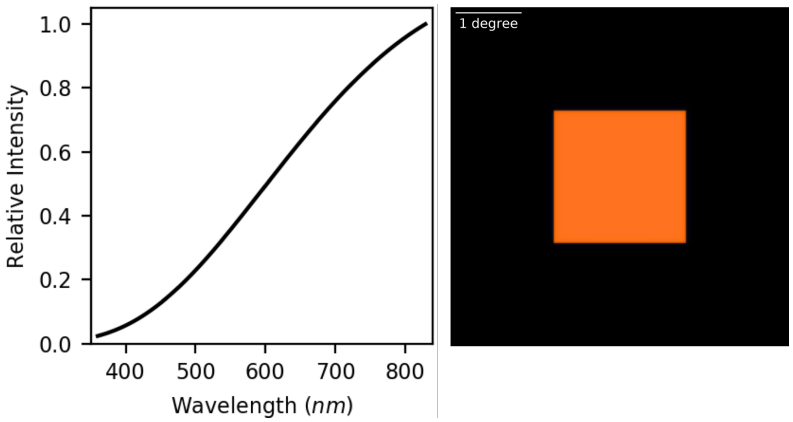

Figure 4.6: The left panel shows the CIE Illuminant A spectrum. The right panel shows the retinal image of a square patch with this spectrum for an eye with natural LCA and a 5mm pupil. The scale bar represents one degree of visual angle. In order for the scale to be accurate the image would need to be viewed from approximately half a meter away.

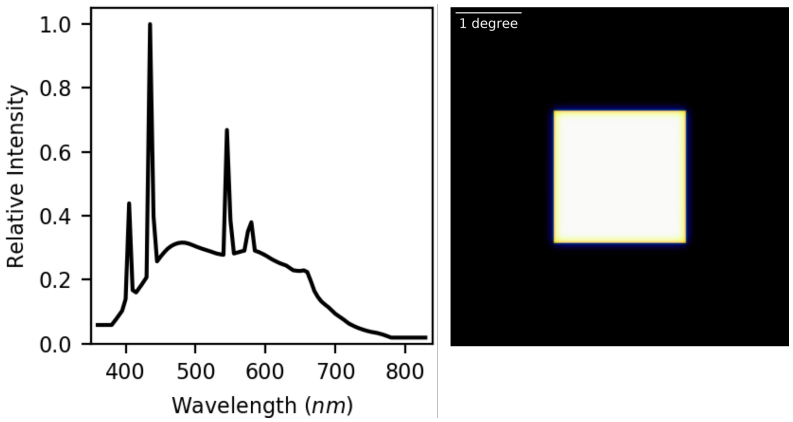

Figure 4.7: The left panel shows the CIE Illuminant F7 spectrum. The right panel shows the retinal image of a square patch with this spectrum for an eye with natural LCA and a 5mm pupil. The scale bar represents one degree of visual angle. In order for the scale to be accurate the image would need to be viewed from approximately half a meter away.

the edge of the square with the inside edge appearing slightly yellowish and the outside edge appearing slightly blue.

These simulations suggest that in fact the shape of the spectrum of light does not have such a dramatic effect on the appearance of the chromatic fringes in the retinal image. It is only when there is very little light at short wavelengths that the fringes are noticeably reduced. However, the experiment described below further explored this question by actually showing participants a variety of spectra and testing whether they saw chromatic fringes more clearly with some spectra than others.

4.5 Experiment

The aim of this experiment was to investigate whether the type of illuminant affected the observer's perception of the strength of chromatic fringes at the edge of a square. This could help us to understand why it is that observers don't generally perceive the chromatic fringes at the edges of objects.

If the participants didn't perceive fringes for any of the stimuli then this would not tell us much. It could indicate that the fringes are too insignificant on the retina to notice, or that the chromatic fringes are lost due to the

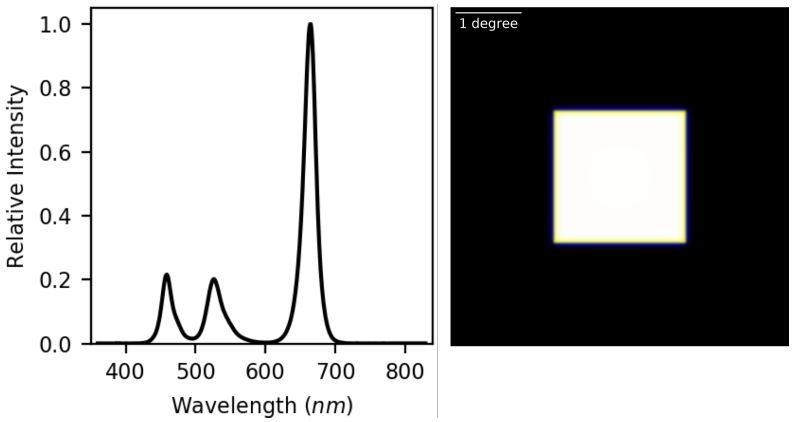

Figure 4.8: The left panel shows the spectrum of a mixture of a red, green and blue LED. The right panel shows the retinal image of a square patch with this spectrum for an eye with natural LCA and a 5mm pupil. The scale bar represents one degree of visual angle. In order for the scale to be accurate the image would need to be viewed from approximately half a meter away.

inherent nature of the visual processing, or even that there is not enough difference between the fringes for the different illuminants and therefore the same adaptation works for all of the illuminants. If we were to find that it was the spectra leading to the strongest fringes on the retina that resulted in the greatest perception of chromatic fringes, this would be consistent with some combination of the first two explanations described above but with there being some limit to the strength of fringes that were eliminated by the other optical factors of the eye and the visual processing. If, on the other hand, it was not the stimuli with the strongest fringes, but rather the stimuli with the most unusual fringes that had the highest ratings for the strength of the fringes, this would suggest that there is some sort of adaptation to the specific LCA of the eye taking place, and it is when the fringes deviate significantly from this that the participants perceive fringes. This is in line with the Hay et al. (1963) study where they found that once participants had adapted to the prism goggles some perceived fringes even when looking at monochromatic light because they had adapted to there being fringes on the retina.

This experiment could also be interesting from a more practical perspective. If there are certain types of illuminant that lead to a significantly stronger perception of fringes, we may wish to avoid using these types of illuminant.

4.5.1 Methods

Participants

14 participants took part in this experiment. Their ages ranged from 19 to 34 ($M = 26.5$). None of the experimenters participated and the participants were unaware of what spectra they were being shown. All of the participants were able to see a stimulus placed at 40cm without any optical correction and none of the participants wore glasses or lenses during the experiment. None of the participants were aware of having any colour deficiencies. All participants signed a consent form prior to taking part. The ethics for this experiment were approved by the Department of Physics Ethics Committee at Durham University.

Design

The independent variable in this experiment was the type of illuminant. There were four different illuminants used. One was a single narrowband orange LED (Orange), the second was a mixture of a red and blue narrowband LED (Red+Blue), the third was a mixture of a red, green and blue narrowband LED (LEDWhite), and the final one was a halogen bulb (Bulb). The spectra for each of these illuminants are shown in Figure 4.9.

This experiment had a repeated measured design meaning that each participant viewed each of the illuminants. The order in which the illuminants were presented was randomised for each participant to avoid order effects.

The dependent variable was the rating from 0 to 5 that the participant assigned to the stimulus based on whether they could see coloured fringes at the edge of the square.

Apparatus

The participants viewed the stimulus monocularly with whichever eye they preferred. The stimulus was placed in a metal enclosure with two openings, one for the observer to look through and a second for the illuminant to be shone on the stimulus. The inside of the enclosure was coated in non-reflective black material (Metal velvet foil - Acktar ltd). The stimulus was a 14mm square coated in Permaflect (Labsphere) which is lambertian and has a uniform, diffuse reflectance.

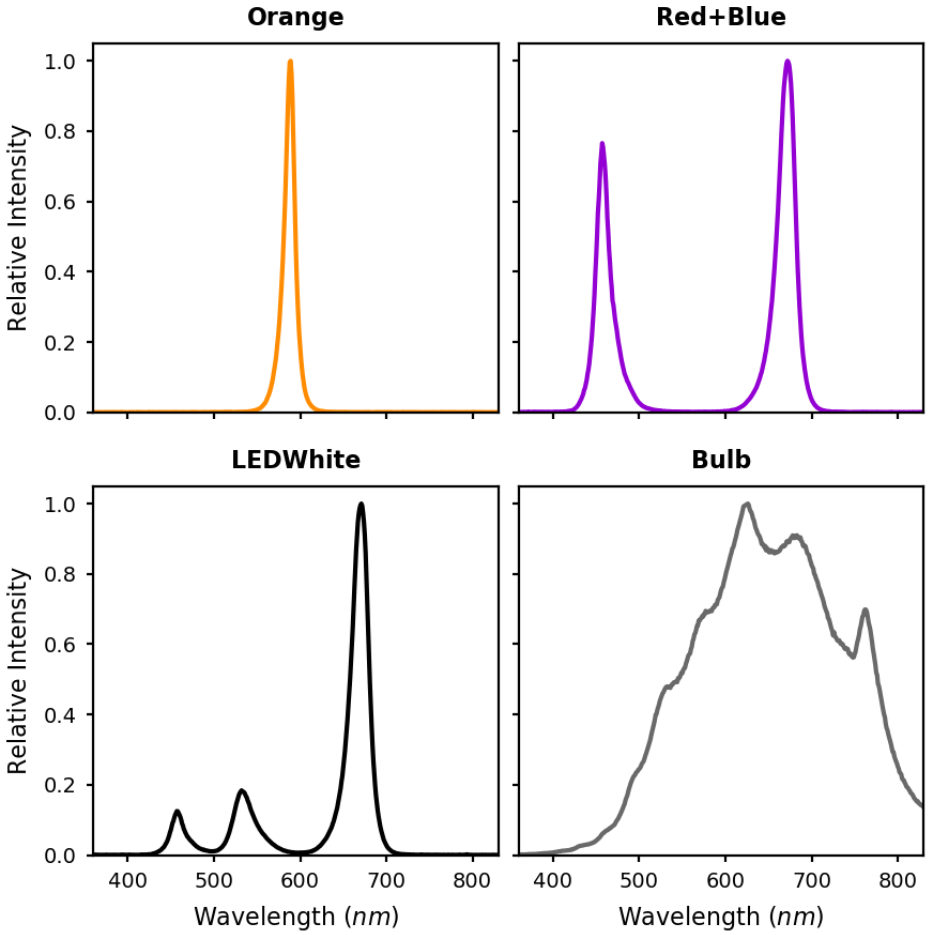

Figure 4.9: The illuminant spectra for the four illuminants in the experiment. The spectra have all been normalised to have peak intensities of 1.

For the LED illuminants, the LEDs were first combined in a custom built integrating sphere made from a ballcock coated with barium sulphate. The combined light from the integrating sphere was then shone into the enclosure onto the stimulus.

Procedure

Prior to the experiment the observers were shown a selection of false colour example images of chromatic fringes to give them an idea of what they were looking for. They were dark adapted for 10 minutes, and then the illuminants were presented one at a time in a random order. For each illuminant the

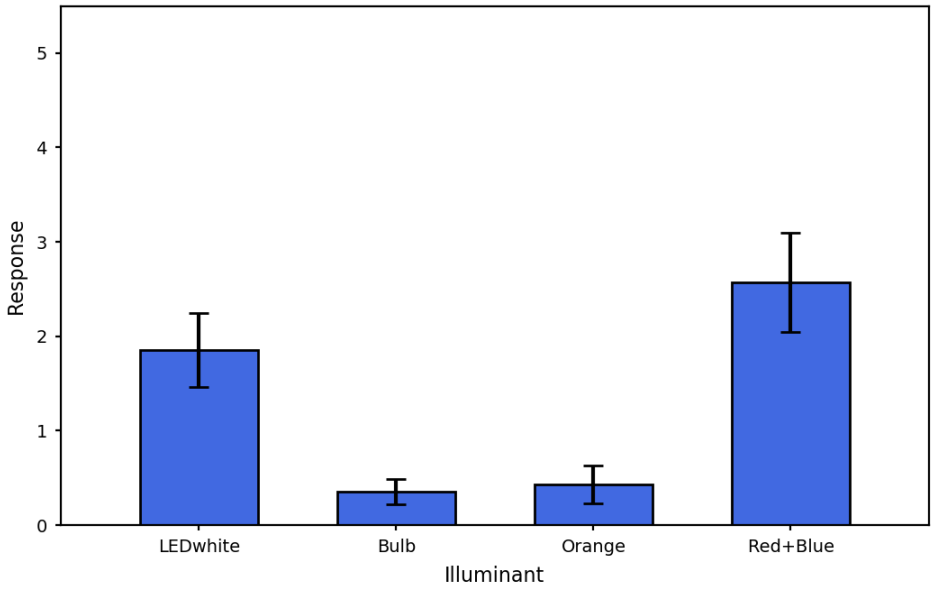

Figure 4.10: The mean rating between 0 and 5 for each of the four illuminants. The error bars represent the standard errors of the means.

participants were able to view the stimulus for as long as they wanted before answering two questions. The first question was "Can you see coloured fringes or halos at the edge of the square?", which had a scale response from 0 to 5, with 0 representing "Not at all" and 5 representing "Definitely yes". The second question was simply "Please describe these fringes" where the observers were given space to describe any fringes that they saw.

4.5.2 Results

The average responses for each condition are shown in Figure 4.10. Here we can see that the Red+Blue illuminant got the highest average rating. The next highest was the LEDWhite stimulus. The Bulb and the Orange illuminants both got average scores below 1 with the very lowest rating for the Bulb.

Figure 4.11 shows a breakdown of the chromatic fringe scores given by each participant for each pair of illuminants. Here the different coloured lines represent different participants. From this we can see that for some illuminant pairs the trend is very consistent across participants. Participants always rated the fringes with the LEDWhite illuminant as either the same or more

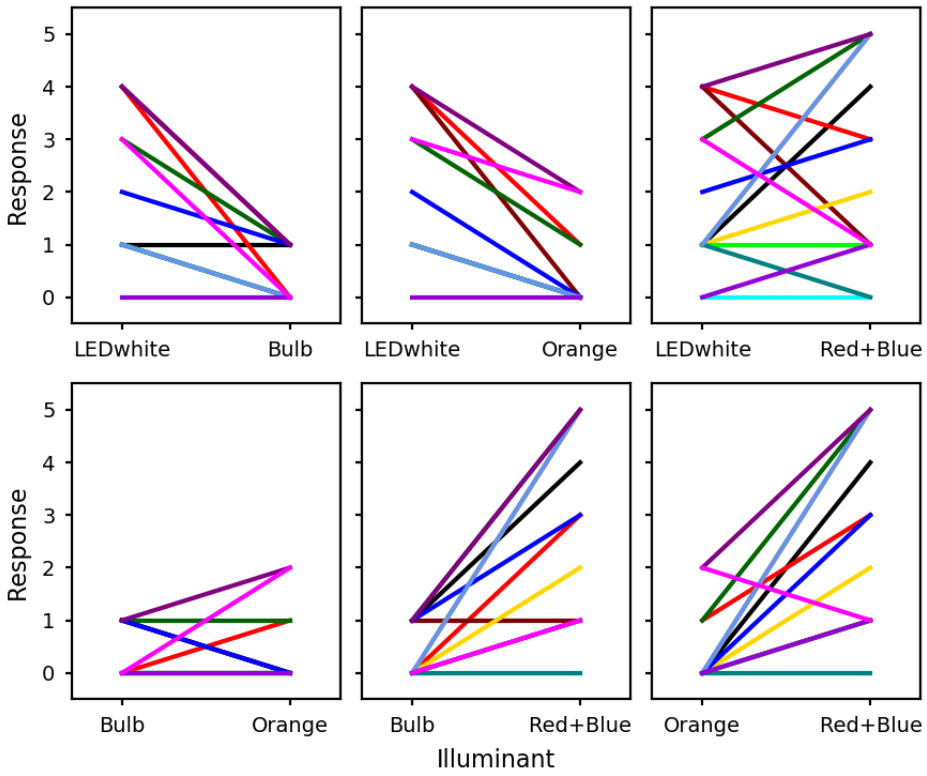

Figure 4.11: The difference in the ratings given for different illuminants. Each graph shows the responses for a different pair of illuminants. Each line colour represents a different participant.

pronounced than with the Bulb illuminant. All participants also gave the LEDWhite illuminant an equal or higher rating than the Orange illuminant. The Red+Blue illuminant also always scored higher than the LEDWhite illuminant and only one participant gave the Orange illuminant a higher score than the Red+Blue illuminant. However, the differences in ratings between the LEDWhite and Red+Blue illuminants, and the Bulb and the Orange illuminants, varied a lot more between participants.

The data did not meet the assumption of normality necessary to conduct an ANOVA. Therefore, a non-parametric, repeated measures Friedman test was used instead. This showed that there was an overall significant difference between the four conditions (X^2 (3) = 25.71, $p < .001$).

Wilcoxon signed rank tests were used to compare each pair of conditions.

These were Bonferroni corrected so that a result was classed as significant if

$$p \leq \frac{0.05}{6} = 0.0083. \tag{4.1}$$

Significant differences were found between 4 of the pairs. The ratings for the LEDWhite were significantly higher than for the Bulb (Z = -2.99, p = .001), and for the Orange (Z = -3.13, p < .001). The ratings for the Red+Blue were also significantly higher than for the Bulb (Z = -2.95, p = .001), and for the Orange (Z = -2.88, p = .002). There was, however, no significant difference between the ratings for the Red+Blue and the LEDWhite (Z = -1.19, p = .257), or between the ratings for the Bulb and the Orange illuminants (Z = -0.33, p = 1.000).

4.5.3 Discussion

Out of all of the illuminants, the halogen bulb should be the one that the subjects were most used to. Therefore if people have adapted to the chromatic fringes that they normally see we might expect the lowest rating for the halogen bulb. However, the orange LED was the most narrowband stimulus and as it was near to monochromatic it should not have resulted in any chromatic fringes in the retinal image. Therefore if it is simply that the chromatic fringes are too subtle to detect or that the inherent nature of the way in which we process visual information prevents us from detecting the chromatic fringes, then we would expect the orange LED to have an equal or even lower rating than the halogen bulb.

In fact, there was no significant difference between the ratings for the halogen bulb and the orange LED. The average rating was slightly lower for the bulb, which could suggest that the subjects had adapted to the specific chromatic fringes in their eyes. However, looking at Figure 4.11 we can see that some of the subjects rated both the halogen bulb and the orange LED illuminants the same, some rated the halogen bulb higher, and some rated the orange LED higher. This could just be down to random chance and order effects or it could be that all three factors play into us not perceiving the chromatic fringes on the retina and there may be individual differences in terms of how strong an influence each of these factors have.

The fringes for the red and blue mixture and the white LED mixture are both the strongest and also the most different from the chromatic fringes that we

might generally be used to. Therefore, the finding that the ratings for the red and blue mixture and the white LED mixture were significantly higher than those for both the halogen bulb and the orange LED does not particularly help us in narrowing down the reason for why we don't generally see chromatic fringes in everyday life. It may be that usually the fringes are too subtle to be detected and it is only with these strange spectra that the fringes become noticeable. Or it may be that because we have adapted to the chromatic fringes for more broadband light, the fringes for these unusual spectra become noticeable. However, what this finding does suggest is that whatever it is that generally prevents us from detecting these chromatic fringes, does not work for the whole range different spectra that we might be exposed to in the modern world. The results of this study show that without altering the actual LCA using lenses, the chromatic fringes on the retina can be made visible just by changing the spectrum of the illuminant. This is an interesting finding in itself as it suggests that we need to be careful when choosing illuminants and primaries for displays, not just because of the colour appearance and the colour rendering index, but also because some spectra may enhance the appearance of coloured fringes across boundaries.

4.6 Stimuli which highlight the longitudinal chromatic aberration of the eye

As has been discussed in the sections above, we do not generally notice the effects of LCA in every day life. It was demonstrated in the previous section that there are certain spectra of light that make the chromatic fringes due to LCA more obvious. There are also certain stimuli which make the effects of the LCA of our eyes more obvious. One good example of such a stimulus is a simple black and white spoke pattern. Figure 4.12 shows a sinusoidal spoke pattern (top left) and the retinal image of this spoke pattern (top right), generated using method 3 described in Appendix A, for the CIE D65 spectrum. Looking at the image on the left you may be able to see colours towards the centre of the pattern even though the image is just black and white. This may be more obvious if the image is viewed from a distance so that the spatial frequency increases. In the image on the right, we can see that the colours in the retinal image are actually quite dramatic. The reason for this chromatic effect is that, as well as defocus in an image leading to a reduction in contrast, it can also

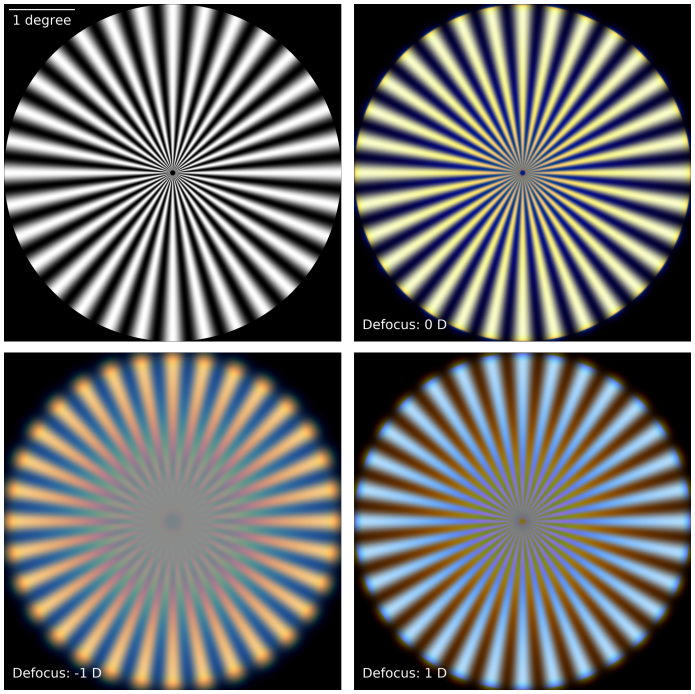

Figure 4.12: The top left panel shows a black and white, sinusoidal, spoke pattern. This is the scene that the retinal images were generated from. The top right panel shows a simulated retinal image of the spoke pattern for a 5mm pupil and LCA but no other aberrations. The bottom left panel shows the retinal image with -1 D of defocus and the bottom right panel shows the retinal image with 1 D of defocus. The scale bar in the top left panel represents one degree of visual angle and applies to all four panels. In order for the scale to be accurate the images would need to be viewed from approximately half a meter away.

lead to phase shifts. The spatial frequencies at which these phase shifts occur depends on the amount of defocus present. In the spoke pattern, the spatial frequency increases towards the centre of the image. Therefore, depending on the level of defocus the phase shifts will occur at different eccentricities. Due to the LCA of the eye, only one wavelength can be in focus at any one time and every other wavelength will be defocussed by a different amount. This means that for each wavelength the phase shifts will occur at slightly different eccentricities resulting in the colour of the spoke pattern changing with eccentricity.

If it is the case that one of the main reasons we do not generally notice

chromatic fringes due to LCA is that we do not use the colour information to detect the boundaries, especially when there is also a luminance edge present, then this could help to explain why some people do see the chromatic effects in the spoke pattern. This is because in the spoke pattern it is not just that for some wavelengths the line is not as sharp but rather that for some wavelengths it is the 'dark' rather than the 'light' regions that are coloured. This may mean that even if the chromatic information is not used to define the boundaries some of the wavelengths are actually in the 'wrong' part of the image defined by the luminance boundaries. It seems unlikely that the inherent nature of the way in which visual information is processed could account for these phase shifts. This could explain why some people do notice the chromatic effects for spoke patterns but not for other stimuli.

The chromatic effects in the spoke pattern become more obvious if there is more defocus. You may be able to see this by looking at the top left image of Figure 4.12 through a defocussing lens, or by focussing the eyes behind or in front of the image while viewing it (if you can). You may notice that the coloured rings come out to greater eccentricities making the coloured effects more dramatic. The lower two images in Figure 4.12 show simulations of the retinal images produced by the spoke pattern for -1 D and 1 D respectively. From these images it is clear that the colours are a lot more dramatic when the spoke pattern is out of focus.

Another situation in which people may become aware of the effects of the LCA of their eyes is when viewing colourful LED or neon signs at night. Because we are more myopic for shorter wavelengths you may notice that although you can read red signs from far away, you will need to be a bit closer before you are able to read the green signs, and closer still before you are able to read the blue signs. Gordon Love developed an illusion based on this concept, in which a red word and a blue word are overlaid. An example of this illusion is shown at the top of Figure 4.13. When standing close the blue word is clearer and easier to read, and when standing at a distance the red word is clearer and easier to read. This effect is most obvious for people who are presbyopic with not much residual accommodation. The bottom left panel in Figure 4.13 shows the retinal image formed with the red writing in focus, as it would be if the person was far away from the image. The bottom right panel shows the retinal image formed with the blue writing in focus, as it would be if the

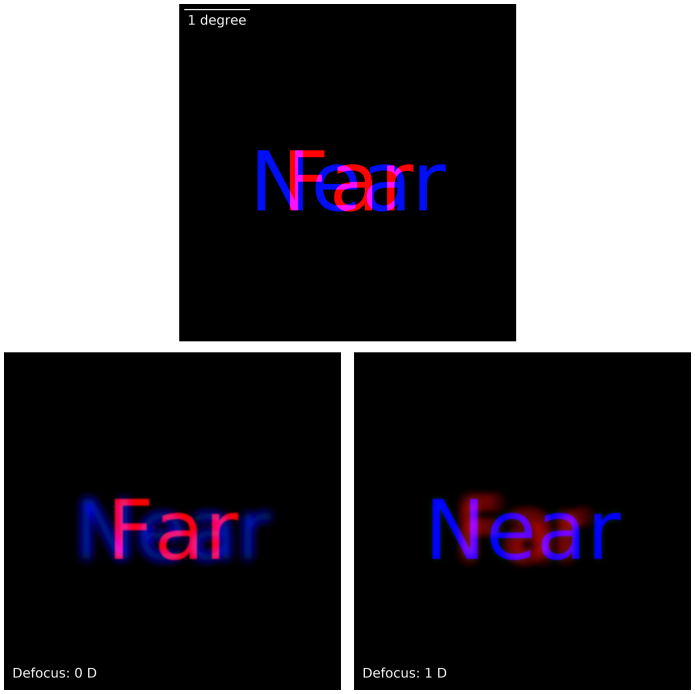

Figure 4.13: The top panel shows the scene that the retinal images were generated for. This scene was multiplied by the R, G, and B primary spectra from a MacBook retina display to give the HSI for the scene viewed on the MacBook display. The bottom left panel shows the retinal image of the scene for a 5mm pupil with LCA and no defocus. The bottom right panel shows the retinal image of the scene for a 5mm pupil with LCA and 1 D of defocus. The scale bar in the top panel represents one degree of visual angle and applies to all three panels. In order for the scale to be accurate the images would need to be viewed from approximately half a meter away.

person was standing close to the image. Both of these retinal images were generated from RGB images using method 2 described in Appendix A.

In this case the LCA is more obvious because the stimulus is different for the red and the blue stimuli. In most cases, when we are focussed on an object we may be able to use the clearer information (e.g. from the luminance channel) to detect the boundaries. This can then guide our perception of where the other colours stop. However, in this case, we can either focus on the image in red or on the image in blue and as the images are different one cannot be used to guide our perception of the other making it more obvious when one is blurred and the other is clear.

4.7 Conclusions

At the start of the chapter three possible explanations were introduced as to why people do not generally perceive the chromatic fringes resulting from the chromatic aberrations of the eye. The first was that it may be that once the other optical imperfections of the eye are taken into account, the chromatic fringes on the retina actually become too subtle to detect. The second was that the inherent nature of the visual processing causes the information about the chromatic fringes to be lost. The third was that we may have adapted to the specific chromatic aberration of our eyes.

Throughout this chapter the evidence for each of these explanations has been explored and it seems that in fact it is some combination of all three. In most everyday scenes and scenarios the chromatic fringes on the retina are actually quite subtle. However, they are not subtle enough, not to be detectable at all, especially for high contrast stimuli. To a certain extent it does seem that the way in which information is processed by the visual system does further reduce our ability to detect chromatic fringes. However, there is also evidence that our visual systems are able to adapt to different chromatic fringes and that they regularly do this (e.g. when we switch to wearing glasses or contact lenses). Therefore it seems that only by some combination of all three explanations can we explain why it is that we do not generally see the chromatic fringes due to chromatic aberration.

The results of the experiment also suggested that changing the illuminant spectra significantly alters the appearance of chromatic fringes. This may be something that needs to be taken into account when choosing what types of illuminants and display primaries to use.

Chapter 5

Chromatic aberration and accommodation to mixed narrowband stimuli.

As has been described in Chapters 2 and 3, accommodation is the process by which the crystalline lens within the eye changes shape and, in doing so, changes the distance at which the eye is focussed. Due to the longitudinal chromatic aberration (LCA) of the eye the defocus changes as a function of wavelength and only one wavelength of light can be in focus on the retina at any one time. For this reason it is conceivable that the eye could accommodate differently for different chromatic stimuli. For example, for a stimulus mostly composed of longer wavelengths it seems reasonable to assume that the eye might bring longer wavelengths into focus and vice versa for a stimulus mostly composed of shorter wavelengths. It is also conceivable that, depending on the cues the eye uses to accommodate, there may be certain spectra for which the eye does not accommodate optimally.

As was described in Chapter 1, in the modern world we are increasingly exposed to unusual illuminant spectra which are often made up of a series of narrowband peaks in intensity rather than having a smooth, broadband intensity distribution as a function of wavelength. This was demonstrated in Figure 1.1 on page 3.

One effect of these modern types of illuminant is that they may alter the appearance of object colours and impair our colour constancy. This is of-

ten considered when selecting illuminants and attempts have been made to quantify this effect using a colour rendering index (CRI). However, what has not been properly addressed is the effect that certain modern illuminants might have on the optimal accommodation response, people's actual accommodation responses, and ultimately on retinal image blur.

5.0.1 Previous Research

Accommodation to different spectra

In narrowband or monochromatic light it has been found that some observers can adjust their accommodation to compensate for the LCA of the eye (Charman and Tucker, 1978). This means that the static accommodation response will differ depending on the wavelength for stimuli presented at the same distance.

There are mixed findings in the literature regarding the wavelength of light we accommodate to under broadband white illumination. Ivanoff (1949) found that the focussing wavelength in white light shifts with accommodation from almost 700nm when the stimulus is presented at infinity to about 500nm when the stimulus is presented at 2.5 D. However, it may be that in this case what was in fact being measured is the apparent lead and lag in the accommodation response function.

Both Charman and Tucker (1978) and Lovasik and Kergoat (1988) found that the static accommodation position for white light was similar to that for green light. However, in a different type of study DeHoog and Schwiegerling (2007) allowed subjects to adjust the focus of a white light source and a series of monochromatic sources and found that the selected best focus for white light was generally equivalent to that for monochromatic light between 590 and 610nm, which is more in the orange or red part of the spectrum. It may be that these differences in findings are due to the different white light spectra used and different viewing distances.

We also measured the static accommodation responses for white light compared to that for narrowband light at various wavelengths (unpublished data). We found that the static accommodation responses for white light generally varied somewhere between that for green light (527nm) and orange light (588nm). This wavelength range aligns roughly with the peak of the luminous

efficiency function. Therefore, it seems reasonable to assume that in white light we accommodate around the wavelengths that we are most sensitive to in the spectrum.

In the modern world we are often exposed to spectra with multiple peaks rather than a continuous broadband spectrum (e.g. LEDs and fluorescent lamps). It is unclear how we might accommodate to such spectra. In the past some research has been done investigating stimuli made up of two different coloured components. Lovasik and Kergoat (1988) ran an experiment in which they investigated accommodation responses to blue letters on a red background, blue letters on a green background and red letters on a green background. They found no clear difference in the accommodative response for these 3 stimuli. They also found that the static accommodation responses for all three of these mixtures (even the blue letters on a green background) was similar to that for red letters on a black background and sometimes even greater. Charman (1989) also ran an experiment in which they measured accommodation responses to a blue C on a red background and a red C on a blue background. They found that observers always accommodated to either the red light or the blue light and never in the middle of the two. From these experimental data we might expect that for spectra made up of 2 peaks at different wavelengths, observers will not focus in between the two wavelengths but rather at around one wavelength or the other.

Accommodation to multiplane displays

Studies have also investigated the accommodation responses in relation to multiplane displays. Multiplane displays are display systems for which there are a series of displays presented at different distances from the eye. Studies have investigated whether it is possible to drive accommodation in between two of the displays by manipulating the intensity ratio between the two displays. This can, in fact, be done by a process known as depth-weighted filtering (Watt et al., 2005). In this process the intensity of the image in each plane is determined by the distance of the desired simulated image plane from the actual display plane in dioptres.

MacKenzie and Watt (2010) found that for image separations up to 1.11 dioptres (D) the accommodation responses could be driven continuously and almost linearly using depth-weighted filtering. However, at larger image plane

separations they found the accommodation response to be biased towards one of the two planes.

These findings can be applied to the topic of accommodation responses to different spectra if we think of the different focal depths for different wavelengths due to LCA being analogous to the different planes of a multiplane display. Therefore, for a spectrum with multiple narrowband peaks we can think of each peak as a separate depth plane. For a spectrum with two peaks, as long as the difference in LCA between the two peaks is less than 1.11 D, we would expect the accommodation position to be somewhere in between the two peak wavelengths and to vary with the relative intensity of the two peaks in line with depth-weighted filtering.

5.0.2 Present Study

The aim of this study is to establish where people accommodate to spectra made up of a mixture of two narrowband components. This is meant as a first step to understanding how we might accommodate to modern spectra with multiple peaks. It may also offer an insight into the cues and rules that the human accommodation system uses.

Firstly, this chapter describes an experiment that was conducted measuring observers' static accommodation responses to a stimulus illuminated from behind by various mixtures of narrowband LEDs. At any one time the stimulus was only illuminated by one or two of the LEDs. Therefore, all of the spectra had either one or two peaks in intensity as a function of wavelength.

There were two possible hypotheses as to where people would accommodate for the mixed stimuli. The first was that people would accommodate to one of the two individual LEDs. This is in line with the findings of Charman (1989). The second hypothesis was that, as long as the dioptric separation between the two wavelengths due to LCA was less than 1.11 D, as the intensity ratio between the two LEDs changed, there would be a roughly linear accommodation response between the two LEDs. This is in line with the findings of MacKenzie and Watt (2010) on multiplane displays.

The paper then goes on to describe a series of simulations to predict where accommodation might be driven for the stimuli used in the experiment. These

simulations were run for a variety of different optimisation rules using a variety of potential optical cues.

The aim of these simulations was to discover the best rule for predicting the measured accommodation responses found in the experiment. Hopefully this rule could then be used to predict the accommodation responses to different chromatic stimuli.

5.1 Experiment

In this section the experiment where the observers' accommodation responses to various combinations of LEDs were measured is described.

5.1.1 Methods

Participants

Initially, 11 participants were recruited. However, six of these were excluded as their refractive state could not be reliably measured by the autorefractor resulting in large gaps in the data. Another participant who completed a previous experiment showed no significant differences in accommodation for the individual LEDs and therefore this participant was also excluded from this experiment.

The 5 participants whose data was used were between the ages of 23 and 28 years (M = 26.2). They all had a visual acuity that was greater than 0.3 logMAR in each eye at both near and far distances without the need for spectacles or lenses.

All participants signed a consent form prior to taking part. The ethics for this experiment were approved by the Department of Physics Ethics Committee at Durham University.

Apparatus

The stimulus was a black Maltese cross printed on transparency film and mounted on a diffuser. This was positioned 3 D away from the observer. At this distance the stimulus window subtended 2^{o} visual angle. Figure 5.1 shows an image of the Maltese cross and its spatial frequency content.

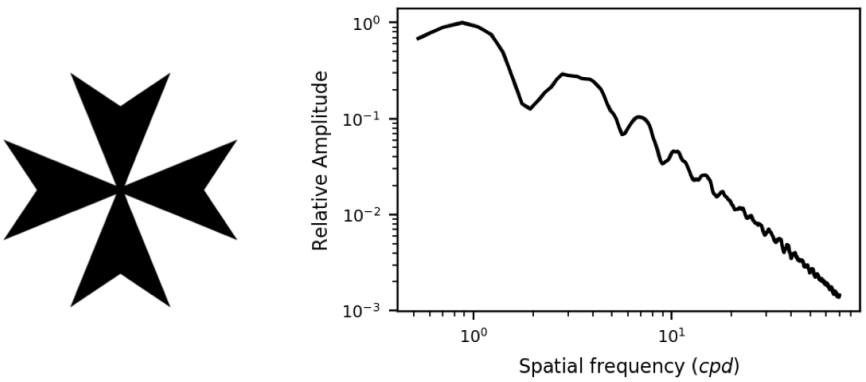

Figure 5.1: The fixation stimulus used in the experiment is shown on the left. The spatial frequency power spectrum is shown on the right.

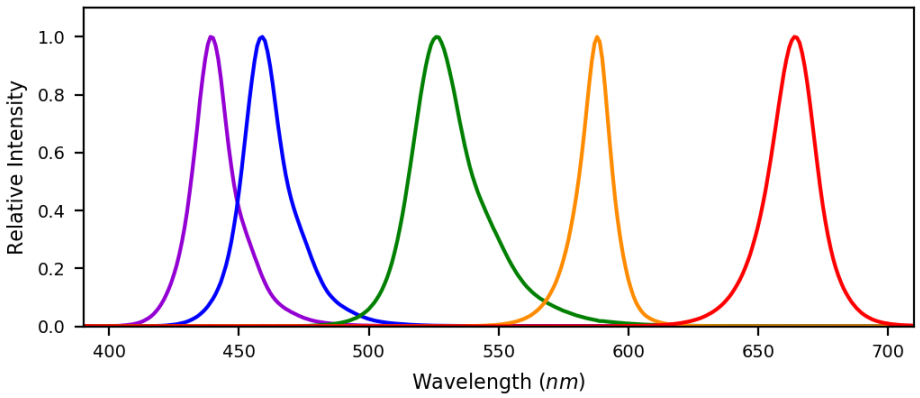

Figure 5.2: Radiance measures for each of the six LEDs. These have been normalised to have peak values of one.

Behind the diffuser there were five narrowband LEDs. The spectra of these LEDs is plotted in Figure 5.2). From now on these LEDs will be referred to as red (peak: 660nm), orange (peak: 588nm), green (peak: 527nm), blue (peak: 461nm), and violet (peak: 441nm). The stimulus was back illuminated by various combinations of these five LEDs. The LEDs were controlled using an Arduino and the intensities were adjusted using pulse width modulation (PWM).

The refractive state of the eye was measured using the PlusOptix PowerRef 3 device while they were viewing the accommodation stimulus. A diagram of the set up is shown in Figure 5.3

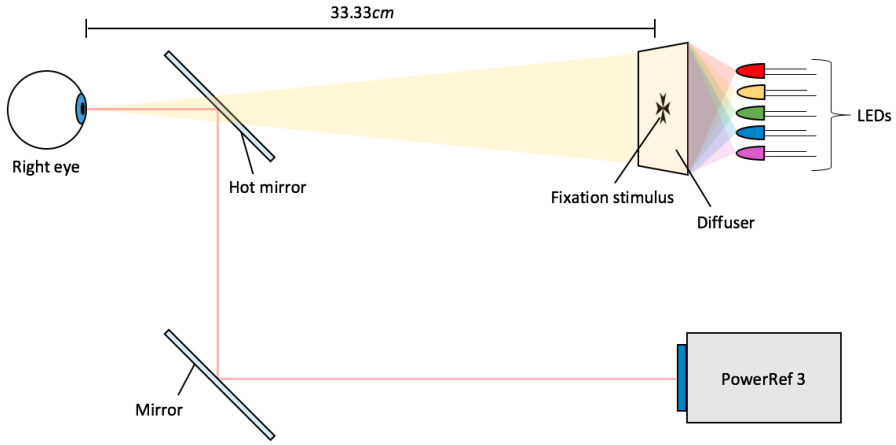

Figure 5.3: A diagram (not to scale) showing the setup of the apparatus. The periscope system, including a hot mirror, allows the participant to view the stimulus while the PowerRef 3 measures the refraction of the eye. The only difference in the set up for the calibration procedure was that the stimulus was at 100cm and the fixation cross was larger to maintain the angular size.

Calibration

To ensure that the relative refraction measures were accurate for each of the participants in this study, we calculated an individual-specific relative calibration factor for each participant as suggested in Sravani et al. (2015).

The stimulus was presented at 1 D from the observer and illuminated from behind by the green LED. The intensity of the green LED was adjusted using PWM until the observers pupil size was roughly 6mm.

An infrared transmitting filter (Edmund Optics, Optical Cast Plastic IR Longpass Filter) was placed in front of the right eye in a trial frame. The observer could not see through this filter but the refractive state of their eye could still be measured. A series of lenses from -4 D to 5 D in 1 D steps were also placed in front of the right eye. The refraction in both eyes was measured for 30 seconds with each of the 10 lenses.

The average difference in refraction between the two eyes was calculated for each of the lenses. The difference in refraction was plotted against the power of the lens and a regression line was fitted to the linear portion of this curve. The slope of the line was taken as the individual-specific relative calibration

factor and applied to all of the subsequent measures.

Procedure

As well as the five LEDs in isolation, six pairs of the LEDs were used to generate the spectra. These were red and green, red and blue, red and violet, orange and blue, orange and violet, and green and violet. For each pair there were 7 mixtures, each with different relative luminances of the two LEDs. The luminances of each of the individual LEDs was increased or reduced in steps of 1.25cd/m^2 while the overall luminance was kept constant at approximately 10cd/m^2. This gave a total of 42 mixtures and 47 test spectra including the five individual LEDs.

Before each trial the orange LED was presented for 2.5 seconds as a 'pre-trial' stimulus. This was followed by the 'trial' stimulus, in which any one of the 47 test spectra was presented for 2.5 seconds.

Each session contained one trial for each of the 47 test spectra in a randomised order. There was no break between trials meaning that each session lasted for 3m 55s. Each participant completed at least 12 sessions, giving 12 repetitions for each of the test spectra.

Participants viewed the target monocularly with their right eye (their left eye was covered). They were instructed to look at the stimulus and keep the cross clear using the same type of effort as when reading a book. There was a pause button that they could press if they needed a break within a session. They were told that they could blink whenever they needed to within the session but that if their eyes were watering or they needed to blink a lot they should use the pause button. Between sessions observers were given a break for as long as they needed.

Data analysis

The data points where the pupil was not found were treated as blinks and excluded along with 80ms before and 160ms after the blink. Data points with a refraction measure that was clearly erroneous (< -20 D or > 20 D) were also excluded. The first 1000ms of data within each trial and and the first 1500ms within each pretrial were excluded to allow the participant time to accommodate.

The static refraction values were calculated as the mean of the remaining data for each trial and pretrial. The trial values were then normalised by subtracting the preceding pretrial value from each. This was based on the assumption that observers always accommodated to the same distance for the pretrial ref and helped correct for longer term measurement errors such as shifts in head position.

5.1.2 Results

Figure 5.4 shows the average static accommodation measures across all of the participants for each of the spectra. There is a clear difference in the average accommodation between the two individual LEDs (plotted at either end of each of the graphs). It also appears that for many of the mixtures the average accommodation lies in between the accommodation for the two individual LEDs. The dashed lines show the accommodation responses needed to reduce the defocus for the peak wavelength of each of the LEDs to zero. The average static accommodation measures for each individual participant can be found in Appendix B.

ANOVAs were performed for each pair of LEDs for each participant. In all cases these showed a significant main effect.

If individual participants were switching their accommodation between the two LEDs for the mixed illuminants, the average results could still show this trend. In order to ensure that this was not the case we calculated the within trial variance and the between trial variance for each spectrum for each observer. The average variances for all observers are shown in Figures 5.5 (within trial) and 5.6 (between trial). If the observers' accommodation responses were switching between the two LEDs then we would expect a symmetrical trend in the variance with an increased variance towards the centre where the mixtures are most even. However, there is no clear symmetrical trend in the variances so we can assume that the accommodation results were not due to switching.

Levene's tests were also used to assess the difference in variances for each pair of LEDs, for each of the participants. Six out of the 24 tests showed an overall significant difference between variances across the different luminance mixtures. A linear contrast was then performed on the Z values to compare the variances for the mixed spectra with those for the single LEDs. This was insignificant in all cases.

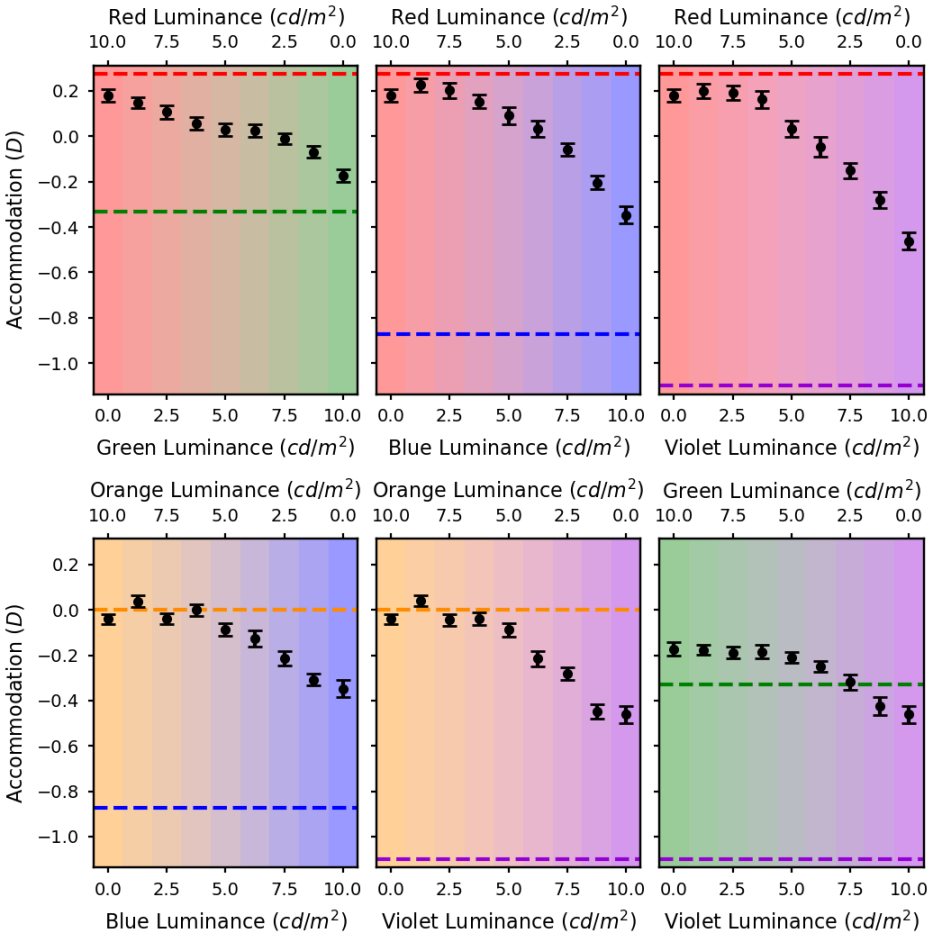

Figure 5.4: The black circles show the relative mean static accommodation responses of all 5 subjects plotted against the luminances of the two LED sources. The different graphs are for the different LED pairs: red and green (top left), red and blue (top middle), red and violet (top right), orange and blue (bottom left), orange and violet (bottom middle), and green and violet (bottom right). The error bars represent the standard error of the mean. The dashed lines indicate the accommodation needed to bring the defocus for the peak wavelength of each LED to zero.

5.1.3 Discussion

The first hypothesis was that there would be a step like pattern in the accommodation responses. With the accommodation always around one of the two LEDs in the mixture and never in the middle of the two. This would align with the findings of Charman (1989). However, looking at the data in Fig-

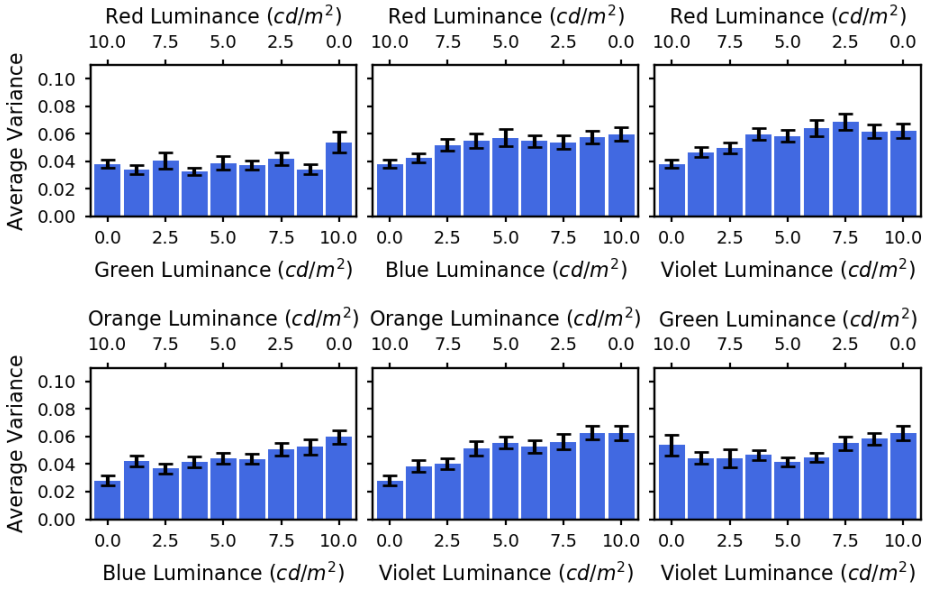

Figure 5.5: The bars show the within trial variances averaged across all five observers for each of the spectra. The different graphs are for the different LED pairs: red and green (top left), red and blue (top middle), red and violet (top right), orange and blue (bottom left), orange and violet (bottom middle), and green and violet (bottom right). The error bars represent the standard error of the mean.

ure 5.4, we can see that for each of the LED pairs there are mixtures for which the accommodation response is clearly in the middle of the responses for the two individual LEDs. This is unsurprising as in the stimuli used by Charman (1989) the red and the blue primaries were not mixed. There was either a red C on a blue background or vice versa. In our stimuli, on the other hand, the two wavelength components were mixed with a diffuser so accommodating to one of the individual components was not such an obvious response.

The second hypothesis was that as long as the difference in defocus between the two LEDs due to LCA was less than 1.11 D, there would be a linear transition in the accommodation response through the mixtures. For the red and green, orange and blue, orange and violet, and green and violet mixtures, the separation between the peak wavelengths due to LCA is less than 1.11 D. Therefore we would expect a linear transition in accommodation across the mixtures. However, Figure 5.4 shows that although there is a smooth transition in accommodation across the mixtures, in most cases there is an

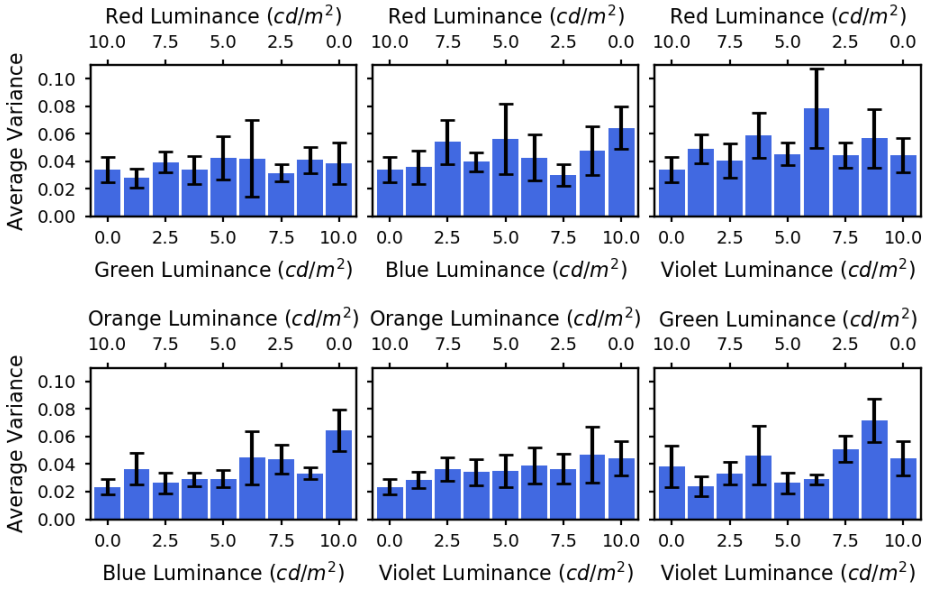

Figure 5.6: The bars show the between trial variances averaged across all five observers for each of the spectra. The different graphs are for the different LED pairs: red and green (top left), red and blue (top middle), red and violet (top right), orange and blue (bottom left), orange and violet (bottom middle), and green and violet (bottom right). The error bars represent the standard error of the mean.

asymmetry in the responses towards the longer of the two wavelengths meaning that the response is not quite linear. The smallest dioptric separation is between the red and green LEDs and in this case the transition in the accommodation responses across the mixtures does seem to be roughly linear. For this reason the findings do at least somewhat agree with the predictions based on the MacKenzie and Watt (2010) study.

Often the measured accommodation responses don't seem to align particularly well with these dotted lines. This may be because the calibration we used only accounted for the relative refraction measures and not the absolute measures. Another possibility is that the optimal accommodation response is not actually the one that minimises the defocus. Certain monochromatic aberrations of the eye, such as spherical aberration, interact with defocus so that a certain magnitude of defocus actually helps to cancel out the blur in the retinal image caused by the other aberrations. Spherical aberration also varies with the accommodative state of the eye and therefore the optimal amount of defocus

will vary depending on the accommodative state. This could also help to explain the offset between the measured accommodation responses and the hypothetical responses for minimising defocus for each of the individual LEDs (as shown by the dotted lines).

5.2 Simulations

In addition to measuring accommodation responses, we ran simulations to attempt to explain these findings. A series of simulations were run using different potential cues to accommodation and employing different rules to determine the eventual focus position. All of the simulations were run in Python using the wave approximation to model the eye.

In the rest of this section a collection of these simulations are described. The results of each simulation is then compared to the measured data.

5.2.1 Maximising Overall Image Quality

The first set of simulations were based on the assumption that the aim of the accommodation response was to maximise the retinal image quality. In the first instance we used visual Strehl Ratio (VSR) calculated from the modulation transfer function (MTF) as our measure of image quality, as this has been shown to be a very good predictor of visual acuity (Cheng et al., 2004; Marsack et al., 2004; Thibos et al., 2004).

The VSR is an image quality metric calculated from the simulated retinal image. It is based on Strehl ratio, which is the peak intensity of the point spread function (PSF) of the optical system divided by the peak intensity of a diffraction limited PSF for the same pupil size. This can be defined as

$$\mathrm{SR} = \frac{\max(\mathrm{PSF})}{\max(\mathrm{PSF_{DL}})}, \tag{5.1}$$

where max(PSF) is the maximum intensity of the PSF and $\max(\mathrm{PSF_{DL}})$ is the maximum intensity of the diffraction limited PSF for an optical system with the same pupil size.

Another version of the Strehl ratio can be calculated in the Fourier domain from the MTF using the equation

$$\mathrm{SR_{MTF}} = \frac{\int_{-\infty}^{\infty} \mathrm{MTF}(f_i) df_i}{\int_{-\infty}^{\infty} \mathrm{MTF_{DL}}(f_i) df_i}, \tag{5.2}$$

where $\mathrm{MTF}(f_i)$ is the MTF and $\mathrm{MTF}_{\mathrm{DL}}(f_i)$ is the MTF for the equivalent diffraction limited eye. f_i is the spatial frequency in the image plane. This is based on the idea that the volume underneath the MTF is equal to the central value of the PSF.

The VSR used for these simulations was computed in the same way as the Strehl ratio is computed from the MTF. However, the MTF was weighted by the neural Contrast Sensitivity Function (nCSF) before integrating. This integrated value was then normalised by the equivalent value for a diffraction-limited system. This can be expressed as

$$\mathrm{VSR} = \frac{\int_{-\infty}^{\infty} \mathrm{nCSF}(f_i)\mathrm{MTF}(f_i)df_i}{\int_{-\infty}^{\infty} \mathrm{nCSF}(f_i)\mathrm{MTF}_{\mathrm{DL}}(f_i)df_i}, \tag{5.3}$$

where the nCSF was calculated using Equations 2.7 and 2.8 on page 12.

The advantage of the VSR over the Strehl ratio is that as well as taking into account the effect of the optics of the eye on the resultant image quality, it aims to capture the effect of the subsequent neural processing that occurs.

In order to simulate the accommodation responses needed to maximise the overall image quality polychromatic PSFs were calculated for a series of defocus values (-1.5 D to 1.5 D in steps of 0.01 D). The polychromatic PSFs were calculated by generating the monochromatic PSFs at a series of wavelengths (400nm to 700nm in 5nm steps) with the LCA and defocus included. The LCA for each wavelength was calculated using Equation 2.14 on page 19 as described in Marimont and Wandell (1994), which gives the LCA of the eye relative to 580nm. Each set of monochromatic PSFs were then weighted by the relevant test spectrum and the luminous efficiency function, and summed across all wavelengths to give the polychromatic PSF.

For each defocus value, the absolute Fourier transform of the polychromatic PSF was then taken to give the polychromatic MTF (see Equation 2.4 on page 11). The VSR was then calculated from the MTF using Equation 5.3. The predicted focus position for each test spectrum was taken to be the defocus value resulting in the peak VSR.

Figure 5.7 shows the calculated VSR as a function of defocus for the test spectra of various mixtures of the red and blue LEDs. It is clear from these graphs that there are two separate peaks in VSR, one around where the peak wavelength of the red LED is in focus and the other around where the peak

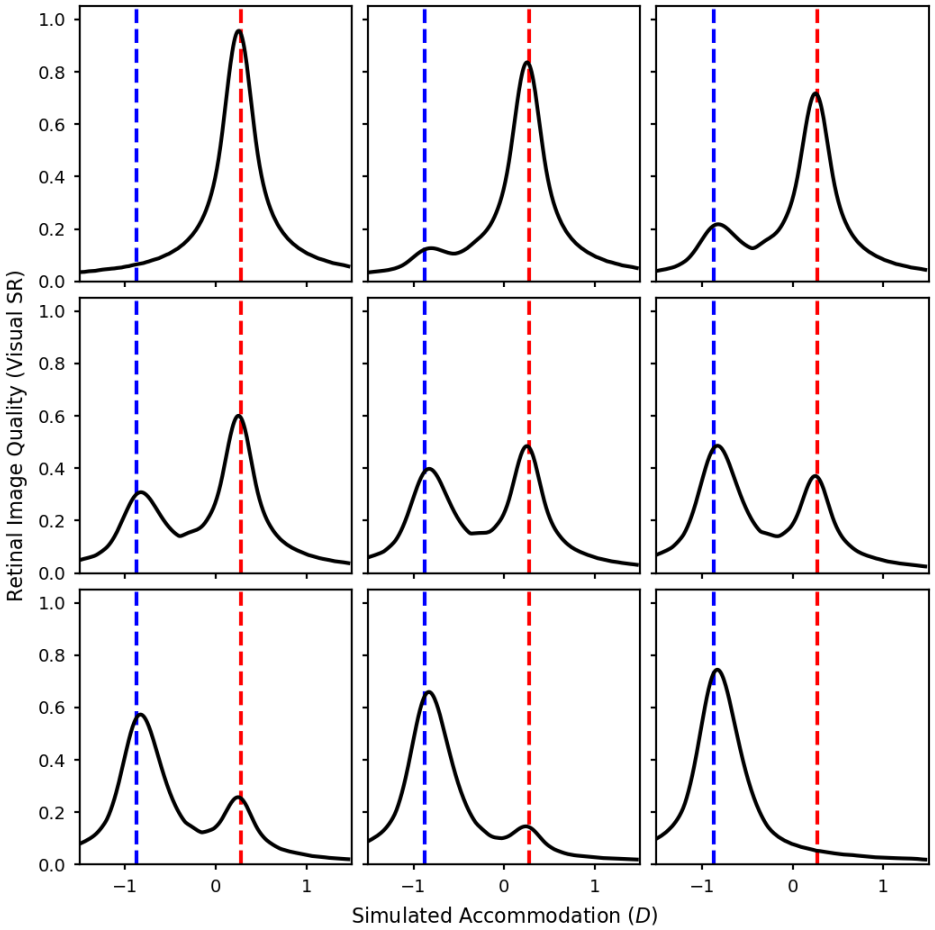

Figure 5.7: Visual Strehl ratios calculated from a wave optics model of the eye with a 5mm pupil over a range of defocus values. The visual Strehl ratios were calculated from polychromatic MTFs weighted by each of the test spectra and the luminous efficiency function. The test spectra are mixtures of the red and blue LEDs. The luminance ratio of these two sources was varied in nine equal steps from completely red (top left) to completely blue (bottom right). The red and blue dashed lines indicate the accommodative response needed to correct the LCA at the peak wavelengths of the red and blue LEDs.

wavelength of the blue LED is in focus. As the luminance of the blue LED increases the peak in the VSR at the blue wavelengths also increases, and vice versa.

In this case we are assuming that the accommodation system finds and accommodates to the overall peak in VSR, which is the highest of the two peaks

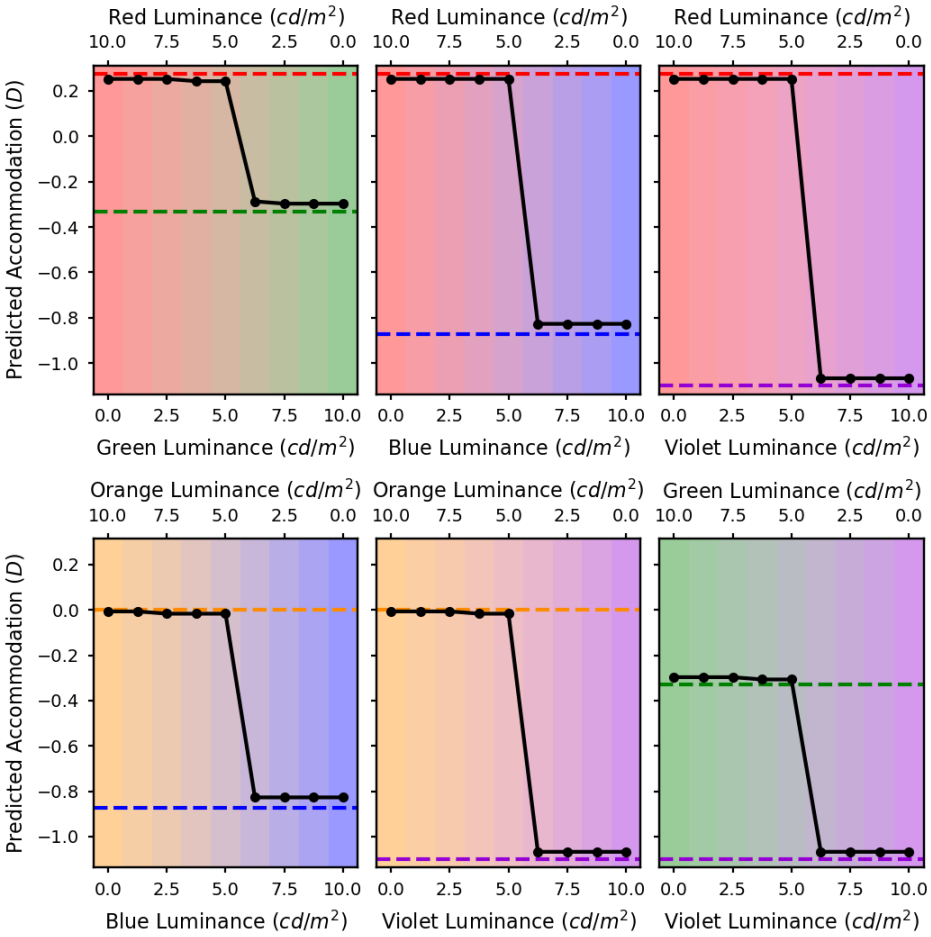

Figure 5.8: The predicted accommodation responses for maximising visual Strehl ratio in the luminance channel for a 5mm pupil. The x axis represents the luminances of the two LED sources. The different graphs are for the different LED pairs: red and green (top left), red and blue (top middle), red and violet (top right), orange and blue (bottom left), orange and violet (bottom middle), and green and violet (bottom right). The dashed lines indicate the accommodative response needed to correct the LCA at the peak wavelengths of the LEDs.

typically shown in Figure 5.7. However, if the visual system was using a trial and error method, for example by using the microfluctuations in defocus to judge the direction of the accommodation response needed, it is conceivable that the actual accommodation response could get stuck in a local maximum rather than reliably finding the overall peak in image quality. Either way,

using this rule we predict a focus position where either the red or the blue LED is focus and not a position between the two.

Figure 5.8 shows the predicted accommodation for each of the LED mixtures. The x-axes of these graphs corresponds to the relative luminances of the two LEDs. The y-axes of these graphs are equivalent to the x-axes from Figure 5.7 although in this case just the defocus value corresponding to the peak VSR is plotted as the predicted accommodation response. The predicted focus values for all of these combinations show the same step pattern as the red and blue mixture, meaning that in all cases the VSR is optimised when one of the two LEDs is in focus.

If observers were accommodating to maximise image quality we would expect that for all of the mixtures, the static accommodation response would be roughly the same as for one of the two individual LEDs making up that mixture and not somewhere in the middle. This is because there is actually a dip in image quality in the middle, as is shown in Figure 5.7. However, looking back to the measured accommodation results in Figure 5.4, it is clear that participants are accommodating in between the two LEDs for some of the mixtures. This suggests that observers may not actually be maximising image quality.

Different Image Quality Metrics

It is possible that the simulation results described above are just due to the specific image quality metric chosen. Perhaps if we used an image quality metric other than VSR we would see different results. In order to ensure that this was not the case we ran exactly the same simulation as that described above but with different image quality metrics.

Firstly we tried using a measure of encircled energy known as 'light-in-the-bucket' (LIB) (Thibos et al., 2004). Encircled energy is defined as the percentage of the total energy falling within a circle that is centred at the peak of the PSF. In the case of LIB the region of interest is the area taken up by the core of the diffraction limited PSF. This can be defined as

$$\mathrm{LIB} = \int_0^{2\pi} \int_0^{\mathrm{DL\ core}} \mathrm{PSF}(r_i, \theta_i) dr_i d\theta_i, \tag{5.4}$$

where the domain of integration is the core of the diffraction limited PSF for the same pupil diameter and PSF is the normalised PSF (sum of energy = 1).

Another metric we tried is one we will refer to as R50. This metric stems from the same principle as encircled energy. However, the value of interest is the radius of the circle containing 50 percent of the energy in the PSF. A smaller value of R50 indicates a more compact PSF and, therefore, a better image quality.

Thibos et al. (2004) defined R50 as being equal to the radius, r, when

$$\int_0^{2\pi} \int_0^{r} \mathrm{PSF}(r_i, \theta_i) dr_i d\theta_i = 0.5. \tag{5.5}$$

We ran the same simulations as described above but this time defining the predicted accommodation response as either the point at which the LIB value was the highest or the point at which the R50 value was lowest. The results were very similar to the VSR predictions. There was generally a reduced image quality in between the two LEDs, and the predicted accommodation was always around one of the individual LEDs and not in between the two.

These findings further support the idea that the way that observers were accommodating to these mixed chromatic stimuli was not maximising the image quality.

5.2.2 Maximising Contrast at Different Spatial Frequencies

The image quality metrics employed in the section above did not break the visual information down into its component spacial frequencies and instead reduced the information from all of the spatial frequencies down to a single measure of image quality. To calculate VSR the MTF was weighted by the nCSF, which places different weights on different spatial frequencies based on real measurements of contrast sensitivity. However, although this weighting of spatial frequencies may describe our ability to detect and distinguish gratings of different spatial frequencies, the same weightings may not be appropriate for the accommodation response.

There is some controversy in the literature as to which spatial frequencies are most important for the accommodative response. One suggestion has been that when there is a large amount of defocus, the lower spatial frequencies are most important, whereas the high spatial frequencies play an important role in fine tuning the response.

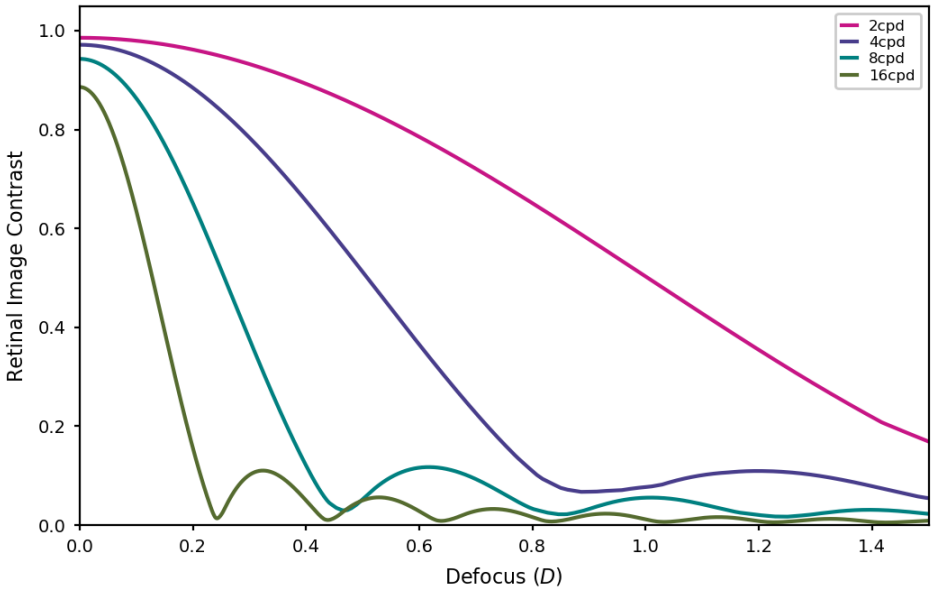

Figure 5.9: Modulation transfer as a function of defocus plotted for 2 (magenta), 4 (purple), 8 (cyan) and 16 (green) cpd.

Figure 5.9 shows modulation transfer as a function of defocus. For higher spatial frequencies the first minimum occurs at a relatively low defocus value. Contrast information at defocus values greater than this first minimum will not be useful because an increase in contrast does not always imply moving closer to the correct focus and there are many local maxima in contrast. However, the lower spatial frequencies provide a reliable cue to the required direction of the accommodation response even at relatively large defocus values. This, therefore, fits with the theory that lower spatial frequencies are more important than high spatial frequencies in guiding the accommodation response for large values of defocus.

For small defocus errors, on the other hand, the contrast gradient at the lower spatial frequencies becomes very shallow. However, the contrast gradient at the high spatial frequencies is very steep for these small defocus errors supporting the idea that the high spatial frequencies could still play an important role in fine tuning the accommodation response. The idea that high spatial frequencies play an important role was supported by an experiment by Charman and Tucker (1978) who measured accommodation responses to sine wave gratings and found that in general responses were more accurate to gratings

with higher spatial frequencies.

There is also evidence to suggest that high spatial frequencies actually have little importance for accommodation. Studies have investigated accommodation responses to sinusoidal gratings with various spatial frequencies and found that optimal accommodation performance was achieved at low to intermediate spatial frequencies (between 3-5 or 1-7 cpd) (Owens, 1980; Stone et al., 1993; Mathews and Kruger, 1994). Similarly Walsh and Charman (1988) investigated participants' sensitivity to blur both for sinusoidal grating targets and for images with a broad spatial frequency bandwidth. They found that the blur sensitivity for the broadband images was most similar to that for gratings at around 5 cpd.

In a very different type of study (Burge and Geisler, 2011) used a set of natural images, and a model of the human eye and early visual system to find a set of optimal filters for extracting defocus information from the environment. They found that these optimal filters were predominantly sensitive to spatial frequencies between 5-15 cpd.

MacKenzie and Watt (2010) measured accommodation to multiplane displays as well as calculating the positions at which the retinal image contrast would be optimised for a range of spatial frequencies. The calculations showed that the optimum focus positions were different for different spatial frequencies, creating a conflict between the information from low and high spatial frequencies. They found that the measured accommodation responses aligned best with optimising retinal image contrast for lower spatial frequencies. This suggests that spatial frequencies above around 6-8 cpd were not contributing to the accommodation response in this case.

It is still unclear which spatial frequencies are most important for accommodation. However, a large amount of the research seems to indicate that lower spatial frequencies between around 3-6 cpd play the most crucial role. It may be that although high spatial frequencies are useful in fine tuning the accommodative response if there is no conflict between the high and low spatial frequencies, when there is a conflict we use the low frequency information over the high frequency information. This makes sense if we look at Figure 5.9, because the higher spatial frequencies give a less reliable cue.

Simulations

The set of simulations described here were carried out in the same way as the ones described above. However, once the polychromatic MTFs had been calculated, instead of calculating the VSRs from these, the contrasts were simply read off for a series of discrete spatial frequencies. The predicted accommodation response for each of these spatial frequencies was then calculated by finding the defocus value at which the contrast for that spatial frequency was at its maximum.

Figure 5.10 shows the simulated retinal image contrasts at 2, 4, 8, and 16 cpd for mixtures of the red and blue LEDs. For each of the LEDs on their own the optimum focus point for maximising spatial frequency was almost identical for all of the spatial frequencies and corresponded roughly to the plane where the peak wavelength of that LED was in focus.

For the mixtures, the general pattern for the higher spatial frequencies of 8 and 16 cpd was similar to that found for the VSR. For these higher spatial frequencies there were always two main peaks in contrast corresponding to the two peaks in the spectrum. As with the VSR the peak corresponding to the red LED increased as more red was added, and vice versa for the peak corresponding to the blue LED.

However, as the spatial frequency reduces, the lines become smoother and the peaks merge into one, so there are no longer two distinct peaks in contrast. For 2 cpd there was just a single peak that moved more towards red wavelengths when more red light was added and towards blue wavelengths when more blue light was added. For the mixture with equal luminances of red and blue, the optimum focus position for maximising contrast at 2 cpd is actually right in the middle of the two LEDs.

This is interesting because the point at which we might focus if we were maximising contrast in the low spatial frequencies actually corresponds to a dip in the contrast for the higher spatial frequencies. This means that, for these types of stimuli, accommodating in order to maximise contrast in lower spatial frequencies, a tactic that would normally maximise contrast across all spatial frequencies, actually results in a loss of contrast at higher spatial frequencies and, therefore, a degradation in the fine details of the image.

Figure 5.11 shows the predicted focus positions for maximising contrast at

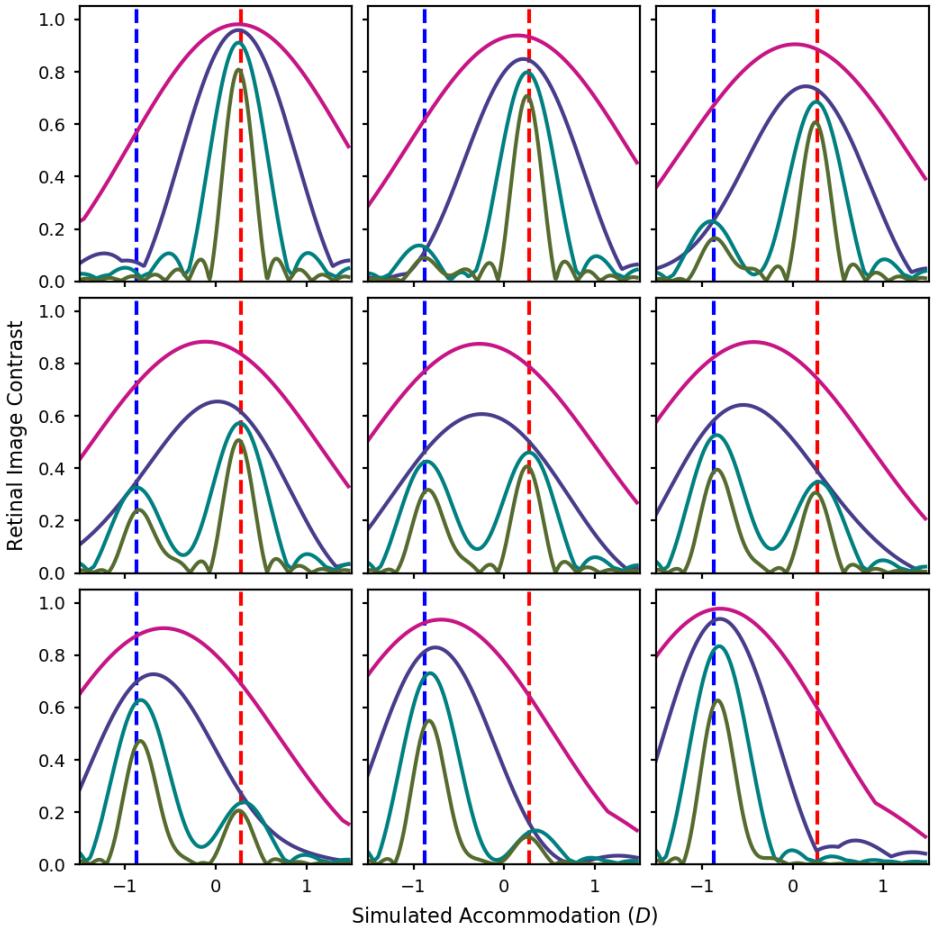

Figure 5.10: Contrast ratios calculated from a wave optics model of the eye with a 5mm pupil over a range of defocus values, at 2 (magenta), 4 (purple), 8 (cyan), and 16 (green) cpd. The contrast ratios were calculated from polychromatic MTFs weighted by each of the test spectra and the luminous efficiency function. The test spectra were mixtures of the red and blue LEDs. The luminance ratio of these two sources was varied in nine equal steps from completely red (top left) to completely blue (bottom right). The red and blue dashed lines indicate the accommodative response needed to correct for the LCA at the peak wavelengths of the red and blue LEDs.

each of the four spatial frequencies. The separate graphs are for different LED combinations. Here we can see a clear step function for the higher spatial frequencies of 16 cpd and sometimes 8 cpd. As the spatial frequency decreases there is a slightly smoother sigmoid shape, and at 2 cpd the transition is even

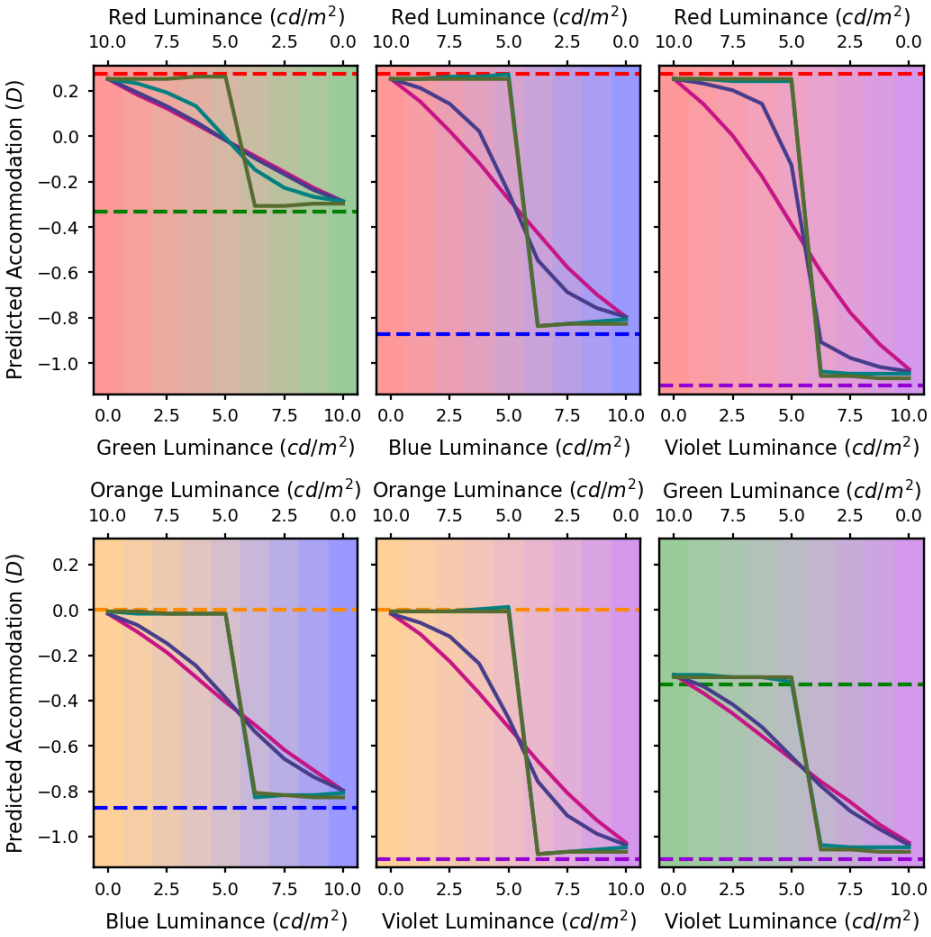

Figure 5.11: The predicted accommodation responses for maximising retinal image contrast in the luminance channel for spatial frequencies of 2 (magenta), 4 (purple), 8 (cyan), and 16 (green) cpd with a 5mm pupil. The x axis represents the luminances of the two LED sources. The different graphs are for the different LED pairs: red and green (top left), red and blue (top middle), red and violet (top right), orange and blue (bottom left), orange and violet (bottom middle), and green and violet (bottom right). The dashed lines indicate the accommodative response needed to correct the LCA at the peak wavelengths of the LEDs.

smoother and almost linear for some combinations. The only real difference between the different LED combinations is that the less dioptric separation there is between the two wavelengths due to the LCA of the eye, the smoother the curves tend to be, and the greater the dioptric separation is, the more

step-like the curves tend to be.

The measured accommodation responses in Figure 5.4 show a relatively smooth line across the mixtures. This seems to correspond best to the lower spatial frequencies of 2 or 4 cpd. There are a number of test spectra for which participants accommodated in between the average responses for the two LEDs alone. This means that they would have had very low contrast for the higher spatial frequency components of the image.

As was mentioned above, it may be that when there is a disagreement between the directions suggested by the high and the low spatial frequencies, the lower spatial frequencies tend to be favoured as they are generally more reliable (see Figure 5.9). Most of the mixed spectra used in this experiment did lead to disagreements in the optimum focus point for different spatial frequencies. This could explain why the behaviour corresponds more closely to the predictions from lower spatial frequencies as these are generally more reliable. However, it is worth noting here that the depth of focus is much lower for the higher spatial frequencies than it is for the lower spatial frequencies. Therefore, arguably, optimising the focus position for high spatial frequencies is more important than optimising for low spatial frequencies. Looking at the middle panel of Figure 5.10 we can see that if we focus at the peak in contrast for 2cpd this would result in a dramatic reduction in contrast at 16cpd. However, if we were to focus at the peak contrast for 16cpd, the reduction in contrast at 2cpd would be much less dramatic.

5.2.3 Accounting for Monochromatic Aberrations

All of the simulations described so far have been based on a model eye that is diffraction limited (other than the LCA and induced defocus). However, real eyes also have monochromatic aberrations, which generally reduce the quality of the retinal image and increase the depth of field.

We measured the monochromatic aberrations up to and including the 4th order for 3 of the participants. We then reran the simulations both for maximising VSR and for maximising contrast at discrete spatial frequencies for each of these sets of aberrations.

For this set of simulations we also made another alteration, aimed at making the results more realistic. All of the simulations described above were

for a fixed pupil size of 5mm. However, measures of the participants' pupil sizes during the experiment indicate that they varied for the different spectra. The average pupil size across participants for each of the spectra is shown in Figure 5.12. These changes in pupil size with the changing spectra make sense because although we equated the luminance for the different spectra, the pupillary light reflex has been shown to have different spectral response characteristics than the luminance channel (Bouma, 1962; Gamlin et al., 2007). In order to account for this we used the average pupil size for each test spectrum for each observer as the baseline pupil size in these simulations.

Pupil size is also known to change with accommodation. Therefore, if the different defocus values are to represent different accommodation values, the simulated pupil size should also change with defocus. Plainis et al. (2005) found that the pupil constricts by 0.18mm for every dioptre of accommodation. We used this value to vary the pupil size with defocus from the baseline for each spectrum in the simulations.

Spherical aberration has also been found to vary systematically with accommodation, becoming more negative as accommodation increases. Plainis et al. (2005) found that spherical aberration varied linearly with accommodation for all subjects. They found the average change in spherical aberration to be 0.048 µm per dioptre of accommodation. We used this value to predict changes in spherical aberration away from a baseline determined by the observers' measured spherical aberration in our simulations.

Visual Strehl Ratio

Here the simulation results are shown for maximising VSR with monochromatic aberrations.

As well as the alterations described above, with these VSR simulations the MTF was weighted by the spatial frequency content of the Maltese cross stimulus in addition to the nCSF.

Figure 5.13 shows the visual Strehl ratios for the blue and red mixture with the aberrations and pupil sizes measured from observer 1. The main difference between these results and those without monochromatic aberrations shown in Figure 5.7 is that the curves are broader and the two peaks are not so distinct. This is because monochromatic aberrations increase the depth of field.

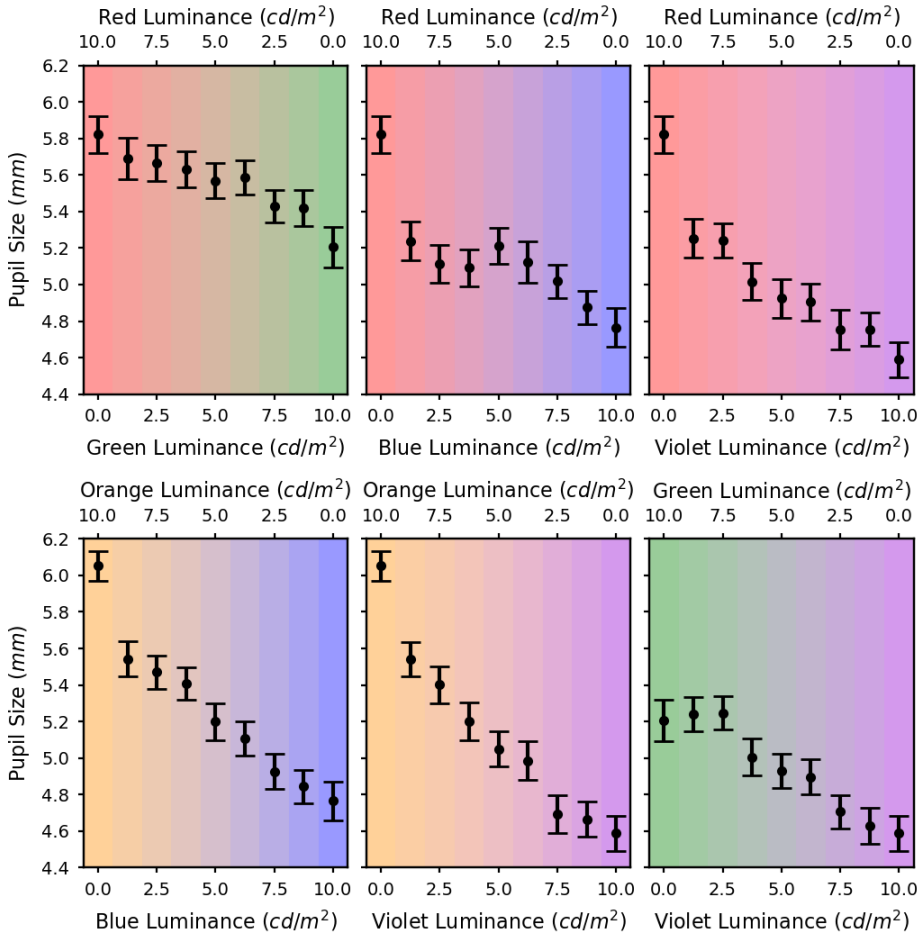

Figure 5.12: The average pupil size across all observers for each of the LED mixtures. The x axis represents the luminances of the two LED sources. The different graphs are for the different LED pairs: red and green (top left), red and blue (top middle), red and violet (top right), orange and blue (bottom left), orange and violet (bottom middle), and green and violet (bottom right). The error bars show the standard error of the mean.

The same simulations were also run for all of the other LED mixtures. The main difference between the different LED combinations was that the greater the dioptric separation between the two peak wavelengths due to LCA, the more of a dip in image quality could be seen between the two peaks, and the smaller the dioptric separation, the more the peaks merged into one. However, it is worth noting here that even in cases where there are two peaks with a dip in VSR in between, this dip is very subtle so there would not be a dramatic

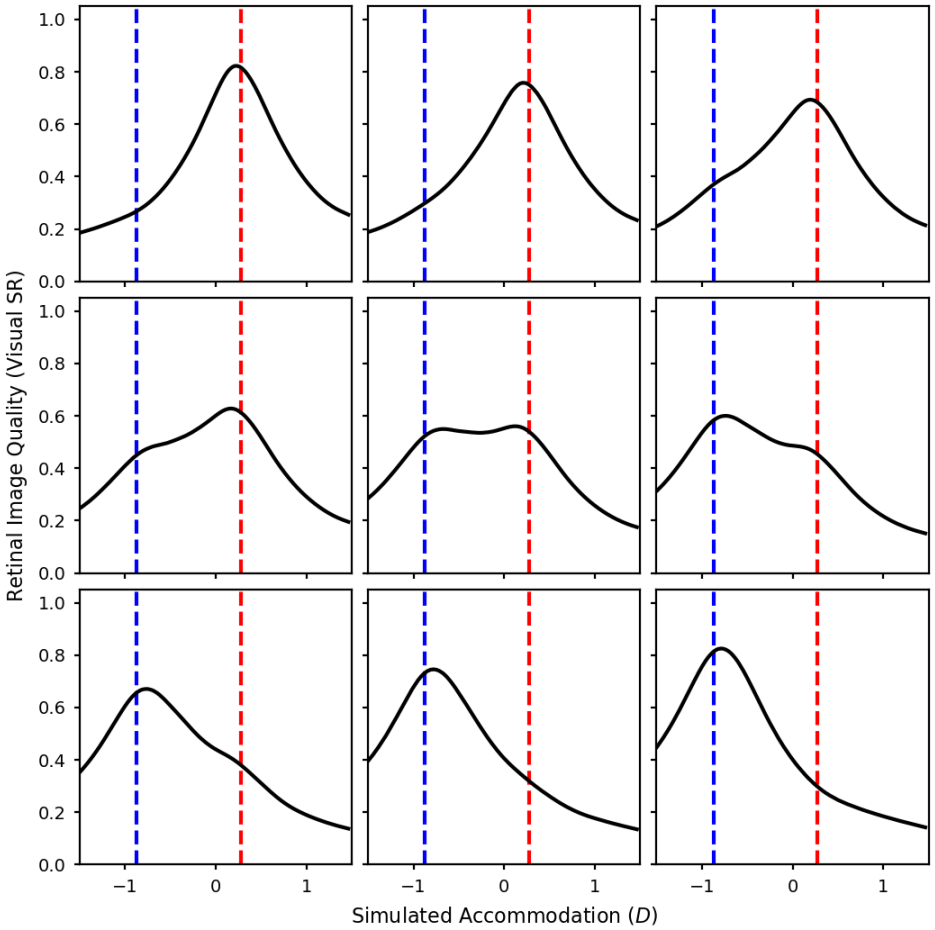

Figure 5.13: Visual Strehl ratios calculated from a wave optics model of the eye with the monochromatic aberrations for Participant 1 over a range of defocus values. The visual Strehl ratios were calculated from polychromatic MTFs weighted by each of the test spectra and the luminous efficiency function. The test spectra are mixtures of the red and blue LEDs. The luminance ratio of these two sources was varied in nine equal steps from completely red (top left) to completely blue (bottom right). The red and blue dashed lines indicate the accommodative response needed to correct the LCA at the peak wavelengths of the red and blue LEDs.

reduction in image quality if the participants were to accommodate in the middle of the two peaks.

Figure 5.14 shows the predicted focus for each of the LED mixtures based on maximising the visual Strehl ratio with the aberrations measured from

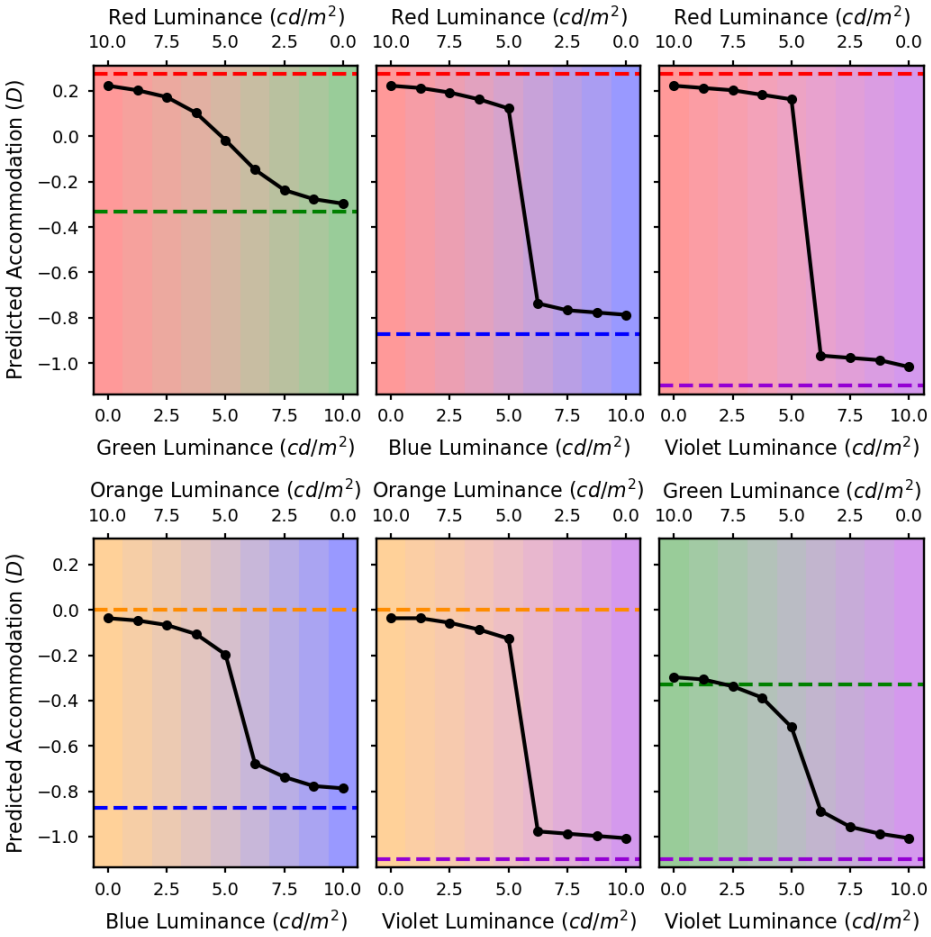

Figure 5.14: The predicted accommodation responses for maximising visual Strehl ratio in the luminance channel with the monochromatic aberrations for Participant 1. The x axis represents the luminances of the two LED sources. The different graphs are for the different LED pairs: red and green (top left), red and blue (top middle), red and violet (top right), orange and blue (bottom left), orange and violet (bottom middle), and green and violet (bottom right). The dashed lines indicate the accommodative response needed to correct the LCA at the peak wavelengths of the LEDs.

observer 1. In comparison to the predicted accommodation responses with no monochromatic aberrations shown in Figure 5.8, these are generally less step like and there is a smoother transition across the mixtures for each of the LED pairs. However, at least for the red and blue, red and violet, and orange and violet LED pairs, the position of optimal focus is still always closer to one or

other of the LEDs and never directly in the middle.

These same simulations were also run using the measured aberrations and pupil sizes of two other participants. The results of these are shown in the Appendix C. The pattern of results for each of these was very similar to those shown above for Participant 1. The main difference for the other two participants was that the curves were even smoother with less of a dip in image quality between the two peaks.

For Participant 5 it is also clear that there is an offset between the two peaks in image quality and the expected best focus for the peak wavelengths of the two LEDs. The most likely explanation for this is that certain aberrations interact with defocus so that the optimum image quality no longer corresponds to the minimum amount of defocus. For example, in an eye with positive spherical aberration, the image quality is better when there is also some positive defocus rather than no defocus. The dotted lines indicate where the defocus will be zero for the peak wavelengths of the two LEDs. However, when monochromatic aberrations are present the optimum defocus at a given wavelength needed for that wavelength to be in focus may be different from 0 D.

If we compare these predicted accommodation values with the actual measured accommodation responses they are slightly more similar than the equivalent predicted accommodation for maximising VSR without monochromatic aberrations. However, generally, if the participants were accommodating to maximise image quality we still would not expect them to accommodate right in the middle of the two LEDs. It is however worth noting that once the monochromatic aberrations have been taken into account, accommodating in between the two LEDs does not have as detrimental an effect on image quality as was initially thought.

Contrast Ratios

Figure 5.15 shows the simulated contrast ratios at a series of spatial frequencies calculated with the aberrations and pupil sizes measured from observer 1. As with the equivalent simulations without monochromatic aberrations shown in Figure 5.10 on page 95, at the higher spatial frequencies there are two distinct peaks in the contrast, corresponding roughly to the best focus positions for each of the two individual LEDs, while for the lower spatial frequencies, there is just a single peak in contrast which moves between the best focus positions

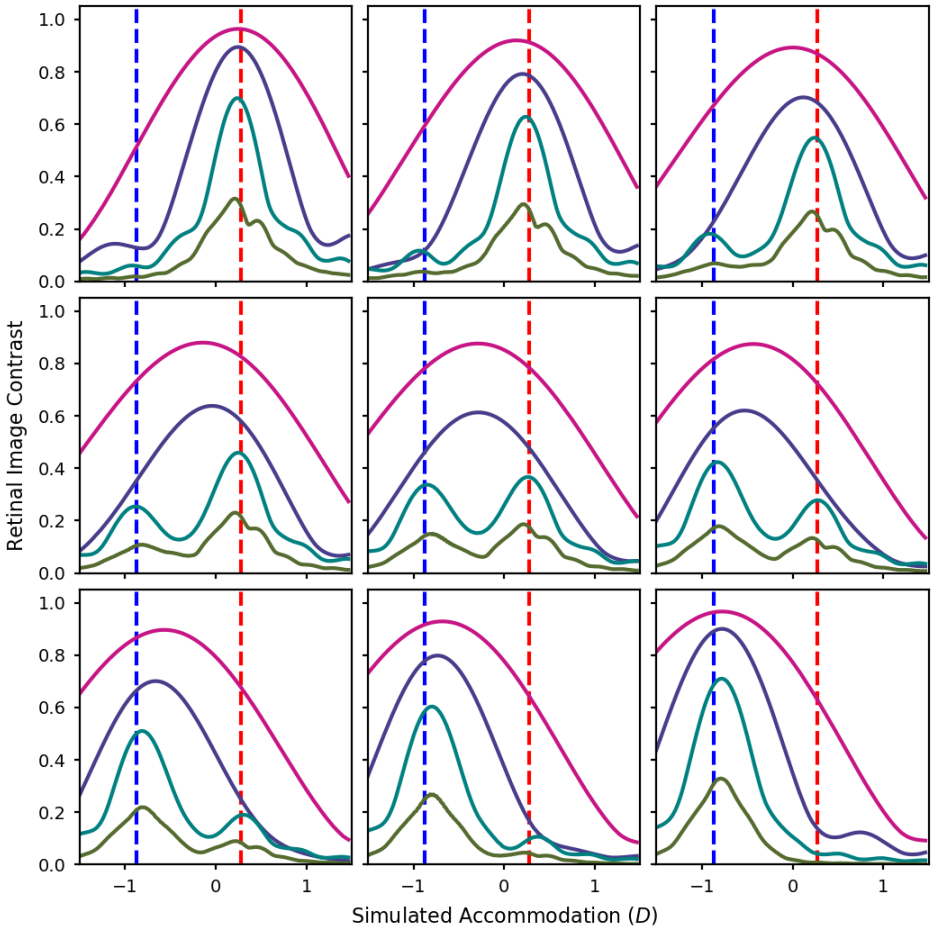

Figure 5.15: Contrast ratios calculated from a wave optics model of the eye with the monochromatic aberrations for Participant 1, over a range of defocus values, at 2 (magenta), 4 (purple), 8 (cyan), and 16 (green) cpd. The contrast ratios were calculated from polychromatic MTFs weighted by each of the test spectra and the luminous efficiency function. The test spectra are mixtures of the red and blue LEDs. The luminance ratio of these two sources was varied in nine equal steps from completely red (top left) to completely blue (bottom right). The red and blue dashed lines indicate the accommodative response needed to correct for the LCA at the peak wavelengths of the red and blue LEDs.

for each of the two individual LEDs as the luminance ratios are changed. The most noticeable difference when the monochromatic aberrations are included is that the shapes of the curves are different at the higher spatial frequencies with reduced and less well defined peaks in contrast.

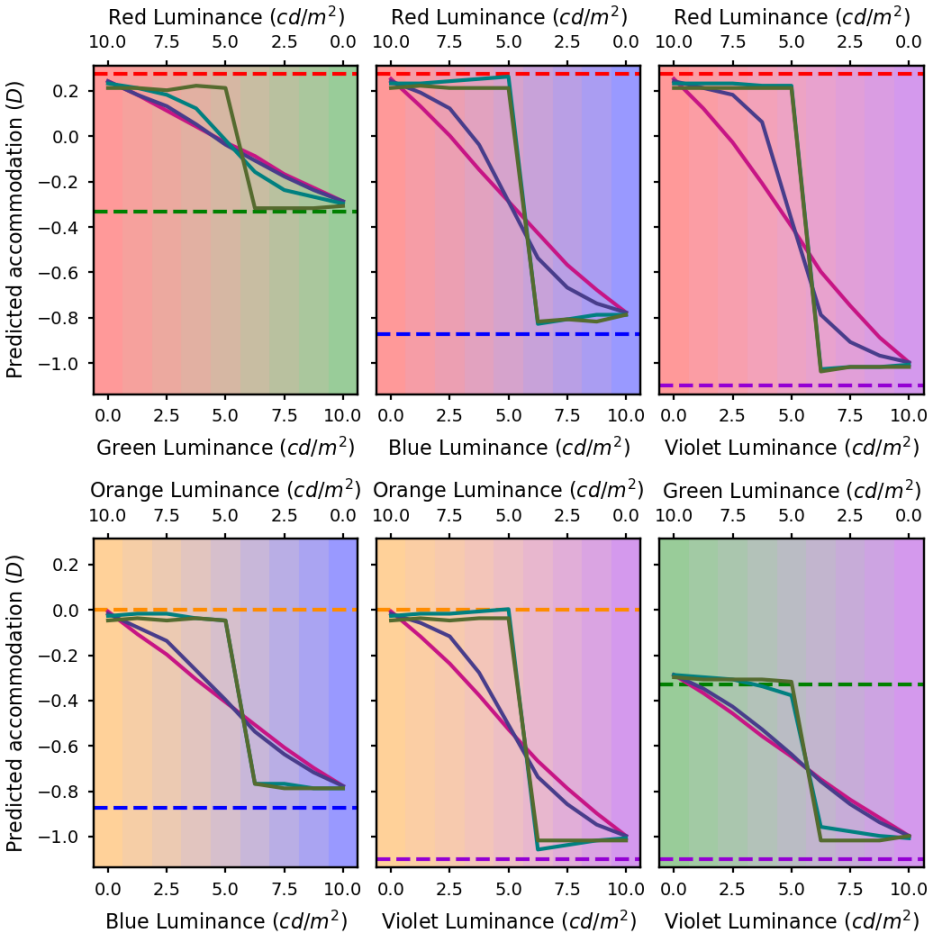

Figure 5.16: The predicted accommodation responses for maximising retinal image contrast in the luminance channel for spatial frequencies of 2 (magenta), 4 (purple), 8 (cyan), and 16 (green) cpd with the monochromatic aberrations for Participant 1. The x axis represents the luminances of the two LED sources. The different graphs are for the different LED pairs: red and green (top left), red and blue (top middle), red and violet (top right), orange and blue (bottom left), orange and violet (bottom middle), and green and violet (bottom right). The dashed lines indicate the accommodative response needed to correct the LCA at the peak wavelengths of the LEDs.

The contrast ratios were also calculated in the same way for each of the other LED combinations. The general pattern was the same in all cases. For each spectrum the predicted focus position was taken for each spatial frequency as the defocus position resulting in the peak contrast at that spatial frequency.

These predicted focus positions are shown in Figure 5.16. If we compare these to the predictions without monochromatic aberrations in Figure 5.11 they are actually very similar. This means that it is the lower spatial frequencies of 2cpd and 4cpd that are the best predictors of the actual accommodation responses.

In this case there was a lot more variation in the predicted accommodation depending on which observers aberrations were used. In the case of Participant 4 the predicted responses as a function of luminance ratio were generally a lot smoother with less of a defined step at the higher spatial frequencies. In the case of Participant 5 on the other hand, there were still clear steps in the predicted accommodation at the higher spatial frequencies. However, as the spatial frequency increased, all of the predicted accommodation positions also seemed to increase. We suspected that this was due to the interaction between the higher order aberrations and defocus.

As was mentioned in the previous section, certain aberrations interact with defocus in such a way that in an eye with those aberrations the defocus value that optimises image quality is not 0 D. We will refer to the level of defocus that optimises image quality in these cases as the baseline defocus. The findings for Participant 5 seem to indicate that this baseline defocus is dependent not only on the monochromatic aberrations present, but also on the spatial frequency. To test this we ran another simulation with just 0.2 µm RMS spherical aberration and a varying level of defocus and calculated the contrast ratio at a series of spatial frequencies for each defocus value. We found that even in this simplified case, the optimal defocus value changed with spatial frequency. Figure 5.17 shows the results of this simulation. This effect has been reported before by Green and Campbell (1965). This is an interesting finding as we had assumed that in general the higher and lower spatial frequencies should agree on the position of best focus and therefore that any apparent disagreement would usually be due to the higher spatial frequency information being unreliable at higher levels of defocus. However, these findings suggest that with sufficient spherical aberration (and possibly other aberrations too) there can be a disagreement in the best focus positions for the high and low spatial frequencies even with monochromatic light where LCA has no effect. Given that spherical aberration has been shown to change by approximately 0.048 µm per dioptre of accommodation (Plainis et al., 2005), this is likely to

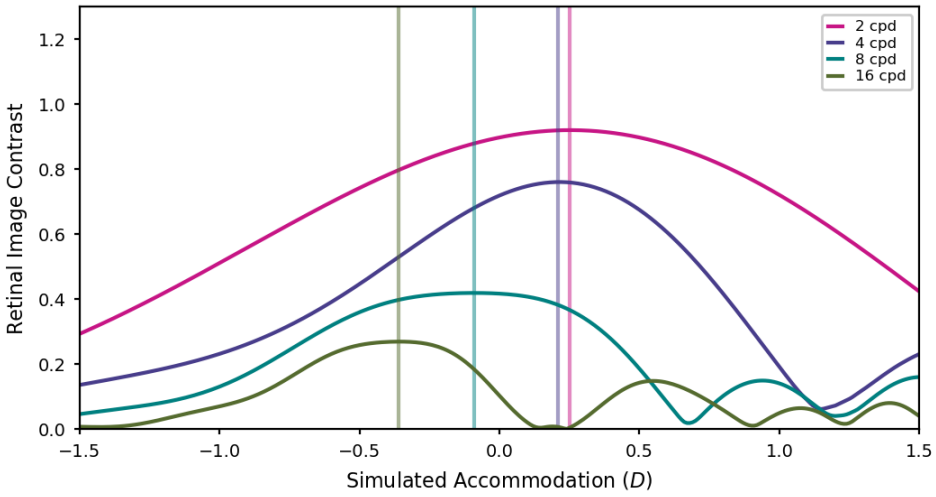

Figure 5.17: The retinal image contrasts calculated for an eye with 0.2 µm RMS spherical aberration and defocus ranging from -1.5 to 1.5 D. The calculations were made for monochromatic 580nm light and a 5mm pupil. The retinal image contrast is plotted for 2, 4, 8, and 16cpd. The vertical lines indicate the defocus values resulting in the optimal contrast at each of the four spatial frequencies.

affect most people. This means that the assumption that generally a conflict between the apparent directions for accommodation at high and low spatial frequencies indicated that the high spatial frequencies were incorrect may be false. In fact there may be many cases in which the high and low spatial frequencies really do have different optimal responses.

5.2.4 Using LCA as a cue

For the simulations described above we have made the assumption that the visual system is able to find the point at which the contrast or the overall image quality is at its highest. However, it is likely that instead of maximising contrast or image quality directly, the visual system uses some other rule to estimate the optimal accommodation response. If the eye was using microfluctuations or monochromatic aberrations as a cue to accommodation, we would expect these to be just as effective under the experimental spectra as under normal lighting conditions. This is because these two types of cue are not wavelength dependent. However, if they were using a cue provided by the LCA of the eye, it may not be so effective for the experimental spectra as it is

wavelength dependent. Therefore, it is possible that under the experimental conditions this cue would not lead to a good approximation for the point of best focus. In this section simulations are described to explore where people might accommodate to the experimental stimuli if they were using LCA as a cue.

Under natural circumstances objects in the environment tend to be illuminated by relatively smooth, broadband spectra. In these cases we can imagine that the optimal accommodation response would involve focussing in the wavelength range that we are most sensitive to (i.e. wavelengths around the peak of $V(\lambda)$). Because $V(\lambda)$ is a combination of the spectral sensitivities of the L and M cones, this means that the ideal focus point would probably be somewhere in between the optimal focus for the L cone channel and the optimal focus for the M cone channel. Therefore, the point at which the image quality or contrast in the L and M cone channels is roughly balanced may provide a good approximation for the optimal focus position for natural illuminants. This will be referred to as the EquateLM rule. If the eye is focussed in front of this then the image quality or contrast would be better in the L cones than the M cones and if the eye is focussed behind this then the image quality or contrast would be better in the M cones than the L cones. A model along similar lines to this was proposed by Flitcroft (1990).

Here I will not go into what exact comparison the visual system may be able to make or how this comparison might be implemented. Instead I will just use the points at which the image quality or contrast in the L and M channels are equal as a rough guide to where the eye might accommodate if it was LCA driving that accommodation response.

Comparing image quality for L and M cone channels

The simulations described in this section were run in a similar way to those for maximising overall image quality described above. However, instead of weighting the spectra by the luminous efficiency function, they were weighted by the L and M cone spectral sensitivities. Then, instead of finding the peak to predict accommodation, we found the point at which the image quality values for the L and M cones crossed over. In cases where there were multiple crossings, this was treated as ambiguous and there were multiple possible focus predictions.

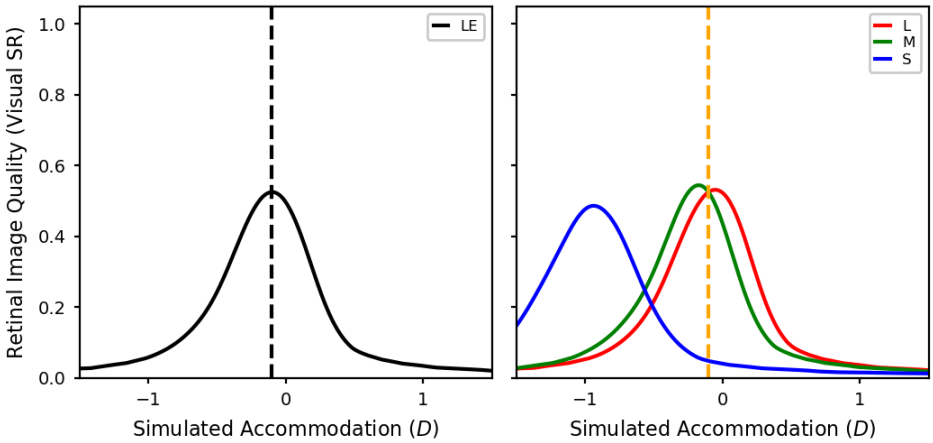

Figure 5.18: The visual Strehl ratios for a range of defocus values with a D65 spectrum. The solid black line in the left graph shows the simulated visual Strehl ratio as a function of defocus for the standard D65 spectrum weighted by the luminous efficiency function. The black dotted line indicates the peak of this function and therefore the predicted accommodation response if the accommodation system were to maximise the visual Strehl ratio in the luminance pathway. The solid red, green and blue lines in the graph on the right show the simulated visual Strehl ratio for the standard D65 spectrum weighted by the L, M, and S cone spectral sensitivities respectively. The dashed orange line indicates the defocus value at which the visual Strehl ratio is equal in the L and M cone channels and therefore the predicted accommodation response for a visual system equating image quality in the L and M cone channels. All of these simulations are for an eye with natural LCA and a 6mm pupil.

Before running the simulations for our test spectra we tested the assumption that the EquateLM rule would provide a good approximation for maximising image quality in the luminance channel under natural illuminants. This is because it is natural illuminants such as skylight that humans have been exposed to as we've evolved so it makes sense that any rule used by the visual system to accommodate should be effective under these spectra. In order to do this we compared the simulated accommodation needed to equate L and M image quality with the simulated accommodation needed to maximise image quality in the luminance channel with the D65 illuminant spectrum (the CIE standard daylight).

The left panel of Figure 5.18 shows the VSR for the D65 illuminant spectrum weighted by $V(\lambda)$ as a function of defocus. The dashed vertical line shows

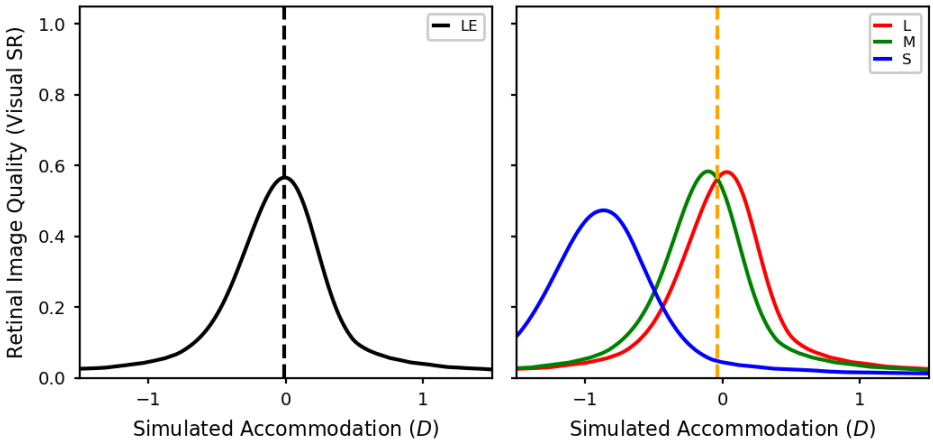

Figure 5.19: The visual Strehl ratios for a range of defocus values with the Illuminant A spectrum. The solid black line in the left graph shows the simulated visual Strehl ratio as a function of defocus for the standard Illuminant A spectrum weighted by the luminous efficiency function. The black dotted line indicates the peak of this function and therefore the predicted accommodation response if the accommodation system were to maximise the visual Strehl ratio in the luminance pathway. The solid red, green and blue lines in the graph on the right show the simulated visual Strehl ratio for the standard Illuminant A spectrum weighted by the L, M, and S cone spectral sensitivities respectively. The dashed orange line indicates the defocus value at which the visual Strehl ratio is equal in the L and M cone channels and therefore the predicted accommodation response for a visual system equating image quality in the L and M cone channels. All of these simulations are for an eye with natural LCA and a 6mm pupil.

the predicted accommodation if the VSR was optimised for the luminance channel, which is at -0.100 D. The right panel of Figure 5.18 shows the VSR for the D65 illuminant spectrum weighted by the L, M, and S cone sensitivities as a function of defocus. The orange dashed line shows the predicted accommodation for the EquateLM rule for VSR, which is at -0.102 D, almost identical to the accommodation value required to optimise image quality in the luminance channel.

Figure 5.19 is equivalent to Figure 5.18 just using the CIE standard Illuminant A instead of D65. Here the predicted accommodation responses for the two rules are also very similar. This suggests that the EquateLM rule is not just effective for D65 but also for other common broadband spectra. Given that

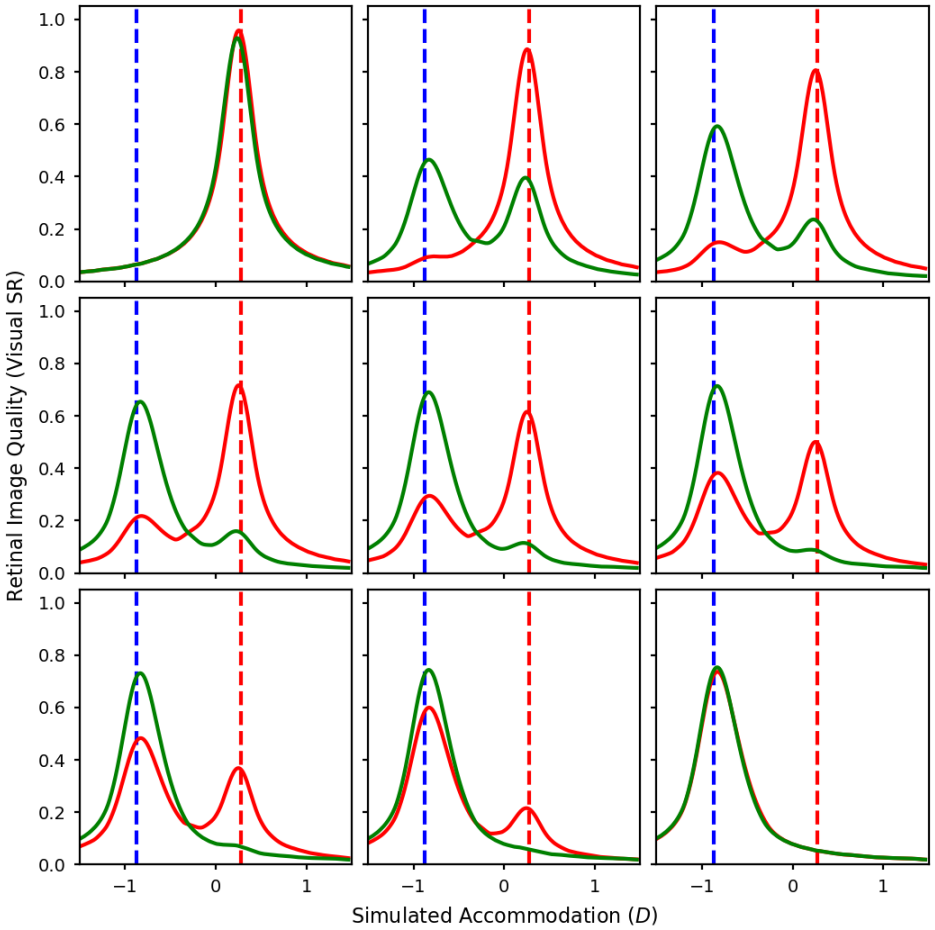

Figure 5.20: Visual Strehl ratios calculated from a wave optics model of the eye with a 5mm pupil over a range of defocus values. The visual Strehl ratios were calculated from polychromatic MTFs weighted by each of the test spectra and the L (red) and M (green) cone spectral sensitivities. The test spectra were made up of the spectra of the red and blue LEDs. The luminance ratio of these two sources was varied in nine equal steps from completely red (top left) to completely blue (bottom right). The red and blue dashed lines indicate the accommodative response needed to correct for the LCA at the peak wavelengths of the red and blue LEDs.

the EquateLM rule seemed to give a good approximation for maximising the image quality in the luminance channel under natural illuminants. We used this rule to predict where people would accommodate for the experimental stimuli.

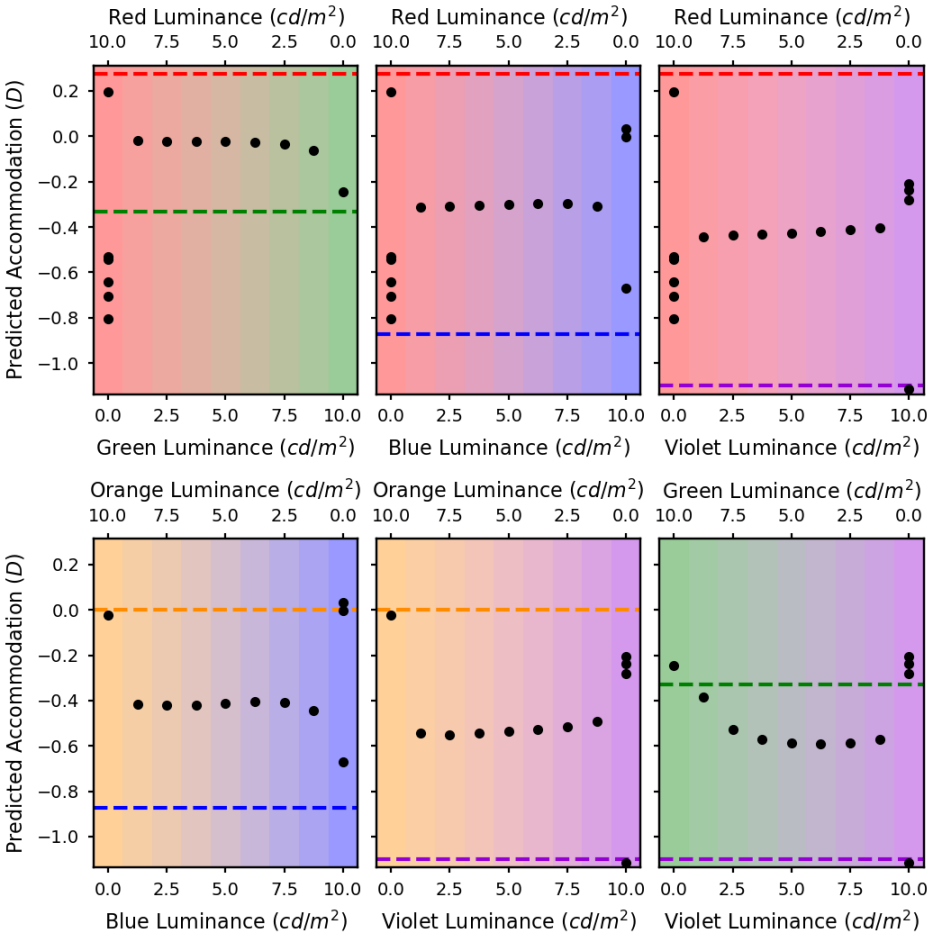

Figure 5.21: The predicted accommodation responses for equating visual Strehl ratio in the L and M channels with a 5mm pupil. The x axes represent the luminances of the two LED sources. The different graphs are for the different LED pairs: red and green (top left), red and blue (top middle), red and violet (top right), orange and blue (bottom left), orange and violet (bottom middle), and green and violet (bottom right). The dashed lines indicate the accommodative response needed to correct the LCA at the peak wavelengths of the LEDs.

Figure 5.20 shows the VSR in the L and M cone channels for each of the mixtures of the red and blue LEDs. For the red and blue LEDs on their own, shown in the top left and bottom right panels respectively, it is clear that the image quality in the L and M channels is almost identical at all defocus values. This indicates that in cases where the illumination is monochromatic or very

narrowband, LCA cannot provide useful cues to accommodation. For the mixtures, there are two peaks in image quality for both the L and the M cone channels, one corresponding to the blue LED and the other to the red LED. However, the blue peak is more pronounced in the M cone channel as this is more sensitive to shorter wavelengths and the red peak is more pronounced in the L cone channel as this is more sensitive to longer wavelengths. For the mixtures the image quality in the two channels always seems to cross almost directly in the middle of the two peaks.

The black filled circles in Figure 5.21 show the predicted accommodation responses for each of the experimental stimuli for the EquateLM rule with VSR. For some of the stimuli there were multiple crossings, which are shown as multiple predicted accommodation responses. For the individual LEDs there are often multiple crossings as the image quality is very similar for the two cone channels at all defocus values. Therefore, for the individual LEDs it is not clear where observers would accommodate if they were using the EquateLM rule. However, for the mixtures, the predicted accommodation response tends to be almost exactly in between the peak wavelengths for the two LEDs regardless of the relative luminances of the two LEDs. Therefore, the predicted image quality with the EquateLM rule corresponds to a dip in overall image quality.

If we compare the simulation results in Figure 5.21 to the actual measured results it seems that the predicted accommodation responses don't fit the actual responses particularly well. This is because for the actual measured values the accommodation responses for the mixtures depend on the relative luminances of the two LEDs with a gradual slope in accommodation as the relative luminance changes. However, for the EquateLM rule the predicted focus position for the mixtures seems to be largely independent of the relative luminances of the two LEDs.

5.3 Conclusion

When viewing stimuli with spectra composed of two distinct peaks at distinct wavelengths, the static accommodation response tends to fall somewhere in the middle of that for each of the two peaks on their own. The focus position also changes as a function of the relative intensities of the two peaks. This

aligns relatively well with the findings of MacKenzie and Watt (2010) for multiplane displays.

Simulations were run to predict the accommodation responses for the following three rules:

1. maximising the overall image quality in the luminance pathway,
2. maximising the contrast at a specific spatial frequency,
3. or equating the image quality in the L and M channels.

Out of all of these it seemed to be maximising the contrast at lower spatial frequencies (e.g. 2 and 4cpd) that best fitted with the observed accommodative response. However, it is worth noting that once the monochromatic aberrations were accounted for, the predicted accommodation positions for maximising the overall image quality in the luminance pathway did not provide such a bad fit to the data.

These findings suggest that the accommodation responses for these chromatic stimuli made up of two distinct wavelength peaks do not generally optimise the overall image quality and may optimise the contrast at low spatial frequencies at the expense of higher spatial frequencies. It may be that, because the depth of focus is increased by the monochromatic aberrations of the eye, this does not have a major affect on visual acuity. However, it is still something that warrants further investigation and something that we may want to consider when designing and selecting lighting and display primaries.

Chapter 6

Is it possible to realistically render blur?

There are two different ways of presenting blurred stimuli. Firstly, the blur can be introduced optically, so that it interacts naturally with the aberrations of the observers eye. For example, this can be done using lenses or a deformable mirror, or even by simply altering the distance between the target and the observer. In this chapter I will refer to blur introduced in this way as optical blur (it has also been described as "observer blur" in past literature). Alternatively, the blur can be rendered in the stimulus itself, for example by convolving the stimulus with a blur disc or point spread function (PSF). The blur presented by this second method will not interact naturally with the aberrations of the eye and may not result in a realistic retinal image depending on how the blur is rendered. In this chapter I will refer to this as rendered blur (it has also been described as "source blur" in some papers).

It would be very useful to be able to render blur realistically as an alternative to introducing the blur optically. This is because in many ways it is simpler to render blur than to optically induce blur. Optically blurring a stimulus requires specialised equipment such as lenses or a deformable mirror. There is also the issue that the eye can accommodate to counteract the optically induced defocus blur meaning that often the accommodation of the eye will need to be controlled or prevented to get the desired blurred image on the retina. Typically, optically blurred images can also only be presented to one observer at a time as the observer will need to be aligned with the optical

set-up. Rendered blur, on the other hand, could potentially avoid these complications.

The ability to render blur effectively could be useful in creating realistic simulations of scenes (e.g. for virtual reality). In real scenes not all objects will be in focus at one time. Therefore to make a two dimensional scene appear realistic the objects that are not in the focal plane will need to be blurred. It may be that the more realistic this blurring is, the more realistic the scene appears to be. In fact Cholewiak et al. (2017) found this to be the case when the rendered blur in a scene was made more realistic by including the chromatic aberration of the eye.

Creating realistic blur could also be useful in more clinical settings. For example, when fitting glasses, contact lenses, or even intra-ocular lenses, it could allow patients to view how certain types of optical correction might affect their vision before they are manufactured and, in the case of intra-ocular lenses, inserted.

Making comparisons between optical and rendered blur is also of interest from a more theoretical perspective. By exploring which factors must be accounted for in order to render blur realistically, we can develop an understanding of how much of an impact different optical features have on our perception of blur and our visual acuity (VA), and which types of blur we are more able to tolerate. It may also give us an insight into which features improve the eye's tolerance to blur.

6.1 Previous Studies

A number of previous experiments have been conducted comparing the effects of optical and rendered blur on VA (Smith et al., 1989; Jacobs et al., 1989; De Gracia et al., 2009; Dehnert et al., 2011; Ohlendorf et al., 2011; Remón et al., 2014). The general trend in these studies has been that we appear to be more tolerant to optical blur than rendered blur, with rendered blur reducing the VA more than the supposedly equivalent amount of optical blur. However, this effect was not always significant.

We have created a table to summarise a selection of previous studies (Table 6.1). This table is colour coded according to whether or not a significant difference was found between rendered and optical blur. The ones highlighted in green

Table 6.1: Summaries of a selection of previous studies. The table is colour coded to indicate whether a significant difference was found in the effect on VA between the two blurring methods. Green indicates that there was a significant difference found, red indicates that there was no significant difference found and orange indicates that there were mixed results with significant effects found for some experiments but not others.

	Smith et al. (1989)	**Jacobs et al. (1989)**	**De Gracia et al. (2009)**	**Dehnert et al. (2011)**	**Ohlendorf et al. (2011)**	**Remón et al. (2014)**
Significant difference	Yes • VA sig. worse for ren blur	Mixed • **Blur threshold:** Sig less ren blur needed • **Blur JND:** No	Yes • VA sig. worse for ren blur	No	Mixed • **Defocus:** No • **Astigmatism:** VA sig worse for ren blur • **Cross-cylinder:** VA sig. worse for ren blur	Mixed • **Defocus:** No • **Astigmatism:** Sig less ren blur needed • **Mixed astigmatism:** Sig less ren blur needed
Stimuli	Landolt C	Landolt C	Landolt C	Landolt C	Landolt C	Landolt C
Type of blur	Defocus	Defocus	Natural aberrations	Defocus	Defocus and astigmatism	Defocus and astigmatism
Blur disc	Circular blur disc with uniform luminance	Circular blur disc with uniform luminance	Realistic PSF based on magnitude of aberrations and pupil size	Realistic PSF based on magnitude of aberrations and pupil size	Realistic PSF based on magnitude of aberrations and pupil size	Realistic PSF based on magnitude of aberrations and pupil size
Preventing accommodation	Cyclopleged for optical blur condition	Cyclopleged for optical blur condition	NA	Target at infinity	Target at 4m	Target at 5m
HOAs accounted for	No	No	Yes • Rendered HOAs • Corrected real HOAs for rendered blur	No	No	No
Stiles Crawford effect	NA	NA	Unknown	Yes	Unknown	Unknown
LCA accounted for	No	No	Unknown	Yes • Narrowband light	No	No
Pupil	Artificial pupil for optical blur	Artificial pupil for optical blur	Artificial pupil	Natural pupil	Artificial pupil	Natural pupil
Lens offset accounted for	NA	NA	NA	Yes • Accounted for difference in power due to offset	No	Unknown

found that the VA was significantly better for optical than rendered blur. The ones highlighted in amber found mixed results, with some experiments showing a significant difference between rendered and optical blur and others showing no significant difference. However, for all of the studies highlighted in amber, the trend, even in the non-significant experiments, was for rendered blur to reduce VA more than optical blur. The Dehnert et al. (2011) study, highlighted in red, is the one exception to this rule. In this study no significant effect was found, and VA was actually slightly better for rendered blur than for optical blur, which is opposite from the trend shown by the other studies.

Another trend from this data is that there was a greater difference between optical and rendered blur for astigmatism than for defocus. Both Ohlendorf et al. (2011) and Remón et al. (2014) found significant effects for astigmatism

and astigmatism plus defocus. However, for defocus alone the results were not generally significant. Dehnert et al. (2011) only investigated defocus and not astigmatism. This could help to explain the differences in their findings from other studies.

In the cases where rendered blur reduced VA more than optical blur, there must have been some aspect of the optically induced blur not captured by those methods for rendering blur, making us more tolerant to the optical blur. Smith et al. (1989) and Jacobs et al. (1989) used a simple blur disc with a uniform luminance as the blur kernel. This is quite different from the actual PSF of an eye and therefore it is not surprising that there was a discrepancy between the effects of the rendered and optical blur. De Gracia et al. (2009), Dehnert et al. (2011), Ohlendorf et al. (2011) and Remón et al. (2014), on the other hand, all generated PSFs based on the magnitude of the defocus (or astigmatism) and the pupil size. It is therefore necessary to investigate further why all but Dehnert et al. (2011) still found a significant difference between the effects of optical and rendered blur. A number of different factors have been suggested as the cause for this discrepancy. These possible factors are discussed below.

1. One possible explanation is that the observers were able to partially accommodate to the stimuli. This could have reduced the blur from the optical defocus and also potentially from the optical astigmatism. Three of the experiments described above did not paralyse the accommodation, and instead relied on the stimulus being presented at or near the far limit of the observers' accommodative range (Dehnert et al., 2011; Ohlendorf et al., 2011; Remón et al., 2014). However, if this distance was incorrect then the observer may have been able to reduce the optical blur by accommodating. Accommodating differently to the rendered stimulus, on the other hand, would not reduce the blur at all as optical defocus can only add to the rendered blur and cannot cancel it out. Remón et al. (2014) presented their stimuli at a distance of 5m, which is 0.2 dioptres (D) from infinity. Similarly, Ohlendorf et al. (2011) presented their stimuli at 4m distance from the observer which is 0.25 D from infinity. Dehnert et al. (2011), on the other hand, accounted for the screen distance in the correction of the refractive error of the eye so that (assuming the refractive correction was correct) the screen was actually at

the limit of the observer's accommodation. It may be that this explains why there was no significant difference between the two types of blur in the Dehnert et al. (2011) study but there was in both the Ohlendorf et al. (2011) and Remón et al. (2014) studies where the stimulus wasn't quite at infinity, leaving room for some residual accommodation.

2. The human eye also has microfluctuations in accommodation, meaning that the accommodative state is not constant even when the eye is fixated at a single distance. It could be that even if the stimulus is aligned to the average far point of the observer's accommodative range, the microfluctuations in one direction actually reduce the optical blur.

3. In three of the studies described above, the optical blur was introduced by placing a lens in a trial frame worn by the observer. These lenses were between 10mm and 16mm away from the cornea and therefore they were not actually in the pupil plane. This means that the aberrations of the lens would not simply add to the aberrations of the eye. Dehnert et al. (2011) placed the lenses at a distance of 16mm from the cornea and accounted for the difference in lens power due to the lens offset from the pupil plane by slightly altering the power of the actual lens so that the effective power for the eye was correct. For 8 D of defocus they actually used a 7 D lens and for the 4 D condition they used a 3.75 D lens. Neither Ohlendorf et al. (2011) or Remón et al. (2014) included an equivalent correction, although they did also have shorter distances between the cornea and the lens of 10mm and 12mm respectively. It is possible that this is one of the factors contributing to the significant effects found in the Ohlendorf et al. (2011) or Remón et al. (2014) studies. Perhaps there was a difference between optical and rendered blur because the optical blur they were introducing was not of the right magnitude due to the offset of the lens from the pupil plane.

4. The separation between the lens and the pupil plane can also cause magnification effects. If this was not accounted for then these magnification effects would affect the retinal image in the optical blur condition but not in the rendered blur condition and therefore may cause some discrepancy between the two conditions. It seems that neither Ohlendorf et al. (2011), Dehnert et al. (2011), or Remón et al. (2014) accounted for

the magnification effects. Ohlendorf et al. (2011) calculated these magnification effects as being less than 5% and concluded that they should not have a significant impact. It therefore seems unlikely that this could account for the significant effects found in the Ohlendorf et al. (2011) and Remón et al. (2014) studies.

5. Most of the studies described above did not account for the longitudinal chromatic aberration (LCA) of the eye so the LCA may have affected the optical blur but not the rendered blur. Because the LCA of the eye increases its depth of field this could help to explain why the VA was better for the optical blur. In fact, one of the differences between the Dehnert et al. (2011) experiment and other similar experiments was that they accounted for the effects of chromatic aberration by using a very narrowband source. It may be because chromatic aberration was not accounted for in other experiments, that there were significant differences between rendered and optical blur. Both Ohlendorf et al. (2011) and Remón et al. (2014) used a broadband light to present all of the stimuli but a monochromatic approximation to generate the PSF for the rendered blur stimuli.

6. The higher order aberrations of the eye also interact with the defocus and astigmatism. It has been shown that these higher order aberrations can increase the depth of focus of the eye (Zhai et al., 2014). Certain aberrations can also help to cancel out other aberrations. For example, it has been shown that when positive spherical aberration is present, the PSF is actually better when there is some positive defocus than when there is no defocus. However, these interactions can only occur with optical defocus. Therefore the higher order aberrations of the eye may interact with the optical defocus and possibly reduce its effect on VA, but the same effect would not be seen for rendered defocus. Ohlendorf et al. (2011) argued that this factor would be too small to explain the magnitude of the difference between the VA for rendered and optical blur found in their study. De Gracia et al. (2009) measured the actual aberrations of the observers' eyes and corrected these optically in the rendered case as well as rendering the images with these aberrations included and still found a significant difference between rendered and optical blur.

7. As well as the aberrations introduced by the eye, diffraction also has a blurring effect on the retinal image. In the case of the rendered blur, generally this diffraction effect is included in the generation of the PSF or blur disc. However, the blurred image is then viewed through the actual optics of the eye which means that the diffraction effects within the eye further distort the image. It may be that this double effect of diffraction reduces the VA in the rendered case to below that in the optical case. However, this effect would have been similar in the Dehnert et al. (2011), Ohlendorf et al. (2011), and Remón et al. (2014) studies. Therefore, it seems unlikely that this could be the main cause of the difference between the rendered and optical blur in the Ohlendorf et al. (2011) and Remón et al. (2014) studies.

8. The rendered stimuli have to be created for a particular pupil size. Some studies, such as Ohlendorf et al. (2011), used an artificial pupil in order to ensure the pupil size was correct and stayed constant. However, if an artificial pupil is not used then it is possible that the pupil size will vary in the optical condition or not be quite the same as that used to generate the PSF. The larger the pupil size is, the smaller the depth of field is, and the greater effect the defocus and other aberrations have on the retinal image. Dehnert et al. (2011) and Remón et al. (2014) used natural pupils and calculated the PSFs for the measured pupil size. Since Dehnert et al. (2011) did not control for the pupil size and found no significant difference between the two blur types it seems unlikely that this could explain the difference found in the Remón et al. (2014) study.

9. Another possible explanation is that the observers could have been squinting their eyes in the optical condition. This could have a similar effect to reducing the pupil size and therefore increase the depth of field and reduce the impact of the aberrated wavefront on the retinal image. In the Remón et al. (2014) study the participants were specifically instructed not to squint their eyes to try and see the stimuli better. However, even in this case it cannot be ruled out as a possibility.

10. When the PSFs are generated, various assumptions and approximations must be made. For example, if the PSF is generated using the wave-optics model, Fourier transforms must be taken. Generally this is done

using an fft (fast Fourier transform) which is an approximation of a true Fourier transform. The Fraunhofer approximations of diffraction are also inherent in the calculations of the PSFs. It may be that the approximations that go into the generation of the PSF cause the PSF to be inaccurate. However, the Dehnert et al. (2011), De Gracia et al. (2009), Ohlendorf et al. (2011), and Remón et al. (2014) studies all will have relied on these same (or similar) assumptions and therefore it seems that this cannot explain the significant findings of the De Gracia et al. (2009), Ohlendorf et al. (2011), and Remón et al. (2014) studies.

11. Even if the process by which the rendered blur was generated was perfect, there are still limitations as to how accurately the display can present these images. Firstly, the display will only have a limited dynamic range, which may mean that it looses some of the information in the original image. The display may also not be linear. This could mean that some parts of the image are brighter than they should be while other parts are dimmer than they should be. These factors of the display could result in differences between the rendered and optical blur. However, most of the studies described above did at least correct for the non-linearity of the displays.

It is worth noting that the fact that Dehnert et al. (2011) did not find any significant difference in VA between the optical and rendered blur does not necessarily mean that the rendered blur was accurate. In fact the two types of blur could still have looked completely different and just happened to have the same effect on VA. In order to ensure that the rendered blur is actually resulting in the same retinal image as the optical blur, a variety of tests using a variety of different stimuli would be needed. The two types of blur may happen to have the same effect on VA for a particular stimulus, but it is possible that this effect would not be robust for different types of stimuli and for different tasks. A subjective test of how similar the different types of blur look would also help to determine whether the rendered blur is equivalent to the optical blur.

6.2 Present Experiment

In this study we have conducted a series of experiments comparing rendered and optical blur for 1 D of defocus. We have investigated the impact of various factors including whether an artificial pupil is used, the use of a pinhole in the rendered condition, and the effect of including monochromatic aberrations in the rendering. In addition to the VA tests, we also conducted a subjective similarity test to check that the conditions that were having the most similar effects on VA were also subjectively the most similar.

There were three main experiments in this study. The first investigated the effects of artificial pupils, pinholes, and monochromatic aberrations on VA for both rendered and optically blurred stimuli. The second experiment, investigated the effect of rendering with the monochromatic aberrations in more detail. The final experiment was a similarity test to investigate which types of rendered blur were subjectively the most similar to the optical blur.

6.3 General Methods

6.3.1 Participants

A single participant participated in all of the experiments described below. This participant was female and 25 years old. The participant was also the experimenter. The ethics for this experiment were approved by the Department of Physics Ethics Committee at Durham University.

6.3.2 Apparatus

A DLP projector (Texus Instruments DLP LightCrafter Display 4710 EVM-G2) was used to present the stimuli to the observer. The primaries in this projector were not as narrowband as was required for the experiment. Therefore, in order to make the primaries narrower, a short pass filter (Omega Optical 535SP) was placed in front of the green LED within the body of the projector, and a multi bandpass filter (Chroma 69002m) was placed at the output of the projector. Figure 6.1 shows the spectra of the three projector primaries with both filters in place. The projector formed an image on a screen positioned 825mm away, as shown in Figure 6.2.

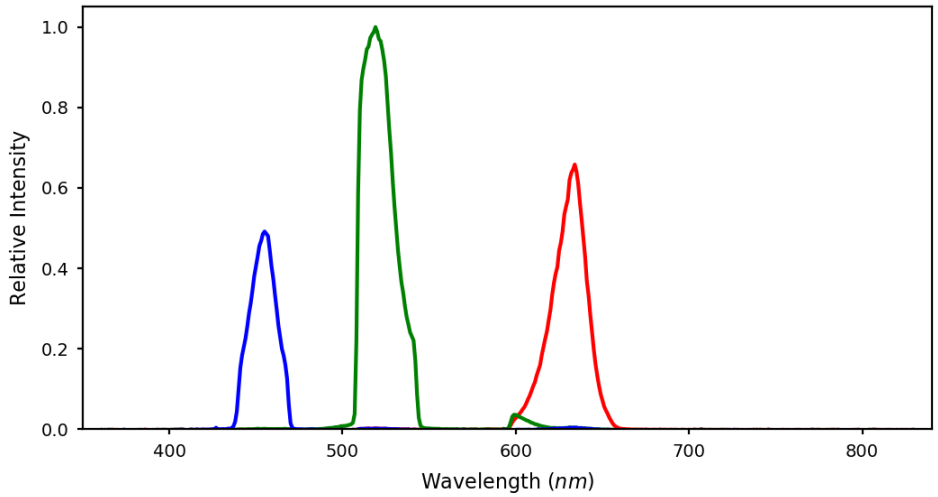

Figure 6.1: The spectra of the red, green, and blue projector primaries after passing through the filters.

The projector display was linearised for each of the colour channels separately. Firstly a ThorLabs power meter was used to measure the power of the light emitted by the projector for each primary at every intensity value from 0 to 255. At each intensity level the power was calculated as the average of 10 measures. These measured intensities were then used to make a lookup table to linearise the display. Figure 6.3 shows the linearity of the display after the linearisation with the lookup table.

The observer viewed the screen monocularly through a relay lens system. The relay was made up of two achromatic doublets with focal lengths of 150mm. The first was positioned 150mm from the observer's eye and the second was positioned 300mm from the first, resulting in a plane conjugate to the pupil at 600mm from the eye. These lenses were aligned in an interferometer to ensure the spacing was correct. This means there should be no unwanted magnification or defocus term introduced. A ThorLabs dual position slider was mounted in the conjugate pupil plane. A 1 D defocusing lens was mounted in one position of the slider and apertures could also be mounted in both positions of the slider depending on the condition. The lens (and any apertures) could then be switched in and out with a command from the computer running the experiment to switch between the optical and rendered blur conditions. Placing the lenses and apertures in the conjugate pupil plane eliminated any

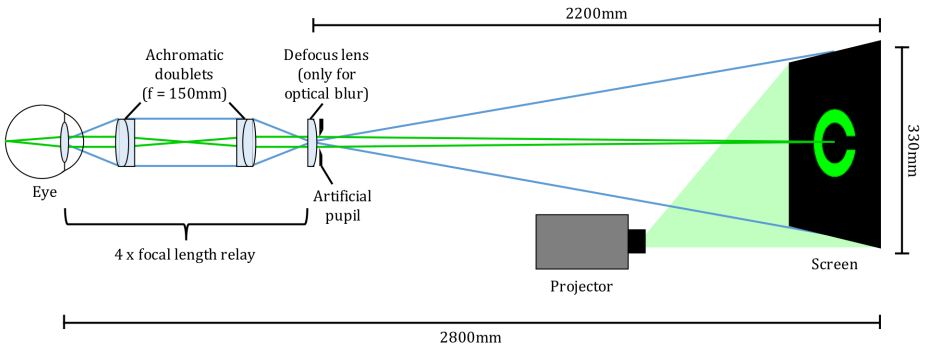

Figure 6.2: A diagram (not to scale) showing the optical layout for the experiments. The projector displayed the stimuli onto a screen at 2800mm from the observer. The observer viewed this screen through a relay lens system composed of two achromatic doublets with focal lengths of 150mm each. This resulted in a plane conjugate to the observer's pupil at 2200mm from the screen. In this plane either a defocus lens, or an artificial pupil, or both, could be placed and switched in and out during the course of the experiments using a ThorLabs dual position slider. The green lines indicate the path of the light from a point on the screen and the blue lines highlight the positions of the conjugate planes.

magnification effects or changes in power due to lens offset. In cases where an aperture and a lens were used they were placed as close as possible to the pupil plane so any offset was minimal. The set-up of the relay lens system is shown in Figure 6.2.

A chin rest was used to keep the observer's head still. To check that the observer was aligned with the relay lens system, the slider switched between a 1 D lens and no lens to ensure the observer could not detect any magnification difference. The observer always viewed the stimulus with her right eye and her left eye was covered with an eye-patch. The conjugate pupil plane was 2200mm from the screen meaning that, without a lens, the screen was at 0.45 D. The observer was slightly myopic and their latest prescription was 0.5 D for their right eye. Therefore, for the rendered case no lens was used and the screen was assumed to be at the far point of the observer's accommodation.

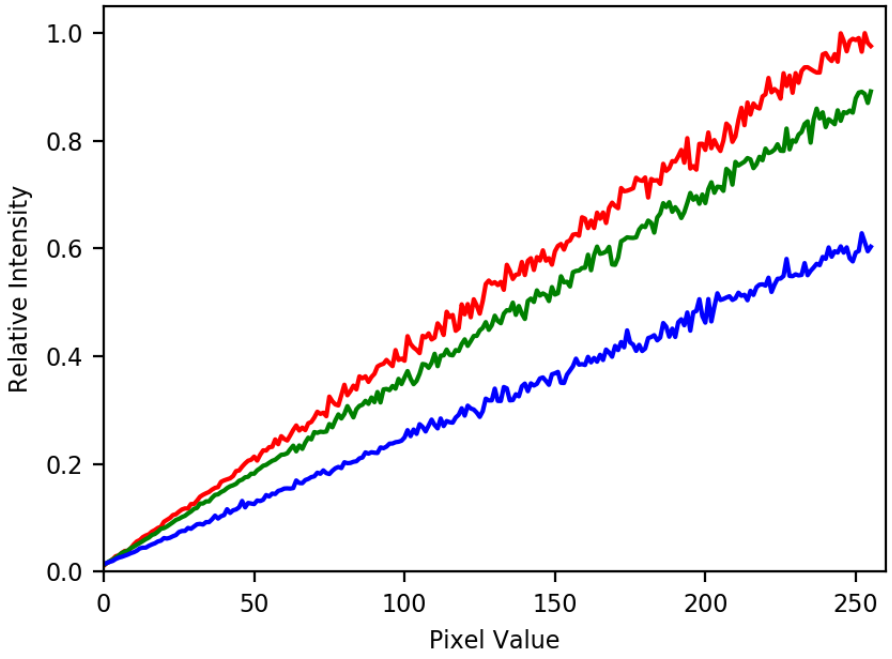

Figure 6.3: The relative measured intensity of the red, green, and blue projector primaries for each input value from 0 to 255 after the linearity correction had been applied. The linearity correction was part of the calibration of the display

6.3.3 Equating luminance

Some of the conditions involved using a smaller pupil for the rendered case than for the optical case. It was therefore important to ensure that the apparent luminance remained the same across all conditions. A simple scaling factor for the difference in pupil area is not sufficient in this case as it does not take into account the Stiles Crawford effect.

A "which is brighter" task was used to determine the exact scaling factor needed for the observer for each pupil size. In this task the observer was shown two stimuli each through a different sized pupil and asked to indicate which was brighter. The two stimuli were generated by illuminating the entire projector screen with the green channel, which, when viewed through the relay lens system, appeared to the observer as a circle of green light. For the larger of the two pupil sizes the intensity of the stimulus was multiplied by the pupil

scaling factor.

This task was carried out for a range of possible pupil scaling factors with 20 repetitions of each. This was then repeated for a series of intensity values and for all of the relevant pupil size combinations. In each case, the average response was plotted against the pupil scaling factor. A curve was fitted to this distribution and the 50% threshold of that curve was taken as the optimum correction factor. The correction factors were then averaged across all intensity values. A separate correction factor was used for the different pupil size combinations.

6.3.4 Measuring the wavefront

The observer's wavefront was also measured prior to the experiments. This was done using the custom built wavefront sensor shown in Figure 6.4. An infrared superluminescent diode (SLD) with a peak wavelength of 875nm was used as the light source so that it was barely visible to the observer and the observer would not accommodate to it. This was collimated and stopped down with an aperture before being directed into the eye. This formed a point source at the back of the eye which was then re-imaged by the wavefront sensor. The wavefront sensor used a Shack-Hartmann design with a 20×20 lenslet array (aμs: APO-Q-P500-R6.3) and CMOS detector behind. The lenslet array was positioned in a plane conjugate to the pupil. The observer focussed on a stimulus of a red cross presented on a monitor screen while the measurements were taken. A tunable lens (optotune) was also placed in a plane conjugate to the pupil. This was adjusted prior to the wavefront measurement so that the stimulus the observer was accommodating to was at the limit of the observer's accommodation. The pupil camera shown in Figure 6.4 was used to help align the observer prior to the measurement.

A series of at least 50 images were taken with the wavefront sensor. These were then analysed using Python to find the best fit of Zernike polynomials up to the 4th order. The averages for each of these Zernike coefficients was taken across all of the images. These average Zernike coefficients were then used to generate the observer's wavefront.

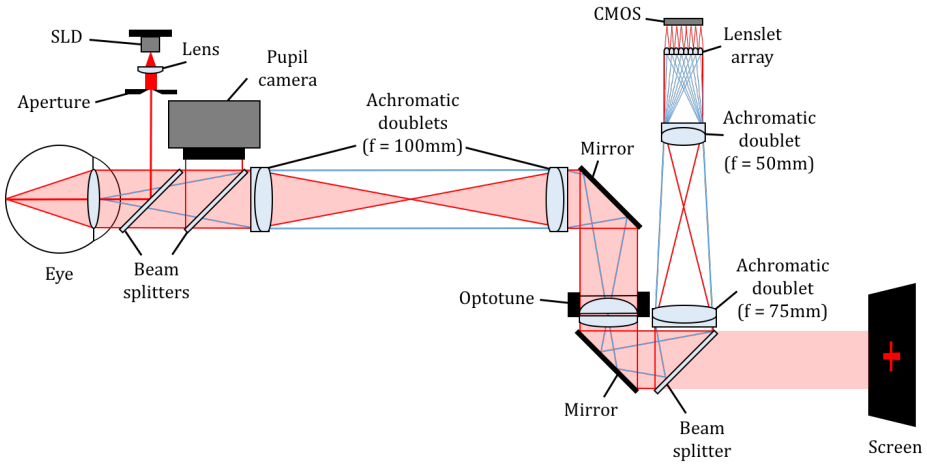

Figure 6.4: A diagram (not to scale) of the wavefront sensor used to measure the aberrations of the observer's eye. The light from the SLD (indicated by the red lines) passed through a collimating lens and an aperture before being directed into the observer's eye with a beam splitter. The light that returned from the eye (still indicated by red lines) was then directed through a relay lens system made up of two achromatic doublets with focal lengths of 100mm. Two mirrors in a periscope arrangement, then guided the light through an tunable lens (optotune) which was in a plane conjugate to the observer's pupil. The third beam splitter then directed the light from the eye up through a second relay made up of one 75mm focal length lens and one 50mm focal length lens. A Shack-Hartmann wavefront sensor consisting of a lenslet array and a CMOS detector was placed in a second conjugate plane to the pupil. A fixation stimulus was displayed on a monitor screen and the path that the light from the screen took to reach the observer's eye is shown by the pale red shaded region. The blue lines highlight the conjugate planes.

6.4 Experiment 1

The aim of this experiment was to investigate the effects of the following four factors on the VA for blurred stimuli.

1. The type of blur, which was either optical or rendered.
2. Whether or not an artificial pupil was used. An artificial pupil ensures that the pupil size is constant and that the rendered blur has been calculated for the correct pupil size. However, if the artificial pupil is

too different from the pupil plane it may cause artefacts in the retinal image.

3. The aperture size through which the rendered stimulus is viewed. If the rendered stimulus is viewed though a pinhole, then the real aberrations of the eye cannot affect the image optically. This is important as the aberrations would not interact with the rendered defocus as they would with the optical defocus. However, the smaller the pinhole is, the greater the effect of diffraction will be as well.

4. Whether or not the monochromatic aberrations of the eye were included in the rendering of the blur.

We hypothesised that when there was a difference between rendered and optical blur it would be the rendered blur that resulted in a poorer VA. Because the artificial pupil was conjugate (or at least almost conjugate) to the pupil plane, we hypothesised that the rendered and optical blur would be more similar with an artificial pupil than without. We ran some simulations to attempt to find the optimal aperture size for viewing the rendered stimuli through. From these it seemed that a 3mm pupil might give the best compromise between diffraction and aberrations and therefore we expected that the rendered and optical blur would be most similar when the rendered stimuli were viewed through a 3mm aperture. We expected the rendered and optical blur to be least similar when the rendered stimuli were not viewed through a reduced aperture. We expected that including the monochromatic aberrations would improve the rendering and therefore that the rendered and optical blur would be more similar when the monochromatic aberrations were included in the rendering than when the blur was rendered just for the defocus.

6.4.1 Methods

Design

This experiment investigated four different independent variables. The first was the blur type, which was either optical blur or rendered blur. The second was the pupil type, which was either a 5mm artificial pupil or the observer's natural pupil (i.e. no artificial pupil). The third independent variable was the aperture size through which the rendered stimulus was viewed, and was

Table 6.2: Experiment 1 conditions.

	Natural pupil	Artificial pupil		
		5mm optical 5mm rendered	5mm optical 3mm rendered	5mm optical 1.5mm rendered
Rendered no HOAs	1	2	3	4
Rendered HOAs	5	6	7	8
Optical	9	10		

only applicable when the pupil type was an artificial pupil and when the blur type was rendered. This had three levels, 5mm, 3mm, or 1.5mm. The final independent variable was the higher order aberrations (HOAs). Either the blur was rendered for defocus only, or the rendering also accounted for the observer's measured aberrations.

There were 10 conditions in this experiment. Each was a unique combination of the independent variables described above, as can be seen from Table 6.2. There were 10 repetitions for each of the 10 conditions. The order of the trials was pseudo-randomised so that there were 10 sessions, each with 1 trial for each of the 10 conditions. Across the 10 sessions each of the 10 conditions came first once, and each came second once, and so forth.

The dependent variable was the visual acuity (VA). This was measured by altering the stimulus size in a staircase procedure to find the threshold for performance in the task. The VA was calculated as,

$$\mathrm{VA}_{\mathrm{logMAR}} = \log_{10}(\mathrm{gapsize}), \tag{6.1}$$

where $\mathrm{VA}_{\mathrm{logMAR}}$ is the VA expressed as the logarithm of the minimum angle of resolution (logMAR), and gapsize is the angular size of the smallest detail to be detected, in this case the gap in the Landolt C, in minutes of arc (arcmin).

Stimuli

The stimuli were standard Landolt C stimuli generated in Python. These were displayed using only the green channel of the display. The intensity of the C was set to 90% of the maximum and the background was also green at

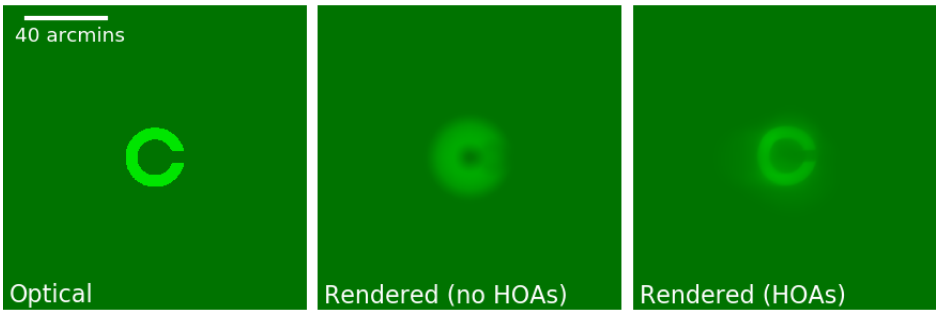

Figure 6.5: Examples of stimuli from Experiment 1. The optical stimulus with no blurring is shown on the left. In the middle is the rendered blur stimulus with a 5mm pupil, 1 D of defocus, and no HOAs. On the right is the rendered blur stimulus with a 5mm pupil, 1 D of defocus and the observer's higher order aberrations up to the 4th order. The 40 arcmin scale bar applies to all three images. In order for the scale to be accurate the images would need to be viewed from approximately 1 meter.

45% of the maximum. The reason for using a green background was that the projector did not have a spatially uniform black background and had some residual light from the projector primaries. This gave the stimuli a Weber's contrast of 0.99. The orientation of the C was randomised so that on each trial the gap was either on the left, right, top, or bottom.

In the optical blur condition the normal Landolt C was presented with a 1 D defocussing lens in the conjugate pupil plane. In the rendered blur condition the Landolt C was first convolved with a PSF. The PSF was generated using the wave-optics model accounting for the pupil size and 1 D of defocus, or in the HOAs condition, accounting for the pupil size, magnitude of defocus, and other monochromatic aberrations of the eye. Figure 6.5 shows an example of an optical blur stimulus (left), a rendered blur stimulus with no HOAs (middle), and a rendered blur stimulus with the observer's measured aberrations (right).

Procedure

The observer's pupil size was measured prior to the experiments using a Ximea MQ022RG-CM camera. An infrared LED with a peak wavelength of 890nm was used to illuminate the pupil without affecting the pupil size. The observer viewed the experimental stimuli and performed a mini version of the task while

their pupil was imaged. The average pupil size of 6.18mm (taken from over 30 images) was used to generate the PSFs for the rendered blur conditions with a natural pupil. The measured pupil size did not drop below 5mm therefore it was never smaller than the artificial pupil.

The task was a 4 alternative forced choice (4afc) task where the observer was asked to indicate the orientation of the Landolt C using the arrow keys on a keyboard. Each stimulus was shown for as long as it took the observer to respond. After the response, the C disappeared and the observer could press the space bar when they were ready for the next stimulus. During this period the observer could also indicate if they had made an error in their response and if they did so that the previous response was discounted.

The thresholds were determined using the accelerated stochastic approximation method or ASA staircase as described in Lu and Dosher (2013). The initial step size for the staircase was set to 0.1 degrees of visual angle and the convergence accuracy level was set to 0.625 (halfway between chance performance and 100% correct). When the observer correctly identified the orientation of the C, the stimulus size decreased, and when they gave an incorrect response, the stimulus size increased. At the end of each staircase the VA estimate was calculated from the size that the next stimulus would have been.

6.4.2 Results

The average VA values across the 10 repetitions are shown in Figure 6.6. From this graph the general trends are that the VA is better when the blur is rendered with HOAs than when the blur is rendered without HOAs. For each blur type the natural pupil always led to the poorest VA. For the rendered blur, the VA continued to improve as the viewing aperture size was reduced with the 1.5mm aperture leading to the best VA. It appears that the VA for the optical blur falls somewhere between those for the various types of rendered blur.

A one-way ANOVA was conducted for all 10 conditions. This showed an overall significant difference in the logMAR scores between conditions ($F(9, 90) = 108.78$, $p < .001$). The differences between conditions were investigated further using Bonferroni corrected t-tests. There were 16 t-tests in total meaning

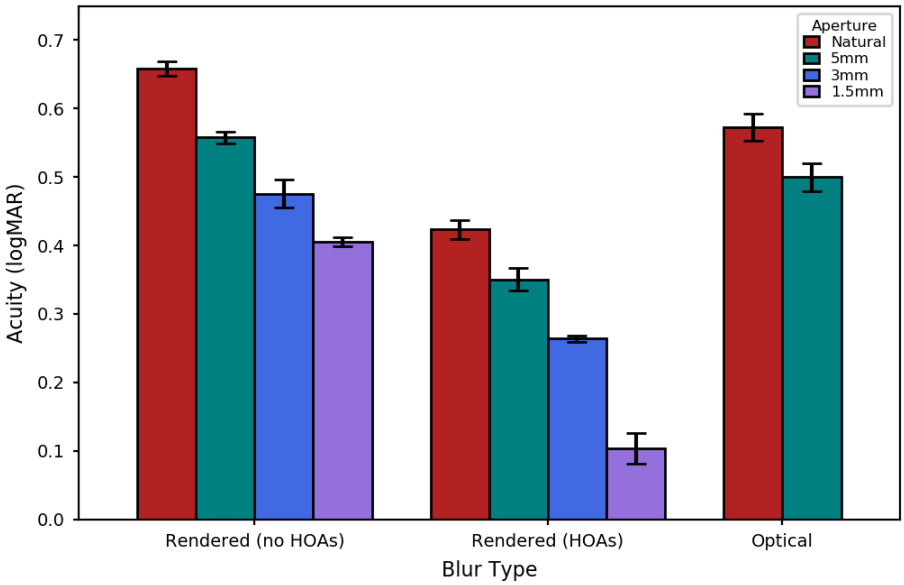

Figure 6.6: The average logMAR values from each of the 10 conditions in Experiment 1. Each bar represents one of the conditions listed in Table 6.2. The error bars show the standard error of the mean.

that a result was classed as significant if

$$p \leq \frac{0.05}{16} = 0.0031. \tag{6.2}$$

First we investigated, whether there was a significant difference between rendered and optical blur. We compared each of the rendered conditions with the equivalent optical condition and the difference was found to be significant for six out of the eight rendered conditions. In the conditions without monochromatic aberrations there was a significant difference for the natural pupil (1 vs 9: $t(18) = 3.83$, $p = .001$), with better VA in the optical case ($M = 0.57$, $SD = 0.06$) than in the rendered case ($M = 0.66$, $SD = 0.03$). There was no significant difference between optical and rendered blur with either the 5mm or the 3mm viewing aperture in the rendered condition (2 vs 10: $t(18) = 2.62$, $p = .017$; 3 vs 10: $t(18) = -0.84$, $p = .410$). With the 1.5mm viewing aperture in the rendered condition, there was a significant difference between the optical and rendered blur (4 vs 10: $t(18) = -4.48$, $p < .001$). However, this time the VA was significantly better for the rendered blur ($M = 0.41$, $SD = 0.02$) than for the optical blur ($M = 0.50$, $SD = 0.06$). In the conditions

with HOAs there was always a significant difference between the optical and rendered blur (5 vs 9: $t(18)$ = -6.14, $p < .001$; 6 vs 10: $t(18)$ = -5.74, $p < .001$; 7 vs 10: $t(18)$ = -11.37, $p < .001$; 8 vs 10: $t(18)$ = -13.18, $p < .001$). In every case the blur rendered with monochromatic aberrations led to a better VA than the optical blur.

Secondly we tested whether the use of a smaller physical aperture size for viewing the rendered stimuli (while rendering the blur for the same optical pupil size of 5mm) had a significant impact on the VA. We conducted 4 t-tests comparing the conditions with the 5mm viewing aperture for the rendered stimuli with both the 3mm and the 1.5mm viewing apertures rendered conditions for both the no HOA and the HOA rendering methods. All of these t-tests showed significant results (2 vs 3: $t(18) = 3.69$, $p = .002$; 2 vs 4: $t(18) = 14.22$, $p < .001$; 6 vs 7: $t(18) = 5.07$, $p < .001$; 6 vs 8: $t(18) = 8.93$, $p < .001$) with the smaller aperture size resulting in a better VA in every case.

Finally the effect of including HOAs when generating the PSF for the rendered blur condition was investigated. This was done by comparing each of the 4 conditions rendered without HOAs with their equivalent conditions rendered with HOAs. In all cases there was a significant difference in the VA (1 vs 5: $t(18) = 13.81$, $p < .001$; 2 vs 6: $t(18) = 11.15$, $p < .001$; 3 vs 7: $t(18) = 10.10$, $p < .001$; 4 vs 8: $t(18) = 13.07$, $p < .001$) with the VA being better in the conditions with HOAs than without HOAs in every case.

6.4.3 Discussion

Only two of the rendered conditions showed no significant difference from the equivalent optical condition. These were conditions 2 and 3, neither of which included HOAs in the rendering and both of which used an artificial pupil. For condition 2 the aperture size in the rendered case was 5mm (the same as the optical pupil size that the blur was generated for) and for condition 3 the rendered stimuli were viewed through a 3mm aperture. However, just because these two cases were the ones where the VA was not significantly different from the optical case, this does not mean that these two cases resulted in the most accurate retinal images.

One unexpected finding was that in most of the cases where there was a significant difference between optical and rendered blur, it was in fact the rendered blur that led to the better image quality. As was discussed in the

introduction, in similar previous studies, when a significant difference was found between the VA for rendered and optical blur it was always the case that people were more tolerant to optical blur. This suggests that in this case there is actually something in the optical blur making the image quality worse that we are missing from the rendered blur.

From the results it is clear that there are various factors that worsen the VA and various factors that improve it. For example, it is to be expected that (once the pupil is large enough that diffraction does not have a dramatic effect on the retinal image) a larger pupil size should result in a greater impact of aberrations and therefore a poorer image quality. It is unsurprising, therefore, that there is a trend for the VA to be better with the artificial pupil than with the natural pupil in both the rendered and optical cases because the artificial pupil is smaller than the natural pupil. There is also a significant effect that as the viewing aperture size for the rendered stimuli is reduced, the VA improves. Although in these cases the PSFs are always generated for a 5mm pupil, the images are still affected by the real aberrations of the eye when they are viewed and therefore the VA still improved as the artificial pupil was stopped down. This finding actually suggests that as the VA was best for the 1.5mm aperture, there must have been less distortion to the retinal image from the optics of the eye for the 1.5mm aperture than for the 3mm or 5mm apertures. It follows that the retinal image would have been closer to the stimulus being presented for the 1.5mm aperture. Because the image being presented was generated as what the retinal image should look like, the less distortion there is from the real optics of the eye when it is viewed the better. Therefore, these findings suggest that the best way to present a rendered blur stimulus to the observer is through a 1.5mm aperture, as opposed to a 3mm or 5mm aperture.

Another finding was that the VA was significantly better in the cases where the rendering included HOAs than when the rendering was for defocus alone. This could be because although the HOAs reduce the image quality for an in focus object, they also increase the depth of focus making us more tolerant to defocus and increasing the image quality for out of focus objects.

The stopping down of the aperture for presenting the rendered stimuli and the inclusion of HOAs in the rendered blur should both bring the retinal image in the rendered blur case closer to that for the optical blur. However, in this experiment both of these factors actually seemed to increase the difference in

VA when compared with the equivalent optical blur condition. For every one of the rendered HOA conditions the VA was significantly better than in the equivalent optical condition and for both of the conditions with the 1.5mm pinhole the VA was also significantly better than in the equivalent optical condition. In fact, the only cases where there was no significant difference between optical and rendered blur, were for the 5mm and 3mm aperture sizes, when the HOAs weren't taken into account. We would expect these conditions to lead to a relatively poor approximation of the optical blur. There must, therefore, be another explanation as to why the conditions that we would have expected to give the best approximation of the optical blur lead to a significantly better VA.

There are two explanations which, when combined, could explain this pattern of results. The first is that perhaps rather than the stimulus being presented at the limit of the observers accommodation (infinity for a corrected eye), it was in fact presented beyond this point, meaning that the eye would need to accommodate beyond its limit to bring the stimulus into focus. If this was the case then as well as the desired rendered or optical defocus there would be an additional optical defocus term. This additional optical defocus term would affect the optical and rendered cases differently because optical + optical defocus is different from optical + rendered defocus. However, at least for the rendered cases with the same aperture size as the optical conditions (i.e. the natural pupil or the 5mm aperture), the magnitude of this defocus should be the same and the effect on the retinal image should not be too different from in the optical condition. On the other hand, in the conditions where the rendered stimuli were presented through a smaller aperture, this additional optical defocus would have a less of an effect on the resultant retinal image. If this was the case then this would account for the significantly improved VA in the rendered conditions viewed through a smaller aperture.

The rendered blur with HOAs also led to a significant improvement in the VA compared to the equivalent optical case. This was the case not only with the smaller viewing apertures but even for the natural pupil and 5mm aperture. Therefore this unexpected finding cannot be explained purely by the unintentional defocus offset suggested above. In order to render the defocus blur with the HOAs included 1 D of defocus was used alongside the other aberrations to generate the PSFs. However, this is not actually appropriate.

Defocus interacts with the other aberrations of the eye and therefore in an eye with HOAs the defocus term required to bring an object into best focus is not necessarily 0 D, in fact it generally isn't. One example of an aberration that interacts with defocus in this way is spherical aberration. In an eye with positive spherical aberration, the best image quality is actually obtained with some positive defocus to balance out the spherical aberration. Therefore, when simulating an in focus retinal image for an eye with HOAs the defocus term should not be zero but should instead be that which best balances out the HOAs of the eye. It follows that to simulate the retinal image for an out of focus eye with HOAs the desired defocus should be added to the defocus value which best balances out the other aberrations.

6.5 Experiment 2

The aim of this experiment was to further investigate the effects of rendering blur with and without accounting for the HOAs while correcting the potential issues in Experiment 1.

The first potential issue with Experiment 1 was that the stimulus may not have been presented at the far limit of the observer's accommodation. Due to the experimental setup we were not able to adjust the actual distance of the screen. Therefore, in order to account for the potential offset, the experiment was run both with the green primary (as in Experiment 1) and with the red primary. The eye is less myopic for red light than for green light due to LCA, and in this case the separation between the red and the green primaries was approximately 0.5 D. If the green stimulus was beyond the accommodative range by approximately 0.5 D or less, then the red stimulus should be just within the accommodative range.

The second potential issue with Experiment 1 was that the defocus term used in the simulations with HOAs was the same as the defocussing power of the lens. However, in an eye with monochromatic aberrations the position of best focus is often not actually 0 D defocus. In this experiment the optimal focus, or baseline defocus, was first established for the given aberrations using a simulation. The induced defocus was then added to this baseline defocus to give the defocus value used to generate the PSF.

This experiment also investigated whether the HOAs used in the rendering

needed to be the observer's own. This is because in many situations when rendered blur is used, the observer's HOAs will not be known, or the same stimuli will be presented to multiple observers and therefore cannot be personalised. It would therefore be useful to know if including HOAs generally improves the similarity of the rendered blur with the optical blur even when the HOAs are not the specific HOAs of the observer.

6.5.1 Methods

Design

This experiment had one independent variable, which was the type of blur. There were 4 different conditions corresponding to 4 different types of blur. These were optical blur, rendered blur, rendered blur with HOAs, and rendered blur with another participant's HOAs (other HOAs). The conditions and their corresponding numbers are shown in Table 6.3. In the final condition the PSF was still generated for an eye with HOAs but they were actually the HOAs of another observer measured using the same wavefront sensor. This other participant was male and 29 years old.

There were 10 repetitions for each of the 4 conditions. The order of the trials was pseudo-randomised so that there were 10 sessions each with 1 trial for each of the 4 conditions. Across the 10 sessions each of the 4 conditions came first at least twice, and each came second at least twice, and so forth.

Table 6.3: Experiment 2 conditions.

Type of Blur	Number
Optical	1
Rendered no HOAs	2
Rendered HOAs	3
Rendered other HOAs	4

The dependent variable was the VA. As in Experiment 1, this was determined using an ASA staircase and converted to logMAR using Equation 6.1.

The experiment was carried out three times. The first time was with the green primary and with a 5mm artificial pupil used in the optical case and a 1.5mm pinhole used in the rendered case. The second time was with the red primary and with a 5mm artificial pupil used in the optical case and a 1.5mm pinhole used in the rendered case. The final time was also with the red primary but with a 5mm artificial pupil used in both the optical and the rendered case.

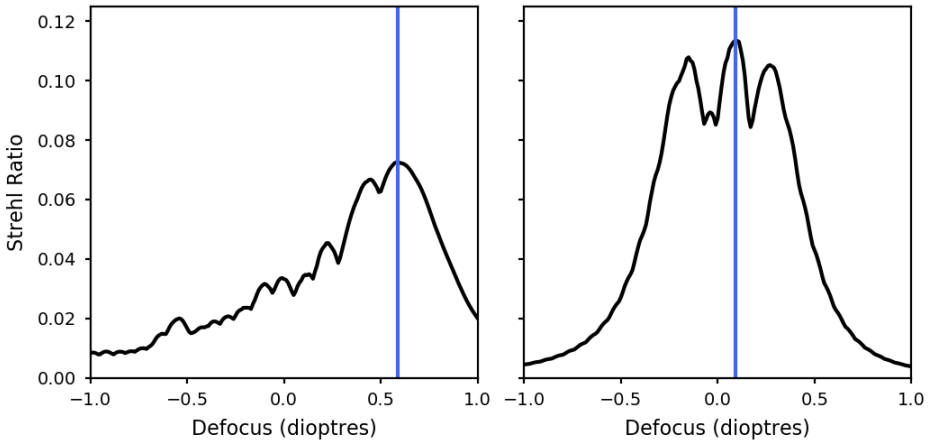

Figure 6.7: The calculated Strehl ratios across a range of defocus values for the observer's own aberrations (left) and the aberrations measured from the other participant (right). The Strehl ratios were calculated assuming a 5mm pupil and a wavelength corresponding to the peak wavelength of the green projector primary. The blue lines indicate the defocus value corresponding to the optimum Strehl ratio. The value indicated by this blue line was taken as the baseline defocus.

Baseline Defocus Simulation

A simulation was carried out for each set of HOAs to determine the defocus value which best balanced out the aberrations. In this simulation the PSFs were generated for the given aberrations and a series of different defocus values in steps of 0.01 D. For each of these PSFs the Strehl ratio was calculated using Equation 5.1. The baseline defocus for that wavefront was then taken as the defocus value that resulted in the highest Strehl ratio. The simulated Strehl ratios and baseline defocus values for each set of aberrations are shown in Figure 6.7.

Stimuli

The stimuli were standard Landolt C stimuli generated in Python as described for Experiment 1. The only difference here was that for two of the experiments the stimuli were rendered for and displayed using the red primary rather than the green.

As in Experiment 1, in the rendered blur conditions the Landolt C was con-

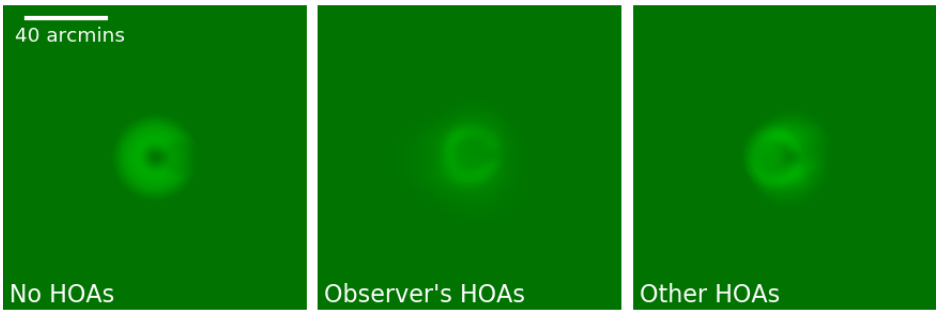

Figure 6.8: Examples of stimuli from Experiment 2. On the left is the rendered blur stimulus with 1 D of defocus and no HOAs. In the middle is the rendered blur stimulus with the observer's higher order aberrations up to the 4th order and 1 D of defocus plus the baseline defocus to best compliment those aberrations. On the right is the rendered blur stimulus with another participant's higher order aberrations up to the 4th order and 1 D of defocus plus the baseline defocus to best compliment those aberrations. The 40 arcmin scale bar applies to all three images. In order for the scale to be accurate the images would need to be viewed from approximately 1 meter.

volved with a PSF. In the case with no aberrations, the PSF was generated for the 5mm pupil size and 1 D of defocus. However for the HOA conditions the PSF was generated for the measured HOAs with 1 D of defocus plus the baseline defocus for those aberrations. Figure 6.8 shows examples of a rendered blur stimulus with no monochromatic aberrations (left), a rendered blur stimulus with the observer's measured aberrations (middle), and a rendered blur stimulus with the other participant's measured aberrations (right).

Procedure

The task was the same 4afc task as described for Experiment 1 above and the thresholds were determined using the same ASA staircase. At the end of each staircase the VA estimate was calculated from what the size of the next stimulus would have been.

6.5.2 Results

The first stage of the experiment involved displaying the stimuli with the green primary of the projector and displaying the optical stimuli through a

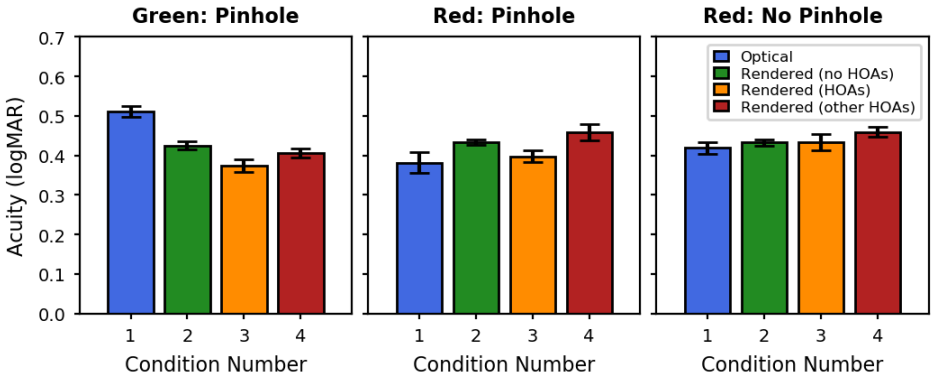

Figure 6.9: The average logMAR values for the 4 blur conditions in shown in Table 6.3. The left hand graph is for the green stimulus with a 1.5mm aperture used to present the rendered blur stimuli. The middle graph is for the equivalent condition with the red stimulus. The right hand graph is for the red stimulus with both the optical and rendered blur stimuli presented through the 5mm pupil. The error bars show the standard error of the mean.

5mm artificial pupil, and the rendered stimuli through a 1.5mm pinhole. The average logMAR scores for each of the 4 conditions can be seen in the left panel of Figure 6.9. This shows that the VA is worst in the optical blur condition (1). Out of the rendered blur conditions, the VA was best when the rendering included the observer's own aberrations (3), and was worst when the rendering did not include any HOAs (2).

An ANOVA showed there to be a significant effect of the type of blur on VA for this first stage of the experiment ($F(3, 36) = 20.13$, $p < .001$). Bonferroni corrected t-tests were then carried out on all 6 possible combinations of conditions to evaluate this effect. With the Bonferroni correction a t-test was classed as significant if

$$p \leq \frac{0.05}{6} = 0.0083. \tag{6.3}$$

The t-tests showed that all three of the rendered blur conditions were significantly different from the optical blur condition (1 vs 2: $t(18) = 5.06$, $p < .001$, 1 vs 3: $t(18) = 6.43$, $p < .001$, 1 vs 4: $t(18) = 6.13$, $p < .001$). In every case the VA was significantly better in the rendered condition than the optical condition.

The t-tests showed no significant differences between any of the different

rendered blur conditions (2 vs 3: $t(18) = 2.59$, $p = .019$; 2 vs 4: $t(18) = 1.27$, $p = .219$; 3 vs 4: $t(18) = -1.60$, $p = .127$).

The second stage of the experiment also involved displaying the optical stimuli through a 5mm artificial pupil and the rendered stimuli through a 1.5mm pinhole, but this time the stimuli were displayed with the red primary. The average logMAR values from this part of the experiment are shown in the middle panel of Figure 6.9. Here, optical blur condition (1) seems to have the best VA and the rendered blur condition with the HOA's from another participant (4) seems to have the worst VA.

The Levenes test for the second part of the experiment showed that the variances varied significantly between conditions ($F(3, 36) = 3.04$, $p = .041$) and although there seemed to be an overall significant effect with the standard ANOVA ($F(3, 36) = 3.47$, $p = .026$) there was not a significant effect with the Welch ANOVA ($F(3, 18.16) = 3.14$, $p = .051$). To be certain we also ran Bonferroni corrected t-tests for each of possible combinations of conditions and none of these came out as significant.

The third stage of the experiment also used the red primary but this time a 5mm artificial pupil was used to present both the optical and the rendered stimuli. The average logMAR values for this part of the experiment are shown in the right panel of Figure 6.9. The VA in all four conditions is very similar with the best performance in the optical blur condition (1) and the worst performance in the rendered blur condition with the HOAs from another observer (4). Here an ANOVA showed no significant difference between any of the conditions ($F(3, 36) = 1.35$, $p = .274$).

6.5.3 Discussion

As was found in Experiment 1, when the green primary was used, with the 1.5mm pinhole to present the rendered stimuli, the rendered blur always resulted in significantly better image quality than the optical blur. This was the case regardless of whether or not HOAs were included in the rendering and whether the HOAs were the observer's own.

Unlike in Experiment 1, there were no significant differences found between any of the rendered blur conditions. This may be because this time the baseline defocus was included for the HOA conditions so that the level of blur was more

similar to that in the rendered condition with no HOAs. This suggests that the main reason for the dramatic difference between the rendered condition with no HOAs and the rendered condition with HOAs in Experiment 1 was that the baseline defocus was not accounted for.

When the red primary was used instead, there was no significant difference between the optical and rendered blur. This was true regardless of whether or not HOAs were included in the generation of the rendered blur and regardless of whether or not a pinhole was used to present the rendered blur. In Experiment 1 using a pinhole for the rendering had a dramatic effect on the VA. The findings from this experiment support the idea that the reason for this dramatic difference in Experiment 1 was that there was some additional optical defocus for both the optical and rendered conditions resulting from the stimulus being placed beyond the far limit of the observer's accommodative range. Therefore, stopping down the pupil was not just lessening the effects of the observer's HOAs but also lessening the effects of this defocus. Using the red primary had the equivalent effect to bringing the stimulus 0.5 D closer to the observer and it seems that this was sufficient to eliminate this additional defocus.

These findings seem to suggest that it does not really matter whether or not the HOAs are included in the rendering and whether a pinhole is used to present the rendering because none of these factors significantly change the resultant VA. In fact, when the red primary was used the VA was not significantly different for the optical versus rendered blur regardless of whether the rendered blur included HOAs, whether the HOAs were those measured from the observer, and whether a pinhole was used. However it is important to remember when interpreting these findings that even if these different conditions do have a very similar effect on VA this does not mean that they are qualitatively the same and they may in fact still appear very different to the observer.

6.6 Experiment 3

In this final experiment, instead of investigating the effects of various types of blur on VA we investigated which type of rendered blur looked qualitatively most similar to the optical blur. We hypothesised that the rendered blur with

the observer's own HOAs would be judged as most similar to the optical blur and that the rendered blur with no HOAs would be the least similar to the optical blur.

6.6.1 Methods

Design

There were two independent variables in this experiment. The first was the types of rendered blur being compared. The types of rendered blur were the same as those used in Experiment 2 and every possible pairing was tested. Therefore, this first variable had three levels: no HOAs versus HOAs, no HOAs versus other HOAs, and HOAs versus other HOAs. The second independent variable was the diameter of the stimulus. This had 4 levels 0.3, 0.5, 0.7, and 0.9 degrees of visual angle. This made 12 different conditions in total.

There were 20 repetitions for each condition. The order of presentation for the two types of rendered blur was counterbalanced so of the 20 repetitions, 10 were for one order of presentation and 10 for the opposite order. In each session there were 24 trials: one for each of the two orders of presentation for each of the 12 conditions. The order of these trials was randomised for each session.

The dependent variable was the type of rendered blur chosen as appearing most similar to the optical blur.

Stimuli

The stimuli were standard Landolt C stimuli generated in Python exactly as described for the Experiment 2. However, for this experiment the 1.5mm pinhole was used to view all of the rendered blur stimuli. The experiment was run twice, once with the green primary and again with the red primary. As in Experiment 2 there were 3 types of rendered blur stimuli: those rendered with no HOAs, those rendered with the observers own HOAs, and those rendered with another participant's HOAs. As with Experiment 2 the baseline defocus values were added to the desired defocus value of 1 D when HOAs were included in the rendering.

Procedure

For each trial three stimuli were shown. The first stimulus was always the optically blurred stimulus. This was presented with a 5mm artificial pupil. This was displayed for 0.5 seconds followed by a black screen for 0.5 seconds. While the black screen was presented the 1 D lens and 5mm artificial pupil were exchanged for a 1.5mm pinhole using the dual position slider. Next the first of the rendered blur stimuli was shown for another 0.5 seconds followed by another black screen for 0.5 seconds. Finally the second rendered blur stimulus was shown for 0.5 seconds followed by a black screen. At this point the subject was able to indicate which, out of the two rendered stimuli, looked most similar to the first, optical blur stimulus, by pressing either the number 1 (for the first rendered stimulus) or 2 (for the second rendered stimulus) on the keyboard.

6.6.2 Results

The frequency with which each type of rendered blur was selected as being closest to the optical blur for each of the 3 comparisons is shown in Figure 6.10 for both the green and the red primary.

Looking at the results for the green primary, for the comparison of the no HOAs condition with the observer's HOAs condition (top left panel), the observer's HOAs condition was chosen as being more similar to the optical blur with a higher frequency for every stimulus size. For the comparison of the no HOAs condition with the other HOAs condition (top middle panel), the other HOAs condition was selected with a higher frequency for 3 out of the 4 stimulus sizes. For the final comparison of the observer's HOAs against the other HOAs condition (top right panel), the results seem to be a lot more mixed.

Looking at the results for the red primary, for the comparison of the no HOAs condition with the observer's HOAs condition (bottom left panel), for the 0.3^{o} and 0.5^{o} stimuli there is a clear trend for the rendered stimuli with the observer's HOAs to look more similar to the optical blur stimuli than the rendered stimuli with no HOAs. However, for the 0.7^{o} and 0.9^{o} stimulus diameters there is no clear trend. For both the comparisons of the no HOAs condition with the other HOAs condition (bottom middle panel) and the HOAs

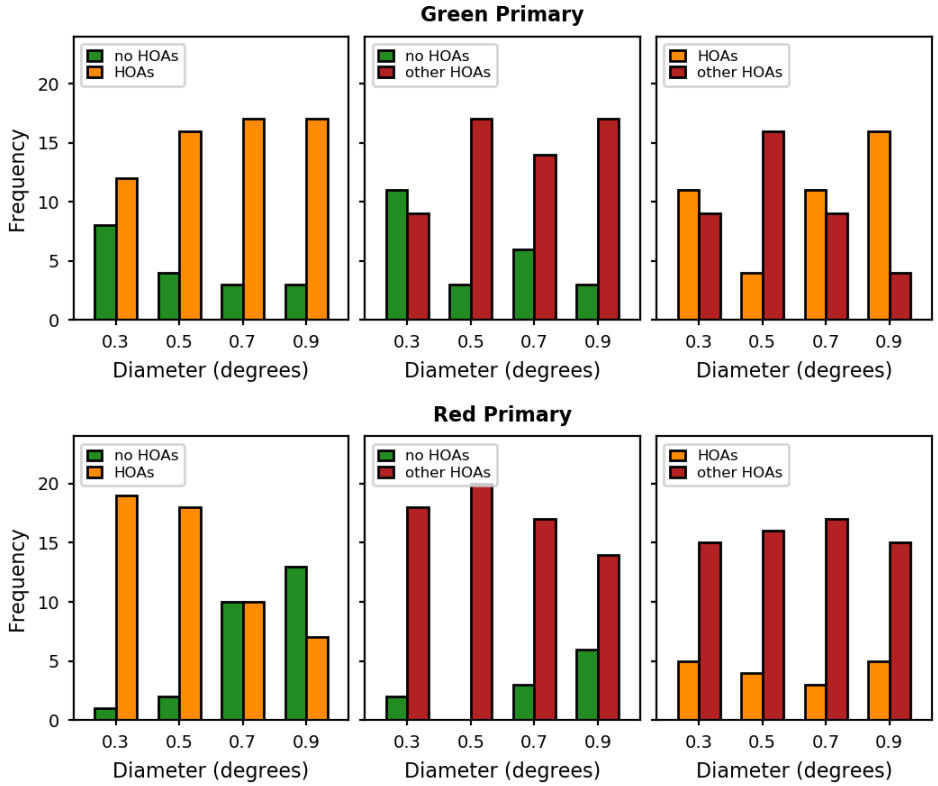

Figure 6.10: The frequencies with which the observer selected each rendered blur conditions as closer to the optical blur stimulus for both the green and the red projector primary. Each graph is for a different comparisons. The results are plotted for each of the 4 stimulus diameters tested.

condition with the other HOAs condition (bottom right panel), there is a clear trend for the other HOAs condition to be judged as more similar to the optical blur condition.

A chi-squared test was carried out for each of the comparisons for both the green and the red primary to determine whether there was a significant difference in the frequencies for the two blur types. A chi-squared test of independence was also carried out for each of the comparisons to establish whether stimulus diameter had a significant effect on the result.

Green primary

For the green primary, there was a significant difference between the frequencies for the no HOAs versus HOAs comparison (X^2 (1, $N = 80$) = 24.20, $p <$ .001), with the HOAs condition being selected significantly more times (62) than the no HOAs condition (18). The frequency with which each of these conditions was selected did not differ significantly with the stimulus diameter (X^2 (3, $N = 80$) = 4.87, $p = .246$).

There was also a significant difference between the frequencies for the no HOAs versus other HOAs comparison (X^2 (1, $N = 80$) = 14.45, $p < .001$), with the other HOAs condition selected significantly more times (57) than the no HOAs condition (23). For this comparison there was a significant interaction between the type of rendered blur selected and the stimulus diameter (X^2 (3, $N = 80$) = 10.43, $p = .018$). To investigate this interaction further, individual chi-squared tests were run for each of the 4 stimulus diameters. There was a significant difference between the no HOAs and the other HOAs frequencies for both the 0.5° stimulus (X^2 (1, $N = 20$) = 9.80, $p = .003$) and the 0.9° stimulus (X^2 (1, $N = 20$) = 9.80, $p = .003$) with the higher frequency for the other HOAs condition in both cases. However, the difference was not significant for the 0.3° stimulus (X^2 (1, $N = 20$) = 0.20, $p = .824$), or for the 0.7° stimulus (X^2 (1, $N = 20$) = 3.20, $p = .115$).

There was no significant difference between the frequencies for the HOAs versus other HOAs comparison (X^2 (1, $N = 80$) = 0.20, $p = .738$). Although the frequency was slightly higher for the HOAs condition (42) than the other HOAs condition (38). There was, however, a significant interaction with stimulus diameter (X^2 (3, $N = 80$) = 14.64, $p = .002$). To investigate this interaction further, individual chi-squared tests were run for each of the 4 stimulus diameters. There was a significant difference found for the 0.5° stimulus (X^2 (1, $N = 20$) = 7.20, $p = .012$), with a higher frequency in the other HOAs case (16) than the HOAs case (16). There was also a significant difference found for the 0.9° stimulus (X^2 (1, $N = 20$) = 7.20, $p = .012$). However, in this case the frequency was higher for the HOAs condition (16) than the other HOAs case (4). There was no significant difference found for either the 0.3° stimulus (X^2 (1, $N = 20$) = 0.20, $p = .824$) or the 0.7° stimulus (X^2 (1, $N = 20$) = 0.20, $p = .824$).

Red primary

For the red primary, there was a significant difference between the frequencies for the no HOAs versus HOAs comparison (X^2 (1, $N = 80$) = 9.80, $p = .002$), with the HOAs condition chosen significantly more times (54) than the no HOAs condition (26). However, there was also a significant interaction between the type of blur chosen and the stimulus diameter (X^2 (3, $N = 80$) = 23.93, $p < .001$). Individual chi-squared tests were run for each of the 4 stimulus diameters to investigate this interaction further. There was a significant difference between the frequencies with which the two blur types were chosen for both the 0.3° stimuli (X^2 (1, $N = 20$) = 16.20, $p < .001$) and the 0.5° stimuli (X^2 (1, $N = 20$) = 12.80, $p < .001$). In both cases the HOAs condition was chosen significantly more times than the no HOAs condition. There was, however, no significant difference for either the 0.7° stimuli (X^2 (1, $N = 20$) = 0.00, $p = 1.000$), or for the 0.9° stimuli (X^2 (1, $N = 20$) = 1.80, $p = .263$).

There was a significant difference between the frequencies for the no HOAs versus other HOAs comparison (X^2 (1, $N = 80$) = 42.05, $p < .001$), with the other HOAs condition chosen significantly more (69) than the no HOAs condition (11). In this case there was no significant interaction with stimulus diameter (X^2 (3, $N = 80$) = 7.91, $p = .050$).

There was also a significant difference between the frequencies for the HOAs versus other HOAs comparison (X^2 (1, $N = 80$) = 26.45, $p < .001$), with the other HOAs condition chosen significantly more times (63) than the HOAs condition (17). There was no significant interaction with stimulus diameter in this case (X^2 (3, $N = 80$) = 0.82, $p = .931$).

Overall results

Figure 6.11 shows the overall frequencies for each of the three types of rendered blur for both the green and the red primary. From this we can see that in both cases the no HOAs condition was clearly selected fewer times than either of the HOA conditions. For the green primary the HOAs condition was selected with a slightly higher frequency than the other HOAs condition. However, for the red primary the other HOAs condition was selected more times than the HOAs condition.

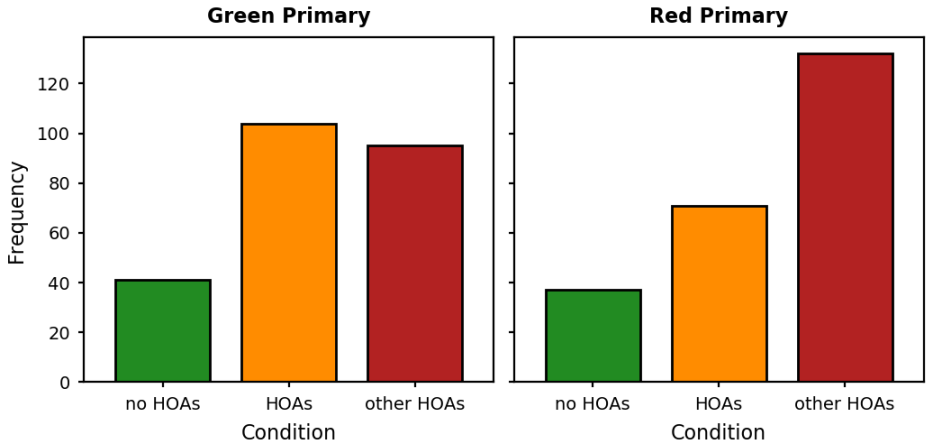

Figure 6.11: The overall number of times that each of the three types of stimuli were selected as being closer to the optical blur stimulus across all of the trials for both the green and the red projector primary.

6.6.3 Discussion

For both the green primary and the red primary the observer judged the HOAs condition to be to more similar to the optical blur than the no HOAs condition. This finding was significant in both cases and in the case of the green primary it was robust regardless of the stimulus size. However, it is worth noting that for the red primary this trend was not seen for the 0.7^{o} and 0.9^{o} stimulus sizes. In fact, for the 0.9^{o} stimulus size there was a non-significant trend for the no HOAs condition to be chosen with a higher frequency than the HOAs condition. These findings indicate that in general rendering with HOAs leads to a more realistic image. However, this effect does seem to be somewhat dependent on stimulus size.

Another interesting question is whether it is important that the aberrations used in the rendering are the observer's own aberrations as there are many cases when the observer's own aberrations will not be known. For both the red and the green primaries, the observer judged the other HOAs condition to be more similar to the optical blur than the rendered blur with no HOAs. This was a significant effect in both cases and it was only for the green primary at the smallest stimulus size that this trend was not seen. This indicates that even in cases when the aberrations used are from another observer this can still make the image appear more realistic.

For the green primary, there was no overall significant difference between the frequencies with which the HOAs condition was chosen and the other HOAs condition was chosen, indicating that the important factor in making the rendered stimuli appear more similar to the optical stimuli was that HOAs were included and it didn't actually make much of a difference whether these aberrations were the observer's own or not. For the red primary, the stimuli rendered with other HOAs were actually chosen with a significantly higher frequency than those rendered with the observer's own HOAs. This was unexpected and may be due to the fact that the experiment with the red primary was carried out a few months after the observer's aberrations were measured. More experiments are required testing a range of observers with a range of aberrations to get a better understanding on whether there is a benefit to using the observer's own aberrations or whether any aberrations can be used.

If these findings are repeatable, this would suggest that HOAs could be used to make rendered blur that appears more realistic even when the stimuli are presented to multiple different people at once or when the specific aberrations of the observer are not known.

6.7 Conclusions

Experiments 1 and 2 indicated that if the distance at which the stimulus is presented is not actually the far point of the observer's accommodative range this can alter the results quite dramatically and lead to significant effects which, when the effective distance is changed slightly, disappear.

They also demonstrated the importance of finding a baseline defocus value when rendering with HOAs and adding the desired defocus term to this baseline defocus. It is relatively well established that the point of best focus for a real eye with HOAs is not actually at 0 defocus, and this is a good example of a practical case where this needs to be accounted for.

Once these two factors above were corrected for in Experiment 2, by using the red primary to effectively bring the stimulus closer to the observer and adding the defocus to a baseline level in the HOA conditions, there was actually no significant difference found between the VA for optical and rendered blur. This was the case regardless of whether or not the rendered stimuli were presented through a pinhole and regardless of whether HOAs were included in

the rendering. It was even the case when the HOAs used in the rendering were measured from another participant's eye. It may seem sensible to conclude from this that it does not really matter whether or not HOAs are included and whether or not the rendered stimuli are viewed through a pinhole. However, just because there was not a significant difference in the VA, this does not mean that there was no significant difference in the stimulus appearance.

Experiment 3 actually indicated that there was a significant difference in how similar to the optical blur the different types of rendered blur appeared. When the rendered blur included HOAs this was chosen significantly more frequently as being closer to the optical blur compared with when the stimulus had no HOAs. This was true regardless of whether or not the HOAs used to render the blur were the observer's own. What was less clear from these results was the effect of using the observer's own aberrations as compared with other aberrations. For the green primary there was no overall significant difference between the frequencies with which the observer selected the two different HOA conditions. This seems to indicate that whether the aberrations are the observer's own does not make a significant difference to how similar the rendered stimuli look to the optical stimuli. For the red primary, on the other hand, the observer selected the stimuli with the other aberrations significantly more times than the ones with their own aberrations. It is unclear what might have caused this affect.

Overall these results suggest that, at least for the two eyes measured in this experiment, the HOAs of the eye don't significantly alter the VA for Landolt C stimuli. However, the images blurred with HOAs are qualitatively different from those blurred without HOAs and the observer judged those blurred with HOAs as more closely resembling the real optically blurred stimuli in almost all cases. This suggests that, in cases where the aim of the rendered blur is to make a stimulus appear to be as realistic as possible, HOAs may well be important. This also shows that there is a lot that a simple comparison of VA will not tell us about how accurate a stimulus with rendered blur is.

Following on from this more experiments are needed testing a greater number of observer's to establish how robust these effects are. A range of different HOAs could also be tested to see whether there is a particular set of HOAs (such as the HOAs for a "standard" observer) which could improve the realism of rendered blur for the majority of the population.

Chapter 7

Conclusions

In this chapter a summary is given of the work and key findings presented in this thesis. This is followed by suggestions for areas of future research.

7.1 Summary

This thesis investigated the monochromatic and chromatic aberrations of the human eye and how they affect our vision. The focus was on updating our understanding of the way that these aberrations affect our vision in the context of the modern world.

7.1.1 Modern illuminant spectra

Increasingly illuminants are being favoured to be more energy efficient and in displays primaries are often chosen to be more narrowband to allow for a wider colour gamut. These modern illuminant spectra are advantageous for many reasons, however, not much research has been done investigating how different illuminant spectra might interact with the longitudinal chromatic aberration (LCA) of our eyes. This thesis aimed to begin investigating this question and explore issues that might arise from certain illuminant spectra due to the LCA of the eye. The focus was particularly on illuminant spectra with one or multiple narrowband peaks.

The question of whether we might see chromatic fringing due to LCA under some illuminant spectra was addressed in Chapter 4 and the question of

whether our accommodation response is compromised under illuminant spectra made up of two narrowband peaks was addressed in Chapter 5.

Is LCA visible under certain illuminant spectra

The simulations presented in Chapter 4 do not give a conclusive answer to the question of whether the fringes due to LCA are more obvious under certain types of illuminant as compared with more natural broadband illuminants. However, the experimental results did indicate that there are certain spectra for which the ratings of the visibility of chromatic fringes were significantly higher. These findings suggest that the chromatic fringes on the retina due to LCA are more obvious under illuminants made up of 2 or 3 narrowband LEDs as compared to the broadband spectrum of a halogen bulb or the near monochromatic spectrum of a single narrowband LED.

Is accommodation compromised under certain illuminant spectra

The measured static accommodation responses for various spectra were presented in Chapter 5. From these it is clear that for mixtures of two narrowband LEDs the accommodation responses tend to be somewhere in the middle of the responses for the two LEDs individually. This suggests that neither of the two peak wavelengths in the spectrum were actually in focus.

Simulations suggested that the image quality is generally better if the focus is nearer to one of the two individual LEDs rather than in the middle of the two. However, the measured accommodation responses show that even for the greatest LED separations every participant was accommodating in between the two LEDs for at least some of the mixtures. This suggests that they were not accommodating optimally.

The accommodation responses aligned better with optimising contrast at lower spatial frequencies than the higher spatial frequencies. It was suggested that this may be because the contrast gradient at the lower spatial frequencies is more reliable at directing accommodation towards the overall peak in contrast over a greater range of defocus values than the higher spatial frequencies. This is potentially problematic as the higher spatial frequencies contain the information relating to the fine detail in the image. The depth of focus is also much lower at the higher spatial frequencies compared to the low spatial

frequencies and therefore arguably accurate accommodation is more important at the higher spatial frequencies.

It is therefore important to consider the spectrum of an illuminant in terms of how much defocus due to LCA there will be in the retinal image and how optimally people can accommodate to that spectrum.

7.1.2 Realistically rendering 3D scenes

Another area that is constantly growing in the modern world is that of displaying very realistic images and scenes. Cinema is becoming more and more realistic with 3D films now commonplace and virtual reality is becoming increasingly popular. In order for a scene presented on a 2D screen to appear realistic and 3D it is not simply a case of getting the best resolution and the highest image quality. In reality objects at different distances are distorted differently by the chromatic and monochromatic aberrations of our eyes and therefore for a scene to appear realistic it seems likely that we will need to attempt to mimic these effects. The ability to render blurred stimuli realistically could also be useful in a more clinical setting, in helping patients to decide which sorts of optical corrections they prefer without going to the expense of manufacturing the lenses. In Chapter 6 a series of experiments were described investigating what is required in order for a stimulus with rendered defocus to have an equivalent effect on visual acuity (VA) and an equivalent appearance to a stimulus with real optical defocus.

One key finding presented in Chapter 6 was that when monochromatic aberrations are included in the rendering of blur it is important to shift the amount of defocus used in the rendering so that instead of being relative to 0 dioptres (D) defocus, it is relative to the baseline level of defocus for those aberrations, where the baseline defocus is the amount of defocus that leads to the best image quality when combined with the aberrations.

There was no evidence that including monochromatic aberrations in the rendering is important in order for rendered defocus to have the same effect on VA as optical defocus. However, the findings did indicate that the rendered stimuli were subjectively more similar to the optically blurred stimuli when monochromatic aberrations were included in the rendering. Interestingly, this effect was still significant even when the aberrations used in the rendering were not the observer's own. This indicates that including monochromatic aberra-

tions in the rendering of blur could improve realism even when the individual's aberrations are not known or when the same stimuli are being shown to many different people.

7.2 Future research

The work presented in this thesis points to many different areas that could be investigated further. Some suggestions for future research are given below.

7.2.1 How different types of illuminant spectrum interact with the LCA of the eye

In this thesis we investigated how participants accommodated to illuminant spectra composed of two individual LEDs. However, more experiments are needed to understand how people accommodate to the full range of different illuminant and display spectra that are used in the modern world.

It would also be useful to determine whether certain types of illuminant spectra and the way we accommodate to them really does have a detrimental effect on the quality of the retinal image. In order to establish this the contrast sensitivity could be measured for a series of different illuminants and compared with that for natural daylight.

Ideally enough research would be done in this area so that we could have a quantifiable scale to indicate how good our vision is under various illuminants and how obvious the chromatic fringes due to LCA are. The colour rendering index (CRI) indicates how similar the colours of objects appear under a given illuminant compared with how the colour of that object would look under natural lighting. However, nothing equivalent exists for how blurred objects appear to be under different illuminants due to the LCA of the eye.

7.2.2 Is it possible to realistically render blur?

The work presented in this thesis only scratched the surface of the question of how to realistically render blur. A lot more work is needed before we can render blur to be indistinguishable from optical blur and it may be that this is not even possible to achieve.

The experiments described in Chapter 6 only tested one participant. This was due to limitations in the optical setup. It would be interesting to carry out the same experiment on multiple participants and see whether the findings are consistent. In particular it would be interesting to know whether it is always the case that including monochromatic aberrations in the rendered blur results in the rendered stimulus looking more realistic even when the aberrations are not the observer's own.

Moving forwards the next step would be to move away from monochromatic light and address realistically rendering blur for RGB displays. This would introduce the question of how to best account for the LCA of the eye in the rendered images. Similar experiments could also be done with more complex scenes, with objects at a range of depths, to see whether the manipulations that made the rendered blur more realistic for a simple scene are still effective.

Appendix A

Simulation method

We made a number of simulations of polychromatic retinal images for Chapter 4. Three different methods were used to simulate the retinal images. Two of these methods were for generating the retinal image for an RGB scene and the third was for generating the retinal image from a greyscale scene.

The first and most simple method (method 1) involved assigning a single wavelength to each of the red, green, and blue channels. In this case 650nm was used for red, 550nm was used for green, and 450nm was used for blue. The point spread functions (PSFs) were then generated for each of the three wavelengths with the appropriate defocus value for the LCA of that wavelength using equation 2.1. Each PSF was then convolved with the relevant channel from the scene bitmap to get the blurred image for that channel using equation 2.2 (i.e. the 650nm PSF was convolved with the R channel of the scene). These blurred images then became the R, G, and B components of the simulated retinal image. The top right panel in figure A.1 shows the retinal image simulated using this method for a scene comprising a simple white square as shown in the top left panel of figure A.1.

Method 2 involved converting the RGB image of the scene into a hyperspectral image. In order to do this the spectra of the red, green and blue primaries from a MacBook Pro (Retina display, 2015) were measured using a USB 2000 spectrometer (Ocean Optics). Using these spectra, a spectrum was calculated for each pixel in the RGB scene as

$$\text{Spectrum} = R \times \text{Spectrum}_R + G \times \text{Spectrum}_G + B \times \text{Spectrum}_B, \quad \text{(A.1)}$$

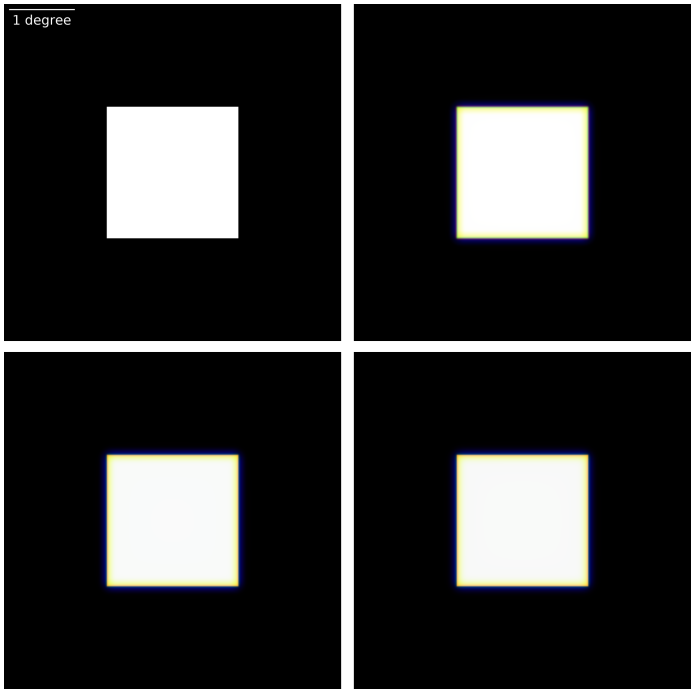

Figure A.1: The top left panel shows a simple 2 degree white square on a black background. This is the scene that the retinal images are based on. The top right panel shows the retinal image of the square generated from a simple 3 wavelength approximation (method 1). The bottom left panel shows the retinal image of the square generated by converting an RGB image to a hyperspectral image using the measured R, B and B spectra from a MacBook display (method 2). The bottom right panel shows the retinal image of the square generated by multiplying the greyscale image by the D65 spectrum and using this as the hyperspectral image (method 3). All of the retinal images were generated for an eye with natural LCA and a 5mm pupil. The 1 degree scale bar for the top left image applies to all of the images. In order for the scale to be accurate the images would need to be viewed from approximately half a meter away.

where R, G, and B are the intensity values for each pixel, Spectrum_R is the spectrum of the red primary, Spectrum_G is the spectrum of the green primary, and Spectrum_B is the spectrum of the blue primary. Once this process was completed for every pixel in the scene, instead of having an image array with 3 different values for each pixel (R, G, and B) we had an image array with 61 values for each pixel going from 400nm to 700nm in 5nm steps (or in the high resolution case 941 values from 360 to 830 in 0.5nm steps) this is known as a

hyperspectral image (HSI).

Once the HSI of the scene had been generated, this was then converted into the HSI of the retinal image. As before a PSF was generated separately for each wavelength and then convolved with the slice of the scene HSI corresponding to that wavelength. This stack of blurred images made up the HSI for the retinal image. Finally, the retinal image HSI needed to be converted back into an RGB format so that it could be viewed on a regular screen. The spectrum for each pixel in the HSI was multiplied by the CIE 1931 2 degree X, Y and Z colour matching functions (CIE, 1932) to give,

$$\begin{aligned} X &= \text{Spectrum} \times X_{\text{cmf}}, \\ Y &= \text{Spectrum} \times Y_{\text{cmf}}, \\ Z &= \text{Spectrum} \times Z_{\text{cmf}}, \end{aligned} \tag{A.2}$$

where X_{cmf}, Y_{cmf}, and Z_{cmf}, are the X, Y, and Z colour matching functions. These X, Y, and Z values were then multiplied by a matrix defined at www.brucelindbloom.com to give the R, G, and B values, so that

$$\begin{bmatrix} R \\ G \\ B \end{bmatrix} = \begin{bmatrix} 3.2404542 & -1.5371385 & -0.4985314 \\ -0.9692660 & 1.8760108 & 0.0415560 \\ 0.0556434 & -0.2040259 & 1.0572252 \end{bmatrix} \begin{bmatrix} X \\ Y \\ Z \end{bmatrix}. \tag{A.3}$$

The R, G, and B values were calculated in this way for each pixel to give the RGB retinal image. The bottom left panel in figure A.1 shows the RGB retinal images calculated in this way for a simple stimulus made up of a white square.

Method 3 used a simple greyscale image, which could then be multiplied by any wavelength spectrum to give an HSI. Once the HSI was generated from the greyscale image, the retinal image was then generated in exactly the same way as described for method 2 above and converted to an RGB image using equations A.2 and A.3 so that it could be displayed. The bottom right image in figure A.1 shows the RGB retinal images calculated in this way for a stimulus made up of a white square with a D65 spectrum.

Appendix B

Individual observers' static accommodation responses

In this section the average static accommodation response measures described in Chapter 5 are plotted separately for each of the five participants. Figures B.1 to B.5 show the accommodation responses for participants 1 to 5 respectively.

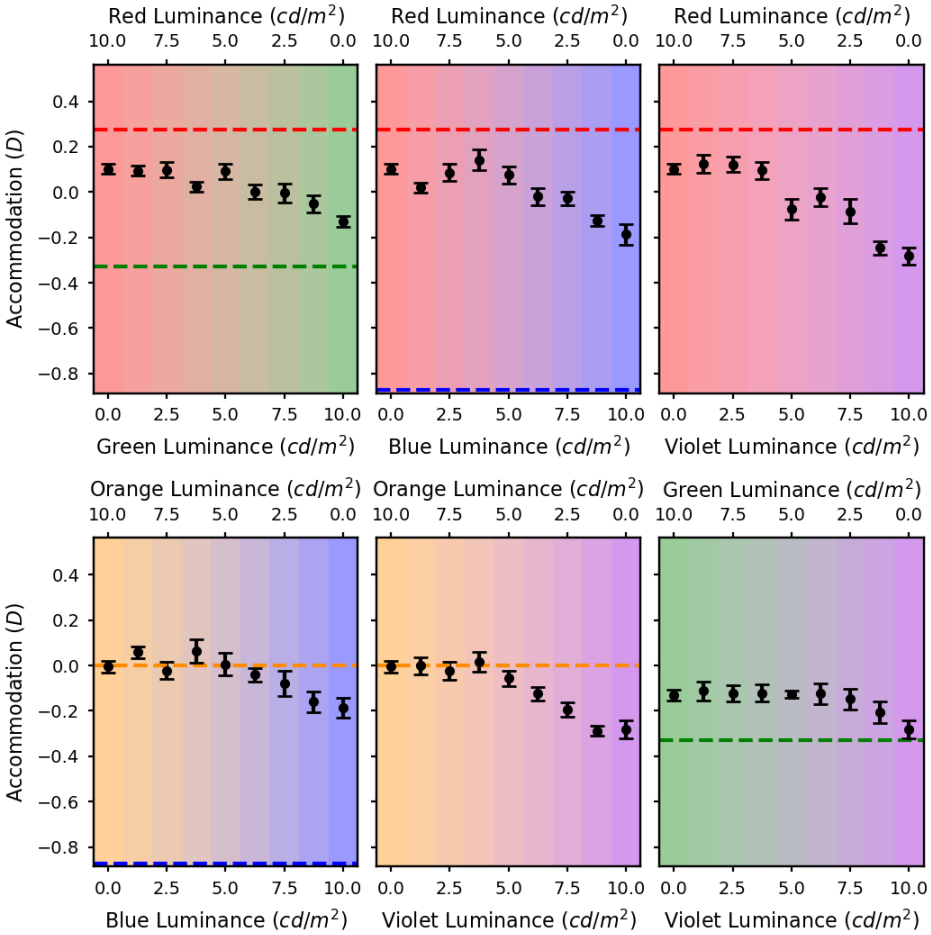

Figure B.1: The black circles show the relative mean static accommodation responses of Participant 1 plotted against the luminances of the two LED sources. The different graphs are for the different LED pairs: red and green (top left), red and blue (top middle), red and violet (top right), orange and blue (bottom left), orange and violet (bottom middle), and green and violet (bottom right). The error bars represent the standard error of the mean. The dashed lines indicate the accommodation needed to bring the defocus for the peak wavelength of each LED to zero.

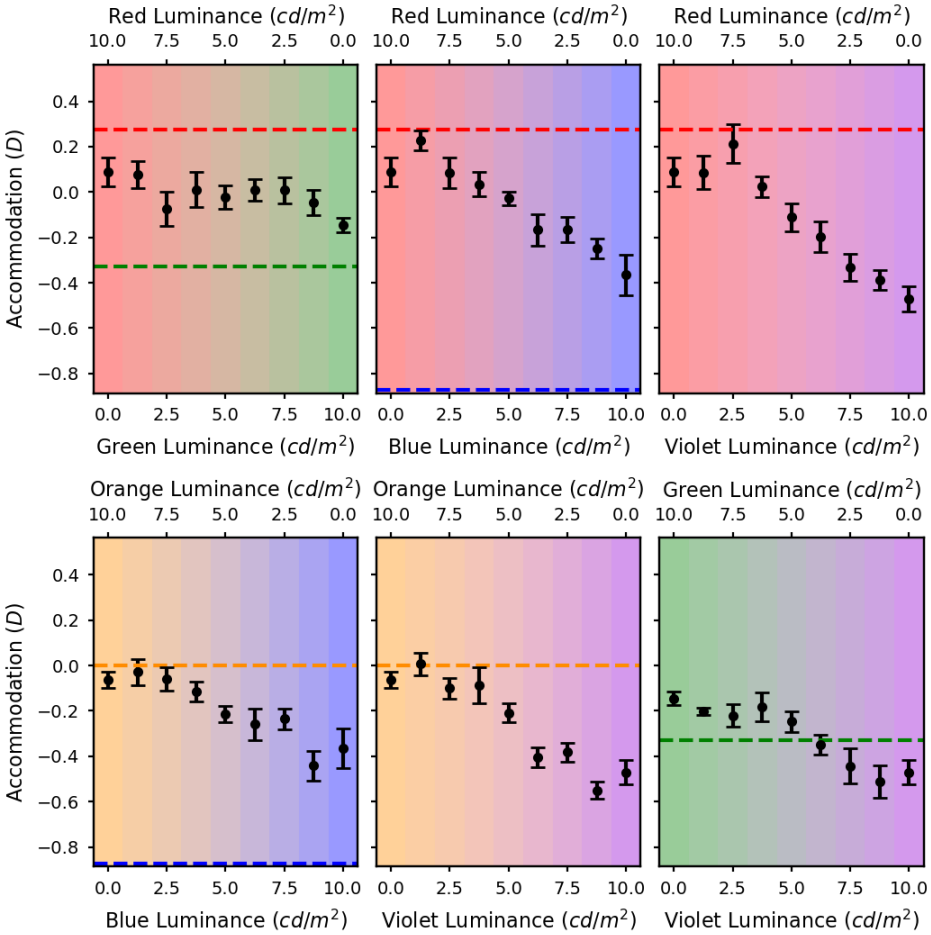

Figure B.2: The black circles show the relative mean static accommodation responses of Participant 2 plotted against the luminances of the two LED sources. The different graphs are for the different LED pairs: red and green (top left), red and blue (top middle), red and violet (top right), orange and blue (bottom left), orange and violet (bottom middle), and green and violet (bottom right). The error bars represent the standard error of the mean. The dashed lines indicate the accommodation needed to bring the defocus for the peak wavelength of each LED to zero.

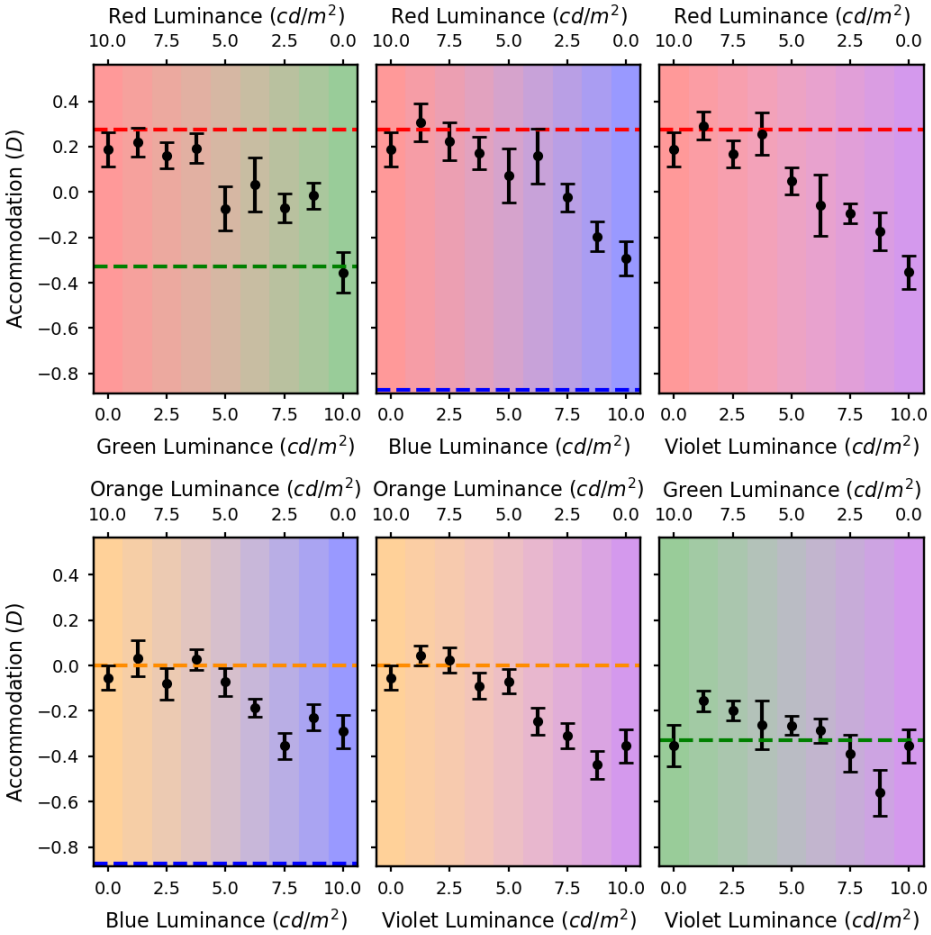

Figure B.3: The black circles show the relative mean static accommodation responses of Participant 3 plotted against the luminances of the two LED sources. The different graphs are for the different LED pairs: red and green (top left), red and blue (top middle), red and violet (top right), orange and blue (bottom left), orange and violet (bottom middle), and green and violet (bottom right). The error bars represent the standard error of the mean. The dashed lines indicate the accommodation needed to bring the defocus for the peak wavelength of each LED to zero.

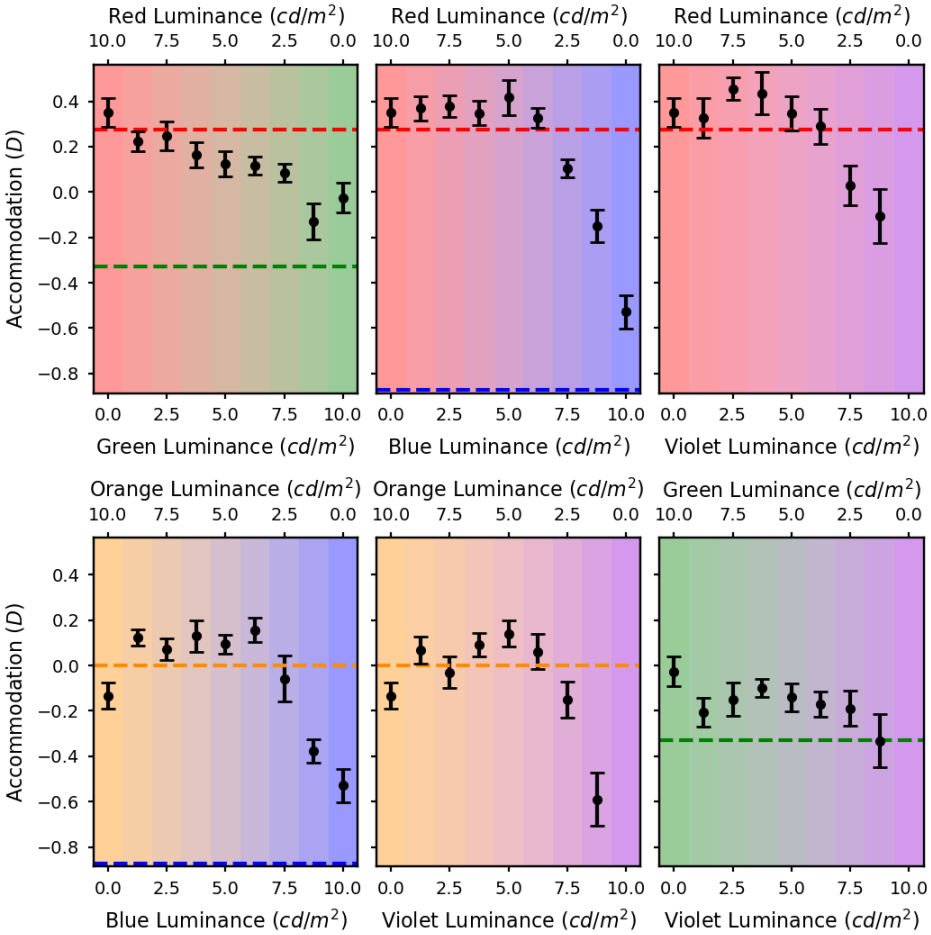

Figure B.4: The black circles show the relative mean static accommodation responses of Participant 4 plotted against the luminances of the two LED sources. The different graphs are for the different LED pairs: red and green (top left), red and blue (top middle), red and violet (top right), orange and blue (bottom left), orange and violet (bottom middle), and green and violet (bottom right). The error bars represent the standard error of the mean. The dashed lines indicate the accommodation needed to bring the defocus for the peak wavelength of each LED to zero.

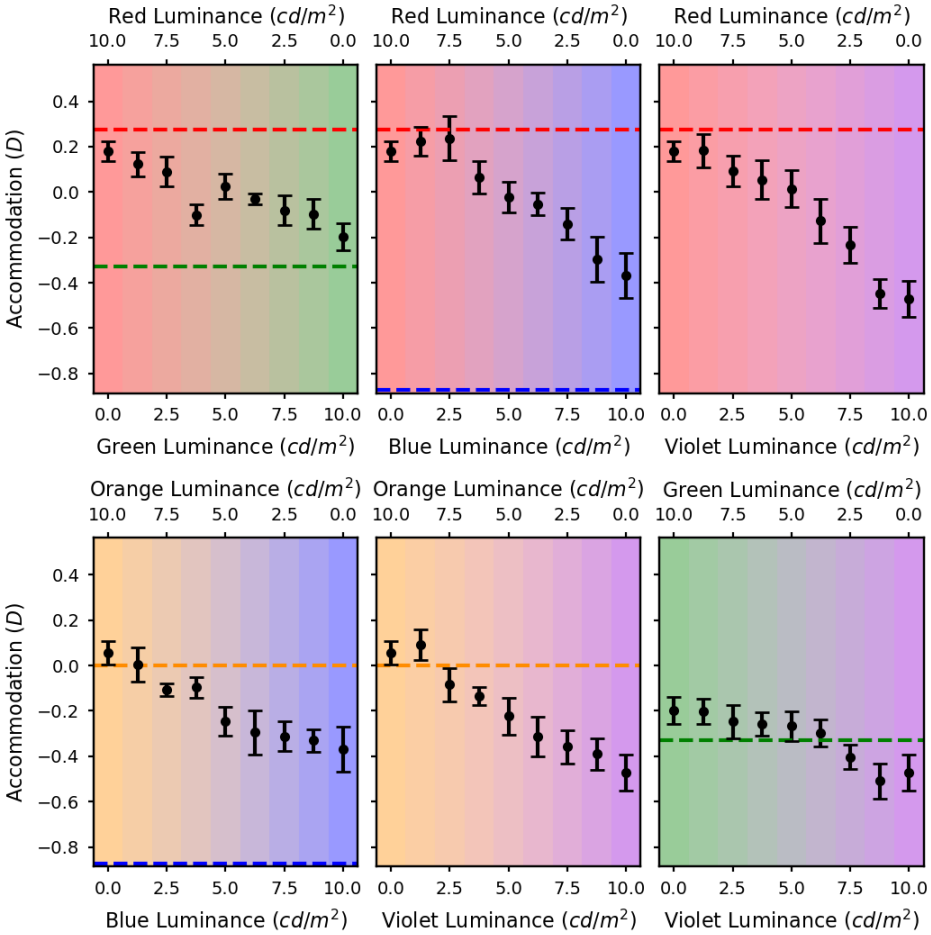

Figure B.5: The black circles show the relative mean static accommodation responses of Participant 5 plotted against the luminances of the two LED sources. The different graphs are for the different LED pairs: red and green (top left), red and blue (top middle), red and violet (top right), orange and blue (bottom left), orange and violet (bottom middle), and green and violet (bottom right). The error bars represent the standard error of the mean. The dashed lines indicate the accommodation needed to bring the defocus for the peak wavelength of each LED to zero.

Appendix C

Visual Strehl Ratio simulations with monochromatic aberrations

Here the visual Strehl Ratio (VSR) simulations described in Chapter 5 are plotted for the measured monochromatic aberrations of participants 4 and 5. Figure C.1 shows the simulated VSR values for the red and blue LED pair with the measured aberrations from Participant 4. Figure C.2 shows the predicted static accommodation responses for maximising the VSR with the aberrations measured from Participant 4 for all of the different LED pairs. Figure C.3 shows the simulated VSR values for the red and blue LED pair with the measured aberrations from Participant 5. Finally, Figure C.4 shows the predicted static accommodation responses for maximising the VSR with the aberrations measured from Participant 5 for all of the different LED pairs. Scales are the same for both participants but the axes have been shifted to fit in all of the data. In some cases this means that some of the dashed lines indicating the LCA of the two LEDs cannot be seen.

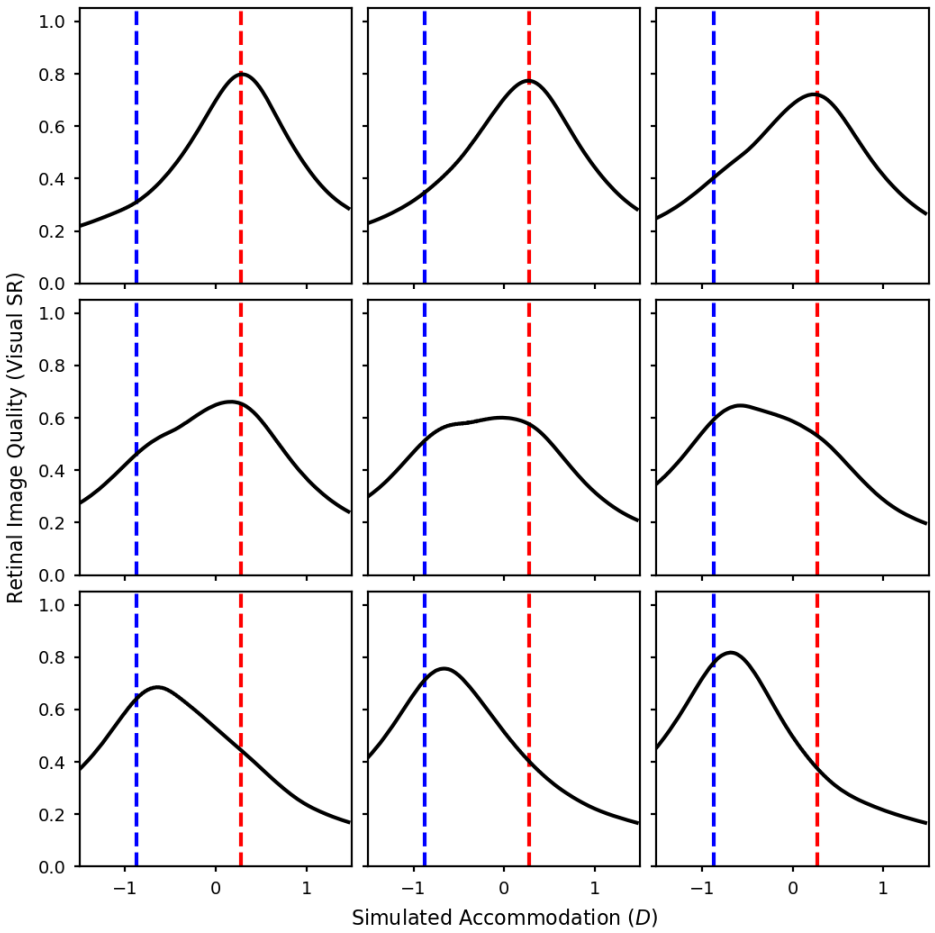

Figure C.1: Visual Strehl ratios calculated from a wave optics model of the eye with the monochromatic aberrations for Participant 4 over a range of defocus values. The visual Strehl ratios were calculated from polychromatic MTFs weighted by each of the test spectra and the luminous efficiency function. The test spectra are mixtures of the red and blue LEDs. The luminance ratio of these two sources was varied in nine equal steps from completely red (top left) to completely blue (bottom right). The red and blue dashed lines indicate the accommodative response needed to correct the LCA at the peak wavelengths of the red and blue LEDs.

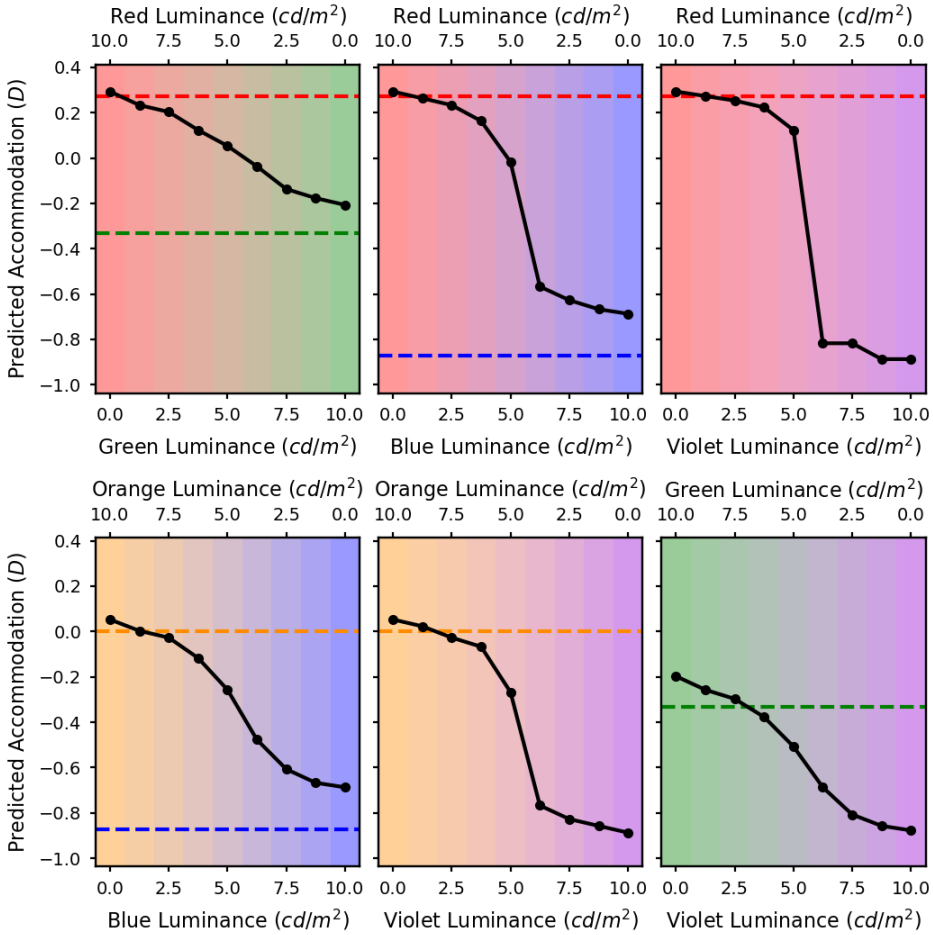

Figure C.2: The predicted accommodation responses for maximising visual Strehl ratio in the luminance channel with the monochromatic aberrations for Participant 4. The x axis represents the luminances of the two LED sources. The different graphs are for the different LED pairs: red and green (top left), red and blue (top middle), red and violet (top right), orange and blue (bottom left), orange and violet (bottom middle), and green and violet (bottom right). The dashed lines indicate the accommodative response needed to correct the LCA at the peak wavelengths of the LEDs.

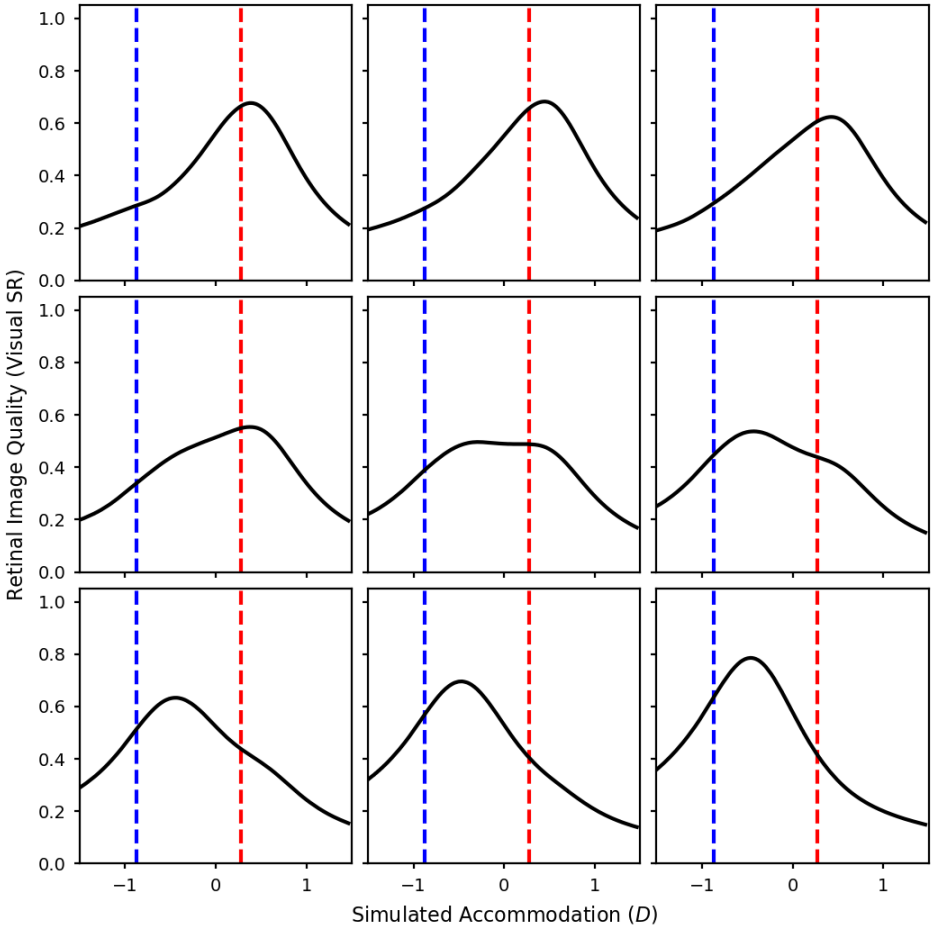

Figure C.3: Visual Strehl ratios calculated from a wave optics model of the eye with the monochromatic aberrations for Participant 5 over a range of defocus values. The visual Strehl ratios were calculated from polychromatic MTFs weighted by each of the test spectra and the luminous efficiency function. The test spectra are mixtures of the red and blue LEDs. The luminance ratio of these two sources was varied in nine equal steps from completely red (top left) to completely blue (bottom right). The red and blue dashed lines indicate the accommodative response needed to correct the LCA at the peak wavelengths of the red and blue LEDs.

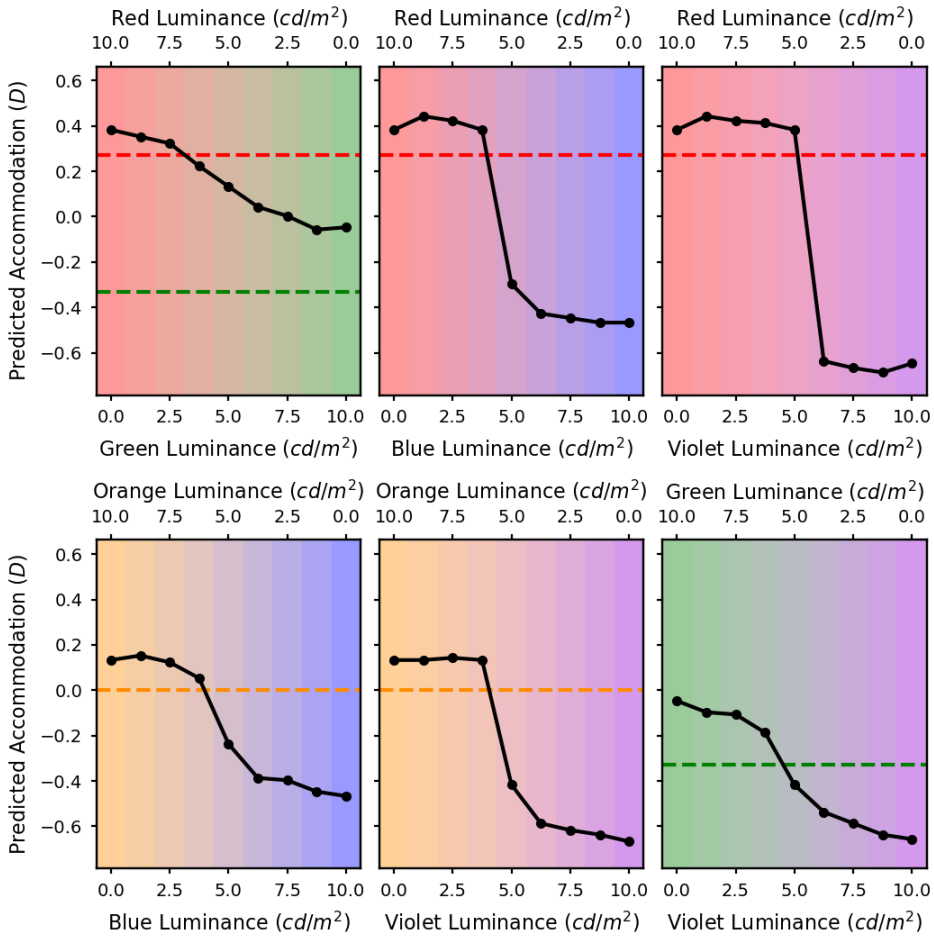

Figure C.4: The predicted accommodation responses for maximising visual Strehl ratio in the luminance channel with the monochromatic aberrations for Participant 5. The x axis represents the luminances of the two LED sources. The different graphs are for the different LED pairs: red and green (top left), red and blue (top middle), red and violet (top right), orange and blue (bottom left), orange and violet (bottom middle), and green and violet (bottom right). The dashed lines indicate the accommodative response needed to correct the LCA at the peak wavelengths of the LEDs.

Appendix D

Contrast Ratio simulations with monochromatic aberrations

Here the simulations described in Chapter 5 for optimising contrast at various spatial frequencies are plotted for the measured monochromatic aberrations of participants 4 and 5. Figure D.1 shows the simulated contrast values for the red and blue LED pair with the measured aberrations from Participant 4. Figure D.2 shows the predicted static accommodation responses for maximising the contrast at various spatial frequencies with the aberrations measured from Participant 4 for all of the different LED pairs. Figure D.3 shows the simulated contrast values for the red and blue LED pair with the measured aberrations from Participant 5. Finally, Figure D.4 shows the predicted static accommodation responses for maximising the contrast at various spatial frequencies with the aberrations measured from Participant 5 for all of the different LED pairs. Scales are the same for both participants but the axes have been shifted to fit in all of the data. In some cases this means that some of the dashed lines indicating the LCA of the two LEDs cannot be seen.

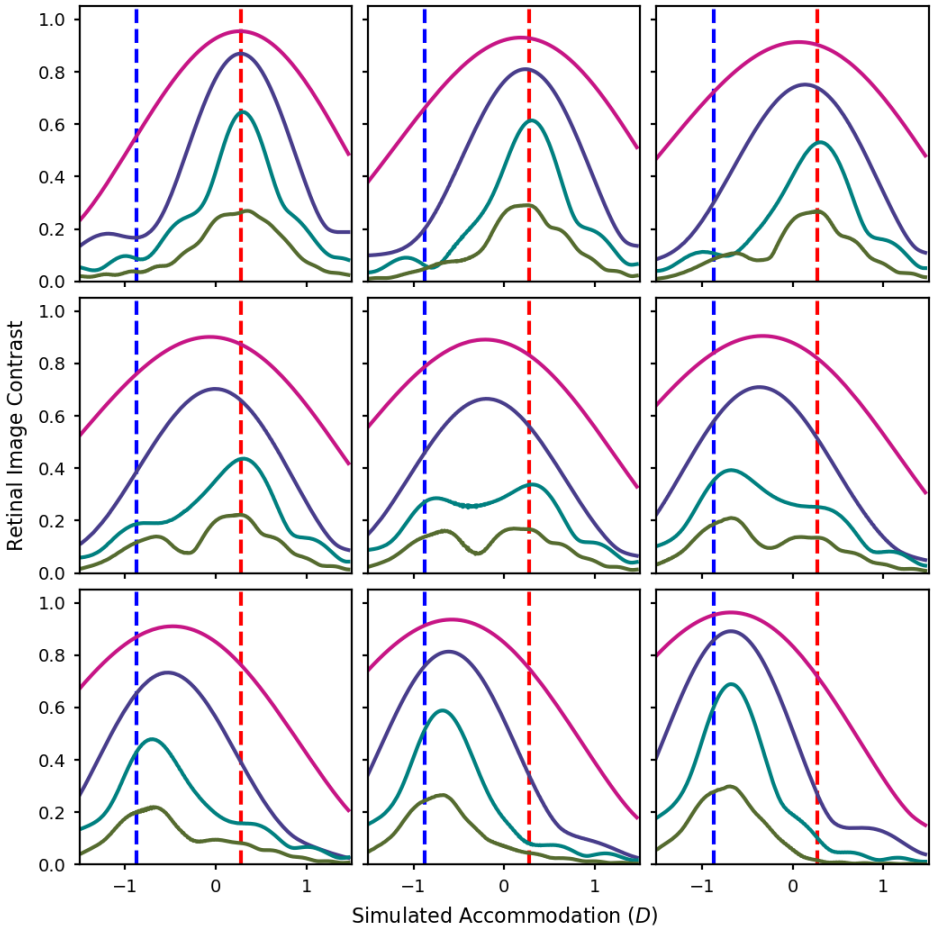

Figure D.1: Contrast ratios calculated from a wave optics model of the eye with the monochromatic aberrations for Participant 4, over a range of defocus values, at 2 (magenta), 4 (purple), 8 (cyan), and 16 (green) cpd. The contrast ratios were calculated from polychromatic MTFs weighted by each of the test spectra and the luminous efficiency function. The test spectra are mixtures of the red and blue LEDs. The luminance ratio of these two sources was varied in nine equal steps from completely red (top left) to completely blue (bottom right). The red and blue dashed lines indicate the accommodative response needed to correct for the LCA at the peak wavelengths of the red and blue LEDs.

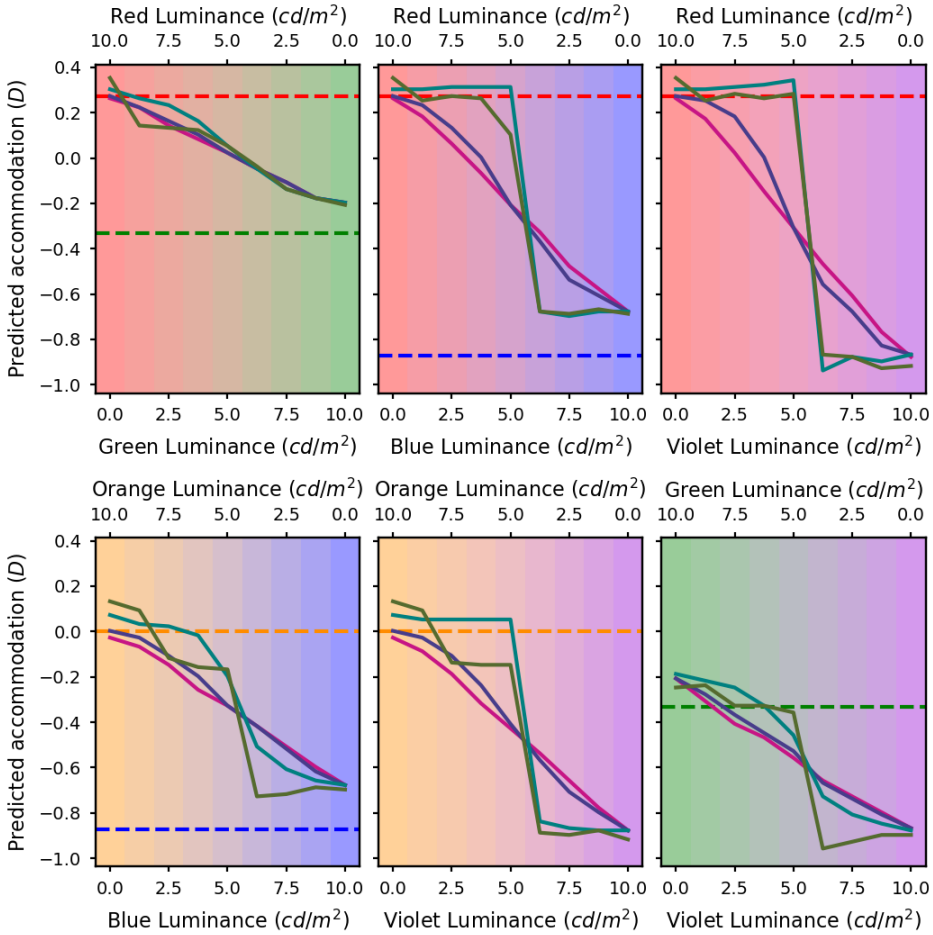

Figure D.2: The predicted accommodation responses for maximising retinal image contrast in the luminance channel for spatial frequencies of 2 (magenta), 4 (purple), 8 (cyan), and 16 (green) cpd with the monochromatic aberrations for Participant 4. The x axis represents the luminances of the two LED sources. The different graphs are for the different LED pairs: red and green (top left), red and blue (top middle), red and violet (top right), orange and blue (bottom left), orange and violet (bottom middle), and green and violet (bottom right). The dashed lines indicate the accommodative response needed to correct the LCA at the peak wavelengths of the LEDs.

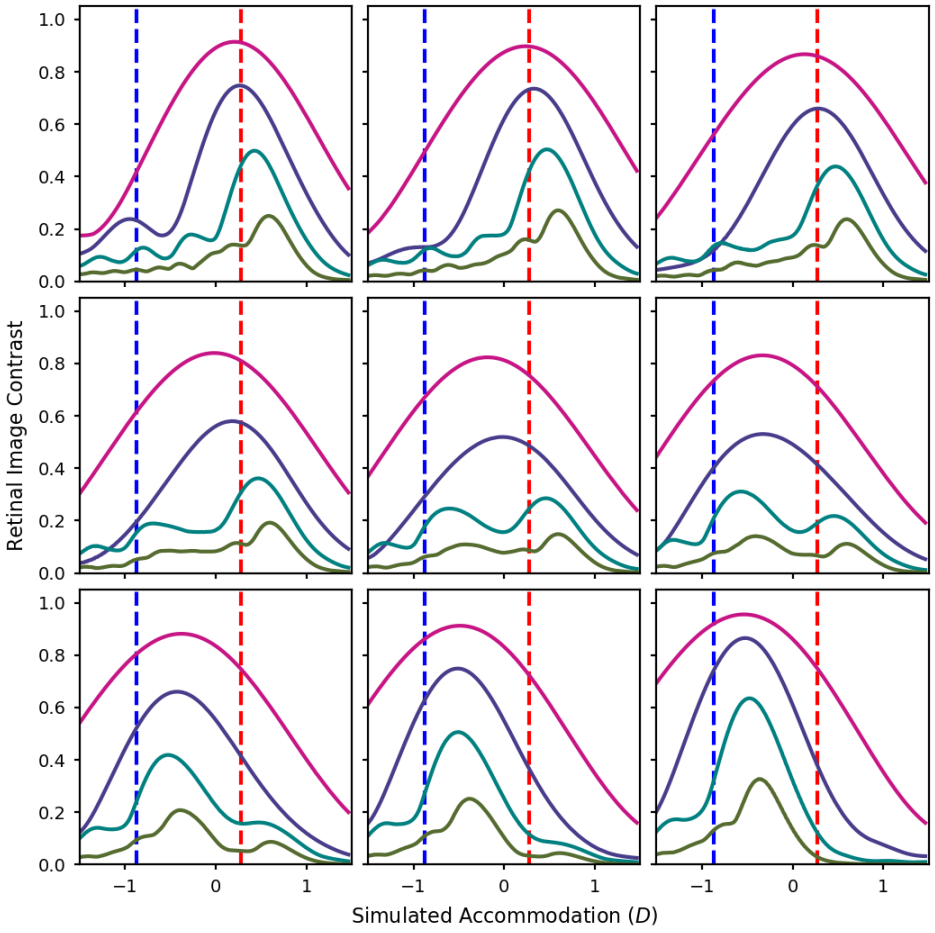

Figure D.3: Contrast ratios calculated from a wave optics model of the eye with the monochromatic aberrations for Participant 5, over a range of defocus values, at 2 (magenta), 4 (purple), 8 (cyan), and 16 (green) cpd. The contrast ratios were calculated from polychromatic MTFs weighted by each of the test spectra and the luminous efficiency function. The test spectra are mixtures of the red and blue LEDs. The luminance ratio of these two sources was varied in nine equal steps from completely red (top left) to completely blue (bottom right). The red and blue dashed lines indicate the accommodative response needed to correct for the LCA at the peak wavelengths of the red and blue LEDs.

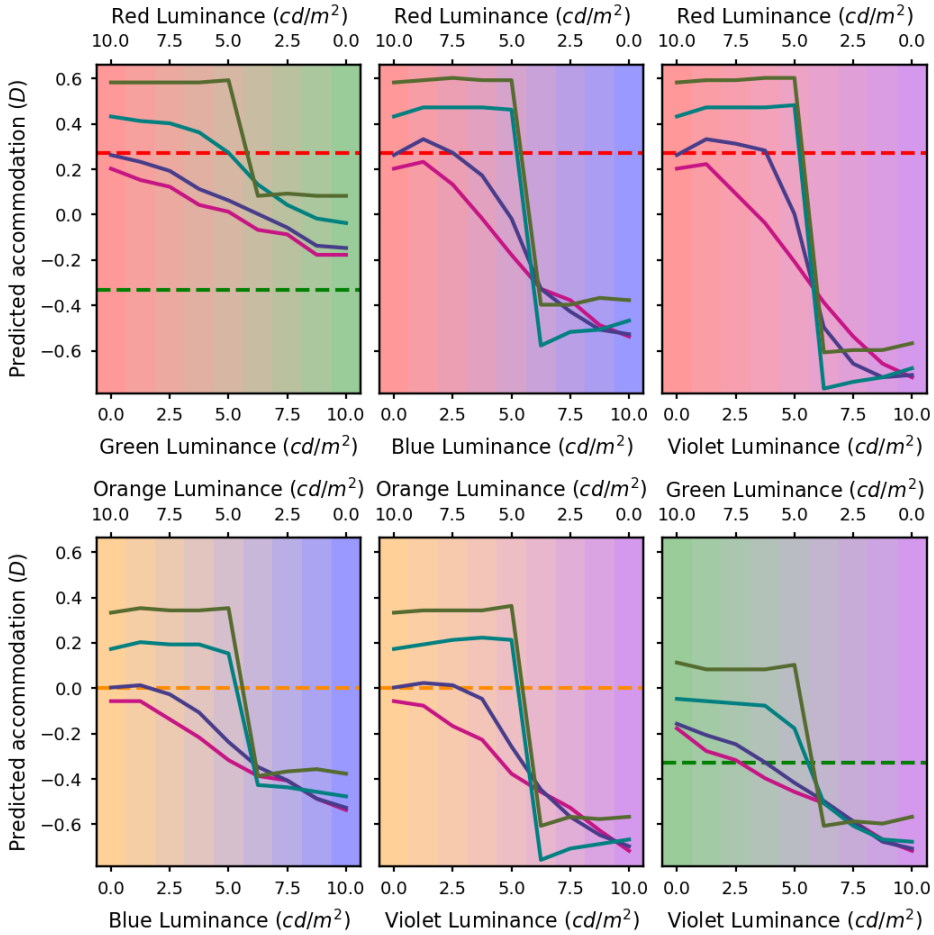

Figure D.4: The predicted accommodation responses for maximising retinal image contrast in the luminance channel for spatial frequencies of 2 (magenta), 4 (purple), 8 (cyan), and 16 (green) cpd with the monochromatic aberrations for Participant 5. The x axis represents the luminances of the two LED sources. The different graphs are for the different LED pairs: red and green (top left), red and blue (top middle), red and violet (top right), orange and blue (bottom left), orange and violet (bottom middle), and green and violet (bottom right). The dashed lines indicate the accommodative response needed to correct the LCA at the peak wavelengths of the LEDs.

Bibliography

K. R. Aggarwala, E. S. Kruger, S. Mathews, and P. B. Kruger. Spectral bandwidth and ocular accommodation. *Journal of the Optical Society of America A*, 12(3):450–455, mar 1995a. ISSN 1084-7529. doi: 10.1364/JOSAA.12.000450. URL http://www.osapublishing.org/viewmedia.cfm?uri=josaa-12-3-450{&}seq=0{&}html=true.

K. R. Aggarwala, S. Nowbotsing, and P. B. Kruger. Accommodation to monochromatic and white-light targets. *Investigative Ophthalmology & Visual Science*, 36(13):2695–2705, 1995b.

M. Alpern. Variability of Accommodation during Steady Fixation at Various Levels of Illuminance. *Journal of the Optical Society of America*, 48(3):193–197, mar 1958. doi: 10.1364/JOSA.48.000193. URL https://www.osapublishing.org/abstract.cfm?URI=josa-48-3-193.

P. Artal. Optics of the eye and its impact in vision: a tutorial. *Advances in Optics and Photonics*, 6(3):340–367, sep 2014. ISSN 1943-8206. doi: 10.1364/AOP.6.000340. URL https://www.osapublishing.org/aop/abstract.cfm?uri=aop-6-3-340.

P. Artal, E. Berrio, A. Guirao, and P. Piers. Contribution of the cornea and internal surfaces to the change of ocular aberrations with age. *Journal of the Optical Society of America A*, 19(1):137, jan 2002. ISSN 1084-7529. doi: 10.1364/JOSAA.19.000137. URL http://www.osapublishing.org/viewmedia.cfm?uri=josaa-19-1-137{&}seq=0{&}html=true.

D. A. Atchison and D. H. Scott. Monochromatic aberrations of human eyes in the horizontal visual field. *Journal of the Optical Society of America A*, 19(11):2180, nov 2002. doi: 10.1364/JOSAA.19.002180. URL https://www.osapublishing.org/abstract.cfm?URI=josaa-19-11-2180.

R. E. Bedford and G. Wyszecki. Axial Chromatic Aberration of the Human Eye. *Journal of the Optical Society of America*, 47(6):564–565, jun 1957. doi: 10.1364/JOSA.47.0564_1. URL https://www.osapublishing.org/abstract.cfm?URI=josa-47-6-564{_}1.

Y. Benny, S. Manzanera, P. M. Prieto, E. N. Ribak, and P. Artal. Wide-angle chromatic aberration corrector for the human eye. *Journal of the Optical Society of America A*, 24(6):1538, may 2007. ISSN 1084-7529. doi: 10.1364/JOSAA.24.001538. URL http://www.osapublishing.org/viewmedia.cfm?uri=josaa-24-6-1538{&}seq=0{&}html=true.

P. Bernal-Molina, I. Marín-Franch, A. J. Del Águila-Carrasco, J. J. Esteve-Taboada, N. López-Gil, P. B. Kruger, and R. Montés-Micó. Human eyes do not need monochromatic aberrations for dynamic accommodation. *Ophthalmic and Physiological Optics*, 37(5):602–609, sep 2017. ISSN 02755408. doi: 10.1111/opo.12398. URL http://doi.wiley.com/10.1111/opo.12398.

D. M. Berson, F. A. Dunn, and M. Takao. Phototransduction by retinal ganglion cells that set the circadian clock. *Science (New York, N.Y.)*, 295 (5557):1070–3, feb 2002. ISSN 1095-9203. doi: 10.1126/science.1067262. URL http://www.ncbi.nlm.nih.gov/pubmed/11834835.

C. Bobier and J. Sivak. Chromoretinoscopy. *Vision Research*, 18(3): 247–250, jan 1978. ISSN 0042-6989. doi: 10.1016/0042-6989(78)90158-X. URL https://www.sciencedirect.com/science/article/pii/004269897890158X.

W. R. Bobier, M. C. W. Campbell, and M. Hinch. The influence of chromatic aberration on the static accommodative response. *Vision Research*, 32(5):823–832, may 1992. ISSN 00426989. doi: 10.1016/0042-6989(92)90025-E. URL http://www.sciencedirect.com/science/article/pii/004269899290025E.

H. Bouma. Size of the static pupil as a function of wavelength and luminosity of the light incident on the human eye. *Nature*, 193:690–691, feb 1962. ISSN 0028-0836. URL http://www.ncbi.nlm.nih.gov/pubmed/13871842.

T. Buehren and M. J. Collins. Accommodation stimulusresponse function and retinal image quality. *Vision Research*, 46(10):1633–1645, 2006. ISSN 00426989. doi: 10.1016/j.visres.2005.06.009.

J. Burge and W. S. Geisler. Optimal defocus estimation in individual natural images. *Proceedings of the National Academy of Sciences of the United States of America*, 108(40):16849–54, oct 2011. ISSN 1091-6490. doi: 10.1073/pnas.1108491108. URL http://www.pnas.org/content/108/40/16849.full.

S. A. Burns. The spatially resolved refractometer. *Journal of Refractive Surgery*, 16(5):S566–S569, 2000. URL http://www.carlomasci.it/biblio/aberrazioni{_}8.pdf.

F. W. Campbell and R. W. Gubisch. The effect of chromatic aberration on visual acuity. *The Journal of physiology*, 192(2):345–58, sep 1967. ISSN 0022-3751. URL http://www.ncbi.nlm.nih.gov/pubmed/6050153http://www.pubmedcentral.nih.gov/articlerender.fcgi?artid=PMC1365561.

F. W. Campbell and G. Westheimer. Factors Influencing Accommodation Responses of the Human Eye. *Journal of the Optical Society of America*, 49 (6):568–571, jun 1959. ISSN 0030-3941. doi: 10.1364/JOSA.49.000568. URL https://www.osapublishing.org/abstract.cfm?URI=josa-49-6-568.

W. Charman and J. Jennings. Objective measurements of the longitudinal chromatic aberration of the human eye. *Vision Research*, 16(9):999–1005, 1976. ISSN 00426989. doi: 10.1016/0042-6989(76)90232-7.

W. N. Charman. Accommodation performance for chromatic displays. *Ophthalmic and Physiological Optics*, 9(4):459–463, oct 1989. ISSN 0275-5408. doi: 10.1111/j.1475-1313.1989.tb00959.x. URL http://doi.wiley.com/10.1111/j.1475-1313.1989.tb00959.x.

W. N. Charman and J. Tucker. Accommodation and color. *J. Opt. Soc. Am*, 68 (4):459–471, apr 1978. ISSN 0030-3941. doi: 10.1364/JOSA.68.000459. URL https://www.osapublishing.org/abstract.cfm?URI=josa-68-4-459.

L. Chen, P. B. Kruger, H. Hofer, B. Singer, and D. R. Williams. Accommodation with higher-order monochromatic aberrations corrected with adaptive optics. *Journal of the Optical Society of America A*, 23(1):1–8, jan 2006. ISSN 1084-7529. doi: 10.1364/JOSAA.23.000001. URL `https://www.osapublishing.org/abstract.cfm?URI=josaa-23-1-1`.

X. Cheng, A. Bradley, and L. N. Thibos. Predicting subjective judgment of best focus with objective image quality metrics. *Journal of Vision*, 4 (4):310–321, 2004. URL `http://jov.arvojournals.org/article.aspx?articleid=2121812`.

S. S. Chin, K. M. Hampson, and E. A. H. Mallen. Role of ocular aberrations in dynamic accommodation control. *Clinical and Experimental Optometry*, 92(3):227–237, 2009a. URL `http://onlinelibrary.wiley.com/doi/10.1111/j.1444-0938.2009.00361.x/full`.

S. S. Chin, K. M. Hampson, and E. A. H. Mallen. Effect of correction of ocular aberration dynamics on the accommodation response to a sinusoidally moving stimulus. *Optics letters*, 34(21):3274–3276, 2009b. URL `http://www.osapublishing.org/ol/fulltext.cfm?uri=ol-34-21-3274`.

S. A. Cholewiak, G. D. Love, P. P. Srinivasan, R. Ng, and M. S. Banks. ChromaBlur: Rendering Chromatic Eye Aberration Improves Accommodation and Realism. *ACM Transactions on Graphics*, 36(6):1–12, nov 2017. ISSN 07300301. doi: 10.1145/3130800.3130815. URL `http://dl.acm.org/citation.cfm?doid=3130800.3130815`.

S. A. Cholewiak, G. D. Love, and M. S. Banks. Creating correct blur and its effect on accommodation. *Journal of Vision*, 18(9):1–29, sep 2018. ISSN 1534-7362. doi: 10.1167/18.9.1. URL `http://jov.arvojournals.org/article.aspx?doi=10.1167/18.9.1`.

C. Cicerone, P. Gowdy, and S. Otake. Composition and arrangement of the cone mosaic in the living human eye. *Investigative ophthalmology & visual science*, 35(4), 1994. URL `https://cloudfront.escholarship.org/dist/prd/content/qt00s720xd/qt00s720xd.pdf`.

CIE. Commission Internationale de l'Éclairage Proceedings, 1931, 1932.

CIE. Fundamental chromaticity diagram with physiological axes - Parts 1 and 2. Technical report, Commission Internationale de l'Eclairage, Vienna, 2006.

H. D. Crane. A theoretical analysis of the visual accommodation system in humans. Technical report, Stanford Research Institute, Menlo Park, California, 1966. URL `https://ntrs.nasa.gov/archive/nasa/casi.ntrs.nasa.gov/19660027855.pdf`.

D. M. Dacey and B. B. Lee. The 'blue-on' opponent pathway in primate retina originates from a distinct bistratified ganglion cell type. *Nature*, 367(6465): 731–735, feb 1994. doi: 10.1038/367731a0. URL `http://www.nature.com/doifinder/10.1038/367731a0`.

D. M. Dacey, H.-W. Liao, B. B. Peterson, F. R. Robinson, V. C. Smith, J. Pokorny, K.-W. Yau, and P. D. Gamlin. Melanopsin-expressing ganglion cells in primate retina signal colour and irradiance and project to the LGN. *Nature*, 433(7027):749–754, feb 2005. doi: 10.1038/nature03387. URL `http://www.nature.com/articles/nature03387`.

P. De Gracia, C. Dorronsoro, L. Sawides, E. Gambra, and S. Marcos. Experimental Test of Simulated Retinal Images Using Adaptive Optics. In *Frontiers in Optics 2009/Laser Science XXV/Fall 2009 OSA Optics & Photonics Technical Digest*, page JWB4, Washington, D.C., oct 2009. OSA. ISBN 978-1-55752-878-0. doi: 10.1364/AOPT.2009.JWB4. URL `https://www.osapublishing.org/abstract.cfm?uri=AOPT-2009-JWB4`.

A. Dehnert, M. Bach, and S. Heinrich. Subjective visual acuity with simulated defocus. *Ophthalmic and Physiological Optics*, 2011. URL `https://www.infona.pl/resource/bwmeta1.element.wiley-opo-v-31-i-6-opo857`.

E. DeHoog and J. Schwiegerling. Position of White Light Best Focus in the Human Eye. *Investigative Ophthalmology & Visual Science*, 48(13):993, may 2007. ISSN 1552-5783. URL `http://iovs.arvojournals.org/article.aspx?articleid=2383876`.

A. Duane. Normal values of the accommodation at all ages. *Journal of the American Medical Association*, 59(12):1010–1013, 1912. URL `https://jamanetwork.com/journals/jama/article-abstract/432623`.

D. H. Fender. Control mechanisms of the eye. *Scientific American*, 211(1): 24–33, 1964. URL https://www.jstor.org/stable/24931558.

E. F. Fincham. The Accommodation Reflex and its Stimulus. *Brit. J. Ophthal*, 35(7):381–393, 1951.

D. Flitcroft. A neural and computational model for the chromatic control of accommodation. *Visual Neuroscience*, 1990. URL https://www.researchgate.net/profile/Ian{_}Flitcroft/publication/21069500{_}A{_}neural{_}and{_}computational{_}model{_}for{_}the{_}chromatic{_}contr links/57cd3bb208ae3ac722b53f8a.pdf.

J. Fourier. Mémoire sur la Propagation de la Chaleur dans les Corps Solides (Extrait). *Nouveau Bulletin des Sciences, par la Société Philomathique de Paris*, 1:112–16, 1808.

E. Gambra, L. Sawides, C. Dorronsoro, and S. Marcos. Accommodative lag and fluctuations when optical aberrations are manipulated. *Journal of vision*, 9(6):1–15, jan 2009. ISSN 1534-7362. doi: 10.1167/9.6.4. URL http://jov.arvojournals.org/article.aspx?articleid=2204022.

P. D. Gamlin, D. H. McDougal, J. Pokorny, V. C. Smith, K.-W. Yau, and D. M. Dacey. Human and macaque pupil responses driven by melanopsin-containing retinal ganglion cells. *Vision Research*, 47(7):946–954, mar 2007. doi: 10.1016/J.VISRES.2006.12.015. URL https://www.sciencedirect.com/science/article/pii/S0042698906005682.

A. Glasser and M. C. Campbell. Presbyopia and the optical changes in the human crystalline lens with age. *Vision Research*, 38(2):209–229, jan 1998. ISSN 0042-6989. doi: 10.1016/S0042-6989(97)00102-8. URL https://www.sciencedirect.com/science/article/pii/S0042698997001028.

D. G. Green and F. W. Campbell. Effect of Focus on the Visual Response to a Sinusoidally Modulated Spatial Stimulus. *Journal of the Optical Society of America*, 55(9):1154–1157, sep 1965. doi: 10.1364/JOSA.55.001154. URL https://www.osapublishing.org/abstract.cfm?URI=josa-55-9-1154.

K. Grieve, P. Tiruveedhula, Y. Zhang, and A. Roorda. Multi-wavelength imaging with the adaptive optics scanning laser Ophthalmoscope. *Optics Express*, 14(25):12230–12242, dec 2006. ISSN 1094-4087. doi: 10.1364/OE.

14.012230. URL http://www.osapublishing.org/viewmedia.cfm?uri=oe-14-25-12230{&}seq=0{&}html=true.

A. Guirao and P. Artal. Off-axis monochromatic aberrations estimated from double pass measurements in the human eye. *Vision Research*, 39(2):207–217, jan 1999. doi: 10.1016/S0042-6989(98)00159-X. URL https://www.sciencedirect.com/science/article/pii/S004269899800159X.

J. C. Hay, H. L. Pick, and E. Rosser. Adaptation to chromatic aberration by the human visual system. *Science (New York, N.Y.)*, 141(3576):167–9, jul 1963. ISSN 0036-8075. doi: 10.1126/science.141.3576.167. URL http://www.ncbi.nlm.nih.gov/pubmed/13953247.

J. He, S. Burns, and S. Marcos. Monochromatic aberrations in the accommodated human eye. *Vision Research*, 40(1):41–48, jan 2000. ISSN 00426989. doi: 10.1016/S0042-6989(99)00156-X. URL http://www.sciencedirect.com/science/article/pii/S004269899900156X.

H. Hofer, J. Carroll, J. Neitz, M. Neitz, and D. R. Williams. Organization of the Human Trichromatic Cone Mosaic. *Journal of Neuroscience*, 25(42):9669–9679, oct 2005. ISSN 0270-6474. doi: 10.1523/JNEUROSCI.2414-05.2005. URL http://www.ncbi.nlm.nih.gov/pubmed/16237171http://www.jneurosci.org/cgi/doi/10.1523/JNEUROSCI.2414-05.2005.

P. A. Howarth and A. Bradley. The longitudinal chromatic aberration of the human eye, and its correction. *Vision research*, 26(2):361–6, jan 1986. ISSN 0042-6989. URL http://www.ncbi.nlm.nih.gov/pubmed/3716229.

A. Ivanoff. Focusing wave-length for white light. *J. Opt. Soc. Am*, 39(8):718, 1949. URL https://www.osapublishing.org/viewmedia.cfm?uri=josa-39-8-718.

R. J. Jacobs, G. Smith, and C. D. C. Chan. Effect of defocus on blur thresholds and on thresholds of perceived change in blur: comparison of source and observer methods. *Optometry & Vision Science*, 66(8):545–553, 1989. URL http://journals.lww.com/optvissci/Abstract/1989/08000/Effect{_}of{_}Defocus{_}on{_}Blur{_}Thresholds{_}and{_}on.10.aspx.

H. Kolb, K. A. Linberg, and S. K. Fisher. Neurons of the human retina: A Golgi study. *The Journal of Comparative Neurology*, 318(2):147–187, apr 1992. ISSN 0021-9967. doi: 10.1002/cne.903180204. URL `http://doi.wiley.com/10.1002/cne.903180204`.

P. B. Kruger and J. Pola. Stimuli for accommodation: Blur, chromatic aberration and size. *Vision Research*, 26(6):957–971, jan 1986. ISSN 00426989. doi: 10.1016/0042-6989(86)90153-7. URL `http://www.sciencedirect.com/science/article/pii/0042698986901537`.

P. B. Kruger, S. Mathews, K. R. Aggarwala, and N. Sanchez. Chromatic aberration and ocular focus: Fincham revisited. *Vision Research*, 33 (10):1397–1411, jul 1993. ISSN 00426989. doi: 10.1016/0042-6989(93)90046-Y. URL `http://www.sciencedirect.com/science/article/pii/004269899390046Y`.

P. B. Kruger, S. Nowbotsing, K. R. Aggarwala, and S. Mathews. Small amounts of chromatic aberration influence dynamic accommodation. *Optometry & Vision Science*, 72(9):656–666, 1995. URL `http://journals.lww.com/optvissci/Abstract/1995/09000/Small{_}Amounts{_}of{_}Chromatic{_}Aberration{_}Influence.9.aspx`.

P. B. Kruger, S. Mathews, M. Katz, K. R. Aggarwala, and S. Nowbotsing. Accommodation without feedback suggests directional signals specify ocular focus. *Vision Research*, 37(18):2511–2526, 1997. doi: 10.1016/S0042-6989(97)00056-4.

P. B. Kruger, N. Lopez-Gil, and L. R. Stark. Accommodation and the Stiles-Crawford effect: theory and a case study. *Ophthalmic and Physiological Optics*, 21(5):339–351, sep 2001. ISSN 0275-5408. doi: 10.1046/j.1475-1313.2001.00599.x. URL `http://doi.wiley.com/10.1046/j.1475-1313.2001.00599.x`.

J. Liang and D. R. Williams. Aberrations and retinal image quality of the normal human eye. *Journal of the Optical Society of America A*, 14(11):2873 – 2883, nov 1997. ISSN 1084-7529. doi: 10.1364/JOSAA.14.002873. URL `http://www.osapublishing.org/viewmedia.cfm?uri=josaa-14-11-2873{&}seq=0{&}html=true`.

J. Liang, D. R. Williams, and D. T. Miller. Supernormal vision and high-resolution retinal imaging through adaptive optics. *Journal of the Optical Society of America A*, 14(11):2884, nov 1997. ISSN 1084-7529. doi: 10.1364/JOSAA.14.002884. URL `http://www.osapublishing.org/viewmedia.cfm?uri=josaa-14-11-2884{&}seq=0{&}html=true`.

N. López-Gil and R. Montés-Micó. New intraocular lens for achromatizing the human eye. *Journal of Cataract & Refractive Surgery*, 2007. URL `http://www.sciencedirect.com/science/article/pii/S0886335007006505`.

J. V. Lovasik and H. Kergoat. Accommodative performance for chromatic displays. *Ophthalmic and Physiological Optics*, 8(4):443–449, oct 1988. ISSN 0275-5408. doi: 10.1111/j.1475-1313.1988.tb01183.x. URL `http://doi.wiley.com/10.1111/j.1475-1313.1988.tb01183.x`.

Z.-L. Lu and B. Dosher. *Visual psychophysics : from laboratory to theory*. The MIT Press, 2013. ISBN 9780262019453. URL `https://mitpress.mit.edu/books/visual-psychophysics`.

K. J. MacKenzie and S. J. Watt. Eliminating accommodation-convergence conflicts in stereoscopic displays: Can multiple-focal-plane displays elicit continuous and consistent vergence and accommodation responses? In A. J. Woods, N. S. Holliman, and N. A. Dodgson, editors, *IS&T/SPIE Electronic Imaging*, pages 752417–752417–10. International Society for Optics and Photonics, feb 2010. doi: 10.1117/12.840283. URL `http://proceedings.spiedigitallibrary.org/proceeding.aspx?articleid=776088`.

J. Mannos and D. Sakrison. The effects of a visual fidelity criterion of the encoding of images. *Information Theory, IEEE ...*, 1974. URL `http://ieeexplore.ieee.org/xpls/abs{_}all.jsp?arnumber=1055250`.

S. Marcos, S. A. Burns, E. Moreno-Barriusop, and R. Navarro. A new approach to the study of ocular chromatic aberrations. *Vision Research*, 39 (26):4309–4323, 1999. URL `http://www.sciencedirect.com/science/article/pii/S0042698999001455`.

S. Marcos, S. A. Burns, P. M. Prieto, R. Navarro, and B. Baraibar. Investigating sources of variability of monochromatic and transverse chromatic aberrations across eyes. *Vision Research*, 41(28):3861–3871, dec

2001. ISSN 00426989. doi: 10.1016/S0042-6989(01)00133-X. URL http://www.sciencedirect.com/science/article/pii/S004269890100133X.

D. H. Marimont and B. A. Wandell. Matching color images: the effects of axial chromatic aberration. *Journal of the Optical Society of America A*, 11(12):3113–3122, dec 1994. ISSN 1084-7529. doi: 10.1364/JOSAA.11.003113. URL https://www.osapublishing.org/abstract.cfm?URI=josaa-11-12-3113.

J. D. Marsack, L. N. Thibos, and R. A. Applegate. Metrics of optical quality derived from wave aberrations predict visual performance. *Journal of Vision*, 4(4):322–328, apr 2004. ISSN 1534-7362. doi: 10.1167/4.4.8. URL http://jov.arvojournals.org/article.aspx?doi=10.1167/4.4.8.

S. Mathews and P. B. Kruger. Spatiotemporal transfer function of human accommodation. *Vision Research*, 34(15):1965–1980, aug 1994. ISSN 0042-6989. doi: 10.1016/0042-6989(94)90026-4. URL https://www.sciencedirect.com/science/article/pii/0042698994900264.

J. S. McLellan, S. Marcos, and S. A. Burns. Age-related changes in monochromatic wave aberrations of the human eye. *... Ophthalmology and Visual ...*, 2001. URL http://www.opt.indiana.edu/people/faculty/burns/pub/waveaberrationsandaging.pdf.

J. S. McLellan, S. Marcos, P. M. Prieto, and S. A. Burns. Imperfect optics may be the eye's defence against chromatic blur. *Nature*, 417(6885):174–6, may 2002. ISSN 0028-0836. doi: 10.1038/417174a. URL http://dx.doi.org/10.1038/417174a.

S. Metlapally, J. Tong, H. Tahir, and C. M. Schor. Evidence that Accommodative Microfluctuations provide Odd-Error Cues to Accommodation and Insights into the Potential Spatial Cues [Abstract]. *Investigative Ophthalmology & Visual Science*, 55(13):3772, apr 2014. URL https://iovs.arvojournals.org/article.aspx?articleid=2269224.

S. Metlapally, J. L. Tong, H. J. Tahir, and C. M. Schor. Potential role for microfluctuations as a temporal directional cue to accommodation. *Journal of Vision*, 16(6):1–11, apr 2016. ISSN 1534-7362. doi: 10.1167/16.6.19. URL http://jov.arvojournals.org/article.aspx?doi=10.1167/16.6.19.

M. A. Miranda, C. O'Donnell, and H. Radhakrishnan. Repeatability of corneal and ocular aberration measurements and changes in aberrations over one week. *Clinical & experimental optometry*, 92(3):253–66, may 2009. ISSN 1444-0938. doi: 10.1111/j.1444-0938.2009.00364.x. URL `http://www.ncbi.nlm.nih.gov/pubmed/19302673`.

R. Navarro, E. Moreno, and C. Dorronsoro. Monochromatic aberrations and point-spread functions of the human eye across the visual field. *Journal of the Optical Society of America A*, 15(9):2522, sep 1998. doi: 10.1364/JOSAA.15.002522. URL `https://www.osapublishing.org/abstract.cfm?URI=josaa-15-9-2522`.

A. Ohlendorf, J. Tabernero, and F. Schaeffel. Visual Acuity with Simulated and Real Astigmatic Defocus. *Optometry and Vision Science*, 88(5):562–569, may 2011. ISSN 1040-5488. doi: 10.1097/OPX.0b013e31821281bc. URL `http://content.wkhealth.com/linkback/openurl?sid=WKPTLP:landingpage{&}an=00006324-201105000-00004`.

D. Owens. A comparison of accommodative responsiveness and contrast sensitivity for sinusoidal gratings. *Vision Research*, 20(2):159–167, 1980. ISSN 00426989. doi: 10.1016/0042-6989(80)90158-3.

J. Parnell. *Depth Perception in Humans and Animals*. PhD thesis, Durham University, 2015.

S. Plainis and I. Pallikaris. Ocular monochromatic aberration statistics in a large emmetropic population. *Journal of Modern Optics*, 55(4-5):759–772, feb 2008. ISSN 0950-0340. doi: 10.1080/09500340701469831. URL `http://www.tandfonline.com/doi/abs/10.1080/09500340701469831{#}.VtRZooQ8E{_}U`.

S. Plainis, H. S. Ginis, and A. Pallikaris. The effect of ocular aberrations on steady-state errors of accommodative response. *Journal of Vision*, 5 (5):466–477, may 2005. ISSN 1534-7362. doi: 10.1167/5.5.7. URL `http://jov.arvojournals.org/article.aspx?doi=10.1167/5.5.7`.

J. Pokorny, V. C. Smith, and M. Lutze. Aging of the human lens. *Applied Optics*, 26(8):1437, apr 1987. ISSN 0003-6935. doi: 10.1364/AO.26.001437. URL `https://www.osapublishing.org/abstract.cfm?URI=ao-26-8-1437`.

S. Ravikumar, L. N. Thibos, and A. Bradley. Calculation of retinal image quality for polychromatic light. *Journal of the Optical Society of America A*, 25(10):2395, sep 2008. ISSN 1084-7529. doi: 10.1364/JOSAA.25.002395. URL http://www.osapublishing.org/viewmedia.cfm?uri=josaa-25-10-2395{&}seq=0{&}html=true.

V. M. Reading and R. A. Weale. Macular pigment and chromatic aberration. *Journal of the Optical Society of America*, 64(2):231, feb 1974. ISSN 0030-3941. doi: 10.1364/JOSA.64.000231. URL http://www.osapublishing.org/viewmedia.cfm?uri=josa-64-2-231{&}seq=0{&}html=true.

L. Remón, J. Benlloch, A. Pons, J. A. Monsoriu, and W. D. Furlan. Visual acuity with computer simulated and lens-induced astigmatism. *Optica Applicata*, 44(4):521–531, 2014. URL http://yadda.icm.edu.pl/baztech/element/bwmeta1.element.baztech-8af5fda9-2868-4f3e-bf76-16bde40e586c.

R. W. Rodieck, K. F. Binmoeller, and J. Dineen. Parasol and midget ganglion cells of the human retina. *The Journal of Comparative Neurology*, 233(1):115–132, mar 1985. ISSN 0021-9967. doi: 10.1002/cne.902330107. URL http://doi.wiley.com/10.1002/cne.902330107.

F. J. Rucker and P. B. Kruger. Accommodation responses to stimuli in cone contrast space. *Vision Research*, 44(25):2931–2944, nov 2004. ISSN 00426989. doi: 10.1016/j.visres.2004.07.005. URL http://linkinghub.elsevier.com/retrieve/pii/S0042698904003542.

C. Schwarz, C. Cánovas, S. Manzanera, H. Weeber, P. M. Prieto, P. Piers, and P. Artal. Binocular visual acuity for the correction of spherical aberration in polychromatic and monochromatic light. *Journal of Vision*, 14(2):1–11, 2014. URL http://jov.arvojournals.org/article.aspx?articleid=2121673.

T. Seiler, M. Mrochen, and M. Kaemmerer. Operative correction of ocular aberrations to improve visual acuity. *Journal of Refractive Surgery*, 16:619–623, 2000. URL https://www.healio.com/ophthalmology/journals/jrs/2000-9-16-5/{%}7B4028cee6-f25b-4e32-a4db-d0269923fe29{%}7D/operative-correction-of-ocular-aberrations-to-improve-visual-acuity.

R. J. Sharman, P. V. McGraw, and J. W. Peirce. Luminance cues constrain chromatic blur discrimination in natural scene stimuli. *Journal of Vision*, 13(4):1–10, mar 2013. ISSN 1534-7362. doi: 10.1167/13.4.14. URL `http://jov.arvojournals.org/Article.aspx?doi=10.1167/13.4.14`.

L. T. Sharpe, A. Stockman, W. Jagla, and H. Jägle. A luminous efficiency function, V*(λ), for daylight adaptation. *Journal of Vision*, 5(11):948–968, 2005. URL `http://jov.arvojournals.org/article.aspx?articleid=2121738`.

G. Smith, R. Jacobs, and C. Chan. Effect of defocus on visual acuity as measured by source and observer methods. *Optometry & Vision Science*, 66(7):430–435, 1989. URL `http://journals.lww.com/optvissci/abstract/1989/07000/effect{_}of{_}defocus{_}on{_}visual{_}acuity{_}as{_}measured{_}by.4.aspx`.

G. Smith, P. Bedggood, R. Ashman, M. Daaboul, and A. Metha. Exploring Ocular Aberrations with a Schematic Human Eye Model. *Optometry and Vision Science*, 85(5):330–340, may 2008. ISSN 1040-5488. doi: 10.1097/OPX.0b013e31816c4449. URL `https://insights.ovid.com/crossref?an=00006324-200805000-00009`.

L. M. Smithline. Accommodative response to blur. *Journal of the Optical Society of America*, 64(11):3–7, 1974.

M. Spitschan, S. Jain, D. H. Brainard, and G. K. Aguirre. Opponent melanopsin and S-cone signals in the human pupillary light response. *Proceedings of the National Academy of Sciences of the United States of America*, 111(43):15568–72, oct 2014. doi: 10.1073/pnas.1400942111. URL `http://www.ncbi.nlm.nih.gov/pubmed/25313040`.

N. G. Sravani, V. K. Nilagiri, S. R. Bharadwaj, D. A. Goss, T. Grosvenor, M. Choi, A. H. Dahlmann-Noor, H. C. Howland, O. A. Hunt, J. S. Wolffsohn, B. Gilmartin, S. R. Bharadwaj, T. R. Candy, S. R. Bharadwaj, J. Wang, T. R. Candy, A. M. Horwood, J. E. Turner, S. M. Houston, P. M. Riddell, R. Suryakumar, D. Kwok, S. Fernandez, W. R. Bobier, J. S. Wolffsohn, O. A. Hunt, B. Gilmartin, F. Schaeffel, H. Wilhelm, E. Zrenner, P. J. Blade, T. R. Candy, S. R. Bharadwaj, Y. L. Chen, B. Tan, J. Lewis, S. R.

Bharadwaj, M. Malavita, J. Jayaraj, M. Erdurmus, R. Yagci, R. Karadag, M. Durmus, S. Hodi, I. C. Wood, A. Roorda, M. C. Campbell, W. R. Bobier, F. C. Delori, K. P. Pflibsen, A. E. Elsner, S. A. Burns, J. J. Weiter, F. C. Delori, R. Dandona, K. S. Naidoo, M. Glickstein, M. Millodot, C. Nischler, D. F. Teel, R. J. Jacobs, J. Copland, D. R. Neal, L. N. Thibos, B. W. Arthur, R. Riyaz, S. Rodriguez, J. Wong, E. A. Ball, L. Marran, C. M. Schor, P. M. Allen, H. Radhakrishnan, D. J. O'Leary, A. Seidemann, F. Schaeffel, K. Wakamatsu, D. N. Hu, S. A. McCormick, S. Ito, L. Semes, A. Shaikh, G. McGwin, J. D. Bartlett, N. Kollias, and A. Baqer. Photorefraction estimates of refractive power varies with the ethnic origin of human eyes. *Scientific Reports*, 5:7976, jan 2015. ISSN 2045-2322. doi: 10.1038/srep07976. URL `http://www.nature.com/articles/srep07976`.

L. R. Stark, P. B. Kruger, F. J. Rucker, W. H. Swanson, N. Schmidt, C. Hardy, H. Rutman, T. Borgovan, S. Burke, M. Badar, and R. Shah. Potential signal to accommodation from the StilesCrawford effect and ocular monochromatic aberrations. *Journal of Modern Optics*, 56(20):2203–2216, nov 2009. ISSN 0950-0340. doi: 10.1080/09500340903184295. URL `http://www.tandfonline.com/doi/abs/10.1080/09500340903184295`.

W. S. Stiles and B. H. Crawford. The luminous efficiency of rays entering the eye pupil at different points. *Proceedings of the Royal Society B: Biological Sciences*, 112(778):428–450, mar 1933. ISSN 0962-8452. doi: 10.1098/rspb.1933.0020. URL `http://rspb.royalsocietypublishing.org/cgi/doi/10.1098/rspb.1933.0020`.

A. Stockman and D. H. Brainard. Color Vision Mechanisms. In M. Bass, C. DeCusatis, J. M. Enoch, V. Lakshminarayanan, G. Li, C. MacDonald, V. N. Mahajan, and E. Van Stryland, editors, *Handbook of Optics, Volume III: Vision and Vision Optics*. McGraw-Hill, New York, 3 edition, 2009. URL `http://www.cvrl.org/people/Stockman/pubs/2010ColorVisionMechanismsSB.pdf`.

A. Stockman and L. T. Sharpe. The spectral sensitivities of the middle- and long-wavelength-sensitive cones derived from measurements in observers of known genotype. *Vision Research*, 40(13):1711–1737, jun 2000. doi: 10.1016/S0042-6989(00)00021-3. URL `https://www.sciencedirect.com/science/article/pii/S0042698900000213`.

A. Stockman, L. T. Sharpe, and C. Fach. The spectral sensitivity of the human short-wavelength sensitive cones derived from thresholds and color matches. *Vision Research*, 39(17):2901–2927, aug 1999. doi: 10.1016/S0042-6989(98)00225-9. URL https://www.sciencedirect.com/science/article/pii/S0042698998002259.

A. Stockman, H. Jagle, M. Pirzer, and L. T. Sharpe. The dependence of luminous efficiency on chromatic adaptation. *Journal of Vision*, 8(16):1–1, dec 2008. doi: 10.1167/8.16.1. URL http://jov.arvojournals.org/Article.aspx?doi=10.1167/8.16.1.

D. Stone, S. Mathews, and P. B. Kruger. Accommodation and chromatic aberration: effect of spatial frequency. *Ophthalmic and Physiological Optics*, 13(3):244–252, jul 1993. ISSN 0275-5408. doi: 10.1111/j.1475-1313.1993.tb00466.x. URL http://doi.wiley.com/10.1111/j.1475-1313.1993.tb00466.x.

J. Tarrant, A. Roorda, and C. F. Wildsoet. Determining the accommodative response from wavefront aberrations. *Journal of Vision*, 10(5):4–4, may 2010. doi: 10.1167/10.5.4. URL http://jov.arvojournals.org/Article.aspx?doi=10.1167/10.5.4.

L. N. Thibos and A. Bradley. Spherical aberration and the sign of defocus. *Optometry & Vision ...*, 2013. URL http://journals.lww.com/optvissci/Abstract/2013/11000/Spherical{_}Aberration{_}and{_}the{_}Sign{_}of{_}Defocus.18.aspx.

L. N. Thibos, M. Ye, X. Zhang, and A. Bradley. The chromatic eye: a new reduced-eye model of ocular chromatic aberration in humans. *Applied Optics*, 31(19):3594–3600, jul 1992. doi: 10.1364/AO.31.003594. URL https://www.osapublishing.org/abstract.cfm?URI=ao-31-19-3594.

L. N. Thibos, R. A. Applegate, J. T. Schwiegerling, and R. Webb. Report from the VSIA taskforce on standards for reporting optical aberrations of the eye. *Journal of Refractive Surgery*, 16:654–655, 2000. URL http://www.carlomasci.it/biblio/aberrazioni{_}27.pdf.

L. N. Thibos, X. Hong, A. Bradley, and X. Cheng. Statistical variation of aberration structure and image quality in a normal population of healthy

eyes. *Journal of the Optical Society of America A*, 19(12):2329–2348, dec 2002. ISSN 1084-7529. doi: 10.1364/JOSAA.19.002329. URL https://www.osapublishing.org/abstract.cfm?URI=josaa-19-12-2329.

L. N. Thibos, X. Hong, A. Bradley, and R. A. Applegate. Accuracy and precision of objective refraction from wavefront aberrations. *Journal of Vision*, 4(4):329–351, apr 2004. ISSN 1534-7362. doi: 10.1167/4.4.9. URL http://jov.arvojournals.org/article.aspx?doi=10.1167/4.4.9.

F. M. Toates. Accommodation function of the human eye. *Physiological reviews*, 52(4):828–63, oct 1972. URL http://www.ncbi.nlm.nih.gov/pubmed/4345068.

E. A. Villegas, E. Alcon, and P. Artal. Optical Quality of the Eye in Subjects with Normal and Excellent Visual Acuity. *Investigative Opthalmology & Visual Science*, 49(10):4688, oct 2008. ISSN 1552-5783. doi: 10.1167/iovs.08-2316. URL http://iovs.arvojournals.org/article.aspx?doi=10.1167/iovs.08-2316.

G. Walsh and W. Charman. Visual sensitivity to temporal change in focus and its relevance to the accommodation response. *Vision research*, 1988. URL http://www.sciencedirect.com/science/article/pii/0042698988900375.

B. A. Wandell. *Foundations of vision.* Sinauer Associates, 1 edition, 1995. URL https://psycnet.apa.org/record/1995-98050-000.

S. J. Watt, K. Akeley, A. R. Girshick, and M. S. Banks. Achieving near-correct focus cues in a 3-D display using multiple image planes. In B. E. Rogowitz, T. N. Pappas, and S. J. Daly, editors, *Electronic Imaging 2005*, pages 393–401. International Society for Optics and Photonics, mar 2005. doi: 10.1117/12.610851. URL http://proceedings.spiedigitallibrary.org/proceeding.aspx?articleid=857734.

R. A. Weale. Age and the transmittance of the human crystalline lens. *The Journal of Physiology*, 395(1):577–587, jan 1988. ISSN 00223751. doi: 10.1113/jphysiol.1988.sp016935. URL http://doi.wiley.com/10.1113/jphysiol.1988.sp016935.

B. J. Wilson, K. E. Decker, and A. Roorda. Monochromatic aberrations provide an odd-error cue to focus direction. *Journal of the Optical Society of America A*, 19(5):833–839, may 2002. ISSN 1084-7529. doi: 10.1364/JOSAA.19.000833. URL `http://www.osapublishing.org/viewmedia.cfm?uri=josaa-19-5-833{&}seq=0{&}html=true`.

K. Y. Wong. A retinal ganglion cell that can signal irradiance continuously for 10 hours. *The Journal of neuroscience*, 32(33):11478–11485, aug 2012. ISSN 1529-2401. doi: 10.1523/JNEUROSCI.1423-12.2012. URL `http://www.ncbi.nlm.nih.gov/pubmed/22895730http://www.pubmedcentral.nih.gov/articlerender.fcgi?artid=PMC3432977`.

G.-Y. Yoon and D. Williams. Visual benefit of correcting the higher order monochromatic aberrations and the longitudinal chromatic aberration in the eye. In *Vision Science and its Applications*, page PD5, Santa Fe, New Mexico, United States, feb 2000. Optical Society of America. URL `http://www.osapublishing.org/abstract.cfm?uri=VSIA-2000-PD5`.

G.-Y. Yoon and D. R. Williams. Visual performance after correcting the monochromatic and chromatic aberrations of the eye. *Journal of the Optical Society of America A*, 19(2):266–275, feb 2002. ISSN 1084-7529. doi: 10.1364/JOSAA.19.000266. URL `http://www.osapublishing.org/viewmedia.cfm?uri=josaa-19-2-266{&}seq=0{&}html=true`.

L. K. Young. *Ocular higher-order aberrations and visual performance*. PhD thesis, Durham University, 2011.

F. Zernike. Diffraction theory of the knife-edge test and its improved form, the phase-contrast method. *Monthly Notices of the Royal Astronomical Society*, 94(5):377–384, 1934. URL `http://adsabs.harvard.edu/full/1934MNRAS..94..377Z7`.

Y. Zhai, Y. Wang, Z. Wang, Y. Liu, L. Zhang, Y. He, and S. Chang. Design of eye models used in quantitative analysis of interaction between chromatic and higher-order aberrations of eye. *Optics Communications*, 332:89–95, 2014. ISSN 00304018. doi: 10.1016/j.optcom.2014.06.051.

Colophon

This thesis was typeset with LaTeX 2_ε. It was created using the *memoir* package, maintained by Lars Madsen, with the *madsen* chapter style. The font used is Latin Modern, derived from fonts designed by Donald E. Kunith.